

หน่วยแปรรูปเชื้อเพลิงเพื่อการผลิตไฮโดรเจนจากเมทานอลสำหรับเซลล์เชื้อเพลิงฟิวเอ็่ม

นางสาว สุธารวดี มัญยานนท์

วิทยานิพนธ์นี้เป็นส่วนหนึ่งของการศึกษาตามหลักสูตรปริญญาวิทยาศาสตรดุษฎีบัณฑิต

สาขาวิชาเคมีเทคนิค ภาควิชาเคมีเทคนิค

คณะวิทยาศาสตร์ จุฬาลงกรณ์มหาวิทยาลัย

ปีการศึกษา 2553

ลิขสิทธิ์ของจุฬาลงกรณ์มหาวิทยาลัย

FUEL PROCESSOR FOR HYDROGEN PRODUCTION FROM METHANOL
FOR PEM FUEL CELL

Miss Sutarawadee Monyanon

A Dissertation Submitted in Partial Fulfillment of the Requirements
for the Degree of Doctor of Philosophy Program in Chemical Technology

Department of Chemical Technology

Faculty of Science

Chulalongkorn University

Academic Year 2010

Copyright of Chulalongkorn University

Thesis Title	FUEL PROCESSOR FOR HYDROGEN PRODUCTION FROM METHANOL FOR PEM FUEL CELL
By	Miss Sutarawadee Monyanon
Field of Study	Chemical Technology
Thesis Advisor	Associate Professor Nuttaya Pongstabodee, Ph.D.
Thesis Co-advisor	Assistant Professor Apanee Luengnaruemitchai, Ph.D.

Accepted by the Faculty of Science, Chulalongkorn University in Partial Fulfillment of the Requirements for the Doctoral Degree

.....Dean of the Faculty of Science
(Professor Supot Hannongbua, Dr. rer. nat.)

THESIS COMMITTEE

.....Chairman
(Professor Pattarapan Prasassarakich, Ph.D.)

.....Thesis Advisor
(Associate Professor Nuttaya Pongstabodee, Ph.D.)

.....Thesis Co-advisor
(Assistant Professor Apanee Luengnaruemitchai, Ph.D.)

.....Examiner
(Associate Professor Tharapong Vitidsant, Ph.D.)

.....Examiner
(Assistant Professor Prasert Reubroycharoen, Ph.D.)

.....External Examiner
(Siriphong Rojluechai, Ph.D.)

ศุขาราวดี มัญยานนท์ : หน่วยแปรรูปเชื้อเพลิงเพื่อการผลิตไฮโดรเจนจากเมทานอลสำหรับ เซลล์เชื้อเพลิงพีอีเอ็ม. (FUEL PROCESSOR FOR HYDROGEN PRODUCTION FROM METHANOL FOR PEM FUEL CELL) อ. ที่ปรึกษาวิทยานิพนธ์หลัก : รศ. ดร. ณัฐชยาน์ พงศ์สถาปติ, อ. ที่ปรึกษาวิทยานิพนธ์ร่วม : ผศ. ดร. อาภาณี เหลืองนฤมิตชัย, 216 หน้า.

วัตถุประสงค์ของงานวิจัยนี้ เพื่อผลิตแก๊สไฮโดรเจนจากเมทานอลสำหรับเซลล์เชื้อเพลิง อีเอ็มโดยใช้กระบวนการรีฟอร์มมิงของเมทานอลรวมกับการกำจัดแก๊สคาร์บอนมอนอกไซด์ สำหรับหน่วยรีฟอร์มมิงของเมทานอลศึกษาตัวเร่งปฏิกิริยาของร้อยละ 5 โดยน้ำหนักบนตัวรองรับ คอปเปอร์ออกไซด์ ตัวรองรับซีเรีย และตัวรองรับออกไซด์ผสม เพื่อทำการเปรียบเทียบกับตัวเร่ง ปฏิกิริยาทางการค้า (MegaMax 700) จากผลการทดลองพบว่าตัวเร่งปฏิกิริยาของร้อยละ 5 โดย น้ำหนักบนตัวรองรับออกไซด์ผสมคอปเปอร์และซีเรียที่สัดส่วน 50 ต่อ 50 โมลอะตอมให้ค่าร้อยละ การเปลี่ยนของเมทานอลเท่ากับ 100 ซึ่งสูงกว่าตัวเร่งปฏิกิริยาทางการค้าและมีความเสถียรในช่วง 540 นาที และสภาวะที่เหมาะสมโดยใช้การออกแบบการทดลองที่ระดับความเชื่อมั่นร้อยละ 95 ณ อุณหภูมิ 306.43 องศาเซลเซียสและสัดส่วนไอน้ำต่อเมทานอลเท่ากับ 2 ซึ่งมีค่าใกล้เคียงกับค่าที่ได้ จากการทดลอง ส่วนหน่วยกำจัดแก๊สคาร์บอนมอนอกไซด์ได้มีการศึกษาชนิดตัวเร่งปฏิกิริยา องค์ ประกอบในตัวเร่งปฏิกิริยา วิธีการเตรียมตัวเร่งปฏิกิริยา การบำบัดตัวเร่งปฏิกิริยา องค์ประกอบใน แก๊สป้อน อุณหภูมิที่ใช้ในการเกิดปฏิกิริยา และสภาวะของเตาปฏิกรณ์ จากผลการทดลองพบว่า ตัวเร่งปฏิกิริยาร้อยละ 1 โดยน้ำหนักโลหะผสมแพลทินัมกับทอง (1 ต่อ 1 โมลอะตอม) บนตัวรองรับ ออกไซด์ผสมซีเรียกับซิงค์ออกไซด์ (1 ต่อ 1 โมลอะตอม) ซึ่งเตรียมด้วยวิธีตกตะกอนร่วมมีความ วงไวมากที่สุดและเสถียรตลอดการใช้งานนาน 60 ชั่วโมง และสภาวะที่เหมาะสมโดยใช้การ ออกแบบการทดลองที่ระดับความเชื่อมั่นร้อยละ 95 ณ อุณหภูมิจาก 100 ถึง 115 องศาเซลเซียสและ มีปริมาณแก๊สคาร์บอนไดออกไซด์ประมาณร้อยละ 9 ถึง 12 เมื่อทำการเปรียบเทียบผลของกระแส ป้อนที่ได้จากการสังเคราะห์และจากหน่วยรีฟอร์มมิงของเมทานอลพบว่าไม่มีความแตกต่างของค่า ความวงไวที่คำนวณจากแบบจำลองและที่ได้จากการทดลอง เมื่อทำการผลิตแก๊สไฮโดรเจนจากเม ทานอลโดยใช้กระบวนการรีฟอร์มมิงรวมกับการกำจัดแก๊สคาร์บอนมอนอกไซด์พบว่า มีการปน เปื้อนของแก๊สคาร์บอนมอนอกไซด์น้อยกว่า 50 ส่วนในล้านส่วน ร้อยละผลได้ของแก๊สไฮโดรเจน ประมาณ 75 ณ อัตราการผลิต 320 ลิตรต่อหนึ่งกรัมตัวเร่งปฏิกิริยาต่อหนึ่งวัน

ภาควิชา วิศวกรรมเทคนิค.....ลายมือชื่อนิสิต.....

สาขาวิชา วิศวกรรมเทคนิค.....ลายมือชื่อ อ. ที่ปรึกษาวิทยานิพนธ์หลัก.....

ปีการศึกษา 2553.....ลายมือชื่อ อ. ที่ปรึกษาวิทยานิพนธ์ร่วม.....

4973854623 : MAJOR CHEMICAL TECHNOLOGY

KEYWORDS : FUEL PROCESSOR / STEAM REFORMING OF METHANOL /
PREFERENTIAL OXIDATION OF CO / PT-AU ALLOY / SOLID SOLUTION /
STATISTICAL DESIGN / RESPONSE SURFACE ANALYSIS

SUTARAWADEE MONYANON : FUEL PROCESSOR FOR HYDROGEN
PRODUCTION FROM METHANOL FOR PEM FUEL CELL.

ADVISOR : ASSOC.PROF. NUTTAYA PONGSTABODEE, Ph.D.,

CO-ADVISOR : ASST.PROF. APANEE LUENGNARUEMITCHAI, 216 pp.

The purpose of this study is to produce H₂-rich stream from methanol by an integration of steam reforming (SRM) and preferential CO oxidation (PROX). In SRM part, a series of supported Au catalysts were compared to MegaMax 700. It was found that 5% Au/(50:50)CuO–CeO₂ expressed complete methanol conversion, being higher than the performance of MegaMax 700. It was also stable and active in whole period test for 540 min. From the statistical analysis of four factors chosen at 95% confidence interval and central composite rotatable design (CCRD) falling response surface analysis, complete methanol conversion at a low CO selectivity was achieved with an operating temperature of 306.43 °C and an steam/methanol ratio of 2. The developed model was adequate. In PROX part, the effects of catalyst type, composition in catalyst, catalyst preparation, pretreatment condition, feedstream composition, operating temperature and mode of reactor was studied and revealed that 1%(1:1)PtAu/(1:1)CeO₂–ZnO prepared by co-precipitation exhibited the highest performance and was stable for ~60 h. From statistical analysis with face-centered central composite design (FCCCD) for PROX part, the optimum statistical conditions were found to lie within an operating temperature from ~100 °C to ~115 °C and 9–12% CO₂ content, in close agreement with the experimental results. When producing hydrogen with CO content less than 50 ppm by an integrating of SRM and PROX, hydrogen was yielded around ~75% at rate of ~320 L d⁻¹ gcat⁻¹.

Department : Chemical Technology Student's Signature

Field of Study : Chemical Technology Advisor's Signature

Academic Year : 2010 Co-advisor's Signature

ACKNOWLEDGEMENTS

This dissertation would have never been successfully without the assistance of the following persons and organizations:

I would like to express my deepest appreciation to my dissertation advisors, Associate Professor Nuttaya Pongstabodee, Ph.D. and Assistant Professor Apanee Luengnaruemitchai, Ph.D., for their endless special guidance, who reviewed this dissertation, offered many helpful suggestions, and much encouraged of my research. They always teach me not only the theoretical knowledge but also the other skills to think and to solve many problems. Moreover, I especially extend my appreciation to Professor Pattarapan Prasassarakich, Ph.D., Associate Professor Tharapong Vitidsant, Ph.D., Associate Professor Prasert Reubroycharoen, Ph.D., and Mr. Siriphong Rojluechai, Ph.D. for their participation on the dissertation chairman and committees.

Secondly, I am sincerest appreciation also extends to The 90th Anniversary of Chulalongkorn University under Ratchadaphiseksomphot Endowment Fund and Center for Petroleum, Petrochemicals and Advanced Materials for their financial support throughout this research.

Thirdly, many thanks are extended to all members and staff, especially, Mr. Theerathad Sakwarathorn of the Department of Chemical Technology, Chulalongkorn University for their assistance, encouragement, and friendships.

The last, I would like to appreciatively thank to my family members and Mr. Akarawut Sukavanawat for their constant support and encouragement. Without their love and support, I would not be able to success my doctoral degree.

CONTENTS

	Page
ABSTRACT (THAI)	iv
ABSTRACT (ENGLISH)	v
ACKNOWLEDGEMENTS	vi
CONTENTS	vii
LIST OF TABLES	xi
LIST OF FIGURES	xiii
CHAPTER I: INTRODUCTION.....	1
1.1. Rationale	1
1.2. Purpose of this study.....	3
1.3. Scope of the dissertation	4
1.4. Format of the dissertation	6
CHAPTER II: THEORY AND LITERATURE REVIEWS	8
2.1. Proton exchange membrane (PEM) fuel cell.....	8
2.2. Hydrogen production process	11
2.2.1. Conventional process	13
2.2.2. Alternative approaches to generating hydrogen	18
2.3. Fuel processing for PEM fuel cell	19
2.3.1. Steam reforming of methanol (SRM)	20
2.3.2. Preferential oxidation (PROX) of CO	21
2.4. Catalysts	22
2.4.1. Catalyst for SRM unit.....	22
2.4.2. Catalyst for PROX unit.....	24
2.5. Catalyst preparation method	25
2.5.1. Impregnation.....	25
2.5.2. Sol-gel.....	30
2.5.3. Precipitation.....	33
2.6. Catalyst characterization.....	38
2.7. Literature reviews	41
2.7.1. Steam reforming of methanol (SRM)	41

	Page
2.7.2. Preferential oxidation (PROX) of CO	46
2.7.3. Design of experiment (DOE).....	51
2.7.4. Fuel processing for PEMFC	54
CHAPTER III: EXPERIMENTAL.....	56
3.1. Materials	56
3.1.1. Chemicals	56
3.1.2. Gases.....	57
3.2. Equipments and apparatus set-up	58
3.2.1. Equipments	58
3.2.2. Apparatus set-up	58
3.3. Experiment procedure.....	60
3.3.1. Steam reforming of methanol (SRM) unit.....	60
3.3.1.1. Catalyst preparation	60
3.3.1.2. Catalyst characterization.....	61
3.3.1.3. Catalytic activity measurement.....	62
3.3.2. Preferential oxidation (PROX) of CO unit	68
3.3.2.1. Catalyst preparation	68
3.3.2.2. Catalyst characterization.....	69
3.3.2.3. Catalytic activity measurement.....	71
3.3.3. Integration of SRM unit and PROX unit	77
CHAPTER IV: HYDROGEN PRODUCTION VIA STEAM REFORMING OF METHANOL.....	79
4.1. Catalyst characterization.....	79
4.2. Catalytic activity	86
4.2.1. Supported Au catalysts	86
4.2.2. Atomic ratio of Cu:Ce	90
4.2.3. Liquid feed rate.....	93
4.2.4. Stability test	93
CHAPTER V: Optimization of methanol steam reforming by statistical design of experiments	96
5.1. Catalytic activity (one-variable-at-a-time)	96

	Page
5.2. Factors screening in a full 2^4 factorial design.....	100
5.3. Response surface methodology (RSM)	107
5.4. Validation of the response surface models	112
CHAPTER VI: PREFERENTIAL OXIDATION OF CARBON MONOXIDE OVER	
SUPPORTED Pt AND Au CATALYSTS.....	
6.1. Part I: Platinum and gold supported on ceria catalysts.....	113
6.1.1. Catalyst characterization.....	113
6.1.2. Catalytic activity	119
6.1.2.1. Monometallic and bimetallic catalysts	119
6.1.2.2. Total metal loading	121
6.1.2.3. Pt–Au ratio in the bimetallic catalyst.....	121
6.1.2.4. Catalyst weight to total gas inlet ratio (W/F ratio)	123
6.1.2.5. H ₂ O and CO ₂ in the feedstream	124
6.1.2.6. Double-stage reactor temperature optimization.....	127
6.1.2.7. Oxygen split ratio optimization	127
6.1.2.8. The total amount of catalyst	129
6.1.2.9. The effect of O ₂ /CO in the feed stream	129
6.2. Part II: Platinum and gold supported on mixed oxide catalysts	133
6.2.1. Catalyst characterization.....	133
6.2.2. Catalytic activity	140
6.2.2.1. Single step sol-gel (SSG) vs co-precipitation method (CP)	140
6.2.2.2. Ce:Zn ratio in the catalyst	144
6.2.2.3. Treatment condition.....	145
6.2.2.4. H ₂ O and CO ₂ in the feedstream	148
6.2.2.5. Single- and double-stage reactor	150
6.2.2.6. Deactivation test	150
CHAPTER VII: OPTIMIZATION OF PREFERENTIAL CO OXIDATION BY	
STATISTICAL DESIGNED SET OF EXPERIMENTS	
7.1. Catalytic activity (one-variable-at-a-time).....	153
7.2. Factors screening in a full 2^3 factorial design.....	156
7.3. Response surface methodology (RSM)	164

	Page
7.4. Validation of the response surface models	169
CHAPTER VIII: INTEGRATION OF STEAM REFORMING UNIT AND PREFERENTIAL OXIDATION UNIT	172
8.1. Yield distribution of SRM unit	173
8.1.1. Single-stage reactor of PROX unit	174
8.1.2. Double-stage reactor of PROX unit.....	176
8.2. Stability test	178
8.3. Characterization of fresh and spent catalysts.....	181
CHAPTER IX: CONCLUSIONS	188
9.1. Steam reforming of methanol (SRM)	188
9.2. Preferential oxidation (PROX) of CO	190
9.3. Fuel processing for hydrogen production	192
9.4. Recommendations.....	192
REFERENCES	193
APPENDICES	206
APPENDIX A Catalyst calculation	207
APPENDIX B Catalyst characterization	213
VITA	216

LIST OF TABLES

	Page
Table 2.1. Major hydrogen production processes	12
Table 2.2. Steam Reforming of Hydrocarbons: Process Steps, Reaction, and Catalysts.....	14
Table 2.3. Influence of the conditions of impregnation and drying on the precursor distribution inside a pellet.....	29
Table 2.4. Catalyst characteristics and methods for their investigation in this dissertation	39
Table 3.1. Experimental variables over Au/CuO–CeO ₂ in coded and actual unit for a full 2 ⁴ factorial design with four central points in the standard order from 1 to 20.	65
Table 3.2. Experimental variables over Au/CuO–CeO ₂ for the central composite rotatable design (CCRD)	66
Table 3.3. SRM unit experiments	67
Table 3.4. Statistically designed set of PROX-experiments over PtAu/CeO ₂ –ZnO catalyst for a full 2 ³ factorial design with three central points	74
Table 3.5. Experimental variables for faced-centered central composite design (FCCCD) of response surface methodology with three central points over PtAu/CeO ₂ –ZnO catalyst.....	74
Table 3.6. PROX unit experiments	75
Table 3.7. Integration of SRM and PROX unit for H ₂ production experiments.....	78
Table 4.1. Characteristics of prepared catalyst	82
Table 5.1. Experimental variables in coded and actual unit for a full 2 ⁴ factorial design with four central points in the standard order from 1 to 20.....	101
Table 5.2. Analysis of variance and validity of regression model for a full 2 ⁴ factorial design with four central points with the methanol conversion as the response.	104
Table 5.3. Analysis of variance for a full 2 ³ factorial design with two central points when maintaining the holding liquid feed rate at a low level (1 cm ³ h ⁻¹)....	106

	Page
Table 5.4. Experimental variables for the central composite rotatable design (CCRD)..	
.....	110
Table 5.5. Validation of the CCRD using different level of operating temperatures and S/M ratios at a constant liquid feed rate ($1 \text{ cm}^3 \text{ h}^{-1}$) and W/F ratio (0.17 g s cm^{-3}).....	112
Table 6.1. BET surface area and ceria crystallite size results of the prepared catalyts..	
.....	115
Table 6.2. Physical properties of Pt–Au supported on various metal oxide catalyts	134
Table 6.3. Physical properties of Pt–Au supported on various ratio of mixed oxide and various calcination temperature	137
Table 7.1. Statistically designed set of PROX-experiments over PtAu/CeO ₂ –ZnO catalyst for a full 2 ³ factorial design with three central points	157
Table 7.2. Analysis of variance of for a full 2 ³ factorial design with three central points of PROX-experiments over PtAu/CeO ₂ –ZnO catalyst when considering CO conversion and CO selectivity as a response	162
Table 7.3. Experimental variables for faced-centered central composite design (FCCCD) of response surface methodology with three central points over PtAu/CeO ₂ –ZnO catalyst	165
Table 7.4. Analysis of variance of for response surface methodology of PROX-experiments over PtAu/CeO ₂ –ZnO catalyst when considering CO conversion and CO selectivity as a response	166
Table 7.5. Validation of FCCCD using various levels of operating temperature and CO ₂ content when feeding (a) simulated reformat gas with 40% H ₂ and 5% H ₂ O in He balance and (b) realistic reformat gas	170
Table 8.1. physical property of the prepared catalyts	182

LIST OF FIGURES

	Page
Figure 1.1. Schematic outline of fuel processor via an integration of steam reforming of methanol (SRM) and CO clean-up (PROX) unit	3
Figure 2.1. Proton exchange membrane fuel cell (PEMFC).....	9
Figure 2.2. Current density of fuel cell at different CO concentration	10
Figure 2.3. Process diagram for hydrogen gas production. Reformer conditions: $P_{H_2O}/P_{CH_4} = 2.5-4.0$, $T_{exit} = 900-1100$ °C, $P_{exit} = 20-30$ atm.....	15
Figure 2.4. Fuel cell drive system.....	20
Figure 2.5. Phenomena of transport involved in (a) dry impregnation and (b) wet impregnation	28
Figure 2.6. General scheme of sol-gel processing in the preparation of solid materials	31
Figure 2.7. The sequence of steps involved in sol-gel processing for the synthesis of porous solid catalytic phases	32
Figure 2.8. Precipitation scheme for precipitated catalysts	36
Figure 2.9. Parameters affecting the properties of the precipitate and the main properties influenced	37
Figure 3.1. Experimental set-up for fuel processor.....	59
Figure 4.1. XRD patterns of the catalysts: (a) (50:50)CuO–CeO ₂ , (b) Au/CeO ₂ , (c) Au/(16:84)CuO–CeO ₂ , (d) Au/(37:63)CuO–CeO ₂ , (e) Au/(50:50)CuO–CeO ₂ , (f) Au/(63:37)CuO–CeO ₂ , (g) Au/(84:16)CuO–CeO ₂ , (h) Au/CuO, and (i) Au/(50:50)CuO–CeO ₂ spent catalyst for 2 h.....	81
Figure 4.2. TPR profiles of the catalysts: (a) (50:50)CuO–CeO ₂ , (b) Au/CeO ₂ , (c) Au/(16:84)CuO–CeO ₂ , (d) Au/(37:63)CuO–CeO ₂ , (e) Au/(50:50)CuO–CeO ₂ , (f) Au/(63:37)CuO–CeO ₂ , (g) Au/(84:16)CuO–CeO ₂ , and (h) Au/CuO.....	84
Figure 4.3. SEM images of the prepared: (a) CuO, (b) CeO ₂ , (c) (50:50)CuO–CeO ₂ , and (d) Au/(50:50)CuO–CeO ₂ catalysts	86
Figure 4.4. Temperature dependent catalytic activity of SRM with (o) MegaMax 700, (♦) (50:50)CuO–CeO ₂ , and 5 wt% Au doped- catalysts: (▲) Au/CuO, (■) Au/(50:50)CuO–CeO ₂ , (●) Au/CeO ₂ catalysts.....	88

	Page
Figure 4.5. Mechanism of H ₂ production via SRM over Au/(50:50)CuO–CeO ₂ catalyst	90
Figure 4.6. Temperature dependent catalytic activity of SRM with (o) MegaMax 700 and supported 5 wt% Au catalysts with various Cu:Ce atomic ratios: (▲) 84:16, (■) 63:37, (●) 50:50, (◆) 37:63, (▼) 16:84 catalysts	91
Figure 4.7. Effect of liquid feed rate on the catalytic activity of Au/(50:50)CuO–CeO ₂ catalyst.	94
Figure 4.8. Stability tests of the commercial MegaMax 700 and the 5% Au/(50:50)CuO–CeO ₂ catalysts.....	95
Figure 5.1. Catalytic performance of 5% Au/CuO–CeO ₂ catalyst in term of methanol conversion and CO selectivity at one-variable-at-a-time	99
Figure 5.2. Statistical analysis for a full 2 ⁴ factorial design with 4 central points by: (a) haft normal probability plot of the effects and (b) The Pareto chart.....	102
Figure 5.3. Half normal probability plot of the effects for a full 2 ³ factorial design with 2 central points when holding liquid feed rate at 1 cm ³ h ⁻¹ : (a) methanol conversion as a response and (b) CO selectivity as a response	105
Figure 5.4. Main effect plot of (a) methanol conversion and (b) CO selectivity.....	108
Figure 5.5. Response surface and contour plot of: (a) methanol conversion response, (b) CO selectivity response and (c) region of the optimum (shaded portion)	111
Figure 6.1. XRD patterns of the prepared catalysts: (a) Commercial ceria, (b) Synthesized ceria, (c) 1% (1:1)PtAu/CeO ₂ -ISG, (d) 1% Au/CeO ₂ -SSG, (e) 1% (1:1)PtAu/CeO ₂ -SSG, and (f) 1% Pt/CeO ₂ -SSG.....	114
Figure 6.2. SEM images of (a) Commercial ceria, (b) Synthesized ceria-SSG, (c) 1% Pt/CeO ₂ -SSG, (d) 1% Au/CeO ₂ -SSG, and 1% (1:1)PtAu/CeO ₂ -SSG catalysts.....	116
Figure 6.3. TPR profiles of (a) 1% (1:1)PtAu/CeO ₂ -SSG, (b) 1% Pt/CeO ₂ -SSG, and (c) 1% Au/CeO ₂ -SSG catalysts	117
Figure 6.4. TEM images of (a) 1% (1:1)PtAu/CeO ₂ -SSG, (b) 1% Pt/CeO ₂ -SSG, and (c) 1% Au/CeO ₂ -SSG catalysts.....	118

Figure 6.5. Catalytic activity of (■) 1%Pt/CeO ₂ -SSG, (▲) 1% Au/CeO ₂ -SSG, (●) 1%(1:1) PtAu/CeO ₂ -SSG, and (◆) 1%(1:1)PtAu/CeO ₂ -ISG	120
Figure 6.6. Catalytic activity of % metal loading (Pt–Au) of (1:1)PtAu/CeO ₂ -SSG: (●) 1%, (▲) 2%, and (■) 3%	122
Figure 6.7. Catalytic activity of Pt:Au ratio of 1%PtAu/CeO ₂ -SSG: 0.2, 0.5, 1, 5, and 10 on CO conversion (solid line) and selectivity (dot line).....	123
Figure 6.8. Catalytic activity of W/F ratio of 1%(1:1)PtAu/CeO ₂ : (●) 0.12 g s cm ⁻³ and (▲) 0.36 g s cm ⁻³	124
Figure 6.9. Effect of H ₂ O and CO ₂ content in the feed of 1%(1:1)PtAu/CeO ₂ : (●) 0% H ₂ O + 0% CO ₂ , (■) 10% H ₂ O + 0% CO ₂ , (▲) 0% H ₂ O + 20% CO ₂ , (○) 10% H ₂ O + 20% CO ₂	126
Figure 6.10. Effect of operating temperature between two stages of the double stage reactor in the first stage: (●) 70 °C, (▲) 90 °C, (■) 110 °C, (◆) 130 °C, of 1%(1:1)PtAu/CeO ₂ at catalyst weight and O ₂ split ratio between two stages = 1:1, O ₂ /CO = 1, and W/F ratio = 0.12 g s cm ⁻³	128
Figure 6.11. Effect of oxygen split ratio between two stages: (▲) 4:1, (●) 3:2, (■) 1:1, (◆) 2:3, (▼) 1:4, of 1%(1:1)PtAu/CeO ₂ at 1 st temperature = 90 °C, catalyst weight and O ₂ split ratio between two stages = 1:1, O ₂ /CO = 1, and W/F ratio = 0.12 g s cm ⁻³	130
Figure 6.12. Effect of catalyst weight to total flow rate (W/F) ratio: (■) 0.12 g s cm ⁻³ and (●) 0.36 g s cm ⁻³ , of 1%(1:1)PtAu/CeO ₂ at 1 st temperature = 90 °C, catalyst weight and O ₂ split ratio between two stages = 1:1, and O ₂ /CO = 1	131
Figure 6.13. Effect of O ₂ /CO in the feedstream and W/F ratio: (●) 1:1 and 0.12 g s cm ⁻³ , (▲) 1:1 and 0.36 g s cm ⁻³ , (■) 2:1 and 0.12 g s cm ⁻³ , and (◆) 2:1 and 0.36 g s cm ⁻³ , of 1%(1:1)PtAu/CeO ₂ at 1 st temperature = 90 °C and catalyst weight and O ₂ split ratio between two stages = 1:1.....	132
Figure 6.14. XRD patterns of the prepared catalysts: (a) PtAu/CeO ₂ -SSG, (b) PtAu/CeO ₂ -CP, (c) PtAu/CeO ₂ -ZnO-SSG, (d) PtAu/CeO ₂ -ZnO-CP, (e) PtAu/CeO ₂ -Fe ₂ O ₃ -SSG, and (f) PtAu/CeO ₂ -Fe ₂ O ₃ -CP.....	134

Figure 6.15. SEM images of the prepared catalysts: (a) PtAu/CeO ₂ -ZnO-SSG, (b) PtAu/CeO ₂ -ZnO-CP, (c) PtAu/CeO ₂ -Fe ₂ O ₃ -SSG, and (d) PtAu/CeO ₂ -Fe ₂ O ₃ -CP.....	135
Figure 6.16. XRD patterns of the prepared catalysts: (a) PtAu/ZnO-CP calcined at 500 °C, (b) PtAu/(1:1)CeO ₂ -ZnO-CP calcined at 200 °C, (c) PtAu/(1:1)CeO ₂ -ZnO-CP calcined at 350 °C, (d) PtAu/(1:10)CeO ₂ -ZnO-CP calcined at 500 °C, (e) PtAu/(1:1)CeO ₂ -ZnO-CP calcined at 500 °C, (f) PtAu/(10:1)CeO ₂ -ZnO-CP calcined at 500 °C, and (g) PtAu/CeO ₂ -CP calcined at 500 °C... ..	137
Figure 6.17. SEM images of the PtAu/(1:1)CeO ₂ -ZnO-CP with various calcination temperature: (a) 200 °C, (b) 350 °C, and (c) 500 °C.....	138
Figure 6.18. TPR profiles of the prepared catalysts: (a) PtAu/ZnO-CP, (b) PtAu/(1:10)CeO ₂ -ZnO-CP, (c) PtAu/(1:1)CeO ₂ -ZnO-CP, (d) PtAu/(10:1)CeO ₂ -ZnO-CP, and (e) PtAu/CeO ₂ -CP.....	139
Figure 6.19. FTIR spectra of PtAu/(1:1)CeO ₂ -ZnO with various calcination temperature: (a) non-calcined, (b) 200 °C, (c) 350 °C, and (d) 500 °C.....	139
Figure 6.20. Addition of ZnO or Fe ₂ O ₃ at 1:1 atomic ratio of Ce:Zn or Ce:Fe into 1%(1:1)PtAu/CeO ₂ catalysts by SSG method: (●) PtAu/CeO ₂ , (▲) PtAu/CeO ₂ -ZnO, and (■) PtAu/CeO ₂ -Fe ₂ O ₃	142
Figure 6.21. Addition of ZnO or Fe ₂ O ₃ at 1:1 atomic ratio of Ce:Zn or Ce:Fe into 1%(1:1)PtAu/CeO ₂ catalysts by CP method: (●) PtAu/CeO ₂ , (▲) PtAu/CeO ₂ -ZnO, and (■) PtAu/CeO ₂ -Fe ₂ O ₃	143
Figure 6.22. Catalytic activity of the PtAu/CeO ₂ -ZnO-CP with various Ce:Zn atomic ratio: (▲) 10:1, (■) 1:1, and (●) 1:10.....	144
Figure 6.23. Catalytic activity of the PtAu/(1:1)CeO ₂ -ZnO-CP with various calcination temperature: (●) 200 °C, (■) 350 °C, and (▲) 500 °C... ..	146
Figure 6.24. Catalytic activity of the PtAu/CeO ₂ -ZnO-CP calcined at 500 °C with various gas pretreatment: (●) non, (■) O ₂ , and (▲) H ₂	147
Figure 6.25. Effect of composition in the feed stream on the PtAu/CeO ₂ -ZnO-CP: (●) 0% H ₂ O + 0% CO ₂ , (■) 10% H ₂ O + 0% CO ₂ , (▲) 0% H ₂ O + 20% CO ₂ , and (◆) 10% H ₂ O + 20% CO ₂	149

	Page
Figure 6.26. Effect of stage reactor in absence and presence 10% H ₂ O + 20% CO ₂ in the feedstream on the PtAu/(1:1)CeO ₂ -ZnO-CP.....	151
Figure 6.27. Deactivation test on the PtAu/(1:1)CeO ₂ -ZnO-CP in single- and double-stage reactor under absence and presence 10% H ₂ O + 20% CO ₂ in the feedstream for 3500 min: (Δ,▲) absence 10% H ₂ O + 20% CO ₂ in single-stage, (○,⊖) absence 10% H ₂ O + 20% CO ₂ in double-stage, (▲,▲) presence 10% H ₂ O + 20% CO ₂ in single-stage, and (●,●) presence 10% H ₂ O + 20% CO ₂ in double-stage.....	152
Figure 7.1. Catalytic performance of 1%(1:1)PtAu/(1:1)CeO ₂ -ZnO catalyst in operating temperature range of 50–190 °C when feeding the feedstream with various compositions	156
Figure 7.2. Normal probability plot of the effects for a full 2 ³ factorial design with 3 central points when using: (a) CO conversion as response and (b) CO selectivity as response.....	159
Figure 7.3. The Pareto diagram for a full 2 ³ factorial design with 3 central points when using: (a) CO conversion as response and (b) CO selectivity as response	160
Figure 7.4. Main effect plot with its response: (a) CO conversion and (b) CO selectivity	163
Figure 7.5. Response surface and contour plot of: (a) CO conversion response, (b) CO selectivity response, and (c) region of the optimum (shaded portion) found by overlaying yield between CO conversion response (solid line) and CO selectivity response (dot line)	168
Figure 7.6. Residual plots of the response surface model: (a) CO conversion response and (b) CO selectivity response.....	171
Figure 8.1. Distribution of product yield from SRM unit over Au/CuO-CeO ₂ catalyst at optimum condition for 2 h: (▲) H ₂ , (■) CO ₂ , and (●) CO, at optimal condition for SRM unit; operating temperature = ~306 °C, S/M ratio = 2, liquid feed rate = 1 cm ³ h ⁻¹ , and W/F ratio = 0.17 g s cm ⁻³	173
Figure 8.2. Catalytic activities of PROX unit in single-stage reactor over PtAu/CeO ₂ -ZnO at W/F ratio of: (●) 0.08 g s cm ⁻³ and (▲) 0.13 g s cm ⁻³	175

	Page
Figure 8.3. Catalytic activities of PROX unit in double-stage reactor over PtAu/CeO ₂ –ZnO at W/F ratio of: (●) 0.13 g s cm ⁻³ and (▲) 0.17 g s cm ⁻³ . Operating temperature and catalyst weight ratio, O ₂ split ratio, and O ₂ /CO ratio = 1:1	177
Figure 8.4. Deactivation test of SRM unit on Au/CuO–CeO ₂ at optimum condition: Operating temperature = ~306 °C, S/M ratio = 2, Liquid feed rate = 1 cm ³ h ⁻¹ , and W/F ratio = 0.17 g s cm ⁻³	179
Figure 8.5. Deactivation test of PROX unit for overall process for 600 min at optimum condition	180
Figure 8.6. TEM images of (a) SRM-Fresh, (b) SRM-Spent, (c) PROX-Fresh, and (d) PROX-Spent catalysts	183
Figure 8.7. XRD patterns of (a) PROX-Fresh, (b) PROX-Spent, (c) SRM-Fresh, and (d) SRM-Spent catalysts	184
Figure 8.8. FTIR spectra of (a) PROX-Fresh, (b) PROX-Spent, (c) SRM-Fresh, and (d) SRM-Spent catalysts.....	186
Figure 8.9. Mechanism of carbonate and hydroxyl group formation on (a) SRM and (b) PROX catalysts surface.....	187
Figure B–1. XRD pattern of 1%(1:1)PtAu/CeO ₂ catalyst.	214
Figure B–2. TEM images of (a) 5% Au/CuO and (b) 5% Au/CeO ₂ catalysts	215

CHAPTER I

INTRODUCTION

1.1 Rationale

The growth of energy consumption, the requirement of the sustainable energy and the rise of a serious air pollution problem are the major force to drive the globe to seek an attractively alternative fuel. Hydrogen (H₂) is one of the most promising clean energy carriers in the near future, especially for proton exchange membrane fuel cells (PEMFCs) as a clean and efficient source of electrical power for portable and micro-devices [1]. Hydrogen can be applied to the modified conventional combustion engine as well. However, the use of hydrogen as energy carrier is suppressed in wide applications due to a technical limitation in storage of hydrogen at a required quantity and density. Therefore, to this end, the hydrogen will likely be generated on site and on demand by reforming available fuels such as methane, natural gas (NG), gasoline, propane (LPG), liquid hydrocarbons or alcohols. Methane and alcohols are an attractively alternative fuel due to their lower cost, compared to the other energy fuels. Comparison steam reforming of methane and alcohols, it is found that alcohol steam reforming, especially methanol (SRM) can be catalytically converted into a H₂-rich stream in a low–moderate range of operating temperature (200–400 °C), whilst the steam reforming of methane is suggested to operate in a range of 600 °C to 900

°C. In addition, methanol is readily available and, since it can be produced from renewable sources, is considered as a potentially sustainable energy carrier [2]. The liquid fuels like methanol give energy higher than gas in unit volume since storage and transportation are very easily and safety. Moreover, the production of H₂ via steam reforming of methanol does not require desulfurization and pre-reforming processes. Methanol has high hydrogen to carbon ratio with no C–C bonds, minimizing the risk for coke formation [3]. Therefore, H₂ production from methanol has received much more attention. Further improvement in the activities of potential catalysts for H₂ production with minimal of CO selectivity via SRM is still needed. Nevertheless, the reformat gas composition always contains ~3–10 % carbon monoxide (CO), which is one of the primary air pollutant and is a poisonous gas for platinum electro-catalyst at the anodic site in a PEMFC. The outlet stream with contaminated CO is further routed to a water–gas shift unit in order to convert CO to yield H₂ and carbon dioxide (CO₂). However, the CO content is still needed to be further reduced to less than 50 ppm in a CO clean-up system. Among the CO removal methods, the preferential oxidation (PROX) of CO seems to be the most promising approach.

This research work studied a fuel processor for producing H₂ from steam reforming of methanol. It supposes to achieve high purity H₂ which contains CO level less than 50 ppm. CO in the reformat H₂-rich stream was then reduced via preferential oxidation of CO process in a CO clean-up unit. The principal concept of a fuel processor for combination of H₂ production from SRM and CO clean-up via PROX process is shown in Figure 1.1

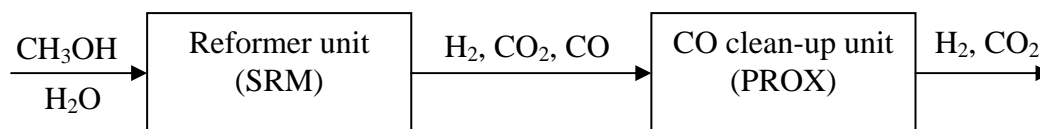


Figure 1.1 Schematic outline of fuel processor via an integration of steam reforming of methanol (SRM) and CO clean-up (PROX) unit.

1.2 Purpose of this study

The purpose of this study is to produce high purity H₂-rich stream from methanol. The methanol is catalytically converted to H₂-rich stream via steam reforming. The CO in the reformat gas is eliminated to less than 50 ppm via PROX process.

Objectives

1. To construct a reactor of a fuel processor to produce pure H₂ which used as a gaseous fuel for PEM fuel cell.
2. To investigate catalytic performance of the prepared catalysts for SRM and PROX.

Hypothesis

To produce pure hydrogen with CO level less than 50 ppm from methanol via an integration of steam reforming of methanol and preferential CO oxidization.

1.3 Scope of the dissertation

1. Construction of system for fuel processor to produce pure H₂ for PEM fuel cell

The experiments were performed using a tubular flow reactor. The system consists of stainless steel tubing (1/4 and 1/8 inch O.D.), fitting and controller equipments, furnaces and gas chromatograph.

2. Investigation of the prepared catalysts for SRM unit

To find the effective catalyst for SRM unit at constant condition of steam to methanol ratio = 1.5, liquid feed rate = 3 cm³ h⁻¹, and catalyst weight to He flow rate ratio = 0.17 g s cm⁻³ in temperature range of 200 °C to 300 °C. The prepared catalysts consist of Au, CuO, and CeO₂.

3. The optimization condition of the effective catalyst

The optimal condition for SRM was studied by statistically designed set of experiments. Four independent factors selected were the operating temperature, steam to methanol (S/M) ratio, the liquid feed rate, and weight of catalyst to He flow rate (W/F) ratio. The methanol conversion and CO selectivity were carried out as a response.

4. Investigation of the prepared catalysts for PROX-CO unit

To find the effective catalyst for PROX-CO unit under simulated gas which contain 1% CO, 1% O₂, 40% H₂, 0–10% H₂O, and 0–20% CO₂ in He balance temperature range of 50 °C to 190 °C. The main parameters were types of catalyst, composition and preparation methods of catalysts, amount of O₂ in the simulated gas, ratio of O₂ to CO, and number of reactor.

5. Development of equation model for PROX-CO performance in single-stage reactor by using statistical analysis of experimental design.

Experimental matrix of a full 2^k factorial design was performed in a randomization to eliminate an error of the data. Three independent factors selected were the operating temperature, H₂O content, and CO₂ content in the reformat gas. The CO conversion and CO selectivity were used as a response.

6. Integration of the SRM and PROX-CO

To combine SRM unit and PROX unit to produce hydrogen for PEM fuel cell application by using the effective catalysts.

7. Catalyst characterization

The prepared catalysts are characterized by analyzer such as

- The Brunauer–Emmett–Teller (BET) method is carried out to determine the surface area and pore size of the prepared catalyst by N₂ adsorption/desorption.
- X-ray diffractometer (XRD) is used for the examination of the crystalline structure.
- X-ray fluorescence (XRF) is used to determine the composition in catalyst.
- Temperature programmed reduction (TPR) is introduced to investigate the reduction temperatures of the catalyst.
- H₂ chemisorption is technique to obtain metallic particle size and metallic surface area in catalyst.
- Scanning electron microscopy (SEM) is employed to determine the morphology of the catalyst.

- Transmission electron microscope (TEM) and scanning electron microscope (SEM) images are employed to obtain information about the morphology and crystal structures of the catalysts.
- Fourier transform infrared (FTIR) spectra is used to record wavenumber range of functional group.

Anticipated benefits

1. To set-up a reactor of a fuel processor system for producing H₂ which used as a gaseous fuel for PEM fuel cell.
2. To obtain an effective catalyst for steam reforming of methanol and preferential oxidation of CO unit.

1.4 Format of the dissertation

The dissertation was formatted in a chapter form. Background, purpose and scope of this research work were presented in Chapter 1. Theoretical information and literature review were mentioned in Chapter 2. Material used in this work and methodology, accompany with catalyst preparation, catalyst characterization, activity measurement, were described in Chapter 3. In this research, there were two main processes involved in this research: hydrogen production via steam reforming of methanol in SRM unit and preferential oxidation of CO in PROX unit. Therefore, hydrogen production via steam reforming of methanol was revealed in Chapter 4, whilst the statistically designed set of experiments for steam reforming of methanol was evaluated in Chapter 5. CO clean-up via preferential oxidation in PROX-CO unit

was determined in Chapter 6 while the statistical analysis for preferential oxidation of CO was evaluated in Chapter 7. The integration of SRM unit and PROX unit was studied in Chapter 8. Finally conclusion and recommendations were introduced in Chapter 9.

CHAPTER II

THEORY AND LITERATURE REVIEWS

In this chapter, a brief detail of proton exchange membrane fuel cell (PEMFC) and the importance of H₂ production on-board PEMFC was mentioned in section 2.1. The conventional process of H₂ production and the limitations of its operation for PEMFC were explained in section 2.2. Fuel processing of H₂ production from steam reforming of methanol (SRM) and CO clean-up unit by preferential oxidation (PROX) of CO were introduced in section 2.3 whilst development of catalysts for both units was remarked in section 2.4. Catalyst preparation method and characterization of catalysts used in this dissertation were displayed in section 2.5 and section 2.6, respectively. In the last section, literature reviews were performed.

2.1 Proton Exchange membrane (PEM) fuel cell

A fuel cell is a device for electrochemical energy conversion, which continuously converts the chemical energy of a fuel directly into electrical energy. Proton exchange membrane (PEM) fuel cell layer (see Figure 2.1) consists of a sandwich of two Pt electrode layers separated by solid polymer electrolyte. It operates at about 80 °C and atmospheric pressure. It is the most promising fuel cell system for residential and transportation applications due to its high energy density.

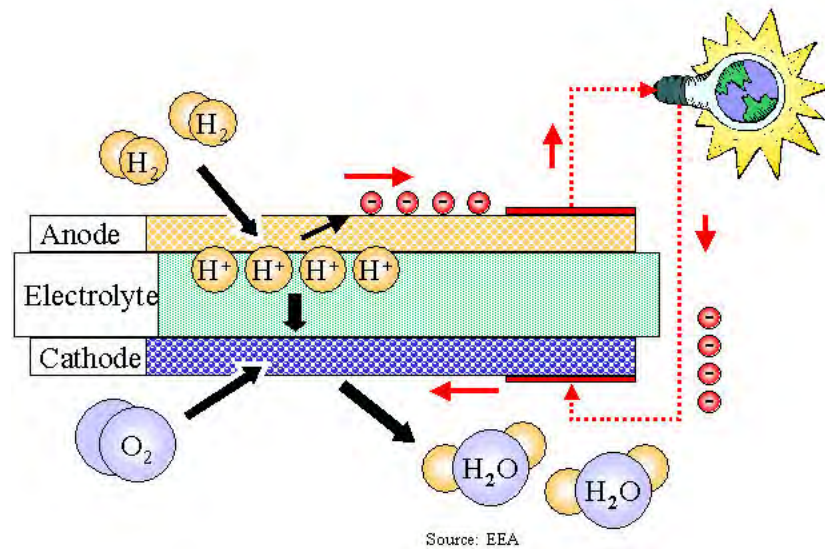
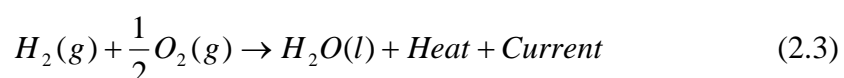
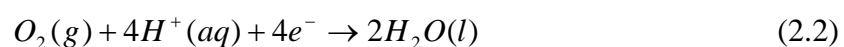


Figure 2.1 Proton exchange membrane fuel cell (PEMFC) operation

[ref: <http://www.eea.europa.eu>]

In an operation, the fuel will be charged to the anode whilst the oxidant will be routed to the cathode. At the anode, the fuel will diffuse into the porous electrode to the reaction zone, where the Pt-catalyst is located, and dissociated into electrons and ions (Eq. (2.1)). Then, the electrons are forced to travel and do work through an external circuit; while the ions will go pass through the electrolyte to the cathode where the oxidant reduction occurs (Eq. (2.2)). The oxidant at the cathode will be reduced by the electrons from the external circuit to combine with the ions from the anode. Overall reaction for The PEM fuel cell is shown in Eq. (2.3). There are some water, heat and current from the reactions. [1]



For PEM fuel cell operation, one of the major content is catalyst which helps H_2 dissociation to proton and electron in anode. The most catalysts widely used are noble metals, especially Pt which is highly active and stable. But it can be deteriorated by CO poisoning that contaminate in H_2 -rich stream. The CO competes the H_2 to adsorb on the active site of catalyst; so, molecules of H_2 cannot dissociate and affect to the performance of fuel cell (shown in Figure 2.2).

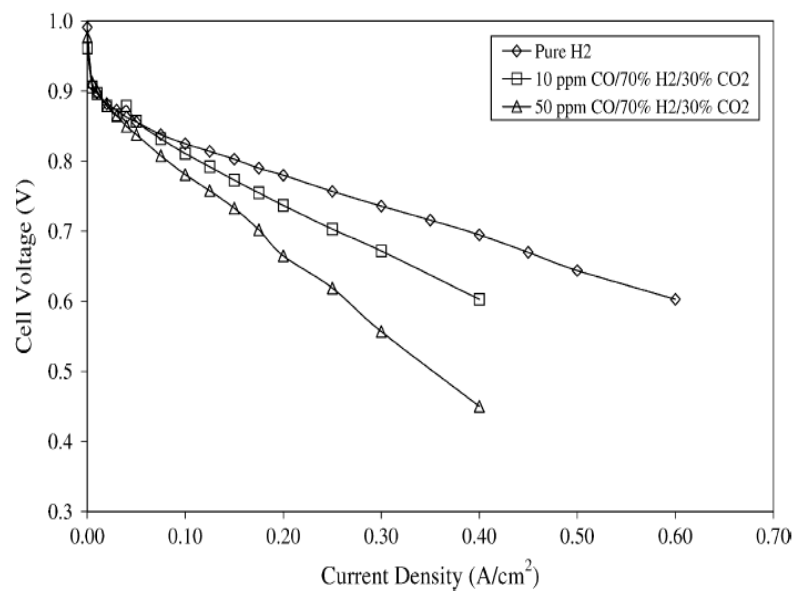


Figure 2.2 Current density of fuel cell at different CO concentration [4]

To solve this problem, one is using CO-tolerant catalysts and another is using pure H_2 as fuel for fuel cell. Nevertheless, pure H_2 is expensive and needs high pressure to form in liquid that is harmful for transportation. Thus, H_2 that is produced on-board from hydrocarbons or liquid fuels are favorable.

2.2 Hydrogen production process [5]

Hydrogen can be produced from a variety of feed stocks. These include fossil resources, such as natural gas and coal, as well as renewable resources, such as biomass and water with input from renewable energy sources. A variety of process technologies can be used, including chemical, biological, electrolytic, photolytic and thermo-chemical. Development in each technology is in a different stage, and each offers unique opportunities, benefits and challenges. Local availability of feedstock, the maturity of the technology, market applications and demand, policy issues, and costs will all influence the choice and timing of the various options for hydrogen production. Table 2.1 presents the major hydrogen production processes.

Currently the dominant technology for direct production is steam reforming from hydrocarbons. Steam reforming of natural gas (Steam methane reforming, SMR) offers an efficient, economical, and widely used process for hydrogen production, and provides near- and mid-term energy security and environmental benefits. The efficiency of the steam reforming process is about 65% to 75%, among the highest of current commercially available production methods. Natural gas is a convenient, easy to handle, hydrogen feedstock with a high hydrogen-to-carbon ratio. It is also widely available from sources in the local, such as U.S. and Canada. The cost of hydrogen produced by SMR is acutely dependant on natural gas prices and is currently the least expensive among all bulk hydrogen production technologies. A well-developed natural gas infrastructure already exists in the U.S., a key factor that makes hydrogen production from natural gas attractive.

Table 2.1 Major hydrogen production processes

Primary Method	Process	Feedstock	Energy	Emissions
Thermal	Steam Reformation	Natural gas	High temperature steam	Some emissions, Carbon sequestration can mitigate their effect
	Thermochemical Water Splitting	Water	High temperature heat from advanced gas-cooled nuclear reactors	No emissions
	Gasification	Coal, Biomass	Steam and oxygen at high temperature and pressure	Some emissions, Carbon sequestration can mitigate their effect
	Pyrolysis	Biomass	Moderately high temperature steam	Some emissions, Carbon sequestration can mitigate their effect
Electrochemical	Electrolysis	Water	Electricity from wind, solar, hydro, and nuclear	No emissions
	Electrolysis	Water	Electricity from coal or natural gas	Some emissions from electricity production
	Photoelectrochemical	Water	Direct sunlight	No emissions
Biological	Photobiological	Water and algae strains	Direct sunlight	No emissions
	Anaerobic Digestion	Biomass	High temperature heat	Some emissions
	Fermentative Microorganisms	Biomass	High temperature heat	Some emissions

(ref: www.hydrogenassociation.org)

2.2.1 Conventional process

Full-scale production of hydrogen by steam reforming (SR) of hydrocarbons involves six different catalytic process steps including desulfurization (Eq. (2.4)), primary and secondary steam reforming (Eqs. (2.5) and (2.6)), high and low-temperature water–gas shift (WGS) reactions (Eqs. (2.7) and (2.8)), and methanation (Eq. (2.9)). Production of syngas involves only steps 1–3. For SR of hydrocarbons heavier than methane, a pre-reformer may be used upstream of the primary reformer to prevent steam cracking in the primary reformer (2-step reforming). Pre-reforming also provides the flexibility to handle a wide range of feedstocks at low sulfur to carbon (s/c) ratios. The corresponding reactions and typical catalysts for all six steps are listed in Table 2.2. The process flow diagram in Figure 2.3 shows inlet and outlet conditions for most of these steps, which together lead to production of 99% H₂. Each of these six process steps is discussed separately below.

The first step for desulfurizing natural gas is CoMo/Al₂O₃ or NiMo/Al₂O₃ hydrodesulphurization catalyzed (Eq. (2.4) of sulfur-containing hydrocarbon (R–S) at about 200 °C and pressures up to about 300 psig (20 bar). Moreover, the H₂S produced is adsorbed on particulate ZnO at about 400 °C (Eq. (2.10)). With this approach, sulfur levels can be decreased to 0.02 ppm or 20 ppb (volume).



Sulfur removal is necessary due to the sensitivity of Ni-based catalysts for primary steam reforming of hydrocarbon (Eq. (2.5)). The CH₄ from primary is continuously reacted with steam in secondary steam reforming (Eq. (2.6)). The steam reforming reaction is highly endothermic and requires high-energy input. The exiting gas from

Table 2.2 Steam Reforming of Hydrocarbons: Process Steps, Reaction, and Catalysts

[5]

Process Step	Reaction(s)	Catalysts
Desulfurization	$R-S + H_2 \rightarrow H_2S + R-H$ Eq. (2.4)	CoMo/Al ₂ O ₃ or NiMo/Al ₂ O ₃
Pre-reforming and Primary steam reforming	$HC + H_2O \rightarrow H_2 + CO + CO_2 + CH_4$ Eq. (2.5)	Ni/MgO (naphtha) Ni/MaAl ₂ O ₄ or Ni/CaAl ₂ O ₄ (CH ₄)
Secondary steam reforming	$2CH_4 + 3H_2O \rightarrow 7H_2 + CO + CO_2$ Eq. (2.6)	Ni/CaAl ₂ O ₄ ; Ni/ α -Al ₂ O ₃
Water gas shift (HT)	$CO + H_2O \rightarrow H_2 + CO_2$ Eq. (2.7)	Fe ₃ O ₄ /Cr ₂ O ₃
Water gas shift (LT)	$CO + H_2O \rightarrow H_2 + CO_2$ Eq. (2.8)	Cu/ZnO/Al ₂ O ₃
Methanation	$CO + 3H_2 \rightarrow CH_4 + H_2O$ Eq. (2.9)	Ni/Al ₂ O ₃

the steam reformer, containing about 10–20% CO, is fed to a high-temperature (350–400 °C) water–gas shift (WGS) reactor containing an Fe–Cr catalyst. This further increases the H₂ content and decreases CO concentration to about 2% as governed by the thermodynamics of this exothermic reaction. The product gas is then fed to a low temperature (200 °C) WGS catalyst, typically Cu/ZnO/Al₂O₃ where the CO is further decreased to less than ~1%, generating additional H₂. The remaining CO, which would poison downstream ammonia or methanol synthesis catalysts, is commonly removed by pressure swing adsorption in beds containing activated carbon, zeolites, or alumino–silicates, although in some cases methanation over a Ni- or Ru-based catalyst at about 250 °C is used.

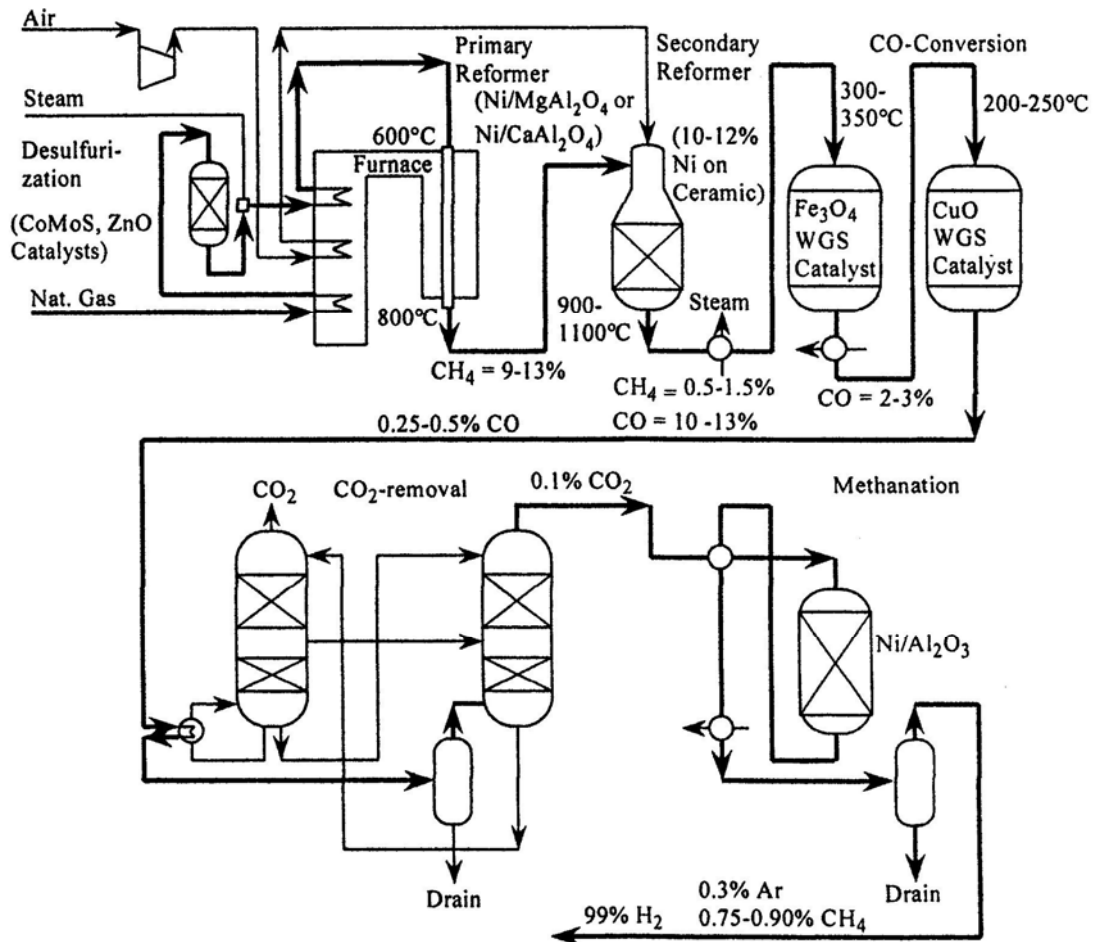


Figure 2.3 Process diagram for hydrogen gas production. Reformer conditions: $P_{\text{H}_2\text{O}}/P_{\text{CH}_4} = 2.5-4.0$, $T_{\text{exit}} = 900-1100\text{ }^\circ\text{C}$, $P_{\text{exit}} = 20-30\text{ atm}$. [5]

Limitations of Conventional Hydrogen Production Technologies when Applied to Fuel Cells

Large-scale H₂ plants typically operate at steady-state over extended periods of time with few shutdowns. They are operated and maintained by experienced operators and engineers. Relatively small-scale, fuel cell units are characterized by transient operations with frequent startups and shutdowns; size, weight, pressure drop,

mechanical integrity, and consumer safety are much more critical compared to large H₂ plants; thus new technologies must be developed to meet these demands.

Commercial steam reforming plants use Ni-based particulate catalysts packed in a large number of parallel metal tubes arranged for maximum heat transfer within a fuel burner that provides the endothermic heat of reaction. They operate more or less at steady state so that turndown ration (range over which capacity or flow can be decreased) and startup and shutdown procedures are not frequent concerns to the plant engineers. Even with an optimum arrangement, the highly endothermic reaction is still heat-transfer limited. The relative low reaction rate requires long tubular catalyst beds that have a slow response to transients. Small fuel cell reformers must be able to respond rapidly to changes in power demand (turndown ratio). Frequent startups and shutdowns will be necessary depending on the duty cycle. A vehicle will start and stop often, as will a residential or portable power system. While the mechanical integrity or attrition resistance of particulate beds may not be a problem for stationary applications, they are certainly important in the design and operation of vehicular applications. Pressure drop due to flow through a particulate bed can be limiting for natural gas residential applications where the line pressure into the home or building is only slightly above atmospheric.

A Ni-based steam reforming particulate catalyst must be well-reduced to be active. If the reduced catalyst is exposed to air either intentionally or accidentally it will spontaneously ignite, liberating the heat of reaction of well-dispersed Ni metal with oxygen. This pyrophoric behavior is an unacceptable safety issue for a consumer-related application. Furthermore, Ni is a toxic heavy metal which forms a highly toxic nickel tetracarbonyl when exposed to a moderately high CO partial

pressure. If exposed to sulfur compounds present in natural gas or any other fuel, nickel catalysts deactivate rapidly and irreversibly as a consequence of sulfur poisoning. Hydrodesulphurization (HDS), used for sulfur removal in traditional plants, requires H₂ recycle pressures in excess of 20 bar, pressures not available in pipeline natural gas brought into the home. A new HDS process reportedly functions at a pressure below 20 bar, but still requires recycled H₂ at temperatures in excess of 200 °C [6].

Activation of Cu- and Fe/Cr-based WGS catalysts requires slow reduction according to a carefully prescribed procedure to avoid large exotherms that would lead to sintering. A detailed, laborious procedure for reducing the catalyst with hydrogen is not likely to be feasible in the field. If reduction is carried out in the plant, the catalyst in its air-sensitive state, must be packaged and shipped with great care as with a flammable material, which adds to transportation costs. Furthermore Cr, like Ni, is also considered a toxic metal and thus should not be incorporated into a processor/fuel-cell system.

Pressure swing adsorption (PSA) is commonly used for the final H₂ purification step in traditional plants. CO, CO₂, H₂O, and any hydrocarbons that have been carried through the process or produced in any of the upstream unit operations are adsorbed in activated carbon, zeolite, or alumino–silicate beds. This process is not applicable for small-scale fuel cells since high pressure is not readily available, especially for those systems that operate with residential pipeline natural gas. PSA will likely be used for on-site hydrogen generation, for example in a H₂ refueling station. Methanation to remove CO is probably not feasible for small fuel processors

since the large amount of CO₂ present consumes a substantial amount of H₂ (four moles H₂ per mole CO₂) and since a runaway reaction exotherm is possible.

Given the serious limitations for applying conventional catalyst and process technologies to fuel cells, it is clear that new catalyst and sulfur removal technologies are necessary, especially for cost-effective fuel processing in small fuel cell systems.

2.2.2 Alternative approaches to generating hydrogen for the fuel cell

Substantial catalyst and reactor technologies have been developed for H₂ generation via steam reforming of methanol principally for transportation applications. Methanol produced by conventional synthesis is a convenient. It has a high hydrogen to carbon ratio with no C–C bonds, minimizing the risk for coke formation and sulfur-free fuel that can be reformed at modest temperature of 200 °C to 400 °C, ideally producing 3 moles of H₂ and 1 mole of CO₂ per mole of methanol. Invariably about 1% CO is produced as an undesirable byproduct that must be removed by preferential oxidation (PROX) (see section 2.3). Therefore no water–gas shift reactor is necessary. The development of a fuel cell membrane that operates above 160 °C and is tolerant to CO would eliminate the need for the PROX reactor. The low-temperature reforming with a traditional Cu/Zn/Al catalyst makes this fuel attractive since rapid startup is possible. It continues to be considered, but emphasis for use in vehicles has stopped due to infrastructure, water solubility, and toxicity problems.

The alternative to the use of either liquid hydrogen or high pressure on board is to carry liquid fuels that have high energy densities and convert them to a hydrogen-rich gas (reformat) via an on-board fuel cell processor. One of the most favorable

liquid fuels used to produce hydrogen on board is methanol. This due to the following superior advantages of using methanol in comparison to other liquid fuels in particular with respect to the on-board reforming process:

- low reaction temperature and atmospheric pressure
- simple molecular with high molar ratio of hydrogen to carbon
- low CO concentration (CO is poison to the fuel cell performance)
- no emission of pollutants, such as NO_x , SO_x
- no formation of soot particles
- minor effort of changing the fuelling station (from gasoline or diesel)

2.3 Fuel processing for PEM fuel cell

Hydrogen production based on SRM for fuel cell drive system consists of the following main devices: a methanol steam reformer, a catalytic burner which provides heat for the reformer and converts all burnable gases in the flue gas into water and carbon dioxide, a gas cleaning unit which reduces CO concentration of the hydrogen-rich product and feeds to the proton exchange membrane fuel cell (PEMFC). A gas storage system is also integrated in the fuel cell system in order to feed the fuel cell during the start-up and speed-up phases. A scheme of the fuel cell drive system based on SRM is shown in Figure 2.4.

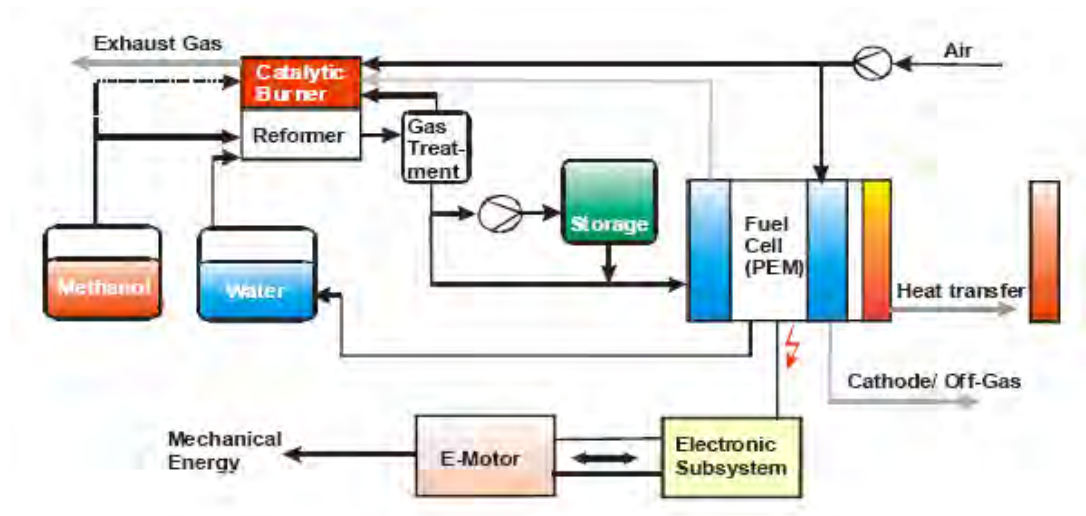
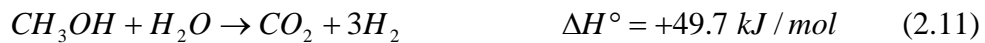


Figure 2.4 Fuel cell drive system. [7]

2.3.1 Steam reforming of methanol (SRM) [8]

SRM is considered to be the most favorable process of hydrogen production in comparison to the decomposition and partial oxidation of methanol. This is because of the ability to produce gas with high hydrogen concentration (75%) and high selectivity for carbon dioxide, reaction as shown below (Eq. (2.11)).

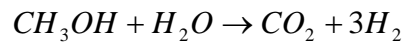


The main products of SRM are hydrogen, carbon dioxide and a low content of carbon monoxide is produced in this process. There have been some controversies in the literature concerning the mechanisms for production of hydrogen and carbon dioxide by SRM. The study of the mechanism of the formation of CO as a by-product has received a high attention. There are two major path ways to present in this research.

I. No formation of CO in the reaction route [9]



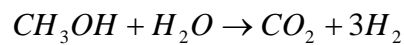
Combination;



II. The decomposition of methanol and water–gas shift reaction [10,11]



Combination;



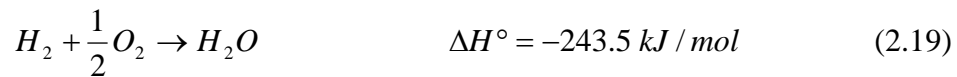
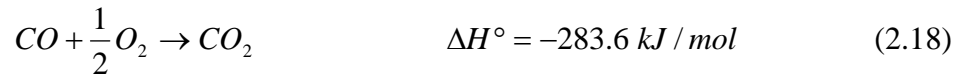
Nevertheless, the WGS reaction is reversible; therefore, CO formation can be come from decomposition of methanol or reverse WGS (Eq. (2.17)).



2.3.2 Preferential oxidation (PROX) of CO [5]

Trace amounts of CO in the H₂-PEMFC deteriorate the efficiency of the fuel cell Pt catalyst via CO poisoning because of competition with H₂ on active species. The CO elimination must be demolish CO to less than 50 ppm. Several approaches are currently applied: CO preferential oxidation, adsorption, membrane separation or catalytic methanation. Among these, preferential oxidation (PROX) is the lowest cost method to reduce CO to the desired level without excessive H₂ consumption. The

main reactions are shown in Eq. (2.18). The side reactions are H₂ oxidation (Eq. (2.19)) and methanation (Eq. (2.20)).



PROX catalysts need to be active and selective without oxidizing a large amount of H₂ at the selected process temperature, usually between the outlet temperature of the WGS reactor and the inlet temperature of fuel cell (~80 °C). The reformat containing mostly H₂, its oxidation leads to a decrease in the overall fuel efficiency. Furthermore, the outlet stream from WGS also has CO, CO₂, and H₂O. As the secondary reactions, reversed WGS (Eq. (2.17)) and methanation (Eq. (2.20)) of CO can occur, depending on temperature, ratio O₂/CO and contact time. For an inlet CO of ~1%, the overall CO conversion has to be higher than 99.995% for a reduction of the CO level to less than 50 ppm. The main effects are type and components in reformat gas, type and preparation method of catalyst and the number of stages.

2.4 Catalysts

2.4.1 Catalyst for SRM unit

Copper-based catalysts have been widely used for many reactions especially, SRM [10–21,22–28]. Cu or CuO/ZnO/Al₂O₃ have been used in commercial catalysts

for SRM because of their high catalytic activity [10,11,13,14,17] that also depended on preparation method [22]. Some [13] suggested that the addition of Pt and Rh to the original CuO/ZnO/Al₂O₃ catalyst has a stabilizing effect. ZrO₂ that added to Cu/Zn-based [23] catalysts plays an important role in enhancing copper dispersion and in forming small sized copper particles on the catalyst surface while the Cu/ZrO₂ catalysts prepared by the microemulsion technique reduced CO formation at high methanol conversions when compared to the commercial Cu/ZnO catalyst [12]. Yang et al. [15] presented that Cu/ZnO–CNTs nano-catalyst by using a chemical reduction and wet impregnation method showed a high activity and selectivity by adding ZnO. Chen et al. [24] reported the Pd–ZnO was coated on CuZnAl from the sol-gel technique by solution-coating have high activity and relatively high stability. Jones et al. [21] pronounced that ZrO₂-promoted catalysts achieve higher methanol conversions and lower CO selectivities. The presence of Cu₂O in CuO/ZrO₂ in Oguchi et al. [25] seems to lead to the durability of the former catalysts. The activity and reduced CO improvement by CuO/ZnO/CeO₂/ZrO₂/Al₂O₃ catalyst because ZrO₂ into CuO/ZnO/Al₂O₃ enhanced the reducibility and the stability while the addition of CeO₂ or Al₂O₃ effected to the weakened interaction between CuO and ZnO in the catalysts [26]. It has been proposed that the catalytic performance of CuO–CeO₂ catalysts in the SRM process is higher than CuO/ZnO/Al₂O₃-based commercial catalysts, due to the fact that CuO particles are integrated into the lattice of CeO₂ and improve the ability to transfer bulk oxygen in CeO₂ to its surface [16,20,21,27]. The improvement in activity and stability of the promoted CeO₂ catalysts was attributed to higher copper dispersion and smaller copper crystallites, and the synergetic effect of ceria [28]. Moreover, the doping of CuO–CeO₂ catalysts with small amounts of Sm

and Zn oxides improves their catalytic performance in SRM [16]. Manzoli et al. [29] found that the different behavior of the two co-precipitated ZnO based catalysts was mainly related to the formation of a solid solution precursor phase. This result was ability of the support towards the oxidative dehydrogenation of methanol to formaldehyde. Au/CuO/ZnO catalysts express a high H₂ production efficiency via POM due to a strong interaction between the Au and CuO species [30]. Bimetallic Au–Cu/TiO₂ catalysts were found to be more active in the POM reaction than the use of the monometallic Au/TiO₂ and Cu/TiO₂ catalysts, because of metal–metal interaction [31].

2.4.2 Catalyst for PROX unit

Supported noble metal catalysts (Pt, Rh, Ru, Pd, Ir) have been effective for the PROX of CO. Especially, Pt is very active and stable for CO removal and minimal loss of H₂ at high temperatures (in the temperature range of 175–200 °C) [33–35]. Some researches [36,37] demonstrated the activity of Au for this reaction. Moreover, at low temperatures, highly dispersed Au on an appropriate oxide support showed high activity and selectivity [38,39]. An Au catalyst is inert for catalytic applications, however, it is more active for selective CO oxidation [40–42], and more for CO oxidation than for H₂ oxidation [43]. In addition, the catalytic activity of Au is enhanced by moisture and is almost insensitive to CO [44,45]. However, it has been reported that the catalytic performance strongly depends on the catalyst preparation. For the supports, mostly metal oxides, ceria is an interesting one because of its unique redox properties and high oxygen storage capacity. The oxygen mobility in the

crystallographic structure, therefore, is greatly facilitated. Moreover, it has been reported that it can promote water–gas shift activity, maintain the dispersion of the catalytic metals and stabilize the surface area of the support [46–48]. For the supported catalysts, mostly metal oxides, ceria is interesting because of its unique redox properties and high oxygen storage capacity. Oxygen mobility in the crystallographic structure is greatly facilitated. It has been reported that it can promote water–gas shift activity, can help to maintain the dispersion of the catalytic metals, and can stabilize the surface area of the support [38,49,50]. Additionally, zinc oxide, which is an important semiconductor material, has been widely investigated for its electrical, optoelectronic, photochemical properties [51–53], and catalytic performance in CO oxidation [54–59]. To enhance the CO oxidation while suppressing the undesired H₂ oxidation, alkali compounds should be added to a noble metal supported on zinc oxide. Another recently reported interesting support is ceria-based composite oxides. They have been extensively investigated for catalytic applications such as in a three-way catalyst, in oxidation, or combustion, and acid–base catalyzed reactions [60–64]. The effectiveness of the oxygen mobility can be manipulated by incorporating metal ions into the ceria lattice and can be promoted by the metals dispersed on the ceria.

2.5 Catalyst preparation method

2.5.1 Impregnation method [65]

Impregnations can be classified in two categories, according to the volume of solution added. The simplest way to execute impregnation is by contacting a previously dried support, of pore volume, with a volume of solution containing the precursor of the active phase. This solution is drawn into the pores by capillary suction (hence “capillary impregnation”).

In the case of proper wetting no excess of solution remains outside the pore space and the procedure is also called “dry” or “incipient wetness” impregnation. The penetration of the liquid phase requires the elimination of air from the pores. If the pore radius is very small, capillary pressure is much larger than the pressure of the entrapped air; compressed air dissolves or escapes from the solid through larger pores. Heat is generally released when a solid/gas interface is replaced by a solid/liquid interface. This might influence the quality of impregnation if the precursor solubility decreases when the temperature increases or if detrimental reactions involving the support take place due to a temperature rise.

In models used for dry impregnation (Figure 2.5a), another equation based on Poiseuille steady states or on the related Darcy’s law is added to represent the pressure-driven capillary flow of the solution inside the empty pores. For low concentrations, strong adsorption of the solute or short times, egg-shell distributions are expected. If the adsorption of the solute is weak and time is long enough, distribution should tend to uniformity. For powders, equilibrium is reached within a few minutes, but it can take a few hours to reach a uniform distribution of the precursor inside a pellet. A blockage of the pores by “bulky species” has been invoked in some cases, when egg-shell distributions persist even after long durations. It must be noted that in physical models, the contact time between support and solvent

is treated as a variable influencing only the transport of the precursor through the pellet. An important parameter from the introduction of Darcy's law is the solution viscosity μ . In the case of aqueous solutions and in the common range of concentrations used for impregnation, viscosity increases almost proportionally with concentration. It also increases with the presence of organic ligands attached to the metal ions. Viscosity and concentration behave contrariwise as far as the precursor diffusion is concerned: a high concentration tends to favor the diffusion of the solute toward the center of the pellet, while a high viscosity tends to curb it.

Impregnation can also be carried out in diffusional conditions, that is, by immersing a water-filled support in the precursor solution ("wet" impregnation). Before water filling, air can be replaced by a water-soluble gas like ammonia to avoid gas bubbles in the pore. Wet impregnation should be avoided when the interaction between precursor and support is too weak to guarantee the deposition of the former. For powders, it can be convenient to suspend the support in an excess of solution and evaporate the solvent under regular stirring. Such a method can be used for the introduction of poorly soluble compounds, but leads to a dispersed phase only if seeds serving the subsequent growth of the particles have time to form all over the support surface before crystallization starts. It is thus advised to check by microscopic methods if the final distribution of the active phase is homogeneous at the scale of the support grain.

In diffusional impregnation, the distribution of the solute inside the wet porosity of the pellet is assumed to be governed by two phenomena (Figure 2.5b): the diffusion of the solute into the pores of the pellet, described by Fick's law, and the adsorption of the solute onto the support, which depends on the adsorption capacity of

the surface and on the adsorption equilibrium constant. These two parameters are experimentally determined from adsorption isotherms, but the final distribution is not fundamentally changed if equilibrium is not reached and adsorption is ruled by kinetics. The distribution of the precursor along the pellet depends on the balance between diffusion and adsorption: when the precursor adsorbs on the support surface, its concentration in solution decreases and as a consequence, diffusion decreases too. Diffusion can be enhanced by imposing a high concentration outside the pellet.

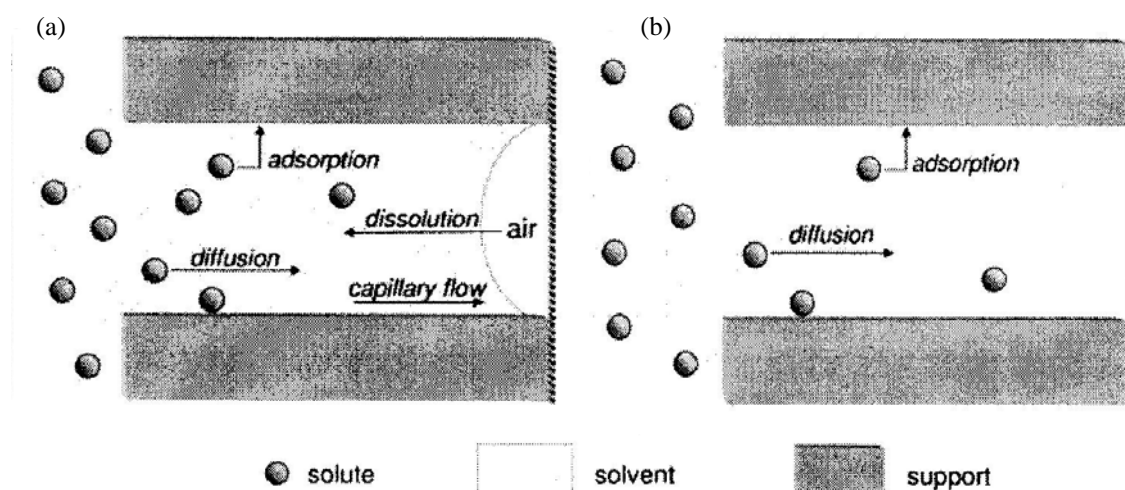

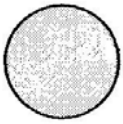
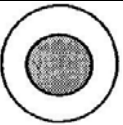


Figure 2.5 Phenomena of transport involved in (a) dry impregnation and (b) wet impregnation. The solute migrates into the pore from the left to the right of the figures. [65]

The step after impregnation is the elimination of the solvent. Typically, the impregnated system, spread in fine layers, is heated in an oven up to the boiling point of the solvent or at a lower temperature for gentle drying, in static conditions or under a flow of gas. The elimination of water from the pores leads to an increase of the

precursor concentration up to saturation and crystallization, preferably on seeds resulting from the interactions with the support, if one wants to obtain a highly dispersed phase. However, hydrated salts like nitrates melt at moderate temperature, which may cause the coalescence of their initially dispersed particles, or even their exclusion from the pores. As a conclusion, Table 2.3 provides a summary of the various conditions of impregnation and drying leading to different types of precursor distributions: egg-shell, uniform, or egg-yolk.

Table 2.3 Influence of the conditions of impregnation and drying on the precursor distribution inside a pellet [65]

Distribution	Conditions of impregnation and drying
 Egg-shell	<ul style="list-style-type: none"> • Strong adsorption of the precursor during impregnation • Impregnation with a very viscous solution • Slow drying regime, in the case of solutions of low concentration and viscosity, or weakly adsorbing precursors
 Uniform	<ul style="list-style-type: none"> • Precursors and competitors equally interacting with the surface^a • Weakly interacting precursor + drying at room temperature • Drying a concentrated, viscous solution • If the migration of the solute has started during drying, transition from the constant-rate period to the falling-rate period
 Egg-yolk	<ul style="list-style-type: none"> • Competitor interacting more strongly with the surface than the precursor^a • Fast drying regime with predominant back-diffusion

^a As long as drying does not modify the precursor distribution obtained during impregnation.

2.5.2 Sol-gel method [66]

Sol-gel processing is one of the routes for the preparation of porous materials by their solidification from a true solution phase, and its physic-chemical principles and applications are well described in the literature. The method is characterized by the formation of stable colloidal solutions (“sol”) in the first step, followed by anisotropic condensation of colloidal particles (micelles) producing polymeric chains with entrapped solution of condensation byproducts, resulting in the formation of a “liogel” or “hydrogel” or “monolith” when external solvent is not used. After washing out the byproducts the solvent removal produces “xerogels” or “aerogels”, depending on the drying mode, with distinct structures of the primary particles and their packing manner (texture). For clarity of terminology, the sol-gel method should be distinguished from other routes of materials solidification from solutions, such as precipitation and deposition–precipitation, crystallization from melts, expansion of supercritical solvent, supercritical anti-solvent method, supramolecular assembling, and others. The main peculiarity — which makes the sol-gel route unique and clearly discernible — is the formation of a clear colloidal solution due to primary condensation of dissolved molecular precursors. The second peculiarity is the merging of these colloidal particles during the subsequent gelation stage into polymeric chains by chemical bonding between local reactive groups at their surface. This prevents flocculation, which is a result of isotropic micelle aggregation. The porous solids (xero- or aerogels) are produced in the next step – desolvation – depending on the drying mode (see Figure 2.6).

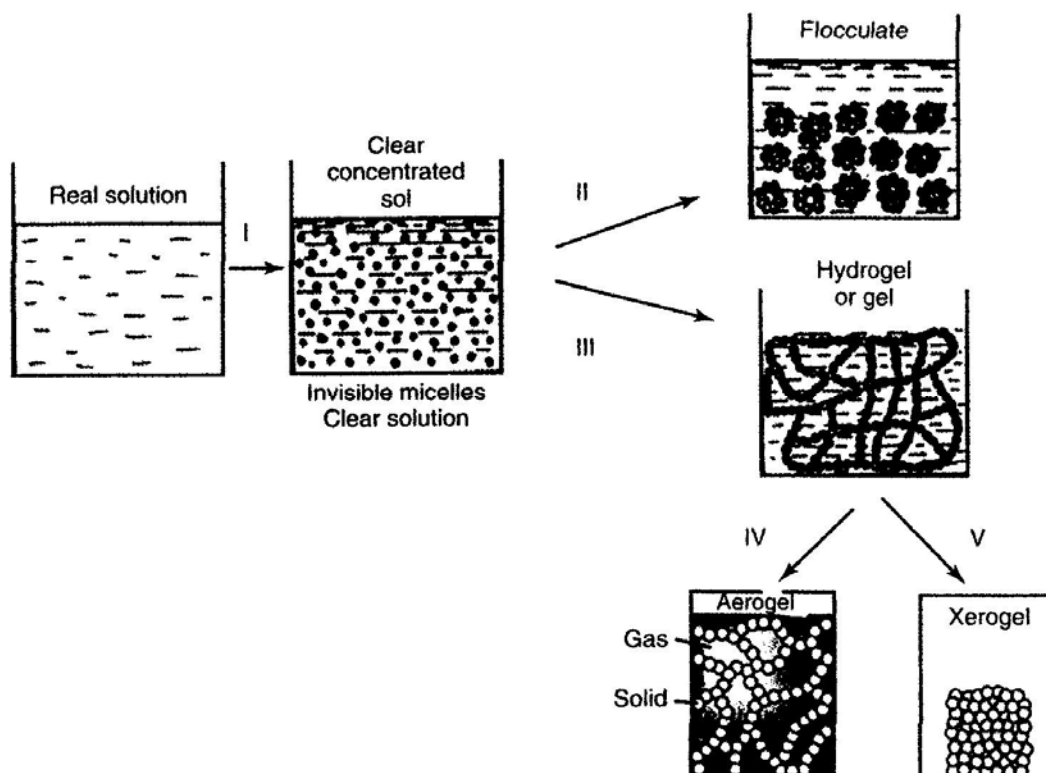


Figure 2.6 General scheme of sol-gel processing in the preparation of solid materials. I = Colloidization; II = Flocculation; III = Gelation; IV = Supercritical fluid processing; V = Drying by evaporation. [66]

Sol-gel processing involves a sequence of operations that includes chemical reactions and physical processes (phase separation, dissolution, evaporation, phase transition, etc.) leading to the formation of porous solids from liquid solutions of molecular precursors. The general principles and the physico-chemical bases of the separate steps have been extensively described and analyzed in many comprehensive books and reviews. The sol-gel processing sequence includes the following seven main stages (see Figure 2.7);

- Conversion (activation) of dissolved molecular precursors to the reactive state
- Polycondensation of activated molecular precursors into nanoclusters (micelles) forming a colloidal solution, the sol
- Gelation
- Aging
- Washing
- Drying
- Stabilization

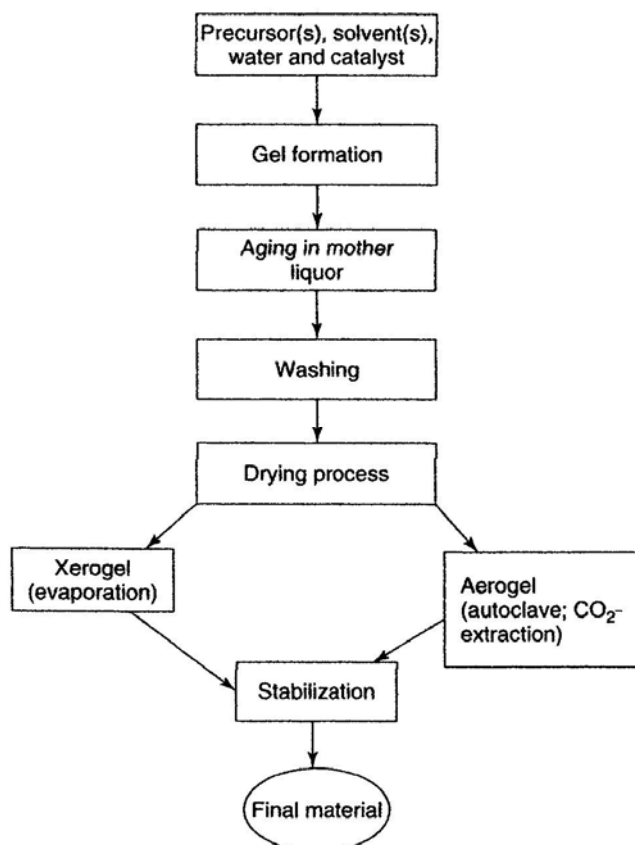


Figure 2.7 The sequence of steps involved in sol-gel processing for the synthesis of porous solid catalytic phases. [66]

The first two steps are hardly distinguished in real sol-gel practice because they occur in parallel after mixing the starting reagents. The preparation of a solid catalyst aims at producing a porous solid with a controlled texture, bulk structure, and chemical functionality of its surface. Here, we will briefly discuss all of the sol-gel steps with regards to their impact on these properties. The chemical nature of the selected precursors determines the reactions involved in sol-gel processing, the required additives (solvents, reagents, catalysts), and the conditions needed to control the properties of a porous solid (pH, reaction time, concentrations, temperature, drying mode). The choice of the chemical strategy depends on the possibility to control the rates of activation/condensation reactions which determine the materials texture, cost/availability of corresponding precursors, and their ease of handling. The choice is also determined by the compatibility of functionalizing substances that should be entrapped in the final gel, with solvents and products liberated during the solids preparation. Choice depends also on the physical properties of the corresponding sols, such as stability, viscosity, and the wetting of substrates, all of which are important for the fabrication of catalytic coatings.

2.5.3 Precipitation method [66]

Precipitation is the process in which a phase-separated solid is formed from homogeneous solution, after super-saturation with respect to the precipitating solid has been achieved. A number of related phenomena are known, which are often not clearly discriminated. Crystallization from solution is a process, in which the solid is directly obtained in crystalline form. Crystallization typically proceeds at relatively

low supersaturation, which is induced mostly by reduction of the temperature or evaporation of the solvent. Precipitation is often used for the description of processes, in which the solid formation is induced by addition of an agent which initiates a chemical reaction or which reduces the solubility (antisolvent). Precipitation normally involves high supersaturation, and thus frequently amorphous intermediates are obtained as the first solids formed. However, no consistent distinction between crystallization and precipitation is made in the literature, although with respect to catalyst synthesis, mostly indeed an agent is added which effects the solid formation — that is, precipitation in the narrow sense of the word is used.

Co-precipitation is very suitable for the generation of a homogeneous distribution of catalyst components, or for the creation of precursors with a definite stoichiometry, which can be easily converted to the active catalyst. If the precursor for the final catalyst is a stoichiometrically defined compound of the later constituents of the catalyst, a calcinations and/or reduction step to generate the final catalyst usually creates very small and intimately mixed crystallites of the components. This has been shown for several catalytic systems, and is discussed in more detail later in the chapter. Such a good dispersion of catalyst components is difficult to achieve by other means of preparation, and thus co-precipitation will remain an important technique in the manufacture of solid catalysts, in spite of the disadvantages associated with such processes. These disadvantages are the higher technological demands, the difficulties in following the quality of the precipitated product during the precipitation, and the problems in maintaining a constant product quality throughout the whole precipitation process, if the precipitation is carried out discontinuously.

The preparation of catalysts and supports by precipitation or co-precipitation is technically very important. However, precipitation is usually more demanding than several other preparation techniques, due to the necessity of product separation after precipitation and the large volumes of salt-containing solutions generated in precipitation processes. Thus, techniques for catalyst manufacture must produce catalysts with better performance in order to compensate for the higher costs of production in comparison, for instance, to solid-state reactions for catalyst preparation.

Precipitation processes are relevant not only for catalysis but also for other industries, as for example the production of pigments. Despite the tremendous importance of precipitation from solution, many basic questions in this field remain unsolved, and the production of a precipitate with properties that can be adjusted at will is still rather more of an art than a science. This is primarily due to the fact that the key step — the nucleation of the solid from a homogeneous solution — is not only very elusive but also difficult to study using the analytical tools currently available. On the one hand, spectroscopies using local probes are not sufficiently sensitive to study larger arrangements of atoms, whereas on the other hand neither are diffraction methods suitable for analysis, as a nucleus is not large enough to produce a distinctive diffraction pattern. Thus, investigations of crystallization and precipitation processes from solution must often rely on indirect and theoretical methods. A general flow scheme for the preparation of a precipitated catalyst is depicted in Figure 2.8.

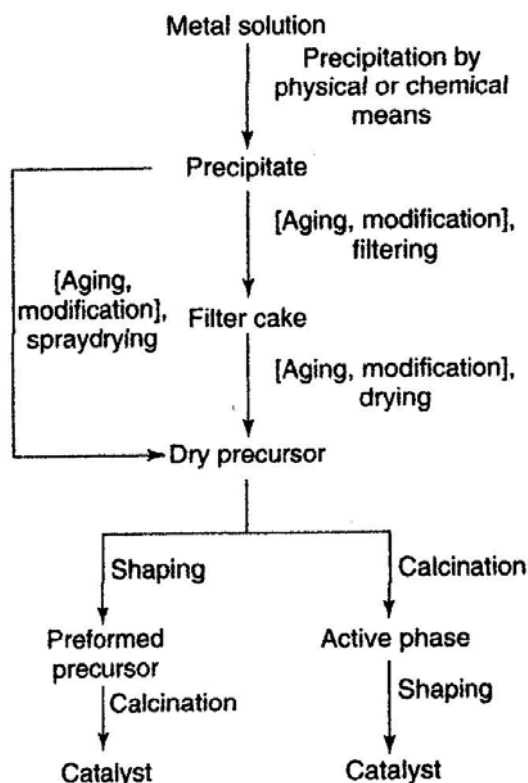


Figure 2.8 Precipitation scheme for precipitated catalysts. Optional steps are indicated by square brackets. [66]

Basically, all process parameters — some of which are fixed and some of which are variable — influence the quality of the final product of the precipitation. Usually, precipitates with specific properties are desired; these properties could be the nature of the phase formed, the chemical composition, purity, particle size, surface area, pore sizes, pore volumes, separability from the mother liquor, and many more, including demands imposed by the requirements of downstream processes, such as drying, pelletizing, or calcinations. It is therefore necessary to optimize the parameters in order to produce the desired material. The parameters which may be adjusted in

precipitation processes, and the properties which are mainly influenced by these parameters, are summarized in Figure 2.9. The main parameters consist of;

- Raw material
- Concentration and composition
- Solvent
- Temperature
- pH
- Aging
- Additives

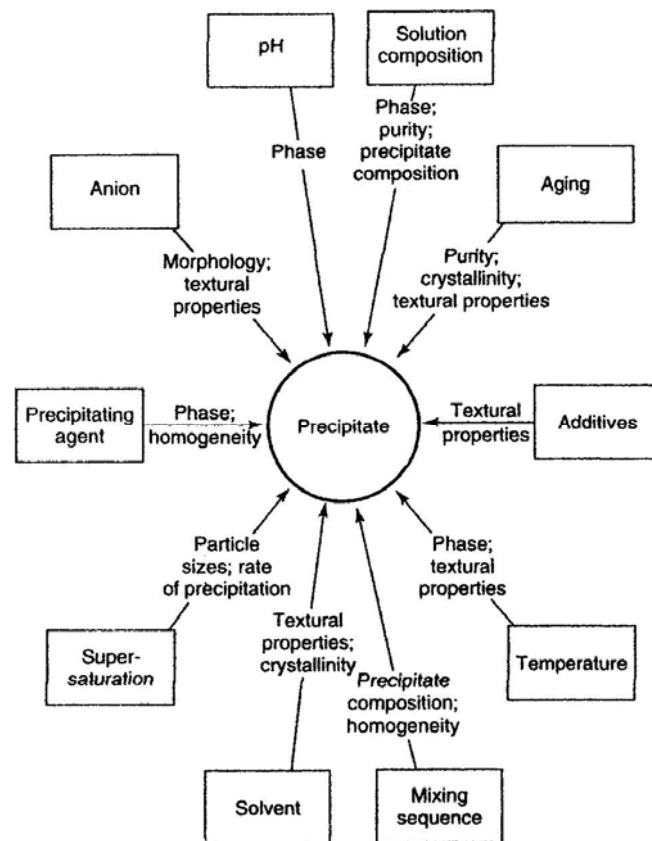


Figure 2.9 Parameters affecting the properties of the precipitate and the main properties influenced. [66]

2.6 Catalyst characterization [5]

Characterization of a heterogeneous catalyst refers to the measurement of its ‘characteristics’, which are those physical and chemical properties of the catalyst assumed to be responsible for its performance in a given reaction. More specifically, the characteristics of a catalyst include:

- The nature of its basic building block, i.e. chemical composition
- The arrangement of these basic building blocks or ‘architecture’, e.g. structure, crystallite size and distribution, crystallite morphology, porosity, and surface area
- Surface chemical properties such as valence state, acidity, reactivity with different molecules, surface energy, and surface electronic states
- The aggregate properties such as aggregate or particle size, magnetic properties, density (bulk, particle, and skeletal), mechanical strength, and attrition resistance
- Catalytic properties, i.e. activity, selectivity, and activity stability.

The characteristics of heterogeneous catalytic materials in this dissertation were discussed in Table 2.4. Some of the most commonly used characterization techniques and their acronyms are defined in the following list.

Table 2.4 Catalyst characteristics and methods for their investigation in this dissertation [66]

Characteristic	Method of Study	ASTM Method
Physical Properties		
• Surface area	Adsorption of N ₂	D3663-84
• Pore size, size distribution	Extended N ₂ and CO ₂ adsorptions	D4567-86
• Catalyst particle size and size distribution	SEM, TEM	D-4513
Chemical Properties		
• Chemical state, bulk	TPR, FTIR	
• Chemical state, surface	FTIR	
• Chemical state, surface • additives	FTIR	
• Composition, bulk	XRF/XRD, SEM, TEM, FTIR	D-3610-83 D-4481-85 D-4642-86
• Homogeneity	SEM, TEM	
• Morphology/structure, bulk	XRD, SEM, TEM	
• Morphology/structure, surface	TEM	
• Dispersion or percentage exposed	Chemisorptions, TEM, XRD	D-3908-82
• Surface reactivity, active site concentration	Chemisorptions	

- BET (Brunauer, Emmett and Teller Method): A widely accepted method for analyzing multi-layer physisorption isotherm of inert gasses to determine the surface area of solids and/or the distribution of mesopore sizes in these solid.

- XRD (X-ray diffraction): The characterization of bulk crystal structure and chemical phase composition by diffraction of an X-ray beam as a function of the angle of the incident beam. Broadening of the diffraction peaks can be used to estimate crystallite diameter. Can detect crystalline materials having crystal domains of greater than 3–5 nm.

- XRF (X-ray fluorescence spectroscopy): Quantitative analysis of the elemental composition of a solid using incident X-ray radiation to eject electrons from inner levels of the atoms. This method is complicated by matrix effects.
- TPR (temperature-programmed reduction): The measurement of the rate of reduction as a function of temperature (at a linear temperature ramp), which allows the study of the oxidation states of the surface and bulk of a solid.
- Chemisorption: It is primarily used for determination of characteristics of catalysts that are necessary for carrying out chemical adsorption. This makes it a very important process for products and manufacturing processes that involved chemical adsorption.
- SEM (scanning electron microscopy): Enable the imaging of the topography of a solid surface by use of backscattered or secondary electrons, with a resolution, at present, of better than 5 nm.
- TEM (transmission electron microscopy): Allows the determination of the microtexture and microstructure of electron transparent samples by transmission of a focused parallel electron beam to a fluorescent screen, with a resolution presently better than 0.2 nm.
- FTIR (Fourier transform infrared spectroscopy): Used to analyze the structures of adsorbed molecules on a catalyst surface under controlled atmosphere conditions. Basically this technique has the same applications as IR, although each FTIR spectrum is of higher intensity than that produced by dispersive IR; in addition, FTIR can be used for kinetic studies because of its rapid scanning resonance (1 ms to 1 s).

2.7 Literature reviews

2.7.1 Steam reforming of methanol (SRM)

Ritzkopf et al. [12] tested over a series of Cu/ZrO₂ catalysts prepared by the microemulsion technique. Catalytic activity was compared to that of a commercial Cu/ZnO catalyst. The synthesized catalysts have been characterized and investigated with respect to methanol conversion, CO formation, and long term stability. Both TPR and XANES/EXAFS indicate that two different Cu species are present in the as-prepared samples. Characterization by XRD and TEM revealed that the Cu/ZrO₂ consisted of small CuO/ZrO₂ particles below 10 nm in size. The catalysts consist of tetragonal zirconia particles with a homogenous distribution of copper and zirconium in the material. Methanol steam reforming over these Cu/ZrO₂ materials results in substantially reduced CO formation at high methanol conversions compared to the commercial Cu/ZnO catalyst.

Huang et al. [13] investigated the performances of catalysts CuO–ZnO–Al₂O₃, CuO–ZnO–Al₂O₃–Pt–Rh, and Pt–Rh in a reformer designed to generate hydrogen. The results show that both of the methanol conversion and the hydrogen yield rates increase with temperature. For the three catalysts tested, catalyst CuO–ZnO–Al₂O₃ provides the best performance at temperatures lower than 320 °C. However, at higher temperatures, the performance of this catalyst deteriorates, while that of CuO–ZnO–Al₂O₃–Pt–Rh and Pt–Rh continue to improve. It suggests that the addition of Pt and Rh to the original CuO–ZnO–Al₂O₃ catalyst has a stabilizing effect upon the reforming process under higher temperature conditions. The results also show that a

higher methanol feed rate reduces the methanol conversion rate, but increases the hydrogen yield rate. It is found that both of the methanol conversion and the hydrogen yield rates reduce as the steam-to-methanol ratio is increased.

Papavasiliou et al. [16] studied a series of doped CuO–CeO₂ catalysts prepared via the urea–nitrate combustion method. XRD analysis showed that at least part of the dopant cations enter the ceria lattice. The addition of various metal oxide dopants in the catalyst composition affected in a different way the catalytic performance towards H₂ production. Small amounts of oxides of Sm and Zn improved the performance of CuO–CeO₂, while further addition of these oxides caused a decrease in catalyst activity. XPS analysis of Zn- and Sm-doped catalysts showed that increase of dopant loading leads to surface segregation of the dopant and decrease of copper oxide dispersion. The addition of oxides of La, Zr, Mg, Gd, Y or Ca lowered or had no effect on catalytic activity, but led to less CO in the reaction products.

Udani et al. [20] studied a series of co-precipitated CuO–CeO₂ catalysts with varying copper content (30–80 at. % Cu) in steam reforming (SRM) and oxidative steam reforming of methanol (OSRM). The effects of copper content, reaction temperature and O₂ concentration on catalytic activity were investigated. The activity of CuO–CeO₂ catalysts for SRM and OSRM increased with the copper content and 70 at. % CuO–CeO₂ catalyst showed stable activities for both reaction. It was observed that the methanol conversion increased considerably with the addition of O₂ into the feedstream, indicating that the partial oxidation of methanol (POM) is much faster than SRM.

Jones et al. [21] reported the study of methanol steam reforming over several ZrO₂- and CeO₂-promoted catalysts prepared by deposition of copper and zinc oxide

precursors onto nanoparticle Al_2O_3 and ZrO_2 supports. It was found that the catalyst activities and CO selectivities are very dependent on both the catalyst preparation method and the ZrO_2 precursor. The best performing catalyst was prepared by co-impregnating Cu and ZnO precursors onto a physical mixture of nanoparticle ZrO_2 and nanoparticle Al_2O_3 resulting in a highly active reforming catalyst which also suppressed CO production. The presence of ZrO_2 nanoparticles promoted a highly active copper surface and addition of high surface area alumina was necessary to assure a reasonable Cu surface area. However, the catalytic activities of the catalysts in this study did not correlate with Cu surface area, total surface area, or reduction temperature. The presence of a monoclinic ZrO_2 phase promotes methanol reforming and also suppresses methanol decomposition

Chen et al. [24] reported the wall coated catalysts in a microchannel reactor for methanol oxidation reforming. The preparation method of the wall coating catalyst was studied in detail, i.e., the sol-gel and solution-coating techniques. To prepare the catalysts for methanol oxidation reforming, the washing-coating layer of CuZnAl was prepared by the sol-gel technique, and then the active layer was coated on it by solution-coating technique with emulsion colloid containing Pd-ZnO particles. Both the Cu-Zn-Al and Pd-Zn alloy particles were distributed uniformly via top view of SEM. The adhesion of coating layer of Cu-Zn-Al with substrate of stainless steel was strong, while the active layer of Pd-Zn exhibited somewhat easy peel off. The reaction experimental results indicated that the catalyst prepared have high activity and relatively high stability. The catalysts developed showed highly activity as indicated by high methanol conversions at high space velocity.

Manzoli et al. [29] studied methanol decomposition and methanol combined reforming to hydrogen on Cu and Au catalysts supported on ZnO and TiO₂ at increasing temperatures. The evolution of the adsorbed species with the increase of the temperature is different on the four catalysts. The reaction mixture, the nature of the metal and the preparation method are the controlling parameters. Although both ZnO supported catalysts have been prepared by the same co-precipitation method, formate species are produced on Cu/ZnO, while they are completely lacking on the Au/ZnO sample during the same thermal treatment in pure methanol. The different behavior of the two co-precipitated ZnO based catalysts is mainly related to the formation of a solid solution precursor phase in the copper catalyst, not produced in Au/ZnO as a consequence of gold size. Therefore, gold is not able to activate the support towards the oxidative dehydrogenation of methanol to formaldehyde and it does not affect the defect equilibria of ZnO. On the contrary, the surface species on the TiO₂ supported catalysts that have been both prepared by deposition–precipitation evolve quite similarly with the temperature. In the methanol combined reforming reaction, the activity towards H₂ production is beneficially influenced on the copper based catalysts and it is negatively affected by the presence of TiO₂ as support.

Yang et al. [30] have studied hydrogen production by partial oxidation of methanol (POM) over Au/CuO/ZnO (Au 3 wt%, Cu 37 wt% and Zn 60 wt%) catalysts, prepared by the co-precipitation method. The Au/CuO/ZnO was more active and exhibited higher hydrogen selectively with smaller amount of CO compared to the CuO/ZnO (Cu 40 wt% and Zn 60 wt%) catalysts. The enhanced activity of Au/CuO/ZnO catalyst is due to the strong interaction between Au and CuO species as evidenced by TPR analysis. The catalytic activity of Au/CuO/ZnO also depended on

calcination temperature that effected to crystalline phases of support and particle size of Au and CuO present on the catalysts. Complete methanol conversion and high hydrogen selectivity of ~97% is attained at 300 °C. The undesired by-product, CO is formed in very small amount throughout the temperature range studied.

Ou et al. [31] have compared catalytic activity of Au/TiO₂ (2 wt% Au), Cu/TiO₂ (2 wt% Cu) and Au–Cu/TiO₂ (1 wt% Au–1 wt% Cu) for partial oxidation of methanol (POM) to produce H₂. The optimum pH for preparing the high active Au–Cu/TiO₂ catalysts by deposition–precipitation method was pH 7 and uncalcined catalyst was chosen. The bimetallic Au–Cu/TiO₂ catalysts are more active, stable and exhibit higher hydrogen selectively with smaller amount of CO compared to the monometallic Au/TiO₂ and Cu/TiO₂ catalysts. The enhanced activity, selectivity and stability of the bimetallic catalysts are due to Au–Cu interaction that creates smaller metal particles, which consequently stabilize the active component for POM to produce hydrogen. The catalytic performance at various reaction temperatures in the range of 200–325 °C showed that at 250 °C, the catalyst exhibited higher methanol conversion, H₂ selectivity with smaller CO selectivity.

Wu et al. [32] have investigated production of H₂ with ultra-low CO concentration via photocatalytic reforming of methanol on Au/TiO₂ catalyst. When the gold particle size is reduced from 10 to smaller than 3 nm the rate of H₂ production is greatly increased while the concentration of CO decreases. They suggested that the byproduct CO is mostly produced via decomposition of the intermediate formic acid species derived from methanol. The smaller gold particles possibly switch the HCOOH decomposition reaction mainly to H₂ and CO₂ products while suppress the CO and H₂O products. In addition, some CO may be oxidized to

CO₂ by photogenerated oxidizing species at the perimeter interface between the small gold particles and TiO₂ under photocatalytic condition.

2.7.2 Preferential oxidation (PROX) of CO

Mariño et al. [33] Investigated covered a wide range of transition metals (Co, Cr, Cu, Ni, Zn) supported on oxides with very different acidic, basic and redox properties (MgO, La₂O₃, SiO₂-Al₂O₃, CeO₂, Ce_{0.63}Zr_{0.37}O₂) for the preferential oxidation of CO. The influence of the metal loading (Cu), the support properties (acidity, basicity, redox, surface area) and the reaction conditions (reaction temperature, feed composition) on the catalyst activity and selectivity was evaluated. Cu-CeO₂ catalysts showed a practically constant and high selectivity towards CO oxidation in the temperature range of 50–150 °C. Due to the strong synergetic effect between copper and ceria, only a small amount of copper (0.3 wt%) was necessary to get an active catalyst. The best catalytic performances were obtained for the samples containing 1–3 wt% copper. Classically, an increase of the oxygen excess led to an increased CO conversion with a simultaneous loss of selectivity towards CO₂. Finally, the presence of CO₂ in the feed negatively affected the catalytic activity. This effect was attributed to the adsorption of CO₂ on the copper sites.

Suh et al. [34] tested various catalysts containing different catalytic materials, supports, and additives for the preferential oxidation (PROX) of CO. Ru/Al₂O₃ is more active than Pt/Al₂O₃, but hydrogen consumption occurs greatly as a result of methanation. When platinum is supported on different supports, the activity for carbon monoxide removal slightly increases in the decreasing order of metal-support

interaction. Addition of base metal to Pt/Al₂O₃ enhances their performances for PROX to a great extent. TPR results indicated that a new active species was formed resulting in the enhancement of catalytic activity. PtCo/Al₂O₃ was tested with a simulated steam-reformed fuel for confirmation of its high activity. It reduces CO concentration to below 10 ppm. under following conditions: space velocity > 30,000, temperature = 70–90 °C, and O₂/CO=1.

Panzer et al. [38] studied ceria-supported Au catalysts for selective oxidation of CO that prepared by co-precipitation method. Fresh and used catalysts were characterized by XRD, XRF and TEM. Air calcination at 500 °C resulted in the establishment of adequate interfacial metal oxide properties which are essential to promote the selective CO oxidation. CO conversion close to 100% was obtained at 120 °C, whereas CO₂ selectivities not higher than 40% were obtained in the entire temperature range investigated (80–120 °C). The presence of CO₂ in the inlet stream negatively affected both CO conversion and CO₂ selectivity. Both calcined and uncalcined Au/CeO₂ catalysts resulted to be very stable, as demonstrated by 120 h endurance tests. TEM investigation of the used catalysts revealed that a surface Au particles reconstruction occurred during reaction.

Souza et al. [59] reported the results related to the preparation of Au/ZnO using the deposition–precipitation technique. There are important parameters in the preparation of gold catalyst by ionic exchange. Many samples were synthesized taking into account different pH values, gold concentration, procedures and contact times between the gold precursor and support. The exposure of gold compounds to radiation in the visible range was also examined during the preparation. It could be observed that exposure to light and competition among anions change the gold

content of the catalyst. The results also show that by using this technique it is possible to prepare active catalysts for the preferential oxidation of carbon monoxide (PROX) reaction giving 100% CO conversion at 40 °C.

Ayastuy et al. [61] studied CO oxidation on Pt/Ce_xZr_{1-x}O₂ (X = 0, 0.15, 0.5, 0.68, 0.8 and 1), both in the absence of H₂ and in H₂-rich streams. Three catalysts were found capable of complete CO depletion with effective oxygen use at $\lambda = 2$: Pt/Ce_{0.8}Zr_{0.2}O₂, Pt/Ce_{0.68}Zr_{0.32}O₂, and Pt/Ce_{0.5}Zr_{0.5}O₂ at temperatures below 112 °C. Catalyst activity was correlated with support reducibility and Pt content. More demanding working conditions, by increasing GHSV from 12,000 up to 18,000 h⁻¹, reduced the adequate catalysts to just two: Pt/Ce_{0.68}Zr_{0.32}O₂ and Pt/Ce_{0.5}Zr_{0.5}O₂, and only the latter would be adequate if the conditions were still more demanding. The only Pt/Ce_{0.5}Zr_{0.5}O₂ remained capable of complete CO removal with effective oxygen use at $\lambda = 2$ when CO₂ and H₂O presented in the feedstream.

Zhou et al. [67] Studied alumina supported Pt group metal monolithic catalysts for selective oxidation of CO in hydrogen-rich methanol reforming gas for proton exchange membrane fuel cell (PEMFC) applications. The results show that Pt/ γ -Al₂O₃ was the most promising candidate to selectively oxidize CO from an amount of about 1 vol% to less than 100 ppm at 170 °C in a single-stage reactor and O₂/CO = 1. Water vapor in the feed could enhance CO preferential oxidation, while CO₂ could retard the reaction. When water vapor and CO₂ were coexisting in the feed, the combined effect was positive at temperatures < 180 °C, and was similar to the effect observed when CO₂ existed alone. The Pt/ γ -Al₂O₃ monolithic catalyst exhibited very stable performance in the durability test. It was scaled up and successfully applied in a 5 kW hydrogen source system via methanol reforming, which had been

successfully integrated and tested with a PEMFC. During the test, the outlet CO concentration from the CO cleaning-up subsystem was below 50 ppm.

Parinyasawan et al. [68] have studied platinum–palladium supported on ceria catalysts for preferential oxidation of CO in the presence of hydrogen. The catalysts were prepared by impregnation method using different supports. The catalytic activity tests were performed using a fixed bed reactor in the temperature range of 50–190 °C atmospheric pressure. Effects of support, ratio of Pt–Pd, O₂ concentration water vapor concentration, CO₂ concentration, and the combination of H₂O and CO₂ in the feed stream on the catalytic performance of Pt–Pd/CeO₂ catalysts were also investigated. The experimental results showed that 1%(1:7)Pt–Pd/CeO₂ (sol-gel) exhibited higher activity than other catalysts examined, ~76% CO conversion at 90–110 °C. The maximum CO conversion of ~99% was obtained at 90 °C when increasing O₂ concentration to 2%. Water vapor in the feed substantially increased the activity of the catalysts, whereas CO₂ in the feed stream drastically decreased the activity of the catalysts. When both H₂O and CO₂ were added in the feed stream, the positive effect of H₂O is more pronounced than the negative effect of CO₂. Their stability results of Pt–Pd/CeO₂ catalyst at the reaction temperature of 90 °C during 24 h showed the high stability of this catalyst.

Srinivas et al. [69] tested the performance of a preferential CO oxidation reactor operating in two modes – single-stage and two-stage. single-stage mode of operation offered a minimum CO outlet composition of around 135 ppm. when operated at 180 °C. The two-stage mode of operation performed significantly better than the single-stage mode by offering a minimum CO outlet composition of 11 ppm with the first stage operating at 230 °C and the second stage at 170 °C. Oxygen split

ratio between the two stages was optimized to obtain best performance, around 60:40. The results proposed that a number of reactor is also the main effect for PROX of CO.

Scirè et al. [70] investigated Selective oxidation of CO in H₂-rich stream over iron oxide supported Au catalysts prepared by deposition–precipitation (AuDP) or co-precipitation (AuCP) and for comparison on commercial gold reference catalyst (AuRef). AuDP and AuCP samples presented CO conversion strongly decreased on increasing calcination temperature while AuRef sample was less evident. On the basis of characterization data (H₂-TPR, XRD, TEM) it was pointed out that, provided gold particles are small enough to be able to activate CO and H₂, the catalytic behavior of the Au/iron oxide system in the PROX reaction is strongly related to the support phase, being sensitive to the microcrystalline structure and the oxidation state of the iron oxide. CO oxidation activity of different iron oxide species was found in the order: ferrihydrite > hematite > magnetite.

Chang et al. [71] tested a series of gold catalysts supported on TiO₂ were prepared by photo-deposition method. They studied the effects of preparation parameters, such as power of UV light, irradiation time, and initial gold concentration, on the characteristics of the catalysts. For catalytic activity of the catalyst, preferential oxidation (PROX) of CO was measured in a fixed-bed plug-flow reactor. The photo-deposition method facilitates to prepare gold particles as small as 1.5 nm on the support and the lower power source lamp can deposit small gold particles on the support. These catalysts were very active and selective in PROX reaction. However, the small gold particles were not stable as long as the reaction temperature was > 50 °C.

2.7.3 Design of experiment (DOE)

In recent year, there are many fields of research work to optimize the operating condition for their work.

Brasil et al. [72] have studied in order to reduce the total number of experiments for achieving the best conditions for Cr(VI) uptake using *Araucaria angustifolia* wastes (named pinhão) as a biosorbent. There are three statistical design of experiments were carried out. A full 2^4 factorial design with two blocks and two central points (20 experiments) was experimented (pH, initial metallic ion concentration— C_0 , biosorbent concentration— X and time of contact— t). The results led to the performance of a Box–Behnken surface analysis design with three factors. Moreover, They also verified the effects of three concomitant ions that gave the best condition to remove completely Cr(VI) from aqueous solution with a ratio of Cr(VI) effluent volume/biosorbent volume of 252.3.

Lima et al. [73] used a full 2^4 factorial design for each adsorbent with two central points to optimize the following factors: mass of adsorbent (m), pH, time of contact (t) and initial metallic ion concentration (C_0). In order to continue the batch adsorption optimization of the systems, a central composite surface analysis design with two factors (C_0 , t). By performing these two sets of statistical design of experiments, the best conditions for Cu(II) uptake using pinhão wastes (PW) and pinhão wastes loaded with Congo red (CRP) using batch adsorption system, where: $m = 30.0$ mg of adsorbent; pH 5.6; $t = 2.5$ h.

Erickson et al. [74] investigated a passive flow disturbance has been proven to enhance the conversion of fuel in a methanol–steam reformer. This study presents a

statistical validation of the experiment based on a standard 2^k factorial experiment design and the resulting empirical model of the enhanced hydrogen producing process. Three input factors, including the number of flow disturbers, catalyst size, and reactant flow rate were investigated for their effects on the fuel conversion in the steam-reformation process. The statistical analysis showed that the number of bluff body packages has a positive significant effect on fuel conversion at a 99.9% confidence level. The model performed more accurately in predicting pelletized catalyst conversion than with crushed catalyst.

Aslan [75] used the application of response surface methodology (RSM) and central composite rotatable design (CCRD) for modeling the influence of some operating variables on the performance of a Multi-Gravity Separator (MGS) for coal cleaning was discussed. Four operating variables of MGS, namely drum speed, tilt angle, wash water and feed solids were changed during the tests based on the CCRD. These equations that are second-order response functions representing ash content and combustible recovery of clean coal were expressed as functions of four operating parameters of MGS. This study has shown that the CCRD and RSM could efficiently be applied for the modeling of MGS for coal and it is economical way of obtaining the maximum amount of information in a short period of time and with the fewest number of experiments.

Meshkini et al. [76] investigated the Cu/ZnO/Al₂O₃ catalysts, prepared by coprecipitation method, have been modified by adding small amount of Mn, Mg, Zr, Cr, Ba, W and Ce oxides using design of experiments (1/16 full factorial design). The oxide additives were found to influence the catalytic activity, dispersion of Cu, Cu crystallite size, surface composition of catalyst and stability of catalysts during their

operations. In addition, the results showed that the Mn and Zr promoted catalysts have high performance for methanol synthesis from syngas.

Thouchprasitchai et al. [77] have studied the catalytic performance of Cu–Zn–Fe composite-oxide catalysts prepared by the urea–nitrate combustion (UNC) method for the WGS reaction. They achieved the optimal condition of CO conversion in the reaction and revealed the interactions among the factors, two sets of statistical designs of experiments were carried-out. From a full 2^5 factorial design with three central points, increased CO conversion is obtained when increasing the H_2O and O_2 concentration in the influent, the W/F ratio, and the reaction temperature. For optimization, the application of the face-centered central composite design (FCCCD) falling under response surface methods was done. The validation of the model was performed and elucidated that the predicted values of the statistical response surface analysis were well fitted with the observed ones.

Charoenchaitrakool et al. [78] investigated the optimum conditions in biodiesel production from waste frying oil using two-step catalyzed process. Box–Behnken design of experiment was carried out followed by using response surface methodology for analyzing. The optimum conditions for biodiesel production were obtained when using methanol to oil molar ratio of 6.1:1, 0.68 wt% of sulfuric acid, at 51 °C with a reaction time of 60 min in the first step, followed by using molar ratio of methanol to product from the first step of 9.1:1, 1 wt% KOH, at 55 °C with a reaction time of 60 min in the second step. The percentage of methyl ester in the obtained product was $90.56 \pm 0.28\%$ and the fuel properties of the produced biodiesel were in the acceptable ranges according to Thai standard for community biodiesel.

2.7.4 Fuel processing of hydrogen production

Wiese et al. [7] studied a compact methanol reformer (CMR) with a specific weight of 2 kg/kW. This CMR contains a methanol and water vaporizer, a steam reformer, a heat carrier circuit and a catalytic burner unit. A hydrogen yield of 10 m³_N/h l_{Cat} can be achieved at 280 °C. In this case, the methanol conversion rate is 95% and the dry product gas contains 0.9% CO. The catalyst was operated for more than 1000 h without having exhibited activity losses.

Pan et al. [79] investigated on-board generation of hydrogen by methanol reforming PEMFC especially for vehicle propulsion purpose. The methanol reforming can take place at temperatures around 200 °C with a nearly 100% conversion at a hydrogen yield of about 400 L (h kg_{catalyst})⁻¹. The CO content in the reformat gas at this temperature is less than 0.2 vol%. The high CO tolerance makes it possible to use the reformat gas directly from the reformer without further CO removal. Considering the fact that a reformer is a consumer of heat and water and a fuel cell stack is a producer of heat and water, integration of the stack and the reformer is expected to improve the system performance.

Men et al. [80] presented a complete and miniaturized methanol fuel processing/fuel cell system composed of microchannel reactors and fabricated at IMM, which consists of a micro-structured evaporator, a micro-structured reformer and two stages of preferential oxidation of CO (PROX) reactor, a micro-structured catalytic burner, and a fuel cell. The methanol steam reformer was fabricated by depositing self-made Cu/ZnO catalyst inside the microchannel reactor and for the PROX reactor a bimetallic Rh–Pt/Al₂O₃ catalyst was applied. Under the optimized operating

condition, the two PROX reactor stages fed by the hydrogen-rich reformat produced by the microreformer effectively reduced the reformat CO content down to 18 ppm at O₂ to CO ratio of 3 at 135 °C. The fuel processing system run stably for over 100 h and exhibited good operating stability.

CHAPTER III

EXPERIMENTAL

In this chapter, materials and equipments used in this dissertation were shown in section 3.1 and section 3.2, respectively. Experiment procedure was divided in three parts; SRM, PROX and integration of SRM and PROX, as considered in section 3.3. Moreover, all experiments can be concluded as shown in Tables 3.3, 3.6, and 3.7.

3.1 Materials

3.1.1 Chemicals

- Gold (III) chloride trihydrate ($\text{HAuCl}_4 \cdot 3\text{H}_2\text{O}$), M.W. = 394.79 g mol⁻¹ from Sigma-Aldrich
- Hydrogen hexachloroplatinic acid hexahydrate ($\text{H}_2\text{PtCl}_6 \cdot 6\text{H}_2\text{O}$), M.W. = 517.93 g mol⁻¹ from Fluka
- Copper (II) nitrate trihydrate ($\text{Cu}(\text{NO}_3)_2 \cdot 3\text{H}_2\text{O}$), M.W. = 241.60 g mol⁻¹ from Merck
- Cerium (III) nitrate hexahydrate ($\text{Ce}(\text{NO}_3)_3 \cdot 6\text{H}_2\text{O}$), M.W. = 434.23 g mol⁻¹ from Merck

- Zinc (II) nitrate tetrahydrate ($\text{Zn}(\text{NO}_3)_2 \cdot 4\text{H}_2\text{O}$), M.W. = 261.44 g mol⁻¹ from Merck
- Ferric (III) nitrate nonahydrate ($\text{Fe}(\text{NO}_3)_3 \cdot 9\text{H}_2\text{O}$), M.W. = 404 g mol⁻¹ from Merck
- Cerium (IV) oxide anhydrous (CeO_2), M.W. = 172.12 g mol⁻¹ from Riedel-de Haën
- Urea (NH_2CONH_2), M.W. = 60.06 g mol⁻¹ from APS Finechem
- Sodium carbonate anhydrous (Na_2CO_3), M.W. = 105.99 g mol⁻¹ from APS Finechem
- Ethanol ($\text{C}_2\text{H}_5\text{OH}$), M.W. = 46.07 g mol⁻¹ from Merck
- Methanol (CH_3OH), M.W. = 32.04 g mol⁻¹ from Merck
- Commercial catalyst (MegaMax 700) from Süd-chemie

3.1.2 Gases

- Ultra high purity (99.999%) He from Thai Industrial Gases Public Co., Ltd.
- High purity (99.99%) H₂ from Thai Industrial Gases Public Co., Ltd.
- 10% CO in He from Thai Industrial Gases Public Co., Ltd.
- 5% O₂ in He from Thai Industrial Gases Public Co., Ltd.
- 20% CO₂ in He from Praxair (Thailand) Co., Ltd.

3.2 Equipments and apparatus set-up

3.2.1 Equipments

- Mass flow controller (AALBORG, model: GFC 1715)
- Temperature controller (PID temperature)
- Syringe pump
- Tube and fitting valve (Stainless steel) from Swagelok
- Gas chromatography (GC, model: Thermo Finnigan 2000 and Agilent Technologies 6890N)
- Stainless steel tube reactor (I.D. = 1/4 in) and Glass tube reactor (I.D. = 6 mm)
- Oven
- Stove
- Conductivity meter

3.2.2 Apparatus set-up

Fuel processor consists of two main parts, hydrogen production unit and CO clean-up unit. Hydrogen is produced from steam reforming of methanol (SRM) reaction and CO is removed by preferential oxidation (PROX). The experiment schematic is shown in Figure 3.1.

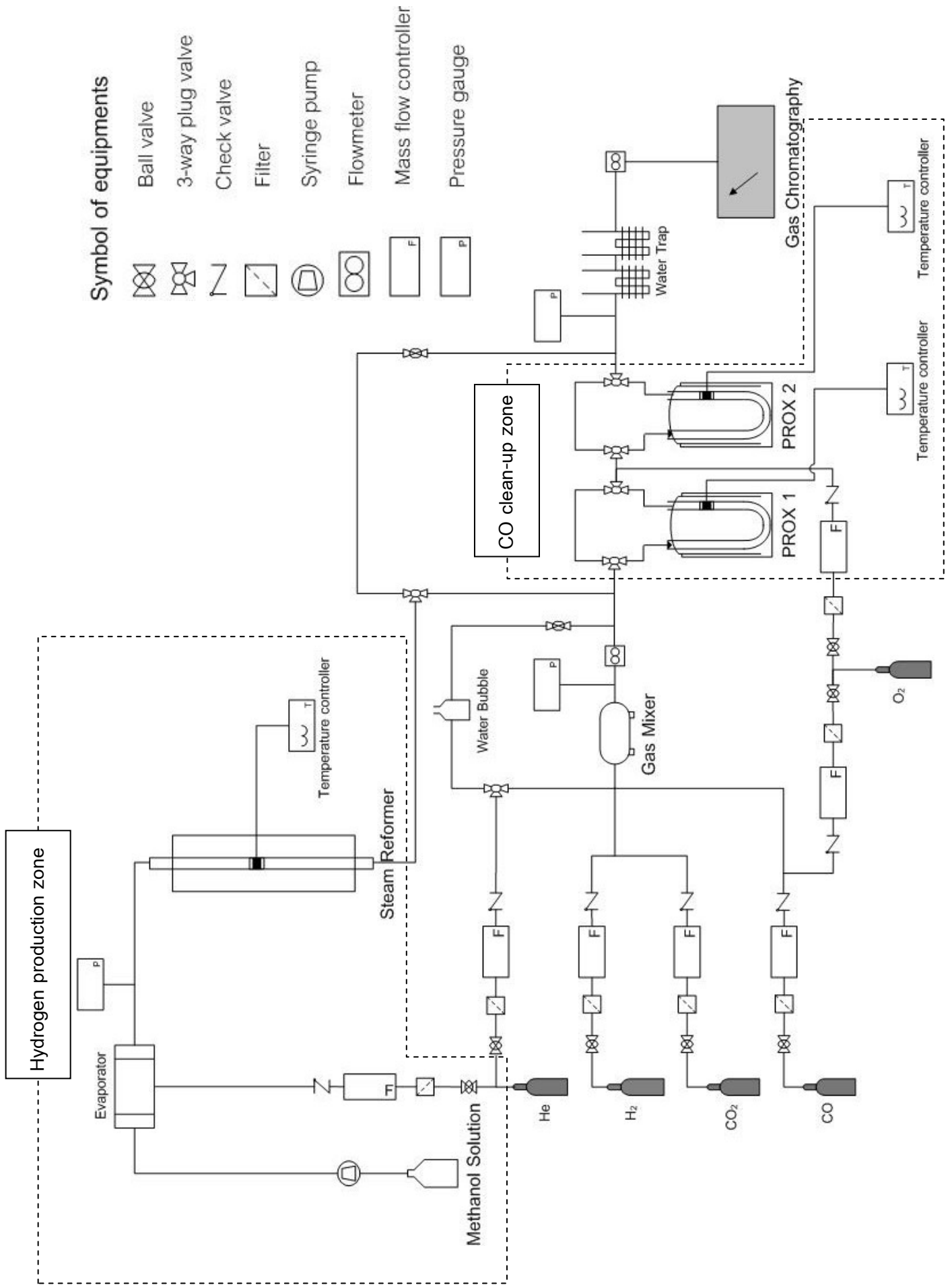


Figure 3.1 Experimental set-up for fuel processor

3.3 Experiment procedure

3.3.1 Steam reforming of methanol (SRM) unit

In this unit, it presented as following: a catalyst preparation method, characterization of the prepared catalysts, catalytic activity measurement. After that statistical design of the experiments over the effective catalyst were then mentioned in order to evaluate an importance of factors chosen. Finally optimization for SRM over the effective catalyst was determine by using response surface methodology (RSM).

3.3.1.1 Catalyst preparation

- Support preparation

CuO, CeO₂, and CuO–CeO₂ were prepared by the simultaneous addition of an aqueous solution of each precursor (Cu(NO₃)₂·3H₂O and/or Ce(NO₃)₃·6H₂O) to the desired atomic ratio of Cu to Ce. The solution was continuously stirred and then co-precipitated by the addition of 0.5 M aqueous sodium carbonate (Na₂CO₃) until the pH of the aqueous solution was stable at 8. The suspension was then aged by heating, with stirring, for 1 h at 80 °C. The resulting precipitate was harvested by filtration, washed with warm deionized (DI) water several times to remove the excess ions. After that, they were dried overnight at 110 °C in air and calcined at 500 °C for 5 h in a flow of air.

- Supported catalyst preparation

A gram of powdered CuO, CeO₂, and CuO–CeO₂, synthesized by co-precipitation (CP) (above), was suspended in 100 cm³ of DI water with constant stirring at room temperature whilst an aqueous solution of HAuCl₄·3H₂O was added

to the suspension to a final Au loading of 5 wt%. Then, 0.5 M Na₂CO₃ aqueous solution was added dropwise to the suspension until pH value was constant at 8. The suspension was continuously stirred for 1 h at temperature of 80 °C for aging. After that the precipitate was filtered and then washed with DI water several times for excess ion removal. The sample was dried overnight at 110 °C in air and calcined at 350 °C for 2 h in a flow of air. The Au/CuO–CeO₂ catalysts with various (x:y) Cu:Ce atomic ratios are denoted as Au/(x:y)CuO–CeO₂.

3.3.1.2 Catalyst characterization

- *Brunauer–Emmett–Teller (BET) surface area*: The BET method was used to determine the surface area of the catalyst by N₂ adsorption/desorption at -196 °C (Micromeritics ASAP 2020).

- *X-ray diffraction (XRD)*: A Rigaku XRD system equipped with a RINT 2000 wide-angle goniometer employing CuK_α radiation ($\lambda = 1.54 \text{ \AA}$) and an X-ray power of 40 kV/30mA was used to examine the crystalline structure. The particle diameter was calculated by the Debye–Scherrer equation at the X-ray line broadening of the (1 1 -1) diffraction peak for CuO and the (1 1 1) diffraction peak for CeO₂.

- *X-ray fluorescence spectrometry (XRF)*: XRF (Philips, model: PW-2400) was used to determine the composition (relative proportion) in the catalyst.

- *Temperature-programmed reduction (TPR)*: TPR was used to investigate the reduction temperature of the catalysts. The catalysts were pretreated in a U-shaped quartz reactor under an Ar flow rate of 40 cm³ min⁻¹ at 300 °C for 2 h. After this pretreatment, the catalysts were cooled to the room temperature. A reducing gas of 10% (v/v) H₂ in Ar was then introduced into the reactor at a flow rate of 40 cm³

min^{-1} and the catalysts were heated up to $350\text{ }^{\circ}\text{C}$ at a rate of $10\text{ }^{\circ}\text{C min}^{-1}$. A thermal conductivity detector (TCD) was employed to determine an amount of H_2 uptake.

- *Scanning electron microscopy (SEM)*: The particle morphology of the catalysts was observed by SEM using a JEOL JSM-5800 LV microscope was operated at 15 kV in bright and dark field modes.

- *Transmission electron microscopy (TEM)*: TEM was carried out using a JEM 2010TEM, operating at 200 kV in bright and dark field modes, to obtain information about the morphology of the catalyst.

- *Fourier transform infrared spectrometer (FTIR)*: The FTIR spectra have been collected on a Perkin-Elmer 2000 spectrometer (Spectrum one) equipped with a MCT detector to record wave number range of functional group.

3.3.1.3 Catalytic activity measurement

- *Catalysts comparison*

An aqueous methanol solution with 1.5:1 of steam to methanol (S/M) mole ratio was fed into the evaporator at $3\text{ cm}^3\text{ h}^{-1}$, controlled by a syringe pump. Simultaneously helium was also fed into the evaporator at $35\text{ cm}^3\text{ min}^{-1}$ as the carrier gas. The final methanol and steam composition nominally set to 10% (v/v) methanol, 15% (v/v) steam, and balance helium. The mixture was then fed into a 1/4 inch inner diameter quartz-tube fixed-bed reactor over reaction temperatures between $200\text{ }^{\circ}\text{C}$ to $400\text{ }^{\circ}\text{C}$ to investigate the SRM catalytic activities at atmospheric pressure. Prior to the activity test, 0.1 g of catalyst sample was placed between two layers of quartz wool in the reactor. The reaction temperature was controlled by a temperature controller and was measured by a thermocouple placed in the center of the catalyst bed. The gaseous effluent was analyzed by an on-line gas chromatograph (Thermo Finnigan 2000)

equipped with a shincarbon column and a thermal conductivity detector (TCD), and using helium as the carrier gas. The experimental data are displayed in terms of methanol conversion (%), H₂ selectivity (%), and CO selectivity (%) as shown in Eqs. (3.1)–(3.3).

$$\text{Methanol conversion (\%)} = \frac{[\text{CO}]_{out} + [\text{CO}_2]_{out}}{\text{CH}_3\text{OH}_{in}} \times 100 \quad (3.1)$$

$$\text{H}_2 \text{ selectivity (\%)} = \frac{[\text{H}_2]_{out}}{[\text{H}_2]_{out} + [\text{CO}]_{out} + [\text{CO}_2]_{out}} \times 100 \quad (3.2)$$

$$\text{CO selectivity (\%)} = \frac{[\text{CO}]_{out}}{[\text{H}_2]_{out} + [\text{CO}]_{out} + [\text{CO}_2]_{out}} \times 100 \quad (3.3)$$

where [CH₃OH]_{in} is the concentration of methanol in the feedstream (mole min⁻¹), [H₂]_{out} is the concentration of H₂ in the effluent (mole min⁻¹), [CO]_{out} is the concentration of CO in the effluent (mole min⁻¹) and [CO₂]_{out} is the concentration of CO₂ in the effluent (mole min⁻¹).

- *Statistical design of experiments* [81]

A factorial design with complete randomization is commonly employed to screen which factors have a significant influence on a given response by varying one factor with the level of the other factors. In this work, the four independent factors chosen were the operating temperature (°C), steam to methanol (S/M) ratio, liquid feed rate (cm³ h⁻¹), and catalyst weight to He flow rate (W/F) ratio. Other factors that also affect the response, such as the amount and type of catalyst and the reactor volume, were held constant throughout the experiments. To achieve the maximum methanol conversion with negligible CO content in the H₂-rich stream, the methanol conversion and CO selectivity were used as the responses for evaluation.

The standard experimental matrix for a full 2^4 factorial design with four central points was designed as shown in Table 3.1. The factor levels on the natural scale were encoded as +1 for the high level, 0 for the central point and -1 for the low level. To minimize errors, the experiments were performed in a completely random order. The Design-Expert 5.0 software package (Stat Ease Inc. Minneapolis, USA) was used for the statistical analysis, such as analysis of variance (ANOVA), regression coefficients, % contribution, evaluation of the half-normal probabilities of the residues and the Pareto chart of absolute standardized effects at a 95% confidence interval. The catalytic performances were displayed in terms of the methanol conversion (%) and CO selectivity (%), computed from Eq. (3.1) and Eq. (3.3), respectively

- *Response surface methodology (RSM) [81]*

After screening the four factors for any significant effects upon the methanol conversion efficiency and CO selectivity with the factorial design, a central composite rotatable design (CCRD) with two independent screened factors was designed as shown in Table 3.2. This model subsequently adopted in order to optimize the conditions for complete methanol conversion with a minimal CO selectivity in a SRM unit with 5 wt% Au/CuO–CeO₂ catalysts.

- *Validation of the model*

To investigate the accuracy of the developed model, the two independent screened factors which were predicted to have the major influence on the methanol conversion with a minimal CO selectivity, as obtained from the RSM were randomly selected within the given levels. The other two screened factors were held

constant at their evaluated optimal levels. Six sets of experiments were then designed and employed.

Table 3.1 Experimental variables over Au/CuO–CeO₂ in coded and actual unit for a full 2⁴ factorial design with four central points in the standard order from 1 to 20

Factors	Variables	Unit	Low (-1)	Medium (0)	High (1)
A	Temperature	°C	250	300	350
B	S/M ratio	–	1	1.5	2
C	Liquid feed rate	cm ³ h ⁻¹	1	2	3
D	W/F ratio	g s cm ⁻³	0.13	0.17	0.24

Standard order	Run order	A	B	C	D
1	8	-1	-1	-1	-1
2	3	1	-1	-1	-1
3	2	-1	1	-1	-1
4	6	1	1	-1	-1
5	20	-1	-1	1	-1
6	1	1	-1	1	-1
7	12	-1	1	1	-1
8	4	1	1	1	-1
9	11	-1	-1	-1	1
10	19	1	-1	-1	1
11	9	-1	1	-1	1
12	16	1	1	-1	1
13	10	-1	-1	1	1
14	18	1	-1	1	1
15	13	-1	1	1	1
16	15	1	1	1	1
17	7	0	0	0	0
18	17	0	0	0	0
19	5	0	0	0	0
20	12	0	0	0	0

Table 3.2 Experimental variables for the central composite rotatable design (CCRD)

Factors	Variables	Unit	Low (-1)	Medium (0)	High (1)
A	Temperature	°C	250	300	350
B	S/M ratio	–	1	1.5	2

Standard order	Run order	A	B
1	9	250	1
2	2	350	1
3	8	250	2
4	10	350	2
5	5	229 (- α)	1.5 (0)
6	1	371 (- α)	1.5 (0)
7	4	300 (0)	0.8 (- α)
8	3	300 (0)	2.2 (- α)
9	7	300	1.5
10	11	300	1.5
11	6	300	1.5

α (Rotatable) = 1.41421

All experiments in SRM unit can be concluded as shown in Table 3.3.

Table 3.3 SRM unit experiments

Section I: Catalysts comparison

Catalyst	Preparation method	Calcination temperature (°C)	Gas treatment	Operating temperature (°C)	Steam to methanol (S/M) ratio	Liquid feed rate (cm ³ h ⁻¹)	Catalyst weight to He flow rate (W/F) (g s cm ⁻³)
MegaMax 700	-	-	-	200–300	1.5	3	0.17
(50:50)CuO–CeO ₂	CP	500	-	200–300	1.5	3	0.17
Au/CuO	DP	350	-	200–300	1.5	3	0.17
Au/(84:16)CuO–CeO ₂	DP	350	-	200–300	1.5	3	0.17
Au/(63:37)CuO–CeO ₂	DP	350	-	200–300	1.5	3	0.17
Au/(50:50)CuO–CeO ₂	DP	350	-	200–300	1.5	1.5–3	0.17
Au/(37:63)CuO–CeO ₂	DP	350	-	200–300	1.5	3	0.17
Au/(16:84)CuO–CeO ₂	DP	350	-	200–300	1.5	3	0.17
Au/CeO ₂	DP	350	-	200–300	1.5	3	0.17

Section II: Statistical design

Catalyst	Preparation method	Calcination temperature (°C)	Gas treatment	Operating temperature (°C)	Steam to methanol (S/M) ratio	Liquid feed rate (cm ³ h ⁻¹)	Catalyst weight to He flow rate (W/F) (g s cm ⁻³)
Au/(50:50)CuO–CeO ₂	DP	350	-	200–400	1–2	1–3	0.13–0.24

3.3.2 Preferential oxidation (PROX) of CO unit

In this unit, it presented as following: a catalyst preparation method, characterization of the prepared catalysts, catalytic activity measurement. After that statistical design of the experiments over the effective catalyst were then mentioned in order to evaluate an importance of factors chosen. Finally, optimization for PROX over the effective catalyst was determine by using response surface methodology (RSM)

3.3.2.1 Catalyst preparation

- Support preparation

Synthesized ceria prepared by sol-gel method. Two solutions of $\text{Ce}(\text{NO}_3)_3 \cdot 6\text{H}_2\text{O}$ and urea were prepared by mixing 0.1 M of $\text{Ce}(\text{NO}_3)_3 \cdot 6\text{H}_2\text{O}$ with 0.4 M of urea solution. The mixed solution was aged at 100 °C for 50 h. After that the precipitate was washed with deionized water and ethanol several times to eliminate excess ions. The support was dried overnight at 110 °C and calcined at 300 °C for 2 h in air.

- Supported catalyst preparation

Impregnation on sol-gel (ISG)

The catalysts were obtained by co-impregnating the appropriate amount of an aqueous solution of $\text{H}_2\text{PtCl}_6 \cdot 6\text{H}_2\text{O}$ and $\text{HAuCl}_4 \cdot 3\text{H}_2\text{O}$ onto the commercial ceria and synthesized ceria supports. The catalysts (denoted as PtAu/CeO₂-ISG) were then dried at 110 °C for 24 h and calcined at 500 °C for 5 h.

Single step sol-gel (SSG)

The catalysts were prepared from aqueous solution of $\text{H}_2\text{PtCl}_6 \cdot 6\text{H}_2\text{O}$ and $\text{HAuCl}_4 \cdot 3\text{H}_2\text{O}$ in an aqueous mixture of solution 3:1 volume ratio of $\text{Ce}(\text{NO}_3)_3 \cdot 6\text{H}_2\text{O}$ and urea. The solution was aged at $100\text{ }^\circ\text{C}$ for 50 h. The precipitate was then washed with deionized water and ethanol several. The catalysts (denoted as PtAu/CeO₂-SSG) were dried at $110\text{ }^\circ\text{C}$ for 24 h and calcined at $500\text{ }^\circ\text{C}$ for 5 h.

Co-precipitation (CP)

An aqueous solution of $\text{H}_2\text{PtCl}_6 \cdot 6\text{H}_2\text{O}$, $\text{HAuCl}_4 \cdot 3\text{H}_2\text{O}$, and $\text{Ce}(\text{NO}_3)_3 \cdot 6\text{H}_2\text{O}$ was placed in a continuously stirred flask, simultaneously adding Na_2CO_3 . During the stirring of the mixed solution, the temperature of the solution was maintained at $80\text{ }^\circ\text{C}$ while the pH was held at around 8 for 1 h. The resulting precipitate was washed with warm deionized water several times. After that, it was dried overnight at $110\text{ }^\circ\text{C}$. The catalysts (denoted as PtAu/CeO₂-CP) were calcined at $500\text{ }^\circ\text{C}$ for 5 h. To prepare the PtAu/(x:y)CeO₂-ZnO catalysts, the method was the same as mentioned above for the PtAu/CeO₂-CP, except for the simultaneous addition of an aqueous solution of $\text{Zn}(\text{NO}_3)_2 \cdot 4\text{H}_2\text{O}$ to the mixed solution at the beginning. The active metal (Pt–Au) of the catalysts was maintained at 1 wt% and the ratio of the Pt to Au was held at 1:1.

3.3.2.2 Catalyst characterization

- *Brunauer–Emmett–Teller (BET) surface area:* The BET method was used to determine the surface area of the catalyst by N_2 adsorption/desorption at $-196\text{ }^\circ\text{C}$ (Micromeritics ASAP 2020).

- *X-ray diffraction (XRD):* A Rigaku XRD system equipped with a RINT 2000 wide-angle goniometer employing CuK_α radiation ($\lambda = 1.54\text{ \AA}$) and an

X-ray power of 40 kV/30mA was used to examine the crystalline structure. The particle diameter was calculated by the Debye–Scherrer equation at the X-ray line broadening of the (1 1 -1) diffraction peak for CuO and the (1 1 1) diffraction peak for CeO₂.

- *X-ray fluorescence spectrometry (XRF)*: XRF (Philips, model: PW-2400) was used to determine the composition (relative proportion) in the catalyst.

- *Temperature-programmed reduction (TPR)*: TPR was used to investigate the reduction temperature of the catalysts. The catalysts were pretreated in a U-shaped quartz reactor under an Ar flow rate of 40 cm³ min⁻¹ at 300 °C for 2 h. After this pretreatment, the catalysts were cooled to the room temperature. A reducing gas of 10% (v/v) H₂ in Ar was then introduced into the reactor at a flow rate of 40 cm³ min⁻¹ and the catalysts were heated up to 500 °C at a rate of 10 °C min⁻¹. A thermal conductivity detector (TCD) was employed to determine an amount of H₂ uptake.

- *H₂ chemisorption*: The analysis was used to obtain metallic particle size and metallic surface area in catalyst. In preparation, the catalysts were pretreated in a reducing gas of 10% (v/v) H₂ in Ar of 40 cm³ min⁻¹ and were heated up to 400 °C at a rate of 10 °C min⁻¹. The catalysts were hold at 400 °C for 2 h and were then cooled to the room temperature. After this pretreatment, 10% (v/v) H₂ in Ar was filled into the catalysts surface as a pulse function until to equilibrium for analyzing.

- *Scanning electron microscopy (SEM)*: The particle morphology of the catalysts was observed by SEM using a JEOL JSM-5800 LV microscope was operated at 15 kV in bright and dark field modes.

- *Transmission electron microscopy (TEM)*: TEM was carried out using a JEM 2010TEM, operating at 200 kV in bright and dark field modes, to obtain information about the morphology of the catalyst.

- *Fourier transform infrared spectrometer (FTIR)*: The FTIR spectra have been collected on a Perkin-Elmer 2000 spectrometer (Spectrum one) equipped with a MCT detector to record wave number range of functional group.

3.3.2.3 Catalytic activity measurement

- *Catalysts comparison*

The catalytic activity was carried out in a fixed-bed reactor at atmospheric pressure. The U-tube reactor had a 6 mm inner diameter. A 0.1–0.3 g catalyst sample was placed between two layers of quartz wool. The total flow rate was equal to $50 \text{ cm}^3 \text{ min}^{-1}$ (W/F ratio = $0.12\text{--}0.36 \text{ g s cm}^{-3}$). The feedstream consisted of 1% CO, 1–2% O₂, 0–10% H₂O, 0–20% CO₂, and 40% H₂ in He balance. The operating temperature was 50 °C to 190 °C. To investigate the effects of the double-stage reactor on the catalytic activity, 1:1 of the catalysts weight ratio were put into each reactor. The effluent from the first reactor was then passed directly to the second reactor, thereby providing the double-stage reactor. The total O₂ was split to two reactors at various ratios. Prior to all of the catalytic tests, the prepared catalysts were subject to various pretreatments with different procedures. In the case of H₂ pretreatment, the catalysts were heated in flowing H₂ at 400 °C (heating rate = 10 °C min^{-1}) for 2 h. In the case of pretreatment under O₂ conditions, the catalysts were heated in flowing O₂ at 110 °C (heating rate = 10 °C min^{-1}) for 30 min. After pretreatment, pure He was then injected into the reactor to cool it down to room temperature. The influent and effluent components were analyzed by an on-line gas

chromatograph (Agilent Technologies, model 6890 N) equipped with a carbosphere column and a thermal conductivity detector (TCD). Helium was used as the carrier gas. The experimental data were displayed in terms of CO conversion and selectivity, which were calculated based on CO consumption, as shown below:

$$CO\ conversion(\%) = \frac{[CO]_{in} - [CO]_{out}}{[CO]_{in}} \times 100 \quad (3.4)$$

$$CO\ selectivity(\%) = \frac{0.5 \times ([CO]_{in} - [CO]_{out})}{[O_2]_{in} - [O_2]_{out}} \times 100 \quad (3.5)$$

where $[CO]_{in}$ is the concentration of CO in the feedstream, $[CO]_{out}$ is the concentration of CO in the effluent, $[O_2]_{in}$ is the concentration of O₂ in the feedstream, and $[O_2]_{out}$ is the concentration of O₂ in the effluent.

- *Statistical design of experiment* [81]

A factorial design was carried out to evaluate the effect of factors and interaction among the factors on the catalytic activities for PROX of CO by varying one factor with the level of the other factors. In this work, the three independent factors chosen were an operating temperature (°C, factor A), H₂O content (% , factor B), and CO₂ content (% , factor C) in the reformat gas. The other factors that affect the catalytic activities, including of a catalyst weight to total gas flow rate (W/F), catalyst type, and reactor volume were held constant throughout the experiments. CO conversion and selectivity were used as a response. The experimental matrix for a full 2³ factorial design with three central points was then designed and employed, as shown in Table 3.4. The experiments were done in a completely random order to minimize errors due to systematic trends in the factors. The factor levels on the natural scale were encoded in a dimensionless scale as +1 for the high level, 0 for the

central point and -1 for the low level. Design–Expert 5.0 software package (Stat Ease Inc. Minneapolis, USA) was employed to treat the experimental data and to generate a statistical analysis at 95% confidence interval, such as normal probability of the residues, the Pareto chart of absolute standardized effect, an analysis of variance (ANOVA) table, and % contribution.

- *Response surface methodology (RSM)* [81]

After screening the three factors for any significant effects upon the CO conversion and selectivity with the factorial design, the first two important factors were selected to a response surface analysis. FCCCD with the two independent screened factors was applied sequentially to optimize the PROX of CO conditions by simultaneously considering CO conversion and CO selectivity, as shown in Table 3.5. A standard ANOVA at 95% confidence interval was then carried out to treat the response surface models.

- *Validation of the model*

The two independent screened factors which were evaluated to have the major influence on CO conversion and CO selectivity were randomly selected within the given levels to investigate the accuracy of the developed model as obtained from the RSM. Another screened factor was held constant at their evaluated levels. Two sets of 6 experiments were then designed and employed under a feed condition of simulating reformat gas. Residual distribution plot, which is a tool of statistical analysis for determining a validation of the model, was then employed.

All experiments in PROX unit can be concluded as shown in Table 3.6.

Table 3.4 Statistically designed set of PROX-experiments over PtAu/CeO₂-ZnO catalyst for a full 2³ factorial design with three central points

Factors	Variables	Unit	Low (-1)	Medium (0)	High (1)
A	Temperature	°C	50	120	190
B	H ₂ O content	%	0	5	10
C	CO ₂ content	%	0	10	20

Standard order	Run order	A	B	C
1	9	-1	-1	-1
2	10	1	-1	-1
3	6	-1	1	-1
4	3	1	1	-1
5	11	-1	-1	1
6	2	1	-1	1
7	1	-1	1	1
8	4	1	1	1
9	5	0	0	0
10	7	0	0	0
11	8	0	0	0

Table 3.5 Experimental variables for faced-centered central composite design (FCCCD) of response surface methodology with three central points over PtAu/CeO₂-ZnO

Factors	Variables	Unit	Low (-1)	Medium (0)	High (1)
A	Temperature	°C	90	120	150
C	CO ₂ content	%	0	10	20

Standard order	Run order	A	C
1	9	90	0
2	2	150	0
3	8	90	20
4	10	150	20
5	5	90	10
6	1	150	10
7	4	120	0
8	3	120	20
9	7	120	10
10	11	120	10
11	6	120	10

Table 3.6 PROX unit experiments

Section I: Catalysts comparison in single-stage reactor

Catalyst	Preparation method	Calcination temperature (°C)	Gas treatment	Operating temperature (°C)	Feed gas composition (%) in He balance	Catalyst weight to He flow rate (W/F) (g s cm ⁻³)
Pt/CeO ₂	SSG	500	H ₂	50–190	H ₂ = 40, O ₂ = 1, CO = 1	0.12
Au/CeO ₂	SSG	500	H ₂	50–190	H ₂ = 40, O ₂ = 1, CO = 1	0.12
PtAu/CeO ₂	ISG	500	H ₂	50–190	H ₂ = 40, O ₂ = 1, CO = 1	0.12
1%(1:1)PtAu/CeO ₂	SSG	500	H ₂	50–190	H ₂ = 40, O ₂ = 1, CO = 1, H ₂ O = 0–10, CO ₂ = 0–20	0.12–0.36
2%(1:1)PtAu/CeO ₂	SSG	500	H ₂	50–190	H ₂ = 40, O ₂ = 1, CO = 1	0.12
3%(1:1)PtAu/CeO ₂	SSG	500	H ₂	50–190	H ₂ = 40, O ₂ = 1, CO = 1	0.12
1%(1:5)PtAu/CeO ₂	SSG	500	H ₂	90	H ₂ = 40, O ₂ = 1, CO = 1	0.12
1%(1:2)PtAu/CeO ₂	SSG	500	H ₂	90	H ₂ = 40, O ₂ = 1, CO = 1	0.12
1%(5:1)PtAu/CeO ₂	SSG	500	H ₂	90	H ₂ = 40, O ₂ = 1, CO = 1	0.12
1%(10:1)PtAu/CeO ₂	SSG	500	H ₂	90	H ₂ = 40, O ₂ = 1, CO = 1	0.12
PtAu/CeO ₂	CP	500	H ₂	50–190	H ₂ = 40, O ₂ = 1, CO = 1	0.12
PtAu/(1:1)CeO ₂ –ZnO	SSG	500	H ₂	50–190	H ₂ = 40, O ₂ = 1, CO = 1	0.12
PtAu/(1:1)CeO ₂ –ZnO	CP	500	H ₂	50–190	H ₂ = 40, O ₂ = 1, CO = 1, H ₂ O = 0–10, CO ₂ = 0–20	0.12–0.36
PtAu/(1:1)CeO ₂ –Fe ₂ O ₃	SSG	500	H ₂	50–190	H ₂ = 40, O ₂ = 1, CO = 1	0.12
PtAu/(1:1)CeO ₂ –Fe ₂ O ₃	CP	500	H ₂	50–190	H ₂ = 40, O ₂ = 1, CO = 1	0.12
PtAu/(1:1)CeO ₂ –ZnO	CP	200	H ₂	50–190	H ₂ = 40, O ₂ = 1, CO = 1	0.12
PtAu/(1:1)CeO ₂ –ZnO	CP	350	H ₂	50–190	H ₂ = 40, O ₂ = 1, CO = 1	0.12
PtAu/(1:1)CeO ₂ –ZnO	CP	500	O ₂	50–190	H ₂ = 40, O ₂ = 1, CO = 1	0.12
PtAu/(1:1)CeO ₂ –ZnO	CP	500	Non	50–190	H ₂ = 40, O ₂ = 1, CO = 1	0.12
PtAu/(10:1)CeO ₂ –ZnO	CP	500	H ₂	50–190	H ₂ = 40, O ₂ = 1, CO = 1	0.12
PtAu/(1:10)CeO ₂ –ZnO	CP	500	H ₂	50–190	H ₂ = 40, O ₂ = 1, CO = 1	0.12

Table 3.6 PROX unit experiments (cont.)

Section II: Optimizing condition in double-stage reactor

Catalyst	Preparation method	Calcination temperature (°C)	Gas treatment	Operating temperature (°C)	Feed gas composition (%) in He balance	O ₂ split ratio	Catalyst weight to He flow rate (W/F) (g s cm ⁻³)
PtAu/CeO ₂	SSG	500	H ₂	50–190	H ₂ = 40, O ₂ = 1–2, CO = 1, H ₂ O = 0–10, CO ₂ = 0–20	4:1, 3:2,1:1, 2:3,1:4	0.12–0.36
PtAu/(1:1)CeO ₂ –ZnO	CP	500	H ₂	50–190	H ₂ = 40, O ₂ = 1, CO = 1, H ₂ O = 0–10, CO ₂ = 0–20	1:1	0.12

Section III: Statistical design in single-stage reactor

Catalyst	Preparation method	Calcination temperature (°C)	Gas treatment	Operating temperature (°C)	Feed gas composition (%) in He balance	O ₂ split ratio	Catalyst weight to He flow rate (W/F) (g s cm ⁻³)
PtAu/(1:1)CeO ₂ –ZnO	CP	500	H ₂	100–140	From SRM unit	Optimum	Optimum

3.3.3 Integration of SRM unit and PROX unit

The effective catalysts in each unit were carried out for producing H₂ via an integration of SRM and PROX unit. The SRM unit was operated the optimum condition from section 3.3.1 while the PROX unit that used the effective catalyst to achieve pure H₂-rich stream. To eliminate CO content to the accepted level (50 ppm), the double-stage reactor in PROX unit was performed at the optimum condition from section 3.3.2.

All experiments in integration of SRM and PROX unit can be concluded as shown in Table 3.7.

Table 3.7 Integration of SRM and PROX unit for H₂ production experiments

SRM unit

Catalyst	Preparation method	Calcination temperature (°C)	Gas treatment	Operating temperature (°C)	Steam to methanol (S/M) ratio	Liquid feed rate (cm³ h⁻¹)	Catalyst weight to He flow rate (W/F) (g s cm⁻³)
Au/(50:50)CuO–CeO ₂	DP	350	-	Optimum	Optimum	Optimum	Optimum

PROX unit

Catalyst	Preparation method	Calcination temperature (°C)	Gas treatment	Operating temperature (°C)	Feed gas composition (%) in He balance	O₂ split ratio	Catalyst weight to He flow rate (W/F) (g s cm⁻³)
PtAu/(1:1)CeO ₂ –ZnO	CP	500	H ₂	100–140	From SRM unit	Optimum	Optimum

CHAPTER IV

HYDROGEN PRODUCTION VIA STEAM REFORMING OF METHANOL*

In this chapter, the production of hydrogen (H_2) with a low concentration of carbon monoxide (CO) via steam reforming of methanol (SRM) over Au/CuO, Au/CeO₂, (50:50)CuO–CeO₂, Au/(50:50)CuO–CeO₂, and commercial MegaMax 700 catalysts were investigated over reaction temperatures between 200 °C to 300 °C at atmospheric pressure. Au loading in the catalysts was maintained at 5 wt%. Supports were prepared by co-precipitation (CP) while all prepared catalysts were synthesized by deposition–precipitation (DP). The characterization of catalysts were presented in section 4.1 The effect of types of supported Au catalysts, atomic ratio of Cu:Ce, and liquid feed rate on the catalytic activities in steam reforming of methanol were determined and discussed in section 4.2. Stability test was also studied and described in section 4.2.

4.1 Catalyst characterization

The crystalline phases of the prepared catalysts were investigated by XRD

* Submitted

(Figure 4.1), where the Au/CuO and Au/CuO–CeO₂ catalysts with various Cu:Ce atomic ratios did not present any reflection peak of Au oxide species ($2\theta = 25.5^\circ$, 30.2° , and 32.5°) or metallic Au species ($2\theta = 38.2^\circ$, 44.4° , and 64.5°). This may be due to the presence of the Au as highly dispersed nano-particles on the surface [33,31] and/or the overlap between CuO and Au peaks. The actual Au loading levels, as determined from X-ray fluorescence (XRF) analysis (Table 4.1), was close to the nominal one. However, the XRD patterns of Au/CeO₂ catalysts reveal the metallic Au phase at $2\theta = 38.2^\circ$ and the CeO₂ phase.

In all fresh catalyst samples except the Au/CeO₂ catalyst, the main reflections of the peaks correspond to CeO₂ phase (cerianite) and CuO phase (tenorite) for Au/CuO–CeO₂ catalysts with various Cu:Ce atomic ratios and to CuO phase for Au/CuO catalyst. The broadened peaks of CeO₂ phase are presented when varying Cu:Ce atomic ratios in the Au/CuO–CeO₂ catalysts. Thus, the CuO particles are seemingly integrated into CeO₂ lattice and form a solid solution. This is in good agreement with that reported before by the others [16,20,21,27]. Moreover, the intensity of XRD peaks that correspond to CuO crystallite phases, especially at $2\theta = 35.5^\circ$ and 38.7° , increased as the copper content in the catalysts increased. Lui et al. [27] explained that only a part of the smaller size Cu²⁺ could enter the CeO₂ lattice to form a solid solution and the rest of the Cu²⁺ forms metal oxide particles on the surface of the CeO₂ lattice. Since the copper in the catalysts is in the form of CuO, the crystallite size of CuO and CeO₂ was determined using the Debye–Scherrer equation, and the results are summarized in Table 4.1.

The ceria crystallite size of all the Au/CuO–CeO₂ catalysts was significantly smaller than that in the Au/CeO₂ catalyst, being smallest at a 50:50 Cu:Ce atomic

ratio (2.5-fold smaller than those in the Au/CeO₂ particles), but even the largest ceria crystallite size in the Au/CuO–CeO₂ catalysts, found in the 16:84 Cu:Ce atomic ratio composition, was still 1.8-fold smaller than that in the Au/CeO₂ catalyst. However, the smallest ceria crystallite size was found in the CuO–CeO₂ catalyst. The CuO crystallite size of all the different Au/CuO–CeO₂ catalysts was also smaller than that of the CuO–CeO₂ catalyst, being minimal at a Cu:Ce atomic ratio of 63:37 (2.7-fold smaller than that in the CuO–CeO₂), and increasing in size with larger or smaller Cu:Ce atomic ratios, but the largest CuO crystal size in the Au/CuO–CeO₂ catalysts, in the 37:63 atomic ratio) was still some 1.2-fold smaller than that in the CuO–CeO₂.

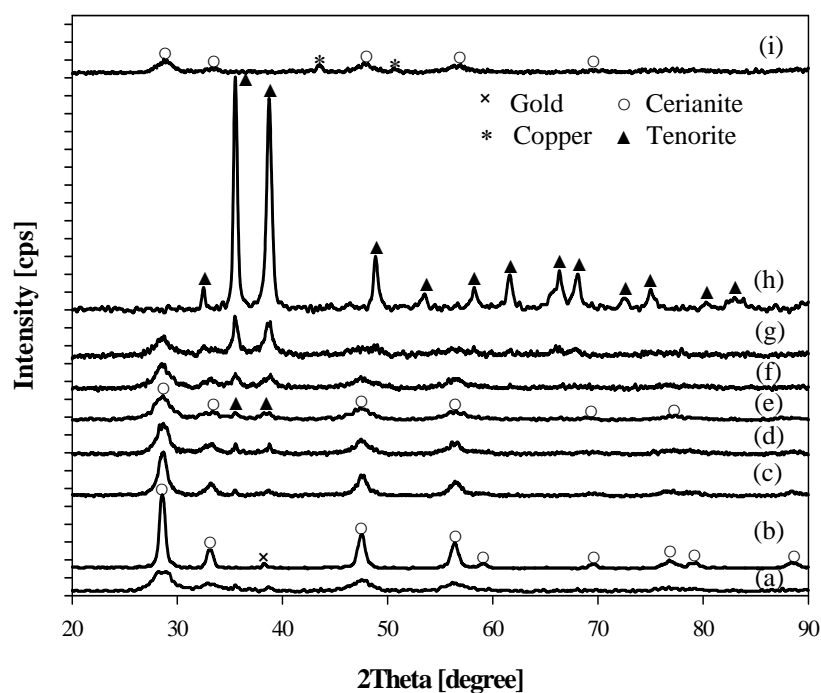


Figure 4.1 XRD patterns of the catalysts: (a) (50:50)CuO–CeO₂, (b) Au/CeO₂, (c) Au/(16:84)CuO–CeO₂, (d) Au/(37:63)CuO–CeO₂, (e) Au/(50:50)CuO–CeO₂, (f) Au/(63:37)CuO–CeO₂, (g) Au/(84:16)CuO–CeO₂, (h) Au/CuO, and (i) Au/(50:50)CuO–CeO₂ spent catalyst for 2 h.

Table 4.1 Characteristics of prepared catalysts

Catalyst	Au (%) nominal	Au (%) real ^a	S _{BET} ^b (m ² g ⁻¹)	Pore volume ^b (cm ³ g ⁻¹)	CuO crystallite size ^c (nm)	CeO ₂ crystallite size ^c (nm)
MegaMax700 [*]	-	-	69.7	0.23	-	-
CuO–CeO ₂	-	-	83.2	0.30	38.6	4.9
Au/CuO	5	4.5	16.5	0.04	22.8	-
Au/(84:16)CuO–CeO ₂	5	4.2	39.3	0.11	17.8	5.9
Au/(63:37)CuO–CeO ₂	5	4.0	74.9	0.26	14.1	6.4
Au/(50:50)CuO–CeO ₂	5	4.3	77.3	0.29	19.7	5.5
Au/(37:63)CuO–CeO ₂	5	4.1	63.0	0.14	33.4	7.2
Au/(16:84)CuO–CeO ₂	5	3.8	22.0	0.14	29.5	7.6
Au/CeO ₂	5	4.8	44.5	0.09	-	13.7

^{*} Commercial catalyst

^a Determined by XRF

^b Determined by BET surface area analyzer

^c Determined by XRD from line broadening of CuO (1 1 -1) peak and CeO₂ (1 1 1) peak

Overall, this most probably indicated that Au had an influence on the interaction between CuO and CeO₂. Along these lines Papavasiliou et al. [16] reported that a smaller dispersion of CuO may be attributed to the perturbation of the interaction between copper and cerium ions by the dopants. The XRD pattern of the spent Au/(50:50)CuO–CeO₂ catalyst (Figure 4.1i) shows that the peaks corresponding to CuO phases at $2\theta = 35.5^\circ$ and 38.7° were not observed, while the peaks at $2\theta = 43.3^\circ$ and 50.4° attributed to metallic copper were observed, consistent with the reduction of CuO to metallic copper during the reaction. Yang et al. [30] and Ou et al. [31] reported that CuO species in their catalysts were reduced by H₂ product stream in POM.

The specific BET surface area and pore volume of the catalysts are also shown in Table 4.1, which reveals that when Au was deposited on the (50:50)CuO–CeO₂, the surface area of Au/(50:50)CuO–CeO₂ is slightly less (1.1-fold) than that of

(50:50)CuO–CeO₂. In the case of Au/CuO–CeO₂ catalysts with various Cu:Ce atomic ratios, the surface area is lower still and varies with the atomic ratios in biphasic manner, being highest at a 50:50 Cu:Ce atomic ratio (still 1.1-fold smaller than that of CuO–CeO₂) and then decreasing with either increasing or decreasing Cu levels to a minimal BET surface area in the 16:84 Cu:Ce atomic ratio support (3.8-fold lower than that of CuO–CeO₂). The pore volumes largely follow the BET surface area, and so the Au/(50:50)CuO–CeO₂ catalyst had the highest surface area and largest pore volume. This biphasic response to changing Cu:Ce atomic ratios is in partial contrast to Udani et al. [20], who reported that the catalyst surface area decreased with increasing copper content.

The reduction property of the catalysts used in this work was investigated by H₂-TPR. From all TPR profiles (Figure 4.2), the reduction process was completed before 275 °C. All the catalysts, except Au/CeO₂ catalyst, presented their instinctive reduction peak. No reduction peak of Au/CeO₂ (see Figure 4.2b) was observed since the gold particles in the catalysts are presented in a metallic state, as confirmed by XRD pattern (see Figure 4.1b) and/or a lower amount of Au oxides is loaded in catalysts [31]. Therefore, it can be concluded that the appeared peaks correspond to the reduction peaks of CuO species. A comparison of the reduction peaks of the (50:50)CuO–CeO₂ catalysts with that for the Au/CuO–CeO₂ catalysts with various Cu:Ce atomic ratios (see Figures 4.2 a, c–g), reveals that the reduction temperature of the (50:50)CuO–CeO₂ catalysts is higher.

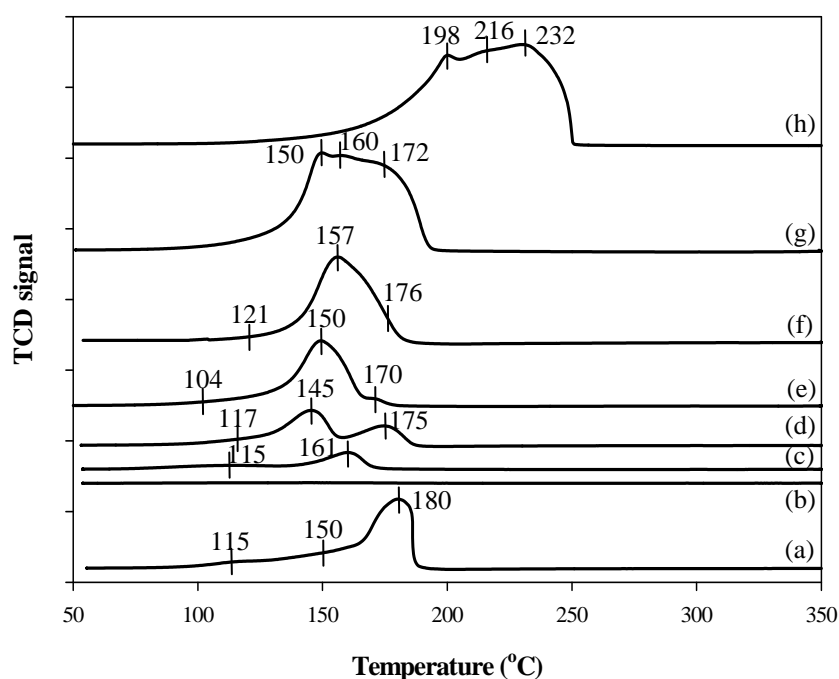


Figure 4.2 TPR profiles of the catalysts: (a) (50:50)CuO–CeO₂, (b) Au/CeO₂, (c) Au/(16:84)CuO–CeO₂, (d) Au/(37:63)CuO–CeO₂, (e) Au/(50:50)CuO–CeO₂, (f) Au/(63:37)CuO–CeO₂, (g) Au/(84:16)CuO–CeO₂, and (h) Au/CuO.

This suggests that Au promotes the CuO reduction and shift to lower temperatures. Additionally, the presence of un-oxidized Au weakened the Cu–O bond, presumably due to some sort of interaction between the Au and CuO, in the Au/CuO–CeO₂ catalysts with various Cu:Ce atomic ratios, and that this interaction can enhance the reducibility of CuO [30,31]. When increasing the Cu:Ce atomic ratio to 50:50 for the Au/CuO–CeO₂ catalysts, reduction peaks were visible that likely represent due to two steps for CuO reduction. CuO is first reduced to Cu⁺ and then the Cu⁺ is reduced

to Cu^0 [30,31]. Avgouropoulos et al. [82] pronounced that there are three overlapping reduction peaks in H_2 -TPR of CuO-CeO_2 : a low intensity, low temperature peak ascribed to the reduction of copper ions strongly interacting with CeO_2 , and two peaks of higher intensity that represent the reduction of larger CuO particles that are less strongly associated with CeO_2 . From Figure 4.2, it is also noteworthy that the peak area and its intensity increased significantly as the Cu:Ce atomic ratio increased [20]. These peaks were overlapping and became a larger single peak as the Cu:Ce atomic ratio increased. Thus, there is more than one step or one copper species involved in the reduction process of CuO . However, the minimum reduction temperature revealed a biphasic response when the Cu:Ce atomic ratio in the Au/CuO-CeO_2 catalysts was increased up to 50:50 and shifted back to a higher temperature with further increases in this ratio. Again, this is in partial contrast to Udani et al. [20] who reported an upward shift in the reduction temperature with increasing copper content in the catalysts.

Figure 4.3 illustrates representative SEM images of the CuO , CeO_2 , (50:50) CuO-CeO_2 , and $\text{Au/(50:50)CuO-CeO}_2$ catalysts. The CuO catalyst shows a cluster of small spherical shapes (Figure 4.3a) while the CeO_2 particles show a more needle-bar shape (Figure 4.3b). The (50:50) CuO-CeO_2 catalysts, with or without the 5% Au show agglomerated particles becoming larger cluster particles (Figures 4.3 c and d).

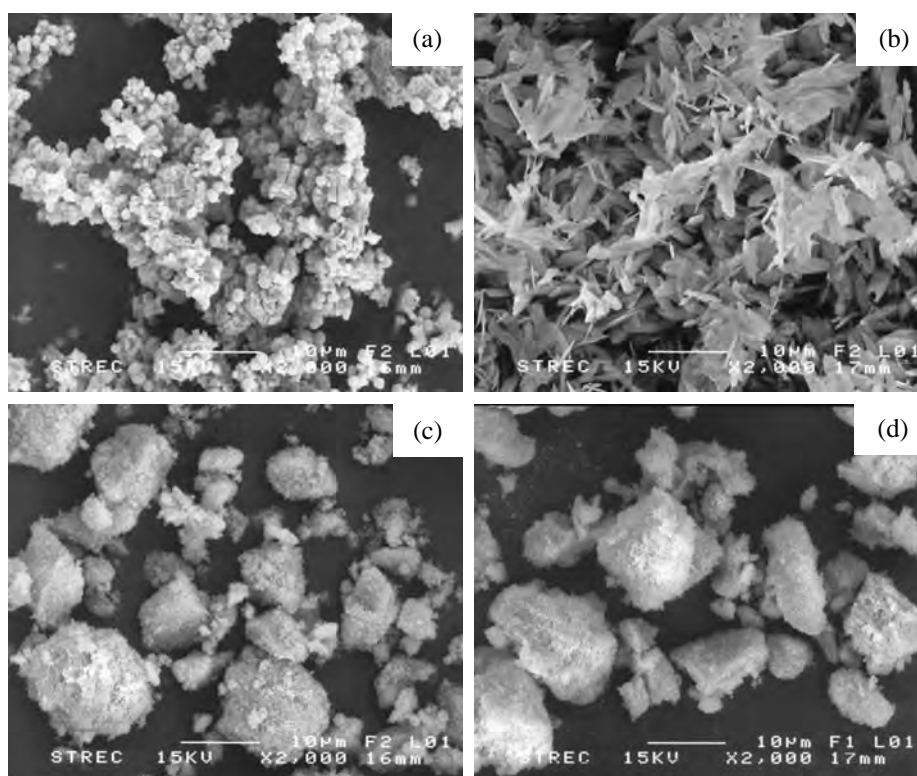


Figure 4.3 SEM images of the prepared: (a) CuO, (b) CeO₂, (c) (50:50)CuO–CeO₂, and (d) Au/(50:50)CuO–CeO₂ catalysts.

4.2 Catalytic activity

4.2.1 Supported Au catalysts

In this research, H₂-rich stream with a low concentration of CO can be produced from SRM. The catalytic activities and product distribution in SRM over the Au/CuO, Au/CeO₂, (50:50)CuO–CeO₂, Au/(50:50)CuO–CeO₂, and commercial MegaMax 700 catalysts are presented in terms of the level of methanol conversion (%), H₂ selectivity (%), and CO selectivity (%) over reaction temperatures between 200 °C to 300 °C, as

shown in Figure 4.4. Steam to methanol (S/M) ratio, liquid feed rate, and catalyst weight to He flow rate (W/F) ratio were constant at 1, 3 cm³ h⁻¹, and 0.17 g s cm⁻³, respectively. The level of methanol conversion (%) and CO selectivity (%) both increased with increasing temperature for all catalysts, albeit to varying degrees between the catalysts. In contrast, the H₂ selectivity showed only a slight numeric decrease in most cases (Au/CeO₂ actually increased from 200 °C to 260 °C and then decreased at 300 °C) within this reaction temperature range. At a reaction temperature of 300 °C, the Au/(50:50)CuO–CeO₂ catalyst produced a slightly higher methanol conversion level than the commercial MegaMax 700, and significantly more than any of the (50:50)CuO–CeO₂, Au/CuO, and Au/CeO₂ catalysts, respectively. However, at lower 300 °C, the % methanol conversion level was significantly higher with the commercial MegaMax 700 catalyst than that seen with any of the other ones. The ordering of CO selectivity over the reaction temperature was commercial MegaMax 700 (3.20) >>>>, Au/CeO₂ (0.95) > Au/CuO (0.70) ≅ (50:50)CuO–CeO₂ (0.65) > Au/(50:50)CuO–CeO₂ (0.43), where the numbers in the parenthesis refer to the CO selectivity at 300 °C. Au/CuO and Au/CeO₂ seem to be least active for the SRM reaction compared to the others.

Normally, Au catalysts are active for CO oxidation and the WGS reaction when supported on a transition metal oxide. Nevertheless, the catalytic performance of supported Au catalysts depends on their size and dispersion [36,37]. In this work, Au/CuO catalysts expressed higher methanol conversion with a lower CO selectivity than that for Au/CeO₂, revealing the likely contribution of CuO as an active component for SRM. Moreover, more CO is consumed in the water–gas shift due to the enhanced CuO reducibility (as shown in Figure 4.2).

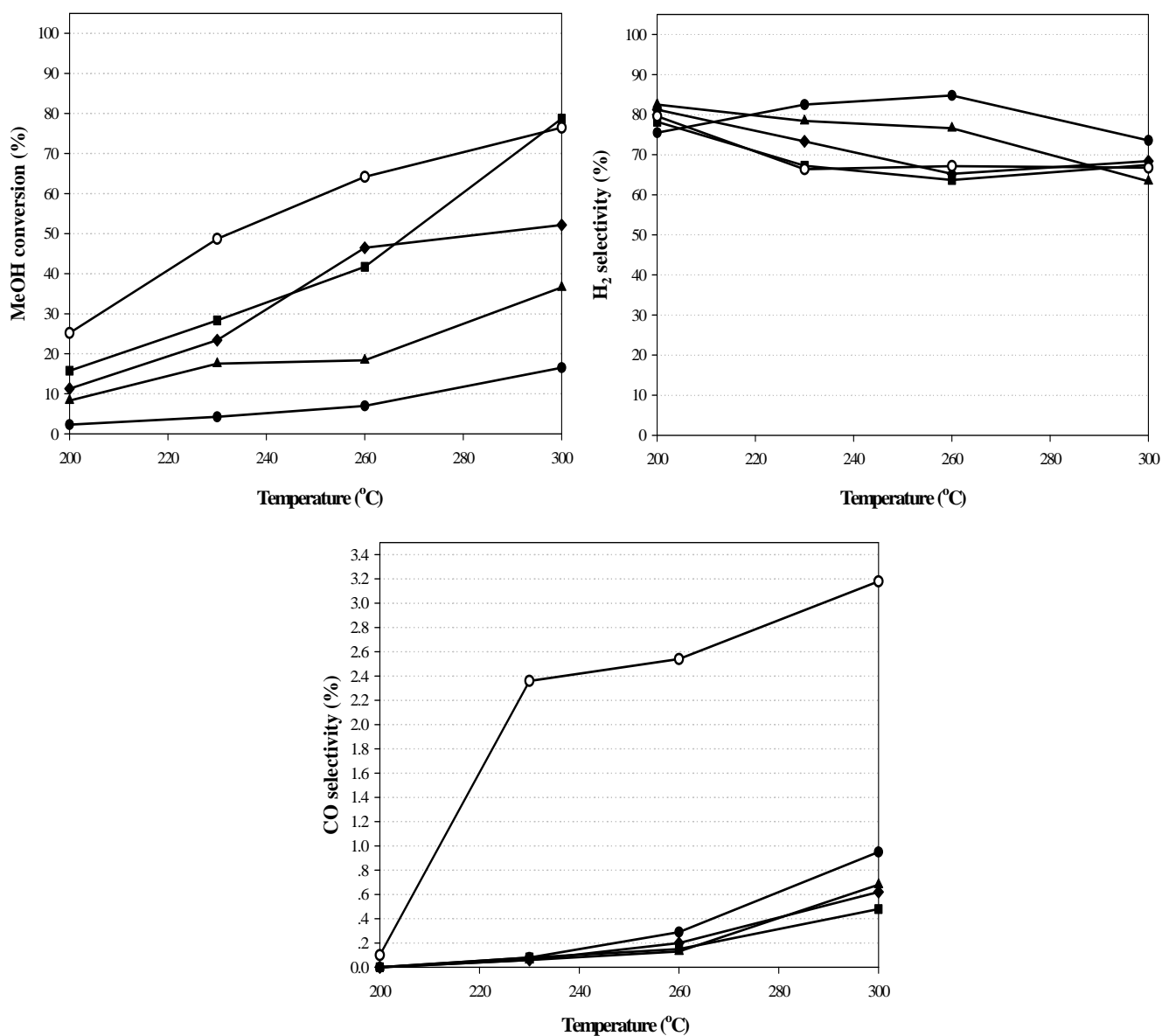


Figure 4.4 Temperature dependent catalytic activity of SRM with (○) MegaMax 700, (◆) (50:50)CuO–CeO₂, and 5 wt% Au doped- catalysts: (▲) Au/CuO, (■) Au/(50:50)CuO–CeO₂, (●) Au/CeO₂ catalysts. Condition: S/M ratio = 1.5, Liquid feed rate = 3 cm³ h⁻¹, W/F ratio = 0.17 g s cm⁻³ at atmospheric pressure.

It is interesting to note that the (50:50)CuO–CeO₂ catalyst presented a higher methanol conversion than that for that Au/CeO₂ and Au/CuO catalysts, but its CO selectivity was not different from that of the Au/CuO. The Au/(50:50)CuO–CeO₂ catalyst at 300 °C displayed a 30% higher methanol conversion than that of the corresponding (50:50)CuO–CeO₂ one, whilst the CO selectivity was reduced 1.5-fold and was the lowest of all the catalysts. As a result, the Au/(50:50)CuO–CeO₂ catalyst exhibited ~80% methanol conversion with ~0.47% CO selectivity. Note that a larger amount of CO production was observed than that with the commercial MegaMax 700 catalyst under the same conditions. The enhanced performance of the Au/(50:50)CuO–CeO₂ catalysts is due to an integration of CuO particles into the CeO₂ lattice to form a solid solution (as evidenced by XRD) and to the strong interaction of Au and CuO species to promote CuO reduction (as evidenced by TPR). However, the slight change in the H₂ selectivity may reflect that only a low level of H₂ is consumed in the reverse water–gas shift.

This result implies that CO in the effluent comes from decomposition of methanol rather than the reverse water–gas shift. The CO will continue to react with water in water–gas shift. The mechanism for this reaction is displayed in Figure 4.5. There are two path ways that is possible. One is decomposition of methanol followed by water–gas shift and another one is an immediate reaction of methanol and water. To investigate this hypothesis, pure methanol was fed into the reactor. The methanol was decomposed to CO and H₂ significantly. In case of methanol solution, the presented H₂O encouraged water–gas shift reaction resulting in a less CO in the product stream. Therefore, it can be proposed that SRM over Au/(50:50)CuO–CeO₂ catalysts proceeds in two path ways via an immediate reaction of methanol and water

and a combination of decomposition of methanol and water–gas shift [10–15,18,19,21]. In this research, the Au/(50:50)CuO–CeO₂ catalyst was found to be an effective catalyst for the enhancement of H₂ production with negligible levels of CO via SRM. Consequently, the effect of the atomic ratio of CuO to CeO₂ on the catalytic activities was then further studied.

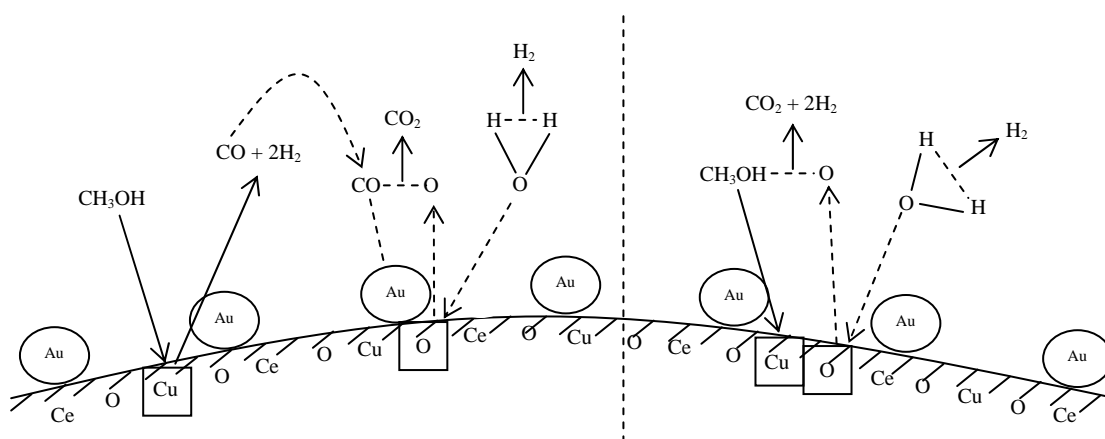


Figure 4.5 Mechanism of H₂ production via SRM over Au/(50:50)CuO–CeO₂ catalyst.

4.2.2 Atomic ratio of Cu:Ce

To study the effect of varying Cu:Ce atomic ratio on the catalytic performance of the resulting supported Au catalysts, the Au loading on the CuO–CeO₂ was fixed at 5 wt%. The level of methanol conversion (%) and the CO selectivity (%) of the Au/CuO–CeO₂ catalysts increased with increasing reaction temperatures for all Cu:Ce atomic ratio based catalysts (a small drop in methanol conversion for the 84:16 atomic ratio as the temperature was increased from 260 °C to 300 °C (Figure 4.6).

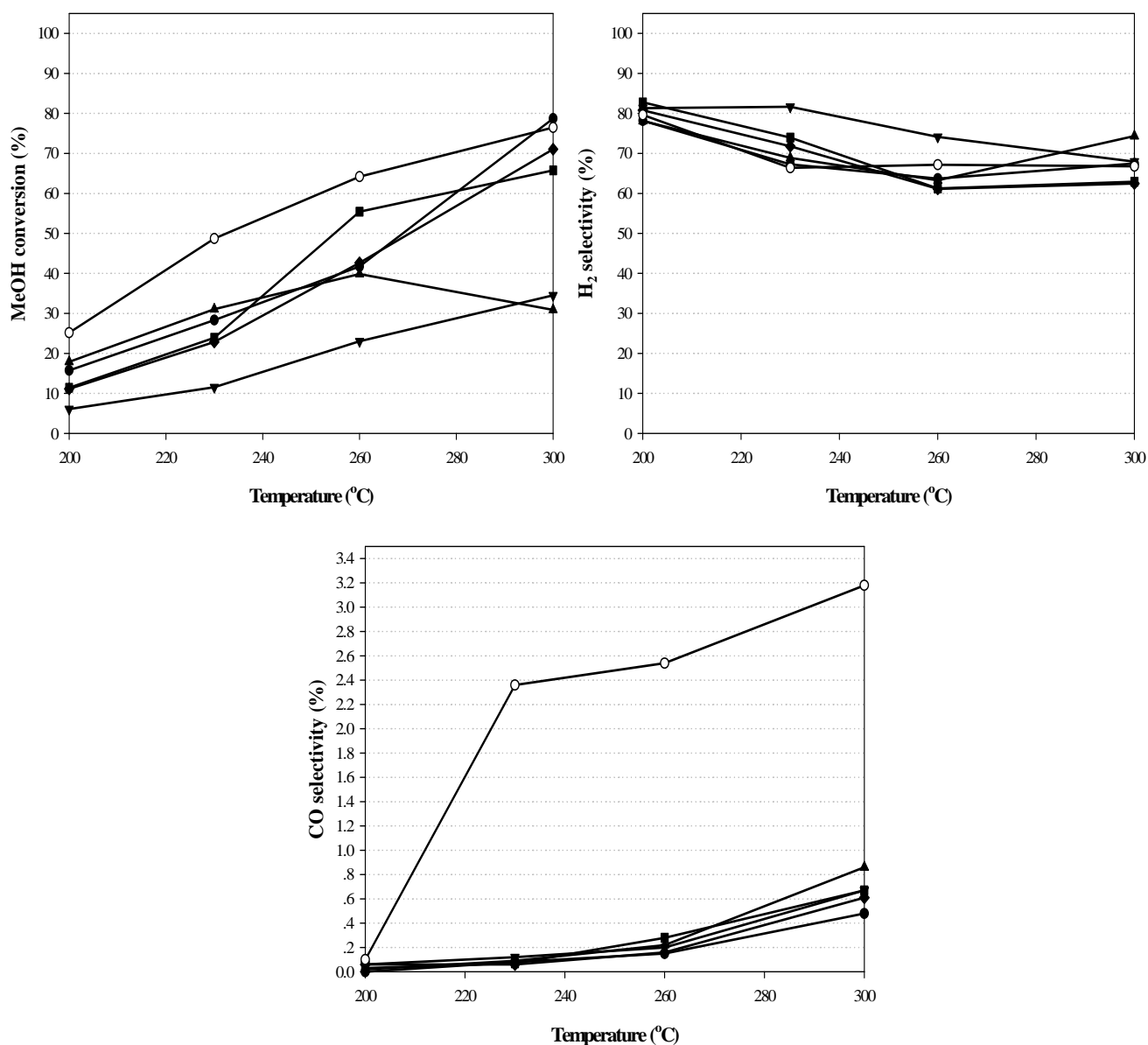


Figure 4.6 Temperature dependent catalytic activity of SRM with (o) MegaMax 700 and supported 5 wt% Au catalysts with various Cu:Ce atomic ratios: (▲) 84:16, (■) 63:37, (●) 50:50, (◆) 37:63, (▼) 16:84 catalysts. Condition: S/M ratio = 1.5, Liquid feed rate = $3 \text{ cm}^3 \text{ h}^{-1}$, W/F ratio = 0.17 g s cm^{-3} at atmospheric pressure.

However, in general a biphasic Cu:Ce ratio-dependence was noted with a higher methanol conversion level and lower CO selectivity being observed with increasing Cu:Ce atomic ratios up to 50:50, with further increasing the Cu:Ce atomic ratio above 50:50 then lowering the methanol conversion level obtained and giving a higher CO selectivity. Nevertheless, the CO selectivity of the prepared catalysts was much lower (e.g. from 4- to 8-fold at 300 °C for the 84:16 and 50:50 Cu:Ce compositions, respectively) than that obtained with the commercial MegaMax 700 catalyst over the whole range of tested reaction temperatures. The methanol conversion, H₂ selectivity, and CO selectivity obtained from the Au/CuO–CeO₂ catalysts with various Cu:Ce atomic ratios were all higher than that of the (50:50)CuO–CeO₂ catalysts, due to the addition of the 5 wt% Au.

Two possible explanations of the Cu:Ce atomic ratio effects on the catalytic performance are the changes in the pore volume and BET surface area of the particles, and the enhancement of the CuO reducibility. Increasing the Cu: Ce atomic ratio up to 50:50 resulted in a larger pore volume and surface area (Table 4.1), which is where the reactions take place. Moreover, more CO is consumed via the WGS reaction due to promoting the reducibility of CuO (Figure 4.2). As a consequence, at 300 °C a higher methanol conversion level (~80%) and H₂ selectivity (~68%), with a significantly lower CO selectivity (~0.47%), is obtained using the Au/(50:50)CuO–CeO₂ catalysts. Increasing the Cu:Ce atomic ratio above 50:50 yielded a lower catalytic activity, presumably due to the resultant smaller pore volume and lower surface area of the catalyst (Table 4.1).

Therefore, this supports the notion that a solid solution of Au supported on CuO–CeO₂ catalysts with an optimum Cu:Ce atomic ratio can promote SRM.

Additionally the catalytic performance depends on the surface area and pore volume of the catalysts. This suggestion is in agreement with our previous work [86], but is in partial contrast to the research reported by Udani et al. [20].

4.2.3 Liquid feed rate

Due to the higher catalytic performance of the Au/(50:50)CuO–CeO₂ catalyst compared to the others tested here, this catalyst formulation was then selected to investigate the effect of liquid feed rate (3 cm³ h⁻¹ and 1.5 cm³ h⁻¹) on its catalytic activities, keeping the other parameters constant. Decreasing the liquid feed rate from 3 cm³ h⁻¹ to 1.5 cm³ h⁻¹ increased the methanol conversion level obtained from ~80% to 100%, the H₂ selectivity from ~68% to ~82% and the CO selectivity from ~0.47% to ~1.3%, respectively (Figure 4.7). Decreasing the liquid feed rate implies a longer reaction time and consequently more reaction can take place. Therefore, an improved catalytic performance for H₂ production from SRM with a lower CO selectivity can be achieved by using a lower liquid feed rate.

4.2.4 Stability test

The stability of the in-house made Au/(50:50)CuO–CeO₂ catalyst and that of the commercial MegaMax 700 catalyst were determined at 300 °C for 540 min with a constant liquid feed rate of 1.5 cm³ h⁻¹. The Au/(50:50)CuO–CeO₂ catalyst gave a higher activity than the commercial MegaMax 700 catalyst for the whole 540 min period of durability testing (Figure 4.8), with both catalysts remaining stable over this

period. Thus, the Au/(50:50)CuO–CeO₂ catalyst is not deactivated during the testing. The XRD pattern (Figure 1i) revealed that CuO was reduced to metallic Cu during the reaction, whilst the durability testing suggested that the catalyst is still active even though the copper is in metallic form. Therefore, it is concluded that metallic Cu is one of active components of the catalysts for SRM. The Au/(50:50)CuO–CeO₂ catalyst prepared by DP appears to be a potential good candidate for a SRM catalyst to produce H₂ with a low CO content.

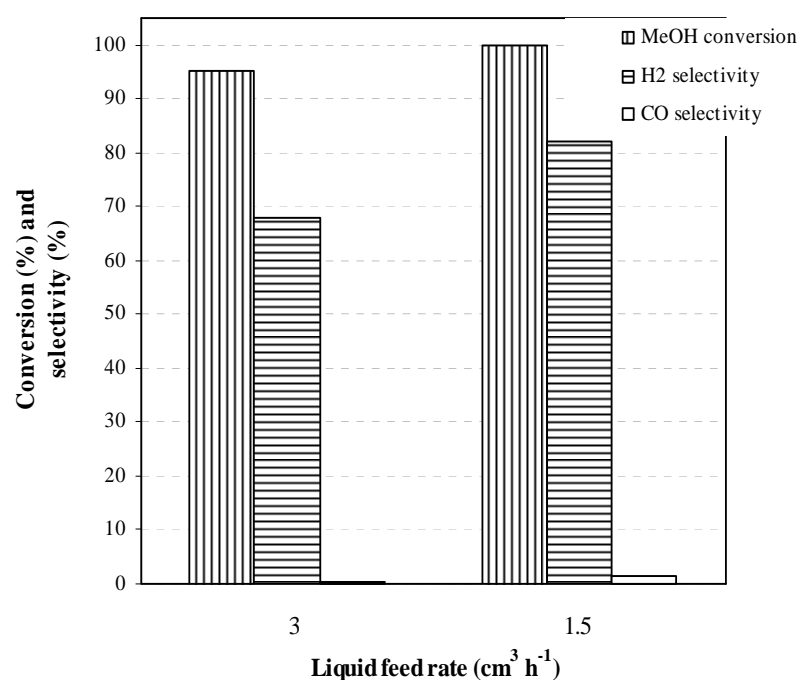


Figure 4.7 Effect of liquid feed rate on the catalytic activity of Au/(50:50)CuO–CeO₂ catalyst.

Condition: Operating temperature = 300 °C, S/M ratio = 1.5, W/F ratio = 0.17 g s cm⁻³ at atmospheric pressure.

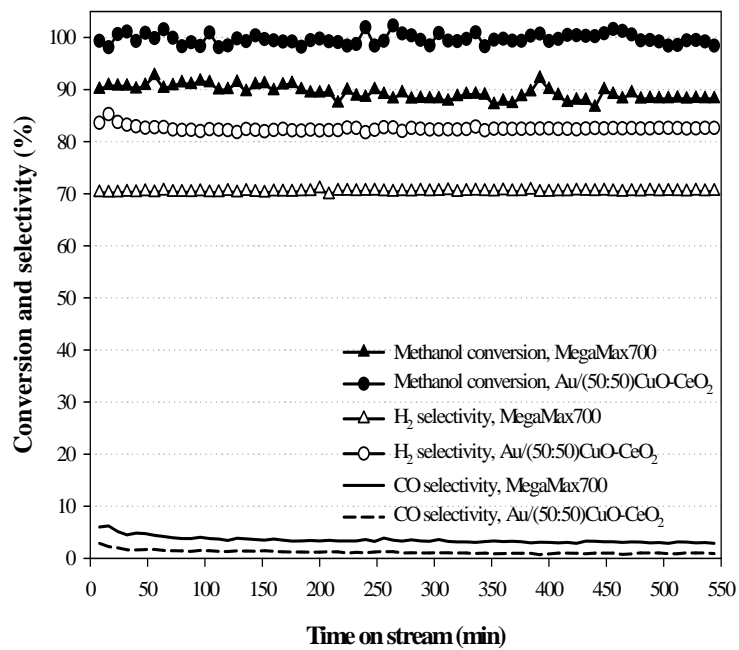


Figure 4.8 Stability tests of the commercial MegaMax 700 and the 5% Au/(50:50)CuO–CeO₂ catalysts.

Condition: Operating temperature = 300 °C, S/M ratio = 1.5, Liquid feed rate = 1.5 cm³ h⁻¹, W/F ratio = 0.17 g s cm⁻³ at atmospheric pressure.

CHAPTER V

OPTIMIZATION OF METHANOL STEAM REFORMING BY STATISTICAL DESIGN OF EXPERIMENTS*

In this chapter, the condition of steam reforming of methanol (SRM) was investigated by statistically designed experiments over 5% Au/(50:50)CuO–CeO₂ catalyst. After describing a role of the factor chosen by method of one-variable-at-a-time (section 5.1), a full 2⁴ factorial design was employed to screen the important factors and interaction among factors; operating temperature (factor A), steam to methanol (S/M) ratio (factor B), liquid feed rate (factor C), and catalyst weight to He flow rate (W/F) ratio (factor D), in section 5.2. In the next section, response surface methodology (RSM) by using central composite rotatable design (CCRD) was performed in order to optimize the conditions for complete methanol conversion with a minimal CO selectivity in a SRM unit. The validation of the developed model was also done.

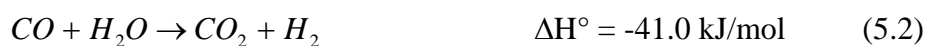
5.1 Catalytic activity (one-variable-at-a-time)

The catalytic activities and product distribution obtained for SRM over the 5% Au/(50:50)CuO–CeO₂ catalyst are presented in terms of the methanol conversion

* Submitted

(%) and CO selectivity (%), as shown in Figure 5.1.

As a result in Figure 5.1a, the level of methanol conversion (%) and CO selectivity (%) increased dramatically from 64.03% to 100% (1.56-fold) and from 0.18% to 1.39% (7.72-fold), respectively, as the operating temperature increased from 230 °C to 300 °C. The composition of the reformed gas was found to contain CO, CO₂, residual methanol and steam in the H₂-rich stream (Chapter IV). This implies that there are two possible path ways for the reaction; (a) a combination of the methanol decomposition (DM, Eq. (5.1)) and water–gas shift (WGS, Eq. (5.2)) reactions and (b) an immediate reaction of methanol and water (Eq. (5.3)). Thus, higher methanol conversion and CO selectivity were obtained with increasing operating temperatures due to the thermodynamic limitations (see Eqs. (5.1)–(5.3)).



From the stoichiometry of either an immediate reaction of methanol and water (Eq. (5.3)) or a combination reaction of DM (Eq. (5.1)) and WGS (Eq. (5.2)), the required molar ratio of methanol to water is around 1:1. It is of noted that, when the S/M ratio was increased from 1 to 2, the methanol conversion was slightly increased from 71.89% to 77.82% (1.08-fold), whilst the CO selectivity was reduced 1.8-fold (from 0.62% to 0.34%) (Figure 5.1b). These results are in good agreement with that reported by Zhang et al. [28]. The excess molar ratio of water is an important driving force to move the immediate reaction between methanol and water forward, accompanied with the DM reaction, leading to a higher methanol conversion level. The excess molar ratio of water also encourages the WGS reaction and so results in a

lower CO level in the product stream. Therefore, a higher methanol conversion efficiency with a lower CO selectivity was achieved at a higher S/M ratio (2.0) than the stoichiometric ratio (1.0).

When the operating temperature, S/M and W/F ratio were fixed at 300 °C, 1.5 and 0.13 g s cm⁻³, respectively, then decreasing the liquid feed rate from 3 cm³h⁻¹ to 1 cm³ h⁻¹ increased the methanol conversion yield some 1.18-fold to a maximal level (100%) and the CO selectivity 1.39-fold (Figure 5.1c). These results agree with that reported by Hwang et al. [80]. Decreasing the liquid feed rate implies a longer reaction time and consequently more reaction can take place. Therefore, an improved catalytic performance in terms of an increased to maximal methanol conversion but with a lower CO selectivity can be achieved by using a low level of liquid feed rate (in this case here, 1 cm³ h⁻¹).

When the W/F ratio was decreased from 0.24 g s cm⁻³ to 0.13 g s cm⁻³, at a constant temperature (350 °C), S/M ratio (1), and liquid feed rate (1 cm³ h⁻¹), the methanol conversion was decreased slightly from 100% to 92.23% (1.08-fold) whilst the CO selectivity was increased from 7.79% to 8.46% (1.09-fold) (Figure 5.1d). A change in the W/F ratio implies a change in the contact time between the catalyst and the substance, with higher W/F ratios resulting in a longer contact time and so a higher catalytic activity [18,21,28].

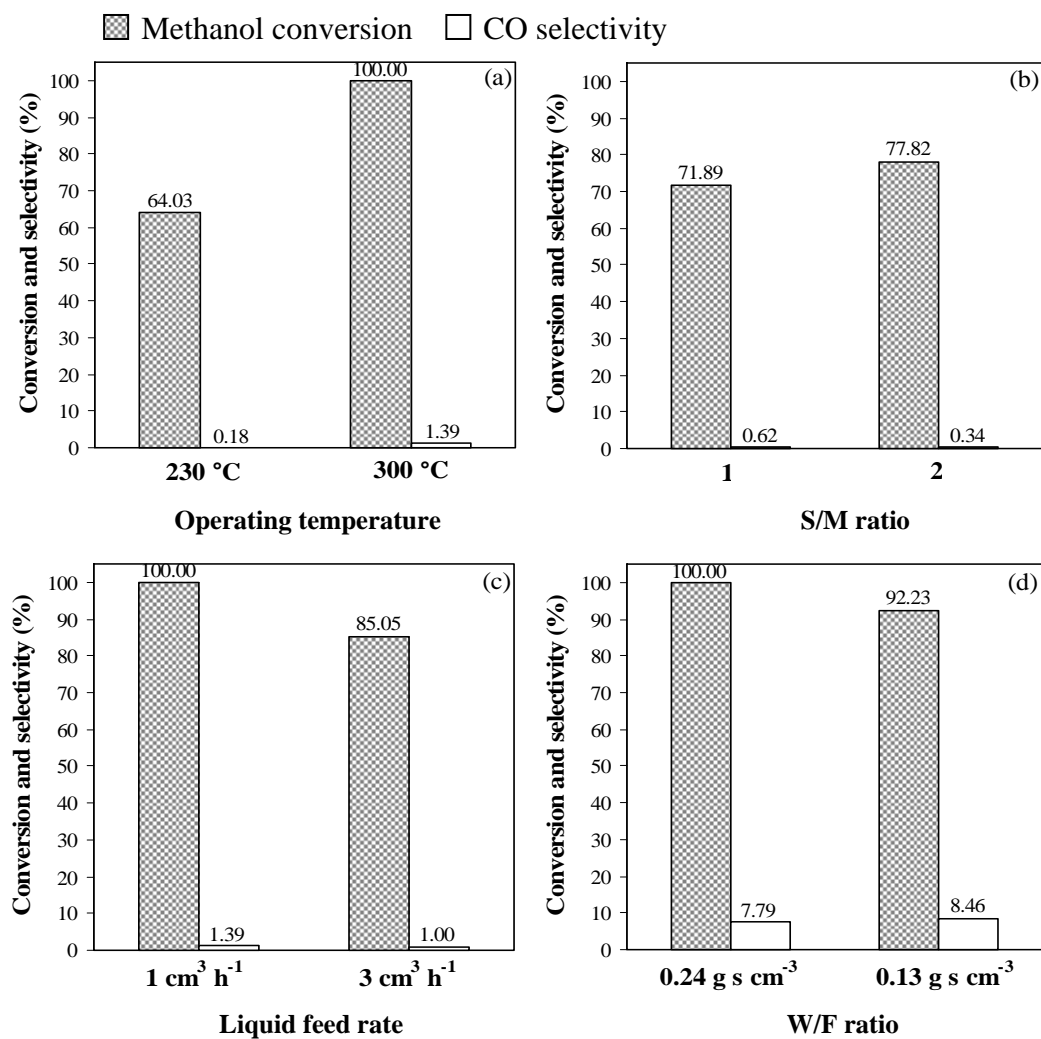


Figure 5.1 Catalytic performance of 5% Au/(50:50)CuO–CeO₂ catalyst in term of methanol conversion and CO selectivity when:

(a) Operating temperature at 230–300 °C, S/M ratio = 1.5, liquid feed rate = 1 cm³ h⁻¹, W/F ratio = 0.13 g s cm⁻³.

(b) Operating temperature = 250 °C, S/M ratio at 1–2, liquid feed rate = 1 cm³ h⁻¹, W/F ratio = 0.24 g s cm⁻³.

(c) Operating temperature = 300 °C, S/M ratio = 1.5, liquid feed rate at 1–3 cm³ h⁻¹, W/F ratio = 0.13 g s cm⁻³.

(d) Operating temperature = 350 °C, S/M ratio = 1, liquid feed rate = 1 cm³ h⁻¹, W/F ratio = 0.13–0.24 g s cm⁻³.

5.2 Factors screening in a full 2⁴ factorial design

To determine the importance of each of the four independent factors on the methanol conversion and CO selectivity, the experimental matrix for a full 2⁴ factorial design with four central points was performed and the results are presented in Table 5.1. Based on the two sequential reactions of methanol decomposition and water–gas shift involved in SRM, as mentioned in the catalytic activities, the statistical analysis of these data, with the methanol conversion efficiency as the response was performed first by constructing a half normal probability plot of the effect estimates (Figure 5.2a) and a Pareto chart (Figure 5.2b).

Of the four investigated factors, three lie along the line but the liquid feed rate is far distant and so is the most important factor determining the methanol conversion. The result was supported by the Pareto chart, which displays the absolute standardized effect at a 95% confidence interval (Figure 5.2b). For the absolute standardized values of the effect of each factor and their interactions, only the liquid feed rate expressed an absolute value higher than 24.98, which again implies that only the liquid feed rate had any significant influence on the methanol conversion obtained. In addition, the analysis of variance (ANOVA) of the catalytic performance at a 95% confidence interval revealed that only the liquid feed rate was significant (P-value < 0.05) and contributed 66.60% of the variance (Table 5.2a). However, the R² and adjusted R² values of the regression model are quite low, suggesting some other factor(s) of importance. From the regression analysis, the methanol conversion could be expressed as:

$$\text{Methanol conversion}(\%) = +56.68 - 32.67C \quad (5.4)$$

Table 5.1 Experimental variables over Au/CuO–CeO₂ in coded and actual unit for a full 2⁴ factorial design with four central points in the standard order from 1 to 20

Factors	Variables	Unit	Low (-1)	Medium (0)	High (1)
A	Temperature	°C	250	300	350
B	S/M ratio	–	1	1.5	2
C	Liquid feed rate	cm ³ h ⁻¹	1	2	3
D	W/F ratio	g s cm ⁻³	0.13	0.17	0.24

Standard order	Run order	A	B	C	D	Methanol conversion (%)	CO selectivity (%)
1*	8	-1	-1	-1	-1	71.17	0.33
2*	3	1	-1	-1	-1	100.00	7.79
3*	2	-1	1	-1	-1	94.21	0.42
4*	6	1	1	-1	-1	100.00	4.36
5	20	-1	-1	1	-1	14.39	0.24
6	1	1	-1	1	-1	8.11	6.84
7	12	-1	1	1	-1	2.09	1.42
8	4	1	1	1	-1	8.91	5.88
9*	11	-1	-1	-1	1	76.00	0.89
10*	19	1	-1	-1	1	92.23	8.46
11*	9	-1	1	-1	1	81.16	0.32
12*	16	1	1	-1	1	100.00	4.06
13	10	-1	-1	1	1	37.49	0.21
14	18	1	-1	1	1	85.49	4.83
15	13	-1	1	1	1	29.61	0.09
16	15	1	1	1	1	5.98	6.25
17	7	0	0	0	0	85.45	0.74
18	17	0	0	0	0	84.85	0.73
19	5	0	0	0	0	75.34	0.71
20	12	0	0	0	0	85.23	0.80
21*	21	0	0	-1	0	100	1.39
22*	22	0	0	-1	0	100	1.37

Note * Experimental variables in coded and actual unit for a full 2³ factorial design with two central points in the standard order from 1–4, 9–16 and 21–22, whilst maintaining the liquid feed rate at a low level (1 cm³ h⁻¹). Data are shown as the mean value from two replicates.

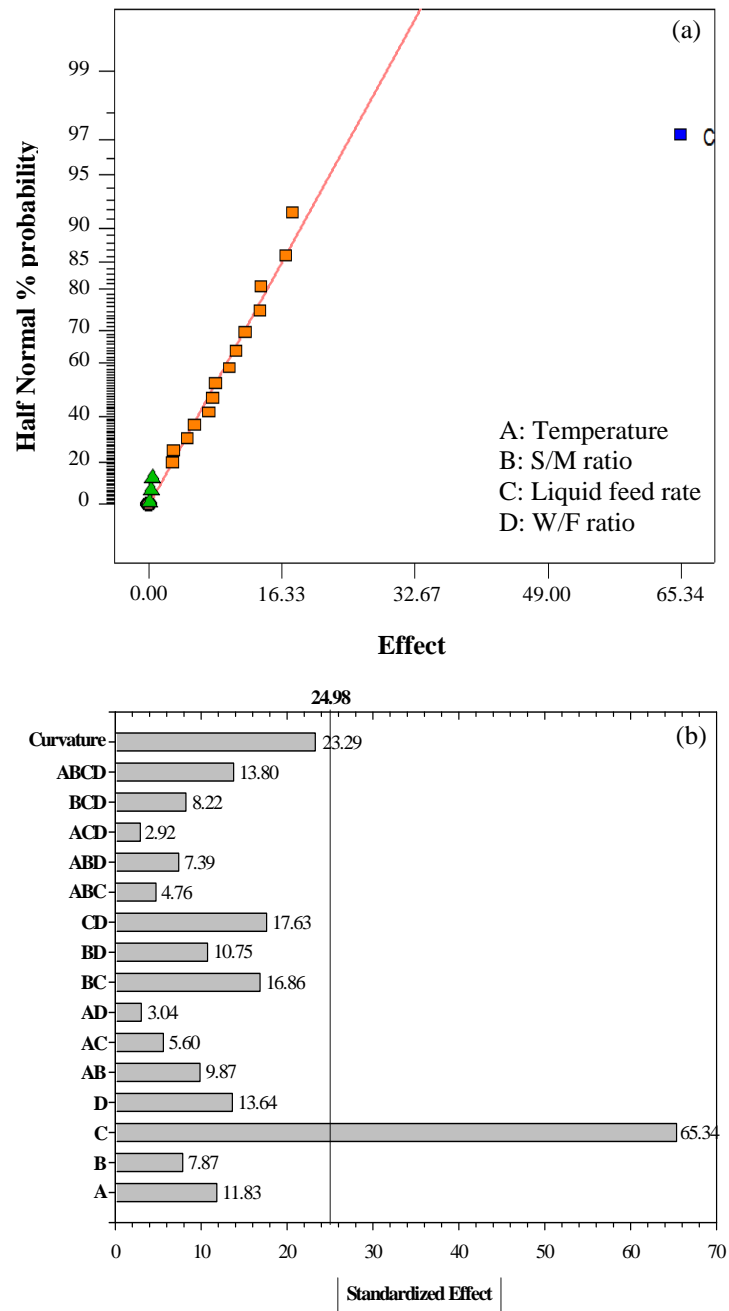


Figure 5.2 Statistical analysis for a full 2^4 factorial design with 4 central points by: (a) half normal probability plot of the effects and (b) The Pareto chart.

The negative sign of the coefficient estimate of the liquid flow rate (C) in the regression equation implies that a decrease in the liquid feed rate leads to an increased methanol conversion, similar to the results shown in Figure 5.1c for a constant 300 °C and S/M and W/F ratios of 1.5 and 0.13 g s cm⁻³, respectively. To test the validity of the regression model, four more treatments with different liquid feed rates were performed (Table 5.2b). The estimated methanol conversions deviated dramatically from those obtained experimentally as the liquid feed rate increased above the lowest (1 cm³ h⁻¹) of the four evaluated rates. This could be explained by the fact that the influence of the liquid flow rate on the methanol conversion (Table 5.2b) is much larger than that of the other factors and so masks their smaller (under these conditions) contributions. Taking into account the adequacy of the model in order to approach complete (100%) methanol conversion with a low CO selectivity, and to verify the importance of the other factors on the methanol conversion and CO selectivity obtained, the liquid feed rate was then maintained at a low level (1 cm³ h⁻¹).

Table 5.2 Analysis of variance and validity of regression model for a full 2^4 factorial design with four central points with the methanol conversion as the response

(a) Analysis of variance

Source	Sum of squares	DF	Mean square	F-value	Probability (P-value)	Contribution (%)
Model	17075.96	1	17075.96	45.41	< 0.0001	
C	17075.96	1	17075.96	45.41	< 0.0001	66.60
Curvature	2169.86	1	2169.86	5.77	0.0580	8.46
Residual	6392.54	17	376.03			24.94
Cor Total	25638.36	19				

R-Squared = 0.7276; Adj R-Squared = 0.7116

(b) Validity of regression model

Run	Liquid feed rate C ($\text{cm}^3 \text{h}^{-1}$)	Methanol conversion (%)	
		Estimated	Experiment
No.1	1	89.35	100.00
No.2	1.5	73.02	97.94
No.3	2	56.68	90.72
No.4	3	24.01	85.05

In all cases the operating temperature, S/M and W/F ratios were 300 °C, 1.5 and 0.13 g s cm^{-3} , respectively.

A new experimental matrix for a full 2^3 factorial design with two central points was then performed and the results presented in Table 5.1, with the statistical analysis of this matrix shown in Figure 5.3 and Table 5.3. From the half-normal probability plot of the effects, it was found that only the operating temperature had a significant influence on the methanol conversion (Figure 5.3a), whilst in addition the operating temperature, the S/M ratio, and their interaction were important in determining the CO selectivity (Figure 5.3b).

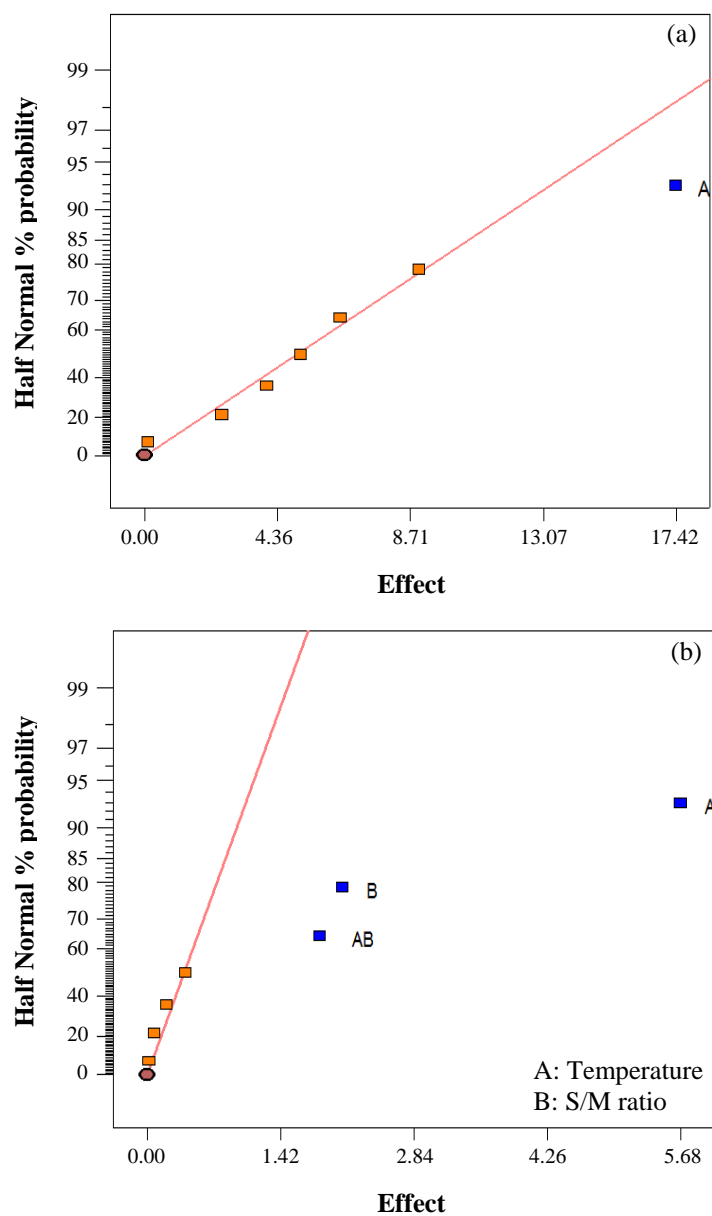


Figure 5.3 Half normal probability plot of the effects for a full 2^3 factorial design with 2 central points when holding liquid feed rate at $1 \text{ cm}^3 \text{ h}^{-1}$: (a) methanol conversion as a response and (b) CO selectivity as a response.

These results were supported by the ANOVA analysis (Table 5.3) with the ordering of the importance of each factor on the CO selectivity and its relative contribution to the variance being temperature (77.09%) > S/M ratio (10.32%) > temperature–S/M ratio interaction (8.08%). It is surprising that the W/F ratio had no significant effect on either the methanol conversion or the CO selectivity obtained. However, of note is that the ANOVA analysis showed that both models displayed a curvature since the probability was lower than 0.05.

Table 5.3 Analysis of variance for a full 2^3 factorial design with two central points when maintaining the holding liquid feed rate at a low level ($1 \text{ cm}^3 \text{ h}^{-1}$)

(a) Methanol conversion as the response

Source	Sum of squares	DF	Mean square	F-value	Probability (P-value)	Contribution (%)
Model	607.09	1	607.09	10.68	0.0171	
A	607.09	1	607.09	10.68	0.0171	57.88
Curvature	100.89	1	100.89	1.78	0.2310	9.62
Residual	340.91	6	56.82			32.50
Cor Total	1048.88	8				

R-Squared = 0.6404; Adj R-Squared = 0.5805

(b) CO selectivity as the response

Source	Sum of squares	DF	Mean square	F-value	Probability (P-value)	Contribution (%)
Model	79.85	3	26.62	246.89	< 0.0001	
A	64.47	1	64.47	597.96	< 0.0001	77.09
B	8.63	1	8.63	80.07	0.0009	10.32
AB	6.75	1	6.75	62.63	0.0014	8.08
Curvature	3.34	1	3.34	30.99	0.0051	4.00
Residual	0.43	4	0.11			0.51
Cor Total	83.63	8				

R-Squared = 0.9946; Adj R-Squared = 0.9906

In order to verify the curvature, the mean changes that occurred in the methanol conversion or CO selectivity when changing the level of each factor from a lower level through the central point to higher level were compared, and revealed that the average response value did not correspond to the response value at the central point for the factors studied (Figure 5.4). This suggested that there should be a quadratic term in both models. In addition, a higher level of methanol conversion is obtained at a higher operating temperature, whilst a lower level of CO selectivity is yielded at a lower temperature and a higher S/M ratio, in agreement with previous reports [18,21,26,27]. Therefore, the operating temperature and the S/M molar ratio were subjected to a surface analysis in order to achieve the maximal methanol conversion (100%) with a minimal CO selectivity.

5.3 Response surface methodology (RSM)

A central composite rotatable design (CCRD), with the two selected independent factors (operating temperature and the S/M molar ratio) was performed in order to optimize the conditions for complete methanol conversion with a minimal CO selectivity in a SRM unit over a 5% Au/(50:50)CuO–CeO₂ catalyst. The criterion of this design is rotatability, which is a spherical property. For a spherical region of interest, the best choice of the distance α of the axial to the design central point is around $2^{1/2}$. The experiments including 2^2 factorial points, four axial points, and three central points were then designed and performed (Table 5.4), with the levels of the screened factors based on the results from the previous full factorial design experiments (section 5.2). From these prior results, the liquid feed rate was held

constant at a low level ($1 \text{ cm}^3 \text{ h}^{-1}$), whereas the W/F ratio was maintained at a medium level (0.17 g s cm^{-3}).

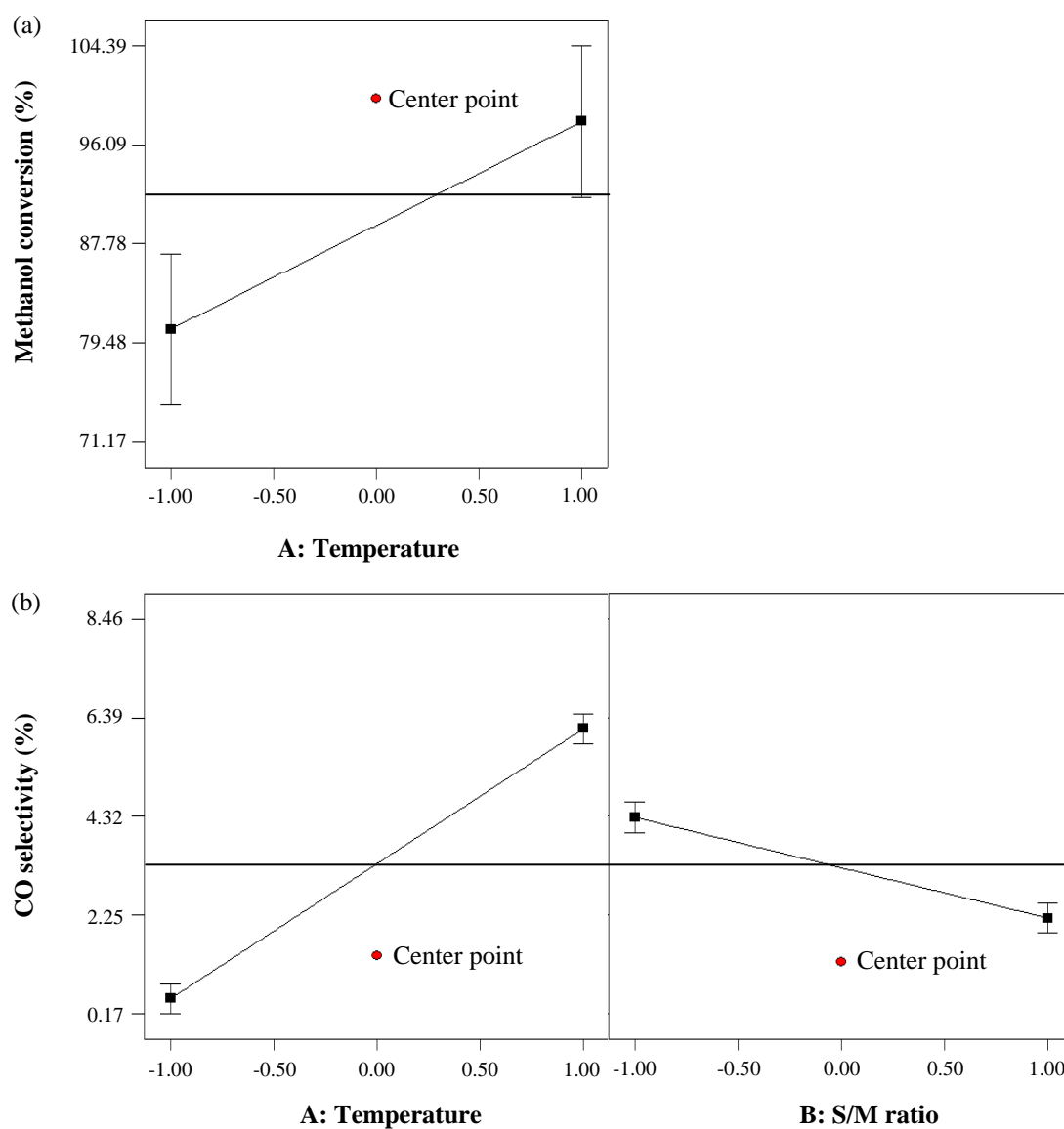


Figure 5.4 Main effect plot of (a) methanol conversion and (b) CO selectivity.

An appropriate RSM for the methanol conversion and for the CO selectivity were analyzed, followed by the simultaneous consideration of them both together to derive the optimized set of both responses. Each corresponding RSM is shown below:

$$\text{Methanol conversion (\%)} = +97.40 + 12.44A + 2.62B - 8.00A^2 - 1.77B^2 - 1.07AB \quad (5.5)$$

$$\text{CO selectivity (\%)} = +2.4 + 2.53A - 1.13B + 0.63A^2 - 0.98AB \quad (5.6)$$

where A, B and AB stand for the temperature, S/M ratio and their interaction, respectively. Figures 5.5a and 5.5b show the three-dimensional response surface and contour plot of the obtained methanol conversion and CO selectivity, respectively. The highest methanol conversion occurred at high operating temperatures and S/M ratios while the lowest CO selectivity was found at low operating temperatures and high S/M ratios. A relatively straightforward approach to optimize the two responses is to overlay the contour plot for each response, as shown in Figure 5.5c. The optimal condition that is estimated by such simultaneous consideration of the maximal methanol conversion and the minimal CO selectivity response is found in the shaded portion (Figure 5.5c), represented by an operating temperature of ~295 °C to ~306 °C and an S/M ratio of ~1.82 to 2.00.

Table 5.4 Experimental variables for the central composite rotatable design (CCRD)

Factors	Variables	Unit	Low (-1)	Medium (0)	High (1)
A	Temperature	°C	250	300	350
B	S/M ratio	–	1	1.5	2

Standard order	Run order	A	B	Methanol conversion (%)	CO selectivity (%)
1	9	250	1	71.17	0.33
2	2	350	1	100.00	7.79
3	8	250	2	94.21	0.42
4	10	350	2	100.00	4.36
5	5	229 (- α)	1.5 (0)	14.39	0.24
6	1	371 (- α)	1.5 (0)	8.11	6.84
7	4	300 (0)	0.8 (- α)	2.09	1.42
8	3	300 (0)	2.2 (- α)	8.91	5.88
9	7	300	1.5	76.00	0.89
10	11	300	1.5	92.23	8.46
11	6	300	1.5	81.16	0.32

α (Rotatable) = 1.41421

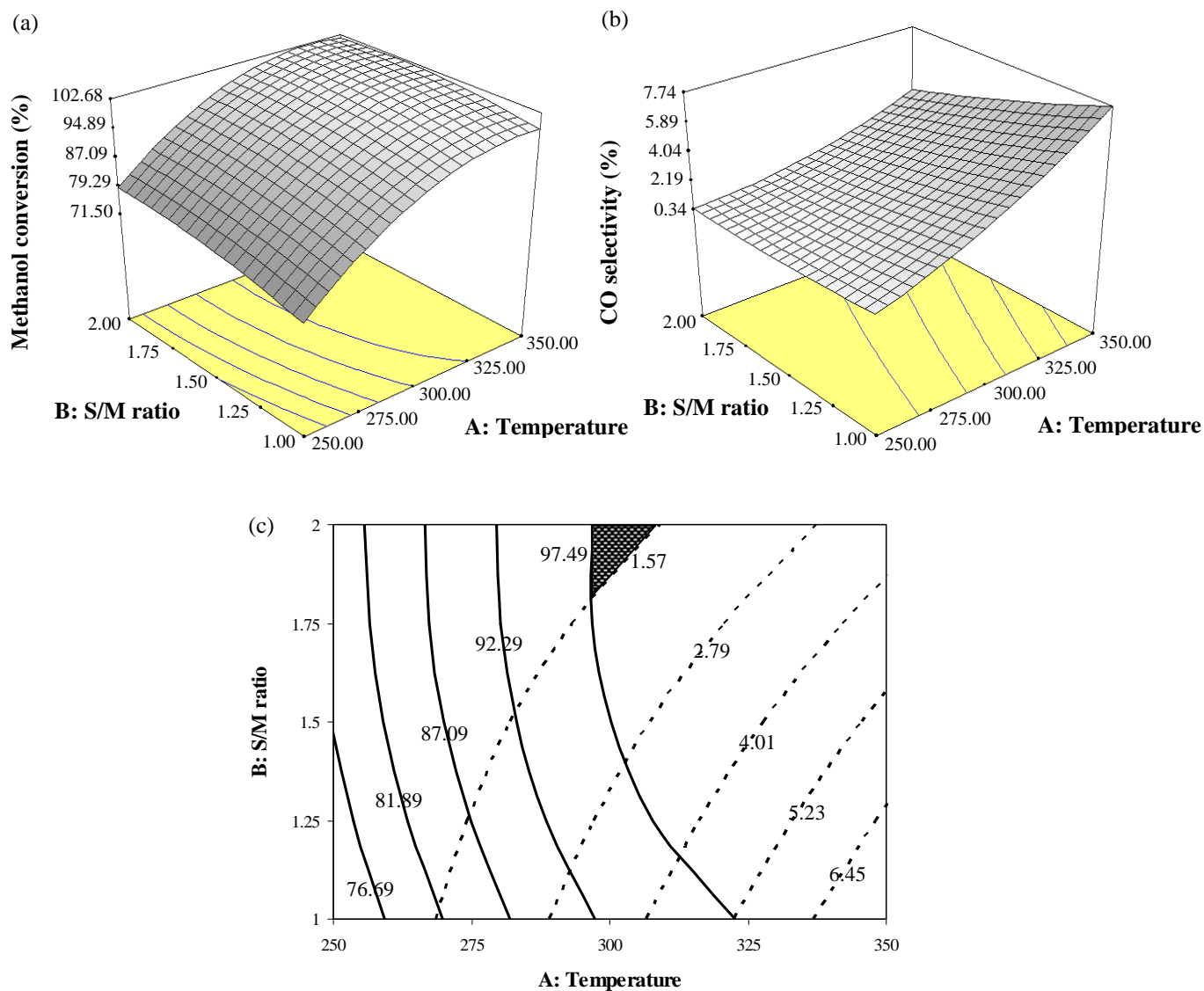


Figure 5.5 Response surface and contour plot of: (a) methanol conversion response, (b) CO selectivity response, and (c) region of the optimum (shaded portion) found by overlaying yield between methanol conversion response (solid line) and CO selectivity response (dot line).

5.4 Validation of the response surface models

To investigate the accuracy of the models, six experimental set ups using different operating temperatures (250–350 °C) and S/M molar ratios (1–2), whilst maintaining the other factors at their optimum level, were evaluated (Table 5.5). Complete methanol conversion at a low CO selectivity was achieved with an operating temperature of 306.43 °C and an S/M ratio of 2. Under the five other conditions the estimated methanol conversion and CO selectivity were very close to the experimentally derived ones. Thus, the RSM analysis provided useful details regarding the efficient process for SRM over 5% Au/(50:50)CuO–CeO₂ catalyst.

Table 5.5 Validation of the CCRD using different level of operating temperatures and S/M ratios at a constant liquid feed rate (1 cm³ h⁻¹) and W/F ratio (0.17 g s cm⁻³)

Operating condition		Methanol conversion (%)		CO selectivity (%)	
Temperature (°C)	S/M ratio	Estimated	Experiment	Estimated	Experiment
306.43	2.00	99.68	100.00	1.48	1.51
250.00	2.00	76.96	77.82	0.50	0.34
260.00	1.50	80.15	81.65	0.95	0.82
300.00	1.50	95.65	94.27	2.97	2.08
250.00	1.00	71.50	71.89	0.65	0.62
350.00	1.00	98.52	98.34	7.67	8.03

CHAPTER VI

PREFERENTIAL OXIDATION OF CARBON MONOXIDE OVER SUPPORTED Pt AND Au CATALYSTS*

In this chapter, CO clean-up by preferential oxidation was studied over series of supported platinum and gold catalysts. There were two main parts in the investigation: part I: platinum and gold supported on ceria catalysts and part II: platinum and gold supported on mixed oxide catalysts, as shown in section 6.1 and 6.2, respectively

6.1 Part I: Platinum and gold supported on ceria catalysts

6.1.1 Catalyst characterization

The patterns of X-ray diffraction of the catalysts are shown in Figure 6.1. All peaks were the peaks of CeO₂ (ceria) crystallite. Major of ceria characteristic peaks were attributed to (1 1 1), (2 0 0), (2 2 0), and (3 1 1) crystal planes at 28.6°, 33.1°, 47.5°, and 56.3° of 2θ, respectively. However, there was no metal peak in the

* - Journal of the Chinese Institute of Chemical Engineers, 38 (2007) 435–441.
- International Journal of Hydrogen Energy, 35 (2010) 3234–3242.

XRD patterns of the catalysts. This was due to the fact that the metallic particle size of the prepared catalysts was either atomically dispersed or too small to be detected by XRD method. By using X-ray line-broadening and the Debye–Scherrer equation, the ceria crystallite size of each catalyst can be obtained. BET surface area, pore volume, and ceria crystallite size results are presented in Table 6.1. The surface area of catalyst was related to its pore volume. The ceria crystallite sizes were calculated at (1 1 1) plane of all samples. The commercial ceria showed a high crystallinity and had a crystallite size of 53.5 nm. The synthesized ceria showed broader shape and had a smaller ceria crystallite about 16.2 nm. There was evident that the method of catalyst preparation had a significant effect on the surface area of the prepared catalysts. The synthesized ceria had higher surface area than the commercial ceria.

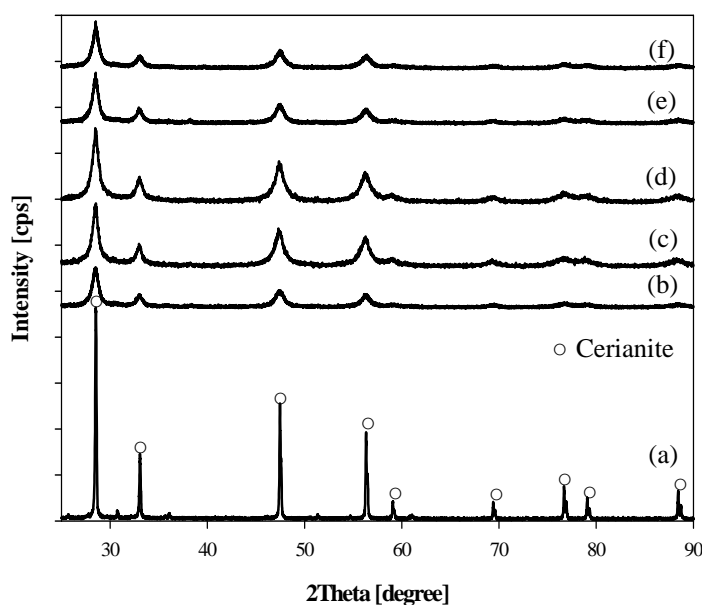


Figure 6.1 XRD patterns of the prepared catalysts: (a) Commercial ceria, (b) Synthesized ceria, (c) 1%(1:1)PtAu/CeO₂-ISG, (d) 1% Au/CeO₂-SSG, (e) 1%(1:1)PtAu/CeO₂-SSG, and (f) 1% Pt/CeO₂-SSG.

This result confirmed that smaller ceria crystallite size led to higher surface area. Furthermore by comparison, a catalyst prepared by ISG had higher surface area than one prepared by SSG. The catalysts prepared by SSG did not much different in the surface area and in the crystallite size.

Table 6.1 BET surface area and ceria crystallite size results of the prepared catalysts

Sample	Preparation method	$S_{\text{BET}}^{\text{a}}$ ($\text{m}^2 \text{g}^{-1}$)	Pore volume ^a ($\text{cm}^3 \text{g}^{-1}$)	CeO ₂ crystallite size ^b (nm)
CeO ₂ commercial	as received	2.3	0.01	53.5
CeO ₂ synthetic	Sol-gel	116.8	0.10	16.2
1%(1:1)PtAu/CeO ₂	ISG	111.9	0.09	16.6
1%(1:1)PtAu/CeO ₂	SSG	83.9	0.09	15.1
1%Pt/CeO ₂	SSG	95.6	0.10	13.7
1%Au/CeO ₂	SSG	79.3	0.08	13.7

^a Determined by BET surface area analyzer

^b Determined by XRD from line broadening of CeO₂ (1 1 1) peak

SEM images were used as a magnifier-glass to identify the shape of the crystallinity of the ceria support. Figure 6.2 (a)–(e) shows the SEM images of commercial ceria, synthesized ceria, 1% Pt/CeO₂, 1% Au/CeO₂, and 1%(1:1)PtAu/CeO₂ prepared by SSG. The SEM results of the both supports showed that the crystallinity of the commercial ceria was higher than that of the synthesized ceria and this was confirmed by the XRD results. It could be seen that the particles of synthesized ceria were mainly of long and thin crystal shaped morphology. In the case of supported catalysts, metal catalysts on the synthesized ceria were predominantly around.

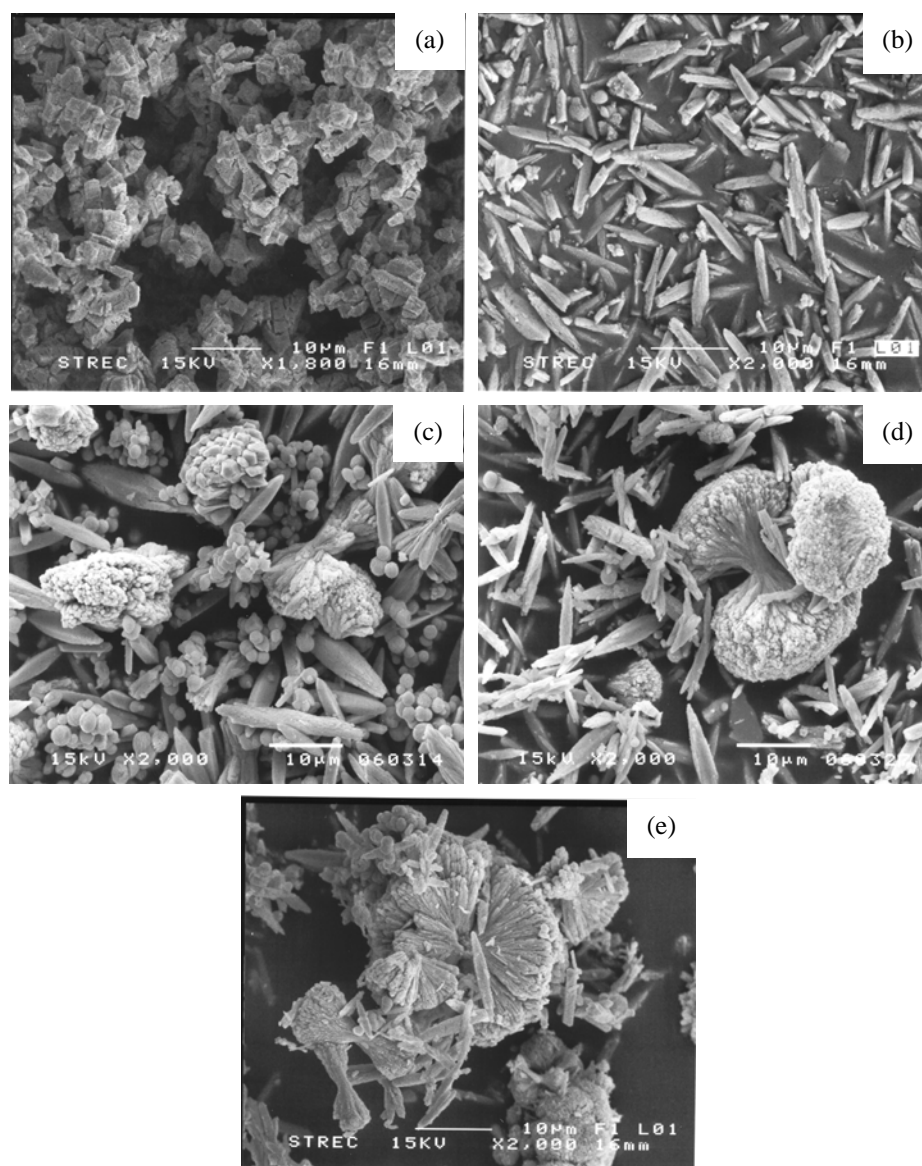


Figure 6.2 SEM images of (a) Commercial ceria, (b) Synthesized ceria-SSG, (c) 1%Pt/CeO₂-SSG, (d) 1%Au/CeO₂-SSG, and 1%(1:1)PtAu/CeO₂-SSG catalysts.

The differences in TPR patterns of monometallic (Pt/CeO₂ and Au/CeO₂) and bimetallic (PtAu/CeO₂) catalyst prepared by SSG are shown in Figure 6.3. The TPR pattern of Au/CeO₂ showed a broad peak at around 150 °C to 450 °C. The TPR profile of Pt/CeO₂ was about 100 °C to 350 °C. Compared to the others, the reduction

peak of PtAu/CeO₂ appeared at a lower temperature range of 50 °C to 250 °C. The results implied that the bimetallic catalyst could be reduced easily by H₂ at lower temperature due to the formation of a new phase.

Figure 6.4 (a)–(c) shows the TEM image of 1% Au/CeO₂, 1% Pt/CeO₂, and 1%(1:1)PtAu/CeO₂ prepared by SSG, respectively. The active components in the dark area were homogeneous with the ceria support in the grey region. However, the active components dispersed throughout the ceria support. An average dimension of Pt–Au metal was approximately 5–10 nm while an average dimension of Pt and Au metal were around 2–3 and 5–6 nm, respectively.

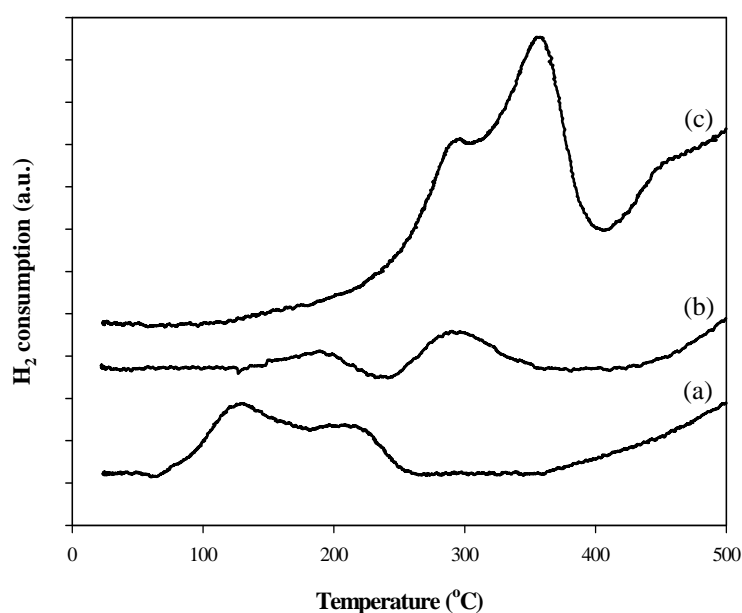


Figure 6.3 TPR profiles of (a) 1%(1:1)PtAu/CeO₂-SSG, (b) 1%Pt/CeO₂-SSG, and (c) 1% Au/CeO₂-SSG catalysts.

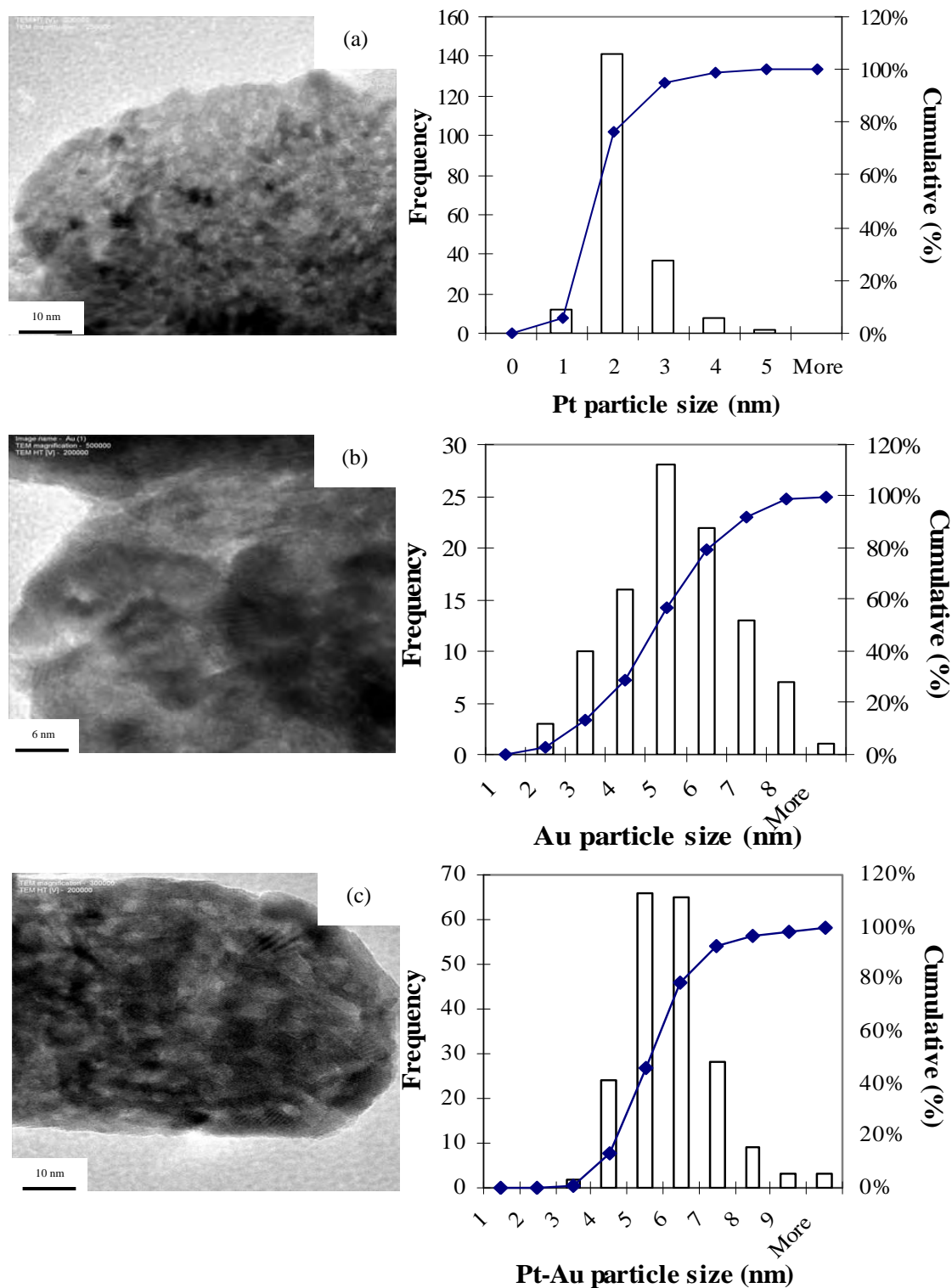


Figure 6.4 TEM images of (a) 1%Pt/CeO₂-SSG, (b) 1%Au/CeO₂-SSG, and (c) 1%(1:1)PtAu/CeO₂-SSG catalysts.

6.1.2. Catalytic activity

6.1.2.1. Monometallic and bimetallic catalysts

The catalyst performance as a function of temperature in terms of CO conversion and selectivity is presented in Figure 6.5. In this study, the active component was fixed at 1 wt% of catalysts. The results showed a similar behavior in which the catalytic activity increased with increasing temperature until reaching a maximum CO conversion. The maximum CO conversion of catalysts were around 80%, 70%, 90% and 65% for 1%Pt/CeO₂-SSG, 1% Au/CeO₂-SSG, 1%(1:1)PtAu/CeO₂-SSG, and 1%(1:1)PtAu/CeO₂-ISG, respectively. At higher temperature, the hydrogen oxidation reaction occurred easier. This led to the reduction of CO conversion and selectivity. For the catalysts prepared by SSG, the bimetallic catalyst (1%(1:1)PtAu/CeO₂) was far more active than the monometallic catalysts in a temperature range of 85 °C to 145 °C because of a formation of a new phase in the bimetallic catalyst. The new phase in bimetallic catalyst was more active for preferential oxidation of CO. The results were in good agreement with Suh et al. [34] even though other catalysts were used.

In a lower temperature range of 50 °C to 100 °C, 1%Au/CeO₂ had a static value at about 70–75% selectivity. Literature reviews have verified that the preparation method had a significant effect on size and dispersion of Au on the support [39,41]. 1%Pt/CeO₂ showed the maximum activity (~80% CO conversion) at 90 °C. The catalytic activity of 1%Pt/CeO₂ was much higher than 1%Au/CeO₂. The presence of Au in PtAu/CeO₂ catalyst caused ~90% CO conversion at 90 °C, which was relatively high compared to the 80% CO conversion of 1%Pt/CeO₂ catalyst. The

advantage of Pt and Au was to improve the catalytic activity of the bimetallic catalyst. Pt atoms strongly interacted with Au atoms and then promoted the reducible oxide support. The results were in good agreement with Suh et al. [34] and Zhang et al. [57].

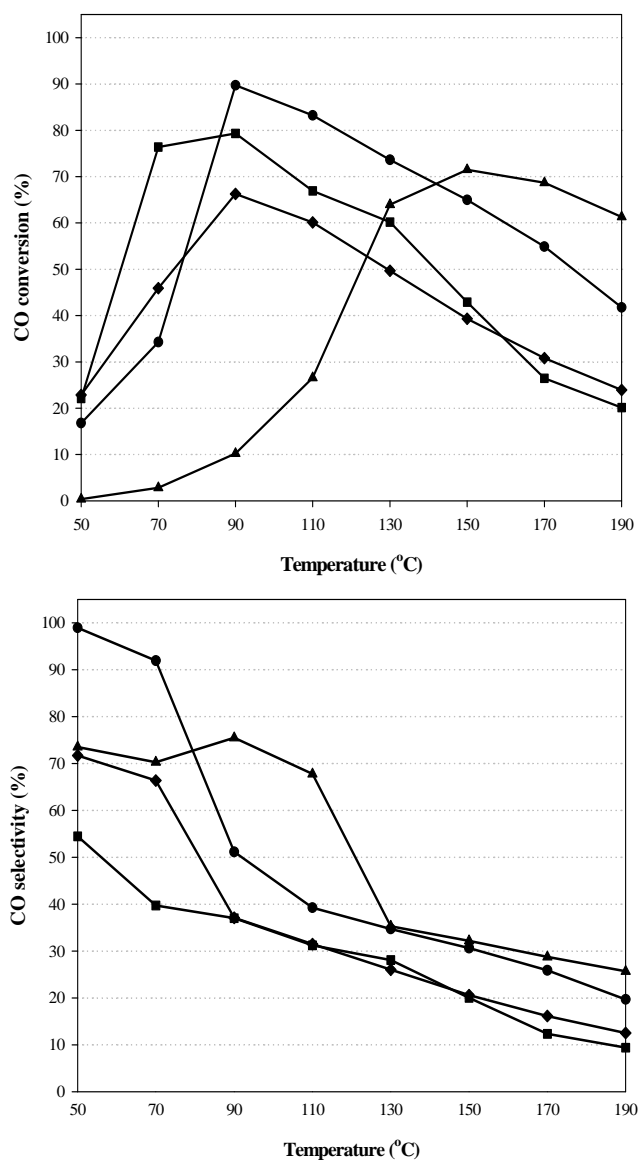


Figure 6.5 Catalytic activity of (■) 1%Pt/CeO₂-SSG, (▲) 1% Au/CeO₂-SSG, (●) 1%(1:1)PtAu/CeO₂-SSG, and (◆) 1%(1:1)PtAu/CeO₂-ISG.

Furthermore, comparison of ISG and SSG method elucidated that the preparation method had strongly effect on CO oxidation reaction. The catalysts prepared by SSG have higher catalytic performance than the catalysts prepared by ISG for bimetallic and monometallic catalysts.

6.1.2.2 Total metal loading

Figure 6.6 shows the effect of 1–3 wt% metal content in (1:1)PtAu/CeO₂ catalysts on catalytic performance. At the low temperature of between 50 °C and 90 °C, there was no significant difference in the CO conversion while the selectivity of 1 wt% metal catalyst was correspondingly higher than that of 2 and 3 wt% metal loading in the catalysts. The dispersion of metal on the support decreased with increasing metal content. Consequently, the surface area of the active site decreased. However, it must be noted that the amount of metal loading in the catalyst also depended on the type of the metal, the support and the catalyst preparation. When the operating temperature increased, 3 wt% metal loading seem to be the highest activities of all due to higher the amount of active site and kinetics energy.

6.1.2.3 Pt–Au ratio in the bimetallic catalyst

The effect of the Pt–Au ratio of 1%PtAu/CeO₂ catalyst on CO conversion and selectivity at reaction temperature of 90 °C is shown in Figure 6.7. The results indicated that the activity increased with increasing Pt content while the selectivity decreased. The maximum CO conversion was achieved at 10:1 of Pt–Au ratio and the maximum selectivity was obtained at 0.2:1 of Pt–Au ratio. It could be seen that the selectivity of 1%(10:1)PtAu/CeO₂ was the lowest value when compared

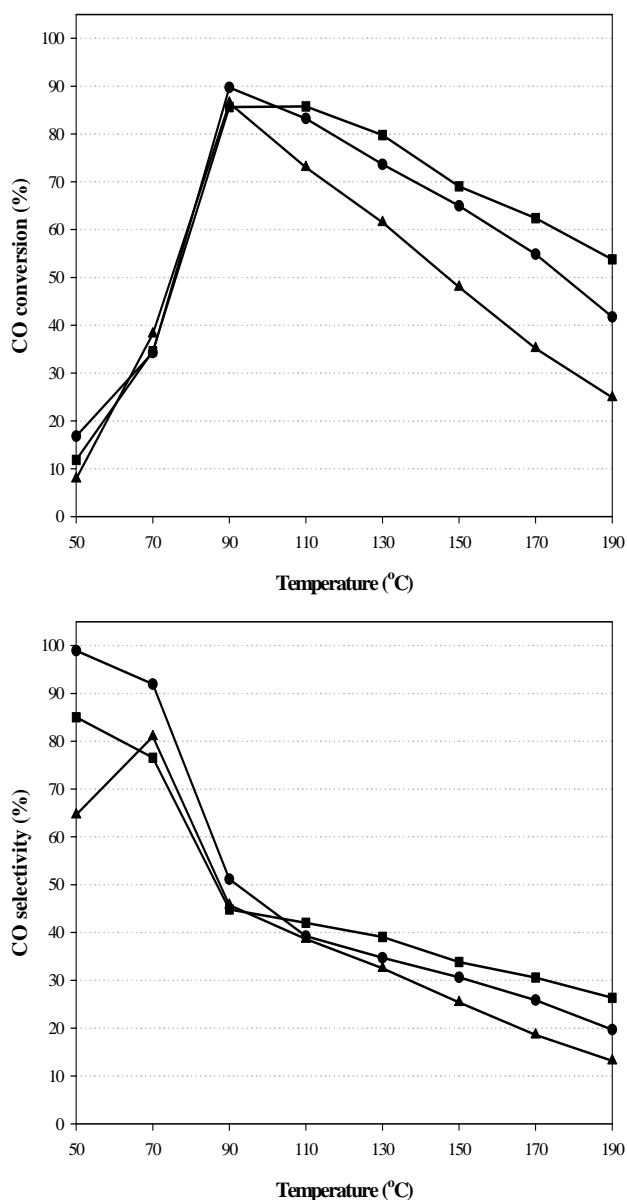


Figure 6.6 Catalytic activity of % metal loading (Pt–Au) of (1:1)PtAu/CeO₂-SSG: (●) 1%, (▲) 2%, and (■) 3%.

to the others. These results suggested that behavior of the catalyst performance depended on the amount of Pt atoms or Au atoms. A 1:1 of Pt–Au ratio showed the best performance (about 90% CO conversion and 50% selectivity) at 90 °C. This

contributed to the highest dispersion of this catalyst, as there was an evidence of its presence in TEM.

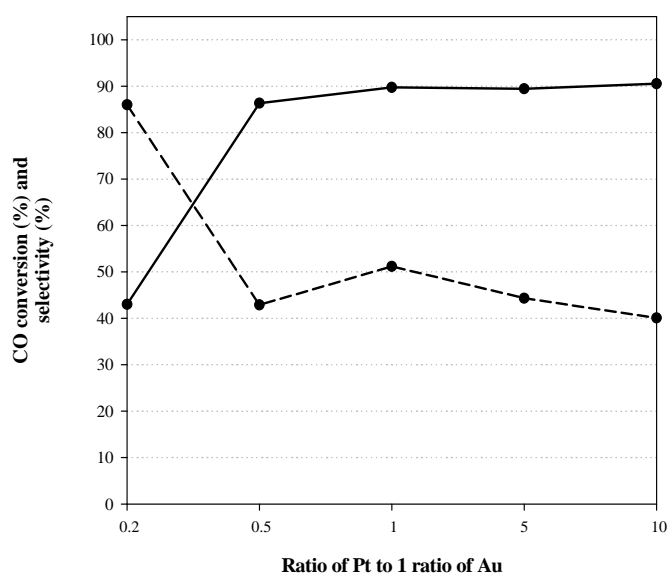


Figure 6.7 Catalytic activity of Pt: Au ratio of 1%PtAu/CeO₂-SSG: 0.2, 0.5, 1, 5, and 10 on CO conversion (solid line) and selectivity (dot line).

6.1.2.4 Catalyst weight to total gas inlet ratio (W/F ratio)

The effect of W/F ratio on the catalytic performance of 1%(1:1)PtAu/CeO₂ prepared by SSG method is shown in Figure 6.8. The CO conversion increased with increasing W/F ratio. At higher W/F ratio, the reactant gas had longer contact time for reaction and thus enhanced the catalytic activity. Additionally, the improvement of the W/F ratio also promoted oxidation of H₂; therefore, the selectivity decreased when increasing in W/F ratio.

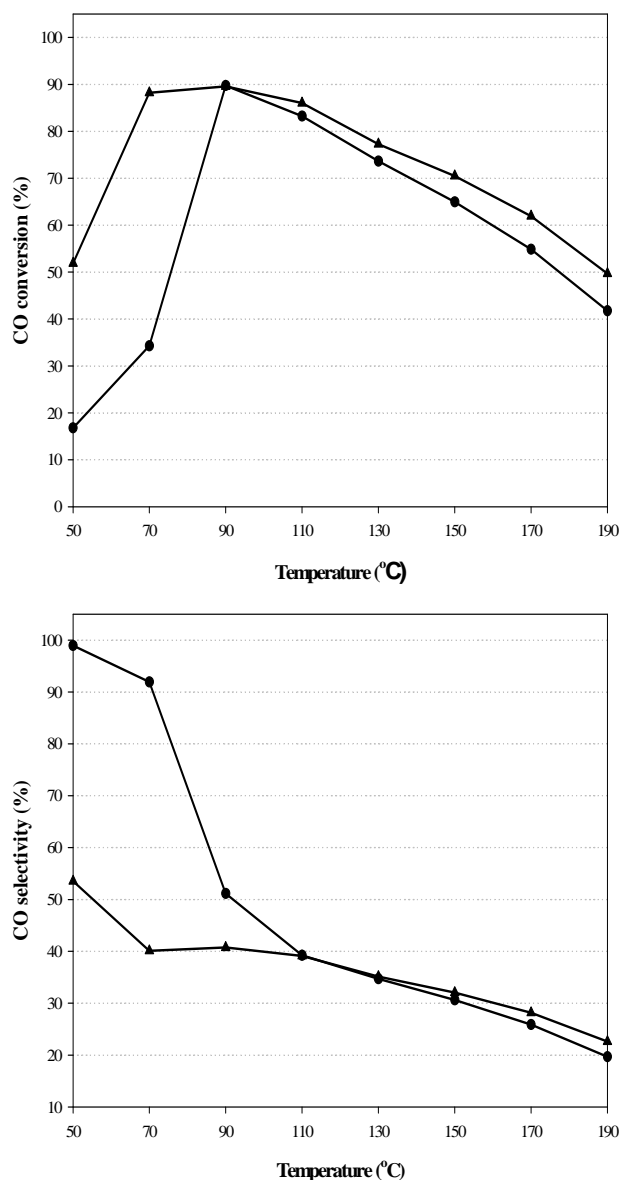


Figure 6.8 Catalytic activity of W/F ratio of 1%(1:1)PtAu/CeO₂: (●) 0.12 g s cm⁻³ and (▲) 0.36 g s cm⁻³.

6.1.2.5 H₂O and CO₂ in the feedstream

Figure 6.9 shows the effect of H₂O and CO₂ in the feed on the catalytic performance of 1%(1:1)PtAu/CeO₂-SSG. The results showed that H₂O and CO₂ in the

feed had a negative effect on catalytic activity. The presence of 10% H₂O in the feed had a slightly negative effect on the catalytic performance. The CO conversion dropped to 75% at 110 °C due to blocking of water on the active sites [84].

The CO conversion dropped to 65% with a shift of 20 °C to higher temperature when 20% CO₂ was present in the feed. Our finding of a decrease in catalytic activity in the presence of CO₂ in the feedstream agreed well with the studies of Panzera et al. [38] and Schubert et al. [85]. The presence of CO₂ in the feed was a cause of forming of carbonate or carboxylate which competed with CO adsorption on the active site of the catalyst. When 10% H₂O and 20% CO₂ were present in the feed, it showed clearly diminishment of the activity because of water blocking and carbonate adsorption on the active sites. The results were in good agreement with Schubert et al. [85] and Parinyaswan et al. [68]. It was also noticed that there was much difference in the selectivity at low temperature range (50–90 °C). However, at the higher temperature, the selectivity of all catalysts did not much change.

In previous work, the results showed that the bimetallic catalyst of Pt and Au displayed the best activity at 90 °C and the maximum conversion and selectivity were approximately 90% and 50%, respectively under simulated gas (dry basis). It means that the bimetallic catalyst has a new phase of Pt–Au metals which helps CO oxidation at lower temperature. Thus, 1%(1:1)PtAu/CeO₂-SSG was chosen to study for the double-stage reactor system.

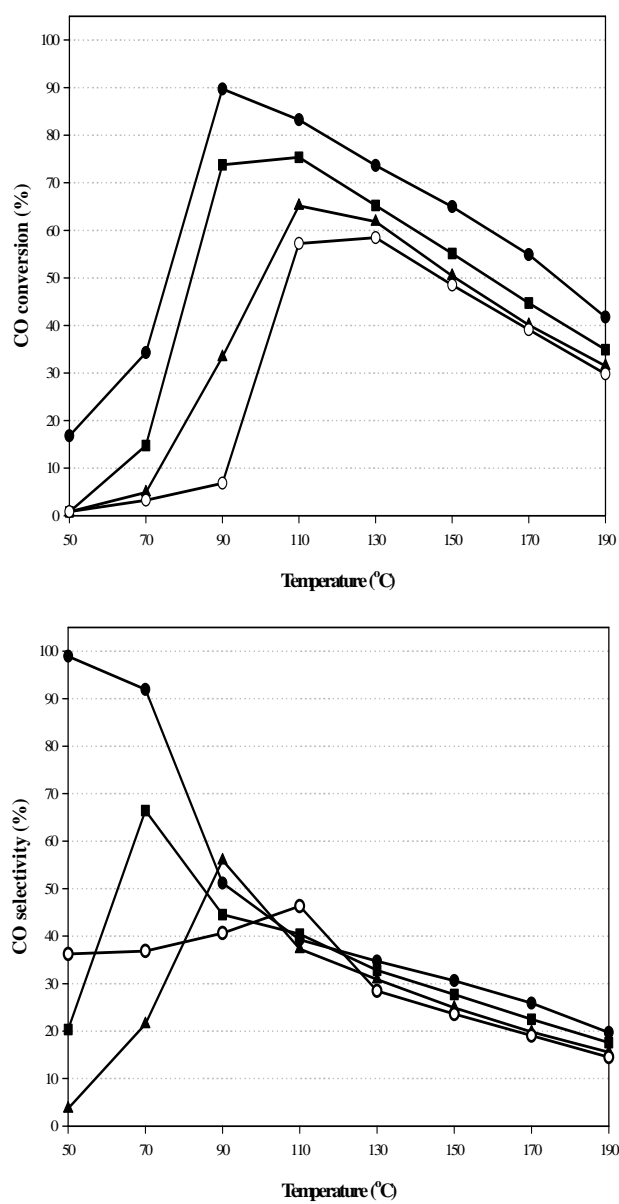


Figure 6.9 Effect of H₂O and CO₂ content in the feed of 1%(1:1)PtAu/CeO₂:
 (●) 0% H₂O + 0% CO₂, (■) 10% H₂O + 0% CO₂, (▲) 0% H₂O + 20% CO₂, (○) 10% H₂O + 20% CO₂.

6.1.2.6 Double-stage reactor temperature optimization

For system of a single stage reactor, the maximum CO conversion was showed at 90 °C by total O₂ in feedstream being 1 vo%l (O₂/CO = 1) and 0.1 g of catalyst. For a double stage reactor at the same condition, it was operated in the temperature range of 70 °C to 130 °C. The oxygen split ratio and the amount of catalyst ratio were 1:1 between the first stage and the second stage. Figure 6.10 shows the results of the operating temperatures affected on the double-stage reactor. It was found that the CO conversion increased rapidly between the temperature range of 90 °C to 110 °C. The maximum CO conversion of ~93% and the selectivity of ~43% were obtained when the temperature of the first and second stage were 90 °C and 110 °C, respectively. Thus, the operating temperature of the first stage reactor at 90 °C was chosen for all of experiment.

6.1.2.7 Oxygen split ratio optimization

To operate in the double-stage reactor, the total amount of O₂ (1 vol%, O₂/CO = 1) was split between two stages in ratios of 4:1, 3:2, 1:1, 2:3, and 1:4. The total amount of catalyst was 0.1 g divided into 1:1 ratio for the first stage to the second stage. The operating temperature of the second stage was heated from 50 °C to 190 °C while the first stage was kept constant at 90 °C. The results are shown in Figure 6.11, indicated that the maximum CO conversion in each oxygen split ratio was in the temperature range of 110 °C to 130 °C. The highest performance is ~93% of CO conversion at 110 °C.

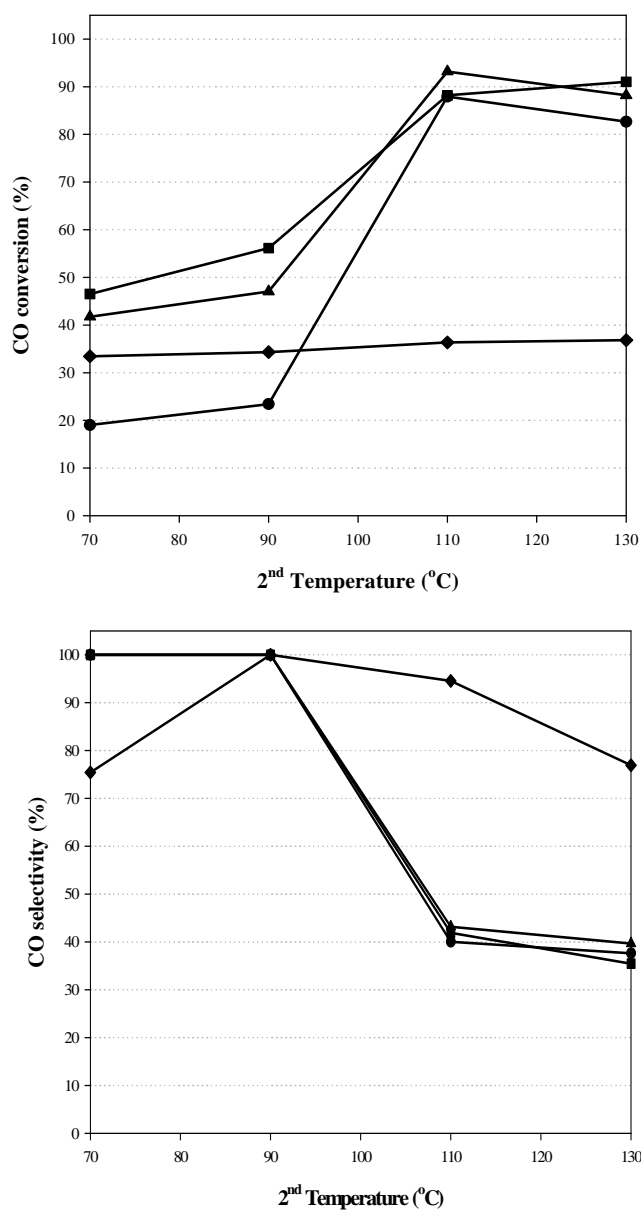


Figure 6.10 Effect of operating temperature between two stages of the double-stage reactor in the first stage: (●) 70 °C, (▲) 90 °C, (■) 110 °C, (◆) 130 °C, of 1%(1:1)PtAu/CeO₂ at catalyst weight and O₂ split ratio between two stages = 1:1, O₂/CO = 1, and W/F ratio = 0.12 g s cm⁻³.

6.1.2.8 Catalyst weight to total gas inlet ratio (W/F ratio)

The total amount of catalyst used in the double-stage reactor was 0.1 g (0.12 g s cm^{-3}) and 0.3 g (0.36 g s cm^{-3}) at 1:1 ratio between the first stage and the second stage. Oxygen split ratio was 1:1 ($\text{O}_2/\text{CO} = 1$). Figure 6.12 illustrates that increasing of the amount of catalyst increased the activity due to a lot of active sites for CO oxidation. The best performance gave ~97% of CO conversion and ~38% of selectivity at 90 °C of the second stage temperature. However, the selectivity decreased because H_2 oxidation also occurred.

6.1.2.9 Effect of O_2/CO in the feedstream

O_2/CO ratio in the feedstream was varied at 1:1 and 2:1 for the double-stage reactor system. The total O_2 inlet stream (1 or 2 vol%) was split between two stages at 1:1 ratio. In this figure, we also compared using of 0.1 g and 0.3 g at 1:1 ratio of the amount of catalyst between two stages. The results display in Figure 6.13, they imply that when the amount of catalyst or the O_2 inlet stream was increased, the CO conversion increased. Nevertheless, when the total O_2 inlet stream increased, the selectivity decreased very clearly because of competition of H_2 oxidation. The best CO conversion was ~99% at 90 °C while the selectivity was ~25% only. Thus, increasing of the amount of catalyst could give better performance at lower temperature because the conversion increased and the selectivity slightly decreased.

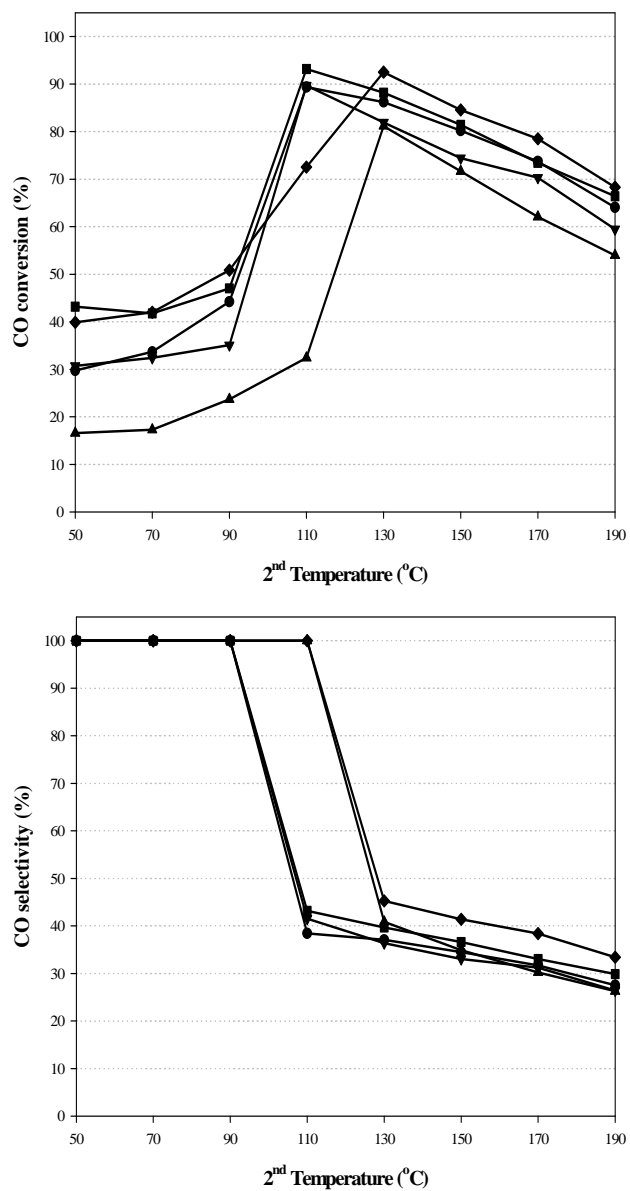


Figure 6.11 Effect of oxygen split ratio between two stages: (▲) 4:1, (●) 3:2, (■) 1:1, (◆) 2:3, (▼) 1:4, of 1%(1:1)PtAu/CeO₂ at 1st temperature = 90 °C, catalyst weight and O₂ split ratio between two stages = 1:1, O₂/CO = 1, and W/F ratio = 0.12 g s cm⁻³.

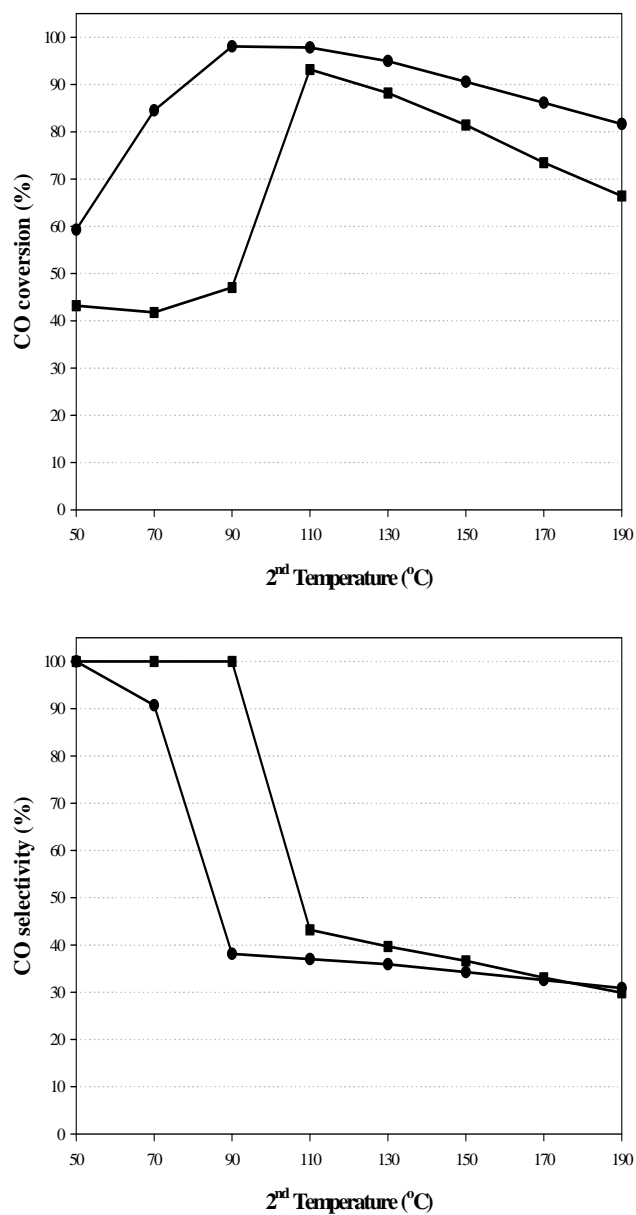


Figure 6.12 Effect of catalyst weight to total flow rate (W/F) ratio: (■) 0.12 g s cm⁻³ and (●) 0.36 g s cm⁻³, of 1%(1:1)PtAu/CeO₂ at 1st temperature = 90 °C, catalyst weight and O₂ split ratio between two stages = 1:1, and O₂/CO = 1.

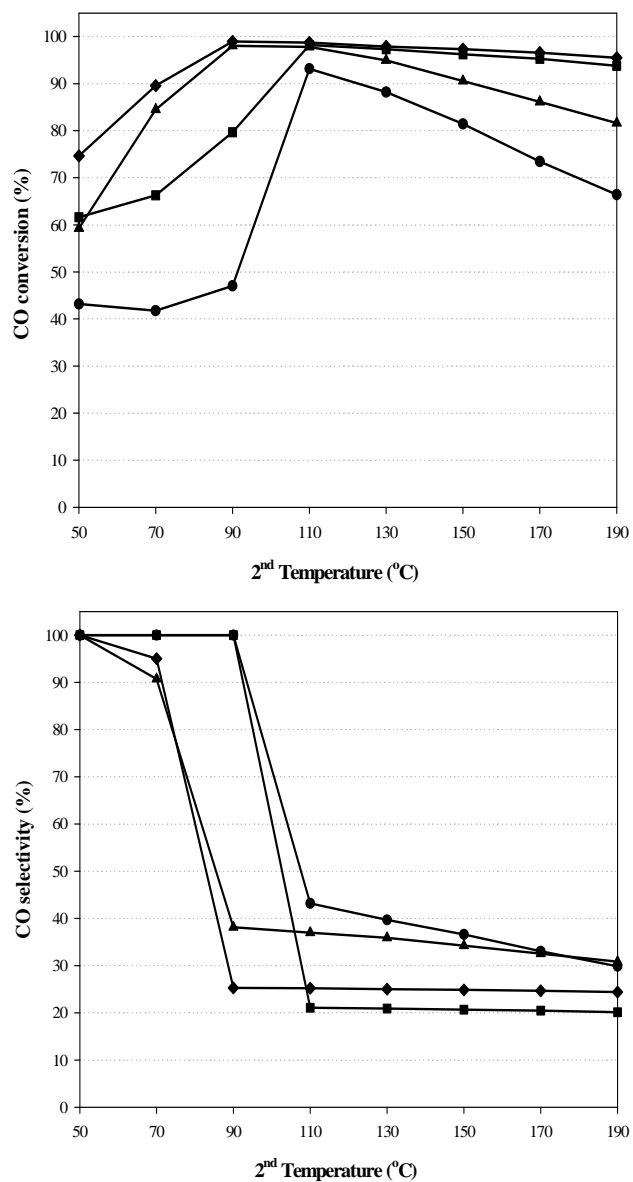


Figure 6.13 Effect of O₂/CO in the feedstream and W/F ratio: (●) 1:1 and 0.12 g s cm⁻³, (▲) 1:1 and 0.36 g s cm⁻³, (■) 2:1 and 0.12 g s cm⁻³, and (◆) 2:1 and 0.36 g s cm⁻³, of 1%(1:1)PtAu/CeO₂ at 1st temperature = 90 °C and catalyst weight and O₂ split ratio between two stages = 1:1.

6.2 Part II: Platinum and gold supported on mixed oxide catalysts

6.2.1 Catalyst characterization

The physical properties of PtAu/CeO₂, PtAu/CeO₂-ZnO, and PtAu/CeO₂-Fe₂O₃ were displayed in Table 6.2. The BET surface area of the catalyst prepared by SSG was greater than the one prepared by CP of all catalysts. The PtAu/CeO₂ (83.9 m² g⁻¹) shows the highest surface area for SSG method while PtAu/CeO₂-ZnO (58.6 m² g⁻¹) is the highest for CP method. Crystallite sizes of metal oxide were determined from X-ray line-broadening using Debye-Scherrer equation. The major peaks at (1 1 1) for CeO₂ (ceria), at (1 0 1) for ZnO (zincite), and at (3 1 1) for Fe₂O₃ (maghemite) have been used for the crystallite size calculation. The catalysts that were prepared by the CP method gave ceria crystallite size smaller than the SSG one. Especially, PtAu/CeO₂-ZnO prepared by CP method gave the smallest ceria crystallite size of all. The ceria crystallite size in the mixed oxide support prepared by CP was smaller than that of the ceria support prepared by CP. Figure 6.14 is a comparison of the XRD patterns of the prepared catalysts which prepared by SSG and CP method. The catalysts that were prepared by CP gave a lower reflection peak intensity when compared to that prepared by SSG. It should be noted that the SSG method provided a more crystalline structure than the CP method and resulted in a greater surface area. The reflection peaks of ceria appeared at 28.6°, 33.1°, 47.5°, 56.3°, 59.1°, 69.4°, 76.7°, 79.1°, and 88.4° of 2θ. All of catalysts presented the major reflection peaks of ceria. For mixed oxide supports, PtAu/CeO₂-ZnO (c and d) also

Table 6.2 Physical properties of Pt–Au supported on various metal oxide catalysts

Catalysts	Preparation method	Pt:Au ratio ^a	S _{BET} ^b (m ² g ⁻¹)	Pore volume ^b (cm ³ g ⁻¹)	CeO ₂ crystallite size ^c (nm)	ZnO or Fe ₂ O ₃ crystallite size ^c (nm)
PtAu/CeO ₂	SSG	0.31:0.30	83.9	0.09	14.8	-
PtAu/CeO ₂	CP	0.30 :0.24	40.0	0.06	12.2	-
PtAu/CeO ₂ –ZnO	SSG	0.22 :0.27	76.9	0.08	15.4	22.3
PtAu/CeO ₂ –ZnO	CP	0.32 :0.29	58.6	0.16	7.7	27.1
PtAu/CeO ₂ –Fe ₂ O ₃	SSG	0.09 :0.19	32.3	0.01	14.6	-
PtAu/CeO ₂ –Fe ₂ O ₃	CP	0.34:0.25	29.5	0.13	10.0	45.0

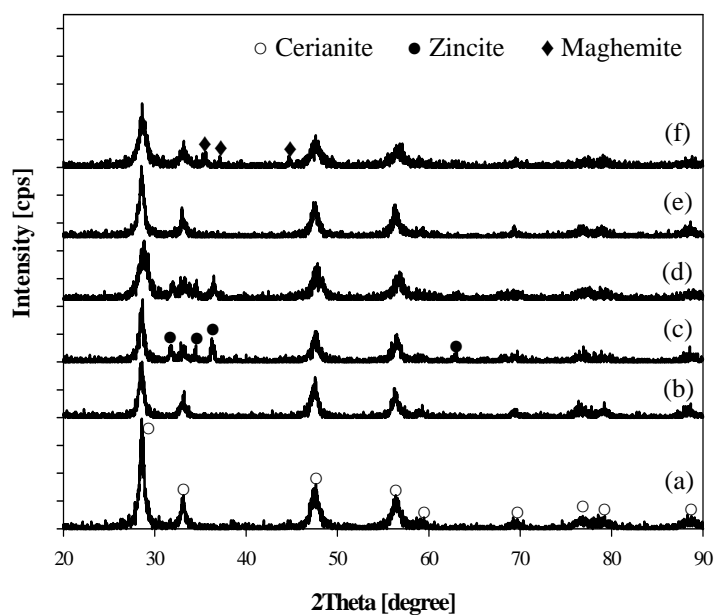
^a Determined by XRF^b Determined by BET surface area analyzer^c Determined by XRD from line broadening of CeO₂ (1 1 1), ZnO (1 0 1), and Fe₂O₃ (3 1 1)

Figure 6.14 XRD patterns of the prepared catalysts: (a) PtAu/CeO₂-SSG, (b) PtAu/CeO₂-CP, (c) PtAu/CeO₂-ZnO-SSG, (d) PtAu/CeO₂-ZnO-CP, (e) PtAu/CeO₂-Fe₂O₃-SSG, and (f) PtAu/CeO₂-Fe₂O₃-CP.

presented the major reflection peaks of zincite at 31.8° , 34.4° , 36.3° , and 62.9° of 2θ . For PtAu/CeO₂-Fe₂O₃ (e and f), the major peaks appeared at 35.6° , 37.3° , and 43.3° were the typical maghemite. However, all of them had no metal peaks (Pt and Au) in XRD patterns of catalysts, implying that the metallic particle size of the prepared catalysts is either atomically dispersed or too small to be detected by XRD (<5 nm). The existent active metal was checked by XRF method. The crystallite size from the XRD calculation was confirmed with SEM images, as shown in Figure 6.15. These images indicate that the SSG provided more crystallinity than the CP and showed a multilayer shape, so the SSG gave a greater surface area than the CP. Moreover, they resulted that the CP gave a smaller particle size than the SSG.

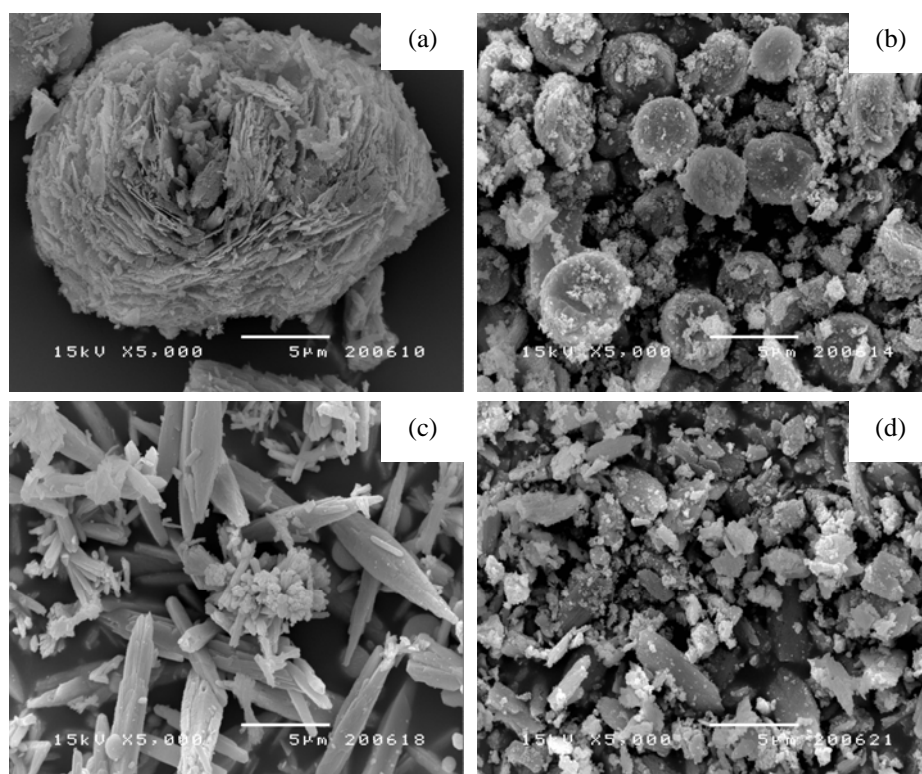


Figure 6.15 SEM images of the prepared catalysts: (a) PtAu/CeO₂-ZnO-SSG, (b) PtAu/CeO₂-ZnO-CP, (c) PtAu/CeO₂-Fe₂O₃-SSG, and (d) PtAu/CeO₂-Fe₂O₃-CP.

Table 6.3 and XRD patterns in Figure 6.16 show physical properties of Pt–Au supported catalyst with various ratio of mixed oxide at different calcination temperature. The ceria crystallite sizes from XRD calculation at the calcination temperatures of 200 °C, 350 °C, and 500 °C were 4.9 nm, 6.3 nm, and 7.7 nm, respectively. This implies that the ceria crystallite size increased with calcination temperature due to sintering of the particles. It resulted in catalyst calcination of 500 °C gave lower surface area than the others due to the highest ceria and zincite crystallite sizes. This results are confirmed by SEM images in Figure 6.17 very clearly. The XRD patterns of the catalysts with various calcination temperatures are shown in line b, c, and e. Broader peaks were obtained when operating at lower calcination temperatures. For mixed oxide support, the diffraction patterns of the pure CeO₂ and ZnO supports revealed more crystallinity compared to the CeO₂–ZnO mixed-phase supports. When varying the Ce–Zn ratios in the mixed-oxide support from 10:1 to 1:1 and to 1:10, the intensity of the zincite reflections at phases (1 0 0), (0 0 2), and (1 0 1) increased rapidly while a broadened peak (1 1 1) of ceria was obtained. This can be explained in that Zn²⁺ had been incorporated into the ceria lattice. Therefore, the ceria crystallite size in the mixed-oxide support is smaller than in the CeO₂ supports. These results are also confirmed by the results shown in Table 6.2 and 6.3. Moreover, it is observed that the peak positions of the ceria in the mixed-oxide support phases – (1 1 1), (2 2 0), and (3 1 1) – had slightly shifted to higher 2θ values when decreasing the Ce–Zn ratio. It can be said that Ce⁴⁺ ions in the lattice were substituted by the Zn²⁺ ions. The incorporation of the Ce⁴⁺ and Zn²⁺ ions cause a shrinkage of the crystal lattice to form a solid solution [87].

Table 6.3 Physical properties of Pt–Au supported on various ratio of mixed oxide and various calcination temperature

Ce:Zn ratio	Calcination temperature (°C)	$S_{\text{BET}}^{\text{a}}$ ($\text{m}^2 \text{g}^{-1}$)	Pore volume ^a ($\text{cm}^3 \text{g}^{-1}$)	CeO ₂ crystallite size ^b (nm)	ZnO crystallite size ^b (nm)
1:1	200	68.7	0.17	4.9	20.2
1:1	350	67.7	0.17	6.3	18.8
10:1	500	43.0	0.09	8.3	-
1:1	500	58.6	0.16	7.7	27.1
1:10	500	63.4	0.40	9.4	16.3

^a Determined by BET surface area analyzer

^b Determined by XRD from line broadening of CeO₂ (1 1 1) and ZnO (1 0 1)

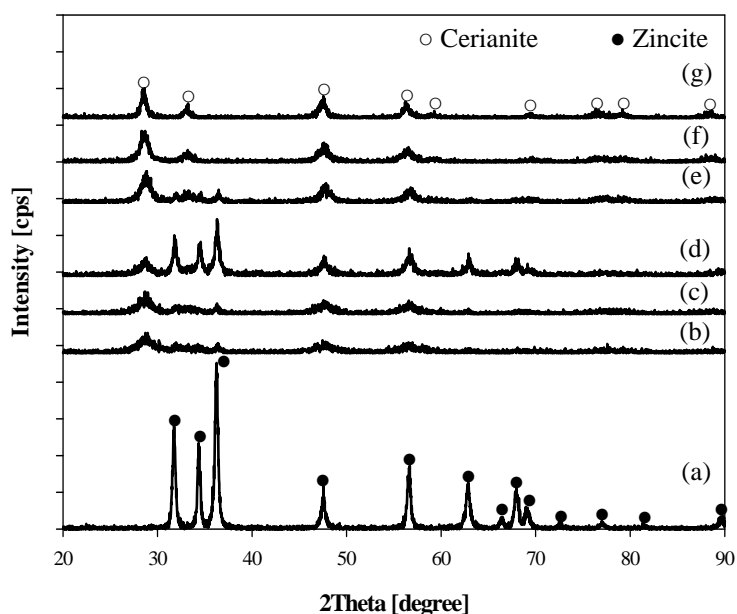


Figure 6.16 XRD patterns of the prepared catalysts: (a) PtAu/ZnO-CP calcined at 500 °C, (b) PtAu/(1:1)CeO₂–ZnO-CP calcined at 200 °C, (c) PtAu/(1:1)CeO₂–ZnO-CP calcined at 350 °C, (d) PtAu/(1:10)CeO₂–ZnO-CP calcined at 500 °C, (e) PtAu/(1:1)CeO₂–ZnO-CP calcined at 500 °C, (f) PtAu/(10:1)CeO₂–ZnO-CP calcined at 500 °C, and (g) PtAu/CeO₂-CP calcined at 500 °C.

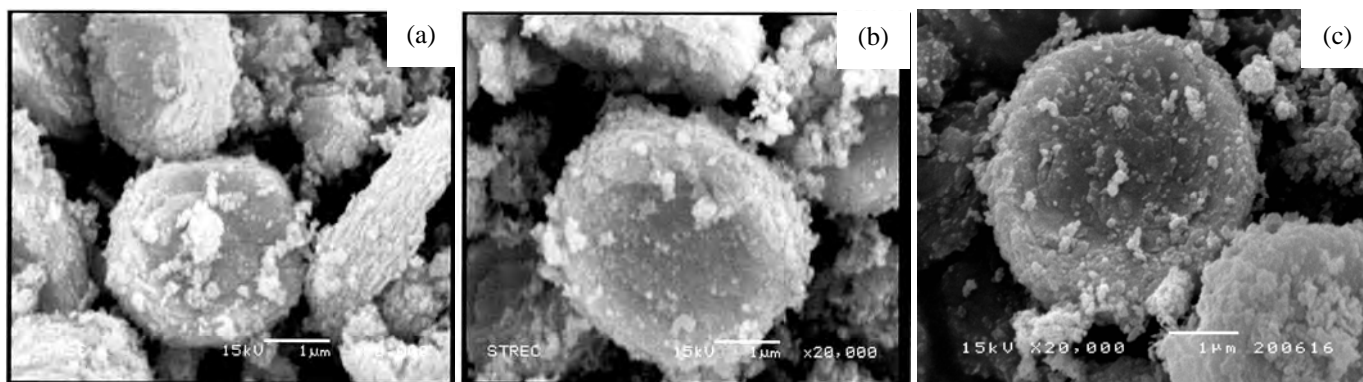


Figure 6.17 SEM images of the PtAu/(1:1)CeO₂-ZnO-CP with various calcination temperature: (a) 200 °C, (b) 350 °C, and (c) 500 °C.

The reduction behavior of the PtAu/(x:y)CeO₂-ZnO, PtAu/CeO₂, and PtAu/ZnO catalysts prepared by CP was determined by TPR, as shown in Figure 6.18. The main reduction peak of the catalysts was in the temperature range of 100 °C to 200 °C, which is the reduction temperature range of the active metal (Pt-Au) [34,86]. This peak also reveals a significant lowering of the reduction temperature of the PtAu/(x:y)CeO₂-ZnO compared to the PtAu/CeO₂. The Zn²⁺ ions help to weaken the surface oxygen on the ceria, thereby improving the reducibility of the catalyst. This interaction may form a solid solution, or a new phase, which shows a lower reduction temperature.

The FTIR spectra of PtAu/CeO₂-ZnO-CP with various calcination temperatures are shown in Figure 6.19. The wavenumber in range of 1200–1700 cm⁻¹ was the adsorption band of carbonate group. The results showed that more carbonate species are removed from the catalysts when increasing in the calcination temperature. Carbonate species on the catalyst surface are removed completely when the catalysts were calcined at 500 °C.

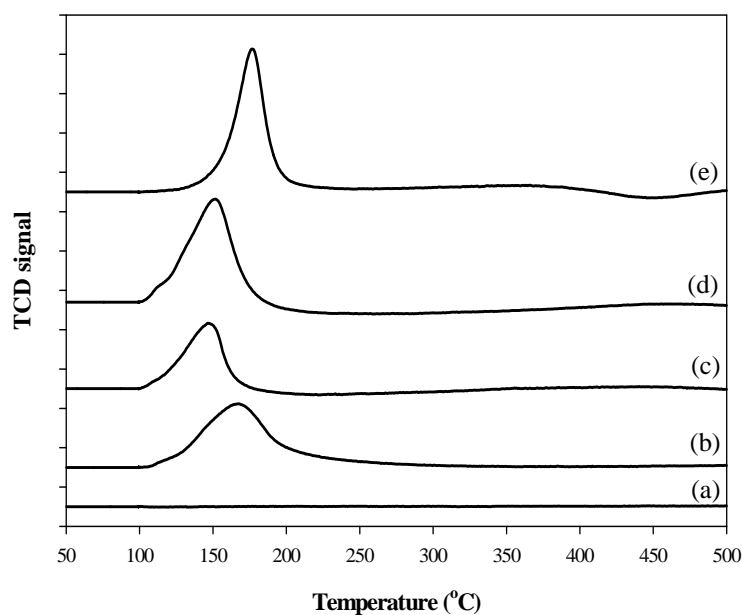


Figure 6.18 TPR profiles of the prepared catalysts: (a) PtAu/ZnO-CP, (b) PtAu/(1:10)CeO₂-ZnO-CP, (c) PtAu/(1:1)CeO₂-ZnO-CP, (d) PtAu/(10:1)CeO₂-ZnO-CP, and (e) PtAu/CeO₂-CP.

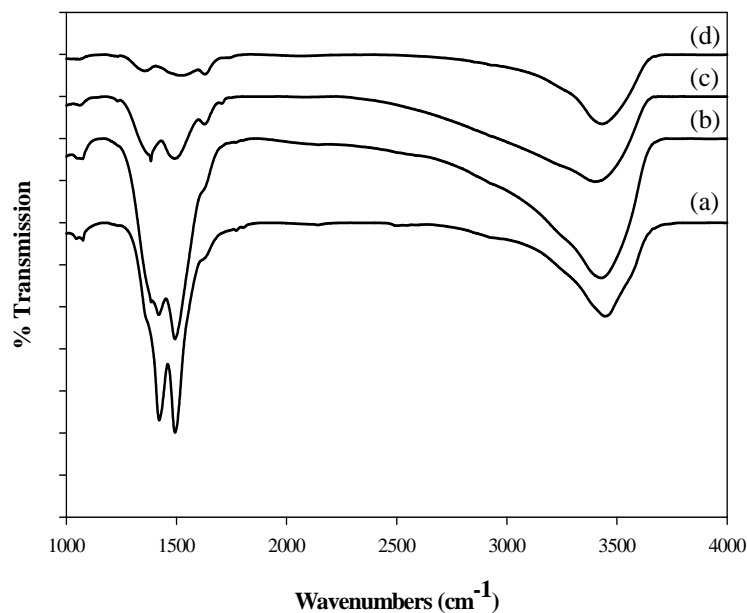


Figure 6.19 FTIR spectra of PtAu/(1:1)CeO₂-ZnO with various calcination temperature: (a) non-calcined, (b) 200 °C, (c) 350 °C, and (d) 500 °C.

6.2.2 Catalytic activity

6.2.2.1 Single step sol-gel (SSG) vs co-precipitation (CP)

The CO conversion and selectivity of the Pt–Au supported on mixed oxide catalysts prepared by SSG and CP are compared in Figures 6.20 and 6.21, respectively. For PtAu/CeO₂ catalysts which prepared by two methods, the catalyst prepared by SSG had a better performance than the catalyst prepared by CP all reaction temperatures. Because SSG method gave smaller particle size and higher surface area than CP method (see Table 6.2). The maximum conversion of the PtAu/CeO₂-SSG and PtAu/CeO₂-CP were ~90% (90 °C) and ~55% (110 °C), respectively. Although the catalyst prepared by SSG method showed a good performance in lower temperature, it can not remove poisoned CO completely. So, improvement of catalyst with other metals is needed.

The different catalyst supports are CeO₂, CeO₂–ZnO and CeO₂–Fe₂O₃ (Ce:Zn or Ce:Fe ratio = 1:1) that prepared by SSG and CP as shown in Figures 6.20 and 6.21, respectively. In case of SSG method, PtAu/CeO₂–ZnO and PtAu/CeO₂–Fe₂O₃ gave lower conversion than PtAu/CeO₂ while they gave higher conversion in case of CP method and maximum CO conversion shift to lower temperature than PtAu/CeO₂. The maximum conversion was PtAu/CeO₂–ZnO (~93%) and then was PtAu/CeO₂–Fe₂O₃ (~80%) at 90 °C. The results showed that the preparation method had effected to catalytic activity significantly. Meanwhile it also had effected to structure and composition in the catalyst. As presented in Table 6.2, addition of Fe₂O₃ by SSG or CP gave the lowest surface area because two methods were not appropriate for Fe₂O₃. It can be seen that the maximum CO conversion shift to lower temperature

(90 °C) when the catalyst was prepared by CP method. From this part, we chose the CP method to improve the performance of PtAu/CeO₂-ZnO for PROX reaction.

When compared the PtAu/CeO₂-ZnO between SSG and CP methods, the catalytic performance prepared by CP gave higher catalytic activity than the one prepared by SSG at a low reaction temperature (80–130 °C). While in the high temperature range (>130 °C), the activity of those catalysts was not very different. The maximum CO conversion is 15% higher when employing the PtAu/CeO₂-ZnO catalysts prepared by CP. From the SEM images (Figure 6.15), the particle size of the PtAu/CeO₂-ZnO prepared by CP is smaller. From the results of the chemisorption analyzer, the metallic surface areas of the PtAu/CeO₂-ZnO prepared by CP and the PtAu/CeO₂-ZnO prepared by SSG are 403.6 m² g⁻¹_{metal} and 117.3 m² g⁻¹_{metal}, respectively. Therefore, the catalytic performance of the PtAu/CeO₂-ZnO prepared by CP is then higher. From the above results, it can be said that the catalytic preparation method had a significant effect on the catalyst characteristics and its activity. This is in good agreement with Scirè et al. [70]. From this result, the PtAu/CeO₂-ZnO prepared CP method was then chosen to prepare the catalysts employed in the rest of the investigation.

6.2.2.2 Ce:Zn ratio in the catalyst

A comparison among the catalytic activities of Pt–Au on different Ce:Zn ratio of support are shown in Figure 6.22. The mixed oxide ratio is varied from 10:1 to 1:1 and to 1:10. The results indicated that the 1:1 of Ce–Zn ratio gave the highest CO conversion (~93%) with ~40% selectivity at 90 °C. This is attributed to the dispersion of active metals (Pt–Au) on the solid solution of CeO₂-ZnO.

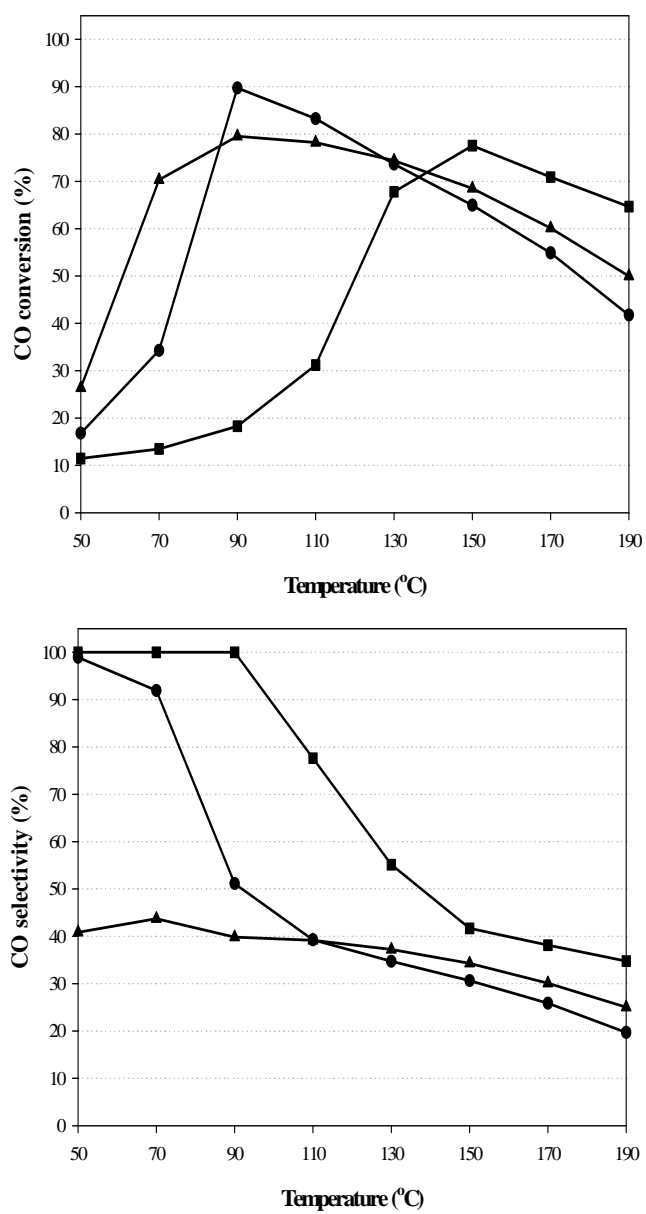


Figure 6.20 Addition of ZnO or Fe₂O₃ at 1:1 atomic ratio of Ce:Zn or Ce:Fe into 1%(1:1)PtAu/CeO₂ catalysts by SSG method: (●) PtAu/CeO₂, (▲) PtAu/CeO₂-ZnO, and (■) PtAu/CeO₂-Fe₂O₃.

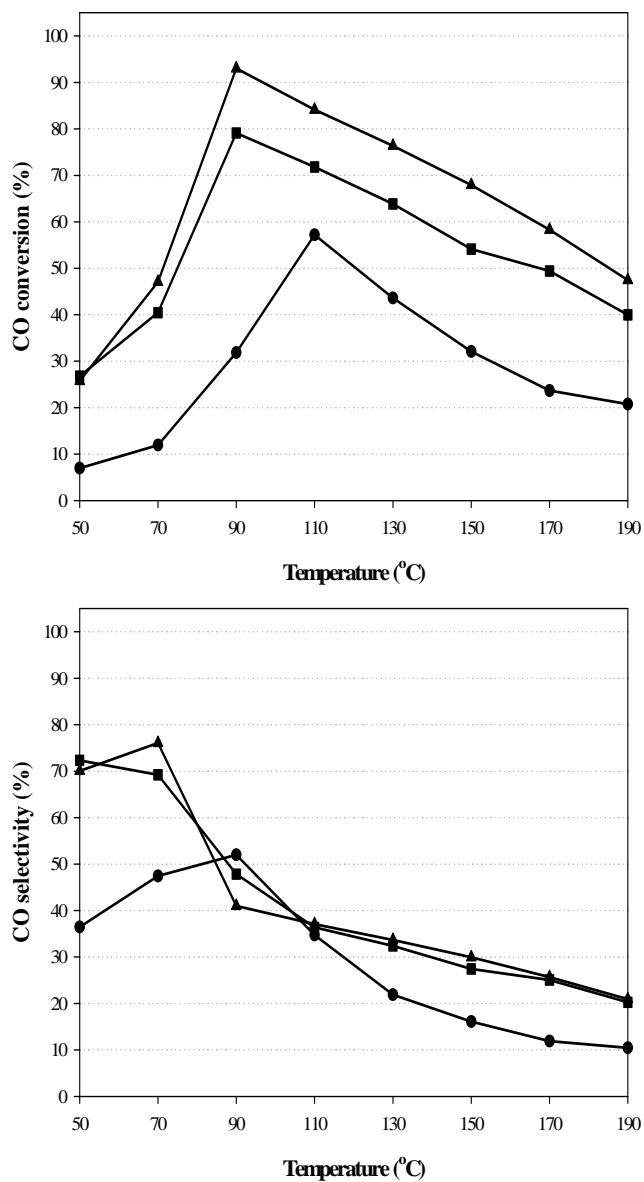


Figure 6.21 Addition of ZnO or Fe₂O₃ at 1:1 atomic ratio of Ce:Zn or Ce:Fe into 1%(1:1)PtAu/CeO₂ catalysts by CP method: (●) PtAu/CeO₂, (▲) PtAu/CeO₂-ZnO, and (■) PtAu/CeO₂-Fe₂O₃.

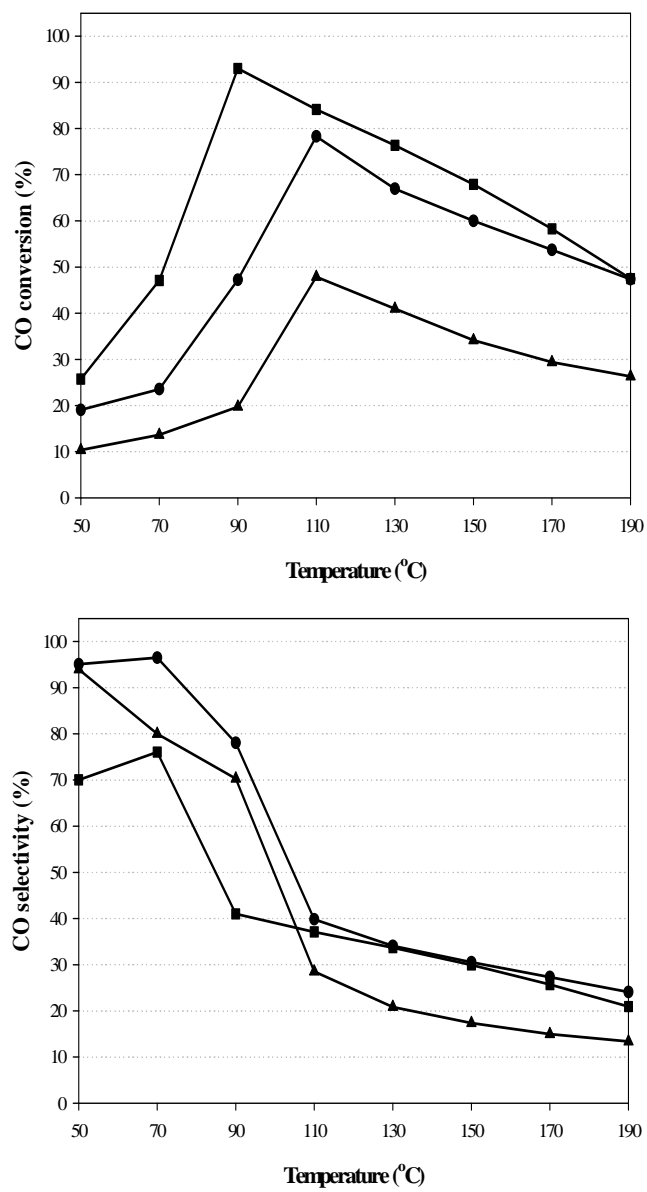


Figure 6.22 Catalytic activity of the PtAu/CeO₂-ZnO-CP with various Ce:Zn atomic ratio: (▲) 10:1, (■) 1:1, and (●) 1:10.

6.2.2.3 Treatment condition

Calcination is an important step to remove impurities in catalysts (such as the carbonate group, which is an inhibitor for the reaction). The calcination temperature is an important parameter for improving the catalytic activity [57]. The activities of the PtAu/CeO₂-ZnO-CP calcined at 200 °C, 350 °C, and 500 °C for 5 h are shown in Figure 6.23. These catalysts were pretreated under H₂ atmosphere. The results indicated that the activities were not different significantly when the operating temperature was higher than 90 °C. However, we have examined the prepared catalysts at various calcination temperatures by FTIR spectrometry (see Figure 6.19). The results show that carbonate groups which is an inhibitor for the reaction in the catalyst were effectively removed when being calcined at higher temperature, particularly at 500 °C. Therefore, we chose the PtAu/CeO₂-ZnO-CP catalysts that calcined at 500 °C to prevent blocking of carbonate groups on catalyst surface. It exhibited the highest CO conversion (~93%) with ~40% selectivity at 90 °C. This is due to its crystallinity and to the complete carbonate removal on the sites of the catalyst surface. Figure 6.24 shows the catalytic performance of the PtAu/CeO₂-ZnO-CP catalysts subjected to different pretreatment procedures. All catalysts were calcined at 500 °C for 5 h. Clearly, the catalytic performance obtained from the H₂-pretreated catalyst is higher than that obtained from the non-pretreated catalyst or the O₂-pretreated catalyst. Reduction with H₂ will change metal oxide form to pure metal form of active sites for reaction. The PtAu/CeO₂-ZnO-CP gave the maximum conversion at 90 °C: ~93% conversion and ~40% selectivity. Thus, the active species of the catalyst are improved by H₂ pretreatment.

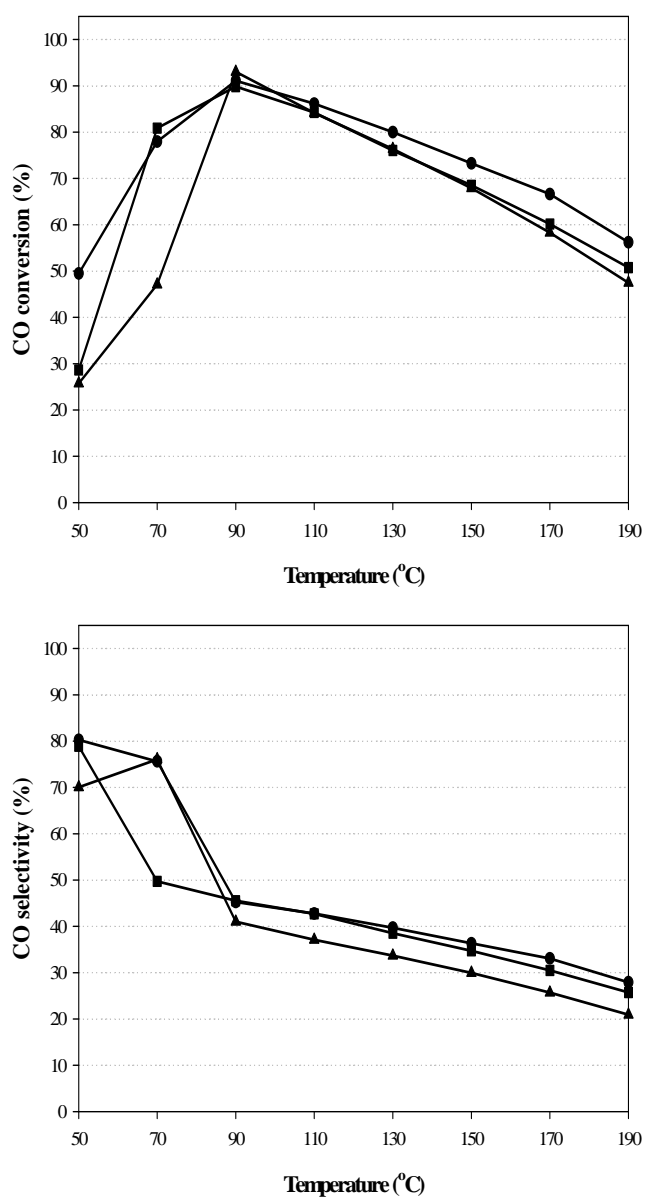


Figure 6.23 Catalytic activity of the PtAu/(1:1)CeO₂-ZnO-CP with various calcination temperature: (●) 200 °C, (■) 350 °C, and (▲) 500 °C.

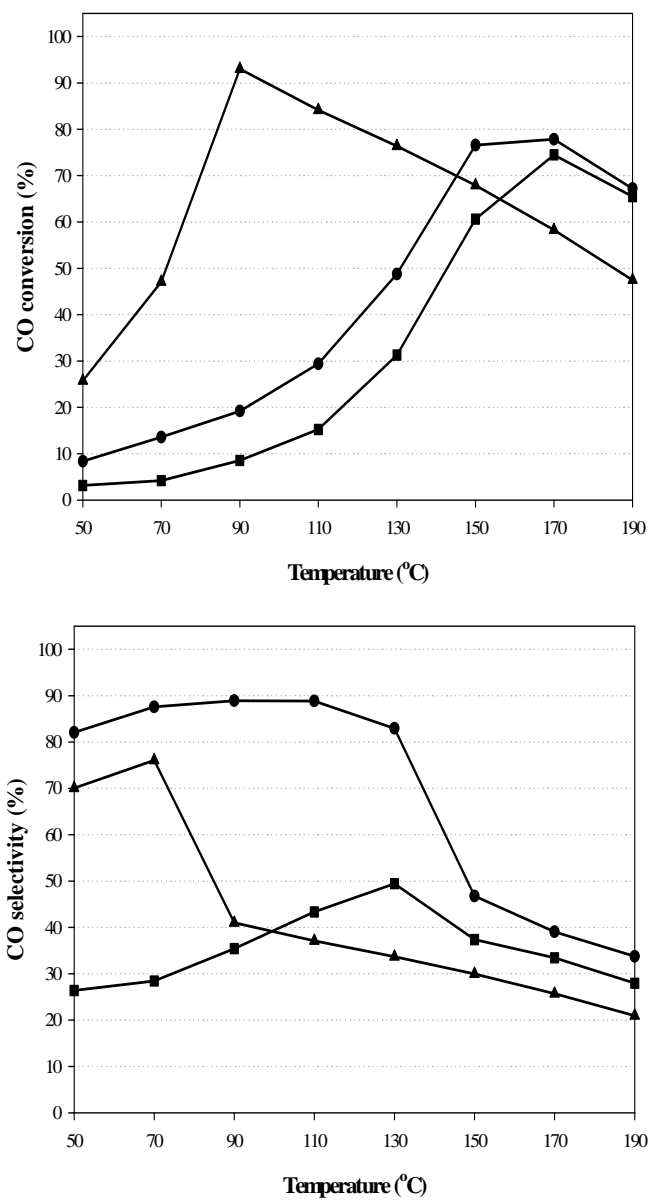


Figure 6.24 Catalytic activity of the PtAu/CeO₂-ZnO-CP calcined at 500 °C with various gas pretreatment: (●) non, (■) O₂, and (▲) H₂.

6.2.2.4 Presence of H₂O and CO₂ in the feedstream

The influence of co-added 10% H₂O and 20% CO₂ to the feedstream on the catalytic performance of PtAu/CeO₂-ZnO-CP catalysts was also investigated, as shown in Figure 6.25. It was found that 10% H₂O in feedstream increased the catalytic activity of catalyst, especially higher temperature (> 90 °C). This can be pronounced that the presence of 10% H₂O promotes oxidation of CO by WGS reaction. This result contrasted to PtAu/CeO₂ catalyst in part I; therefore, the addition of ZnO into PtAu/CeO₂ can improve catalytic activity when H₂O presents in the feedstream. The maximum CO conversion was dropped ~38% with a shift of 60 °C to higher temperature when 20% CO₂ was presented in the feed. Our finding agreed with the studies of Panzera et al. [38] and Schubert et al. [85]. The presence of CO₂ in the feed was a cause of forming of carbonate or carboxylate which competed with CO adsorption on the active site of the catalyst. When 10% H₂O and 20% CO₂ were presented in the feed, the CO conversion and its selectivity were clearly diminished. This can be explained in that the molecules of CO₂ which is significant effect more than H₂O compete for the adsorption with CO on the active sites of the catalysts. Therefore, the CO oxidation was decreased dramatically, which is in agreement with Schubert et al. [85] and Parinyaswan et al. [68]. When considering the maximum CO conversion, we also found that the temperature at the maximum CO conversion shifts from 90 °C to 130 °C when both H₂O and CO₂ are present in the feedstream. Therefore, the competition for adsorption of CO and CO₂ on the active sites is the major causes of the negative effects of catalytic activity; although, H₂O seem to be positive effect at higher temperature.

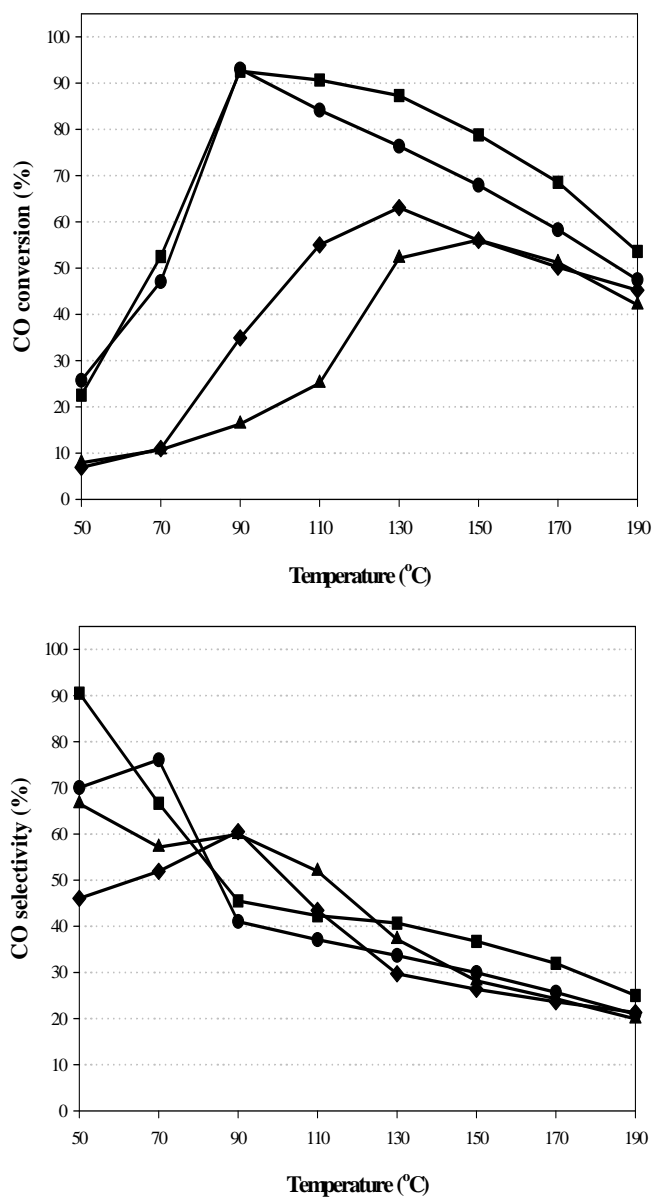


Figure 6.25 Effect of composition in the feedstream on the PtAu/CeO₂-ZnO-CP: (●) 0% H₂O + 0% CO₂, (■) 10% H₂O + 0% CO₂, (▲) 0% H₂O + 20% CO₂, and (◆) 10% H₂O + 20% CO₂.

6.2.2.5 Single and double stage reactor

However, the study of catalyst preparation, addition of metal oxide and pretreatment condition can not remove CO to the desired level. Srinivas et al. [69] had investigated the performance of a PROX reaction in the two-stage mode. They found that the designed reactor had improved the CO elimination. So, we will examine the best catalyst in double-stage reactor. The total amount of catalyst was used 0.1 g ($W/F = 0.12 \text{ g s cm}^{-3}$) by 0.05 g in each reactor and the O_2 split ratio was 1:1 of 1 vol% total O_2 . The results of the reactor effect as shown in Figure 6.26. The experimental data was detected in the steady state region. From the graph presented that using of the double-stage reactor under simulated gas (dry and wet basis) can improve the performance of both condition. For dry basis (0% H_2O + 0% CO_2), can remove CO completely and increase the selectivity from ~40% to ~55% in temperature range of 90 °C to 110 °C. For wet basis (10% H_2O + 20% CO_2), the CO conversion increased from ~60% to ~65% and from ~30% to ~35% for selectivity in temperature range of 90 °C to 130 °C. These results are in good agreement with Srinivas et al. [69].

6.2.2.6 Deactivation test

In our study, we also determine the stability of the PtAu/CeO₂-ZnO-CP catalysts in both single- and double-stage modes for 60 h, as shown in Figure 6.27. Four cases (with and without the presence of 10% H_2O and 20% CO_2 in the feedstream and run in single- and double-stage reactors) are chosen to investigate the deactivation of the catalysts. In the case of no addition of water vapor and CO_2 to the stream, the reaction temperature for the single- and double-stage reactions was maintained at 90 °C to 110 °C. When adding 10% H_2O and 20% CO_2 to the stream, the reaction temperature for the single- and double-stage reactions was kept at 120 °C

to 130 °C. The results showed that the CO conversion for both the single- and double-stage reactions is decreased when adding water vapor and CO₂ to the feedstream. This is due to a blocking by the water vapor and CO₂ at the active sites of the catalysts. Each case also shows that the CO conversion and selectivity are maintained during the deactivation test with only a very slight loss.

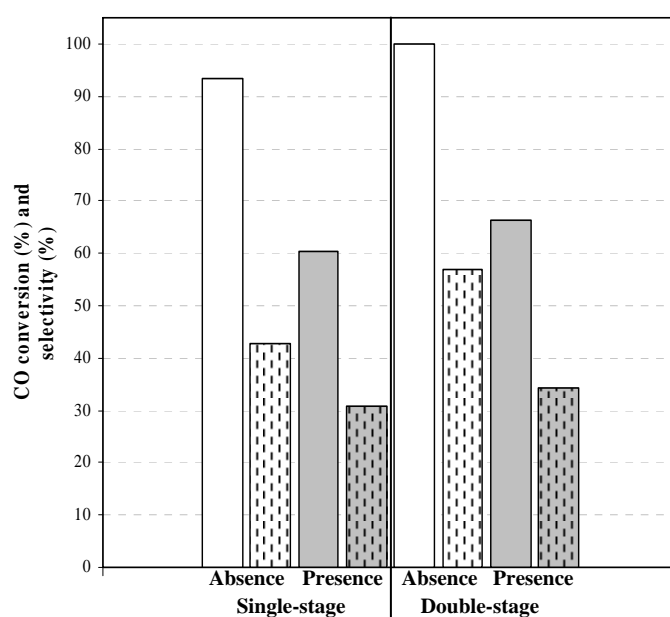


Figure 6.26 Effect of stage reactor in absence (0% H₂O + 0% CO₂) and presence 10% H₂O + 20% CO₂ in the feedstream on the PtAu/(1:1)CeO₂-ZnO-CP.

Single-stage reactor: Operating temperature = 90 °C for absence and 130 °C for presence, O₂/CO = 1, and W/F ratio = 0.12 g s cm⁻³.

Double-stage reactor: Operating temperature of 1st and 2nd stage = 90–110 °C for absence and 120–130 °C for presence, O₂/CO = 1, and W/F ratio = 0.12 g s cm⁻³.

□ ■ CO conversion and ▨ ▩ CO selectivity

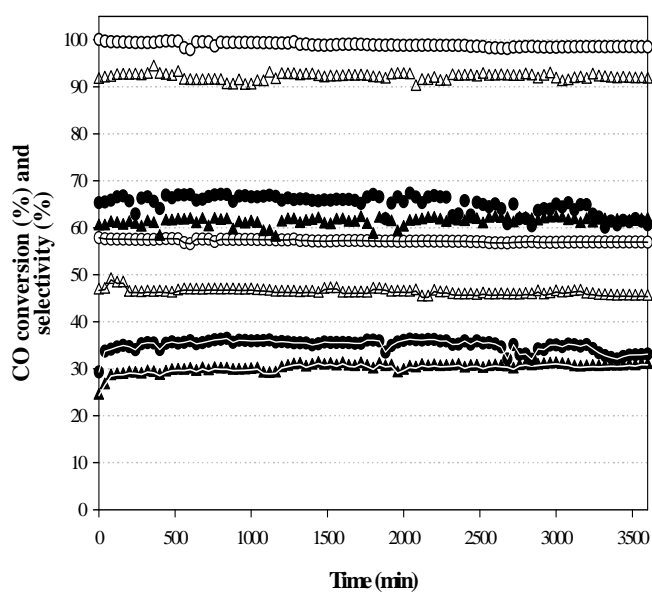


Figure 6.27 Deactivation test on the PtAu/(1:1)CeO₂-ZnO-CP in single- and double-stage reactor under absence and presence 10% H₂O + 20% CO₂ in the feedstream for 3500 min: (Δ,△) absence 10% H₂O + 20% CO₂ in single-stage, (○,⊖) absence 10% H₂O + 20% CO₂ in double-stage, (▲,▲) presence 10% H₂O + 20% CO₂ in single-stage, and (●,●) presence 10% H₂O + 20% CO₂ in double-stage.
 Δ, ▲, ○, ● CO conversion and △, ⊖, ▲, ● CO selectivity

CHAPTER VII

OPTIMIZATION OF PREFERENTIAL CO OXIDATION BY STATISTICAL DESIGNED SET OF EXPERIMENTS*

In this chapter, the catalytic performance for preferential oxidation of CO over 1%(1:1)PtAu/(1:1)CeO₂-ZnO catalyst prepared by co-precipitation was investigated using a statistical design of experiment. The three evaluated factors were the operating temperature (°C), presence of water (%) and CO₂ (%) in the simulating methanol reformat gas. The importance of factors and the interaction among the factors were evaluated by a full 2³ factorial design. Face-centered central composite design (FCCCD) falling under response surface methodology (RSM) was then applied to optimize the responses. The validation of the developed models was tested under both simulating reformat gas and realistic methanol reformat gas.

7.1 Catalytic activity (one-variable-at-a-time)

The catalytic activities of 1%(1:1)PtAu/(1:1)CeO₂-ZnO catalyst when feeding the feedstream with different compositions in operating temperature range of 50 °C to 190 °C are presented in Figure 7.1.

* In preparation

In case of no adding of H₂O and CO₂ in the feedstream, as shown in Figure 7.1a, the CO conversion increased from ~25% to ~93% (3.72-fold) when increasing temperature from 50 °C to 90 °C. Further increasing the temperature from 90 °C to 190 °C, the CO conversion decreased significantly to ~47 (1.98-fold). In a whole range of operating temperatures, CO selectivity was decreased. The maximum CO conversion and selectivity were ~93% and ~41% at 90 °C, respectively. At higher temperature range (> 90 °C), the H₂ oxidation reaction competes with the CO oxidation reaction; therefore, decreasing in the catalytic performance.

Figure 7.1b shows the behavior of catalytic activities when adding H₂O in the feedstream that was similar to that obtained when no adding H₂O and CO₂. In the range of higher operating temperature (> 90 °C), a shift of ~5% to ~10% to higher catalytic performance was obtained when adding 10% H₂O in the feedstream. The possible reason to explain this result is that the presence of 10% H₂O promotes oxidation of CO by WGS reaction. However, the difference in catalytic performance between adding only H₂O and no adding H₂O and CO₂ was less when increasing the operating temperature due to completion of undesired side reaction especially H₂ oxidation. Some [36,60,67] proposed that the presence of H₂O in the feedstream increased the activities at higher temperatures (> 100 °C) whereas Naknam et al. [88] and Schubert et al. [85] showed the enhancing of their catalytic activities at only 30 °C and 80 °C, respectively. Some [89,90] indicated that the maximum CO conversion had shift to the higher temperature.

Effect of CO₂ presence in the feedstream on the catalytic activities is shown in Figure 7.1c. The maximum CO conversion was dropped from ~93% to ~56% with a shift of 60 °C to higher temperature when 20% CO₂ was presented in the feed. Our

finding agreed with the studies of Panzera et al. [38] and Schubert et al. [85], the presence of CO₂ also significantly affected on maximum conversion temperature shift to higher temperature. The presence of CO₂ in the feed was a cause of forming of carbonate or carboxylate which competed with CO adsorption on the active site of the catalyst. The catalyst performance dropped dramatically compare to case of adding 10% H₂O and case of no adding H₂O and CO₂. This implies that influence of CO₂ presence in the feedstream on the catalytic performance is greater than that of H₂O presence in the feed.

Figure 7.1d shows the effect of co-adding 10% H₂O and 20% CO₂ in the feedstream on the catalytic activities. The CO conversion and its selectivity were clearly diminished compare to the others. This can be explained in that the molecules of CO₂ which is significant effect more than H₂O compete for the adsorption with CO on the active sites of the catalysts. Therefore, the CO oxidation was decreased dramatically, which is in agreement with Schubert et al. [85] and Parinyaswan et al. [68]. When considering the maximum CO conversion, we also found that the temperature at the maximum CO conversion shifts from 90 °C to 130 °C when co-adding H₂O and CO₂ in the feedstream. Therefore, the competition for adsorption of CO and CO₂ on the active sites is the major causes of the negative effects of catalytic activity; although, H₂O seem to have a slight positive effect in a range of operating temperature from 90 °C to 190 °C. However, the co-presence of H₂O and CO₂ in feedstream effected significantly on the maximum conversion temperature shift to higher temperature [36,67,85,88–91].

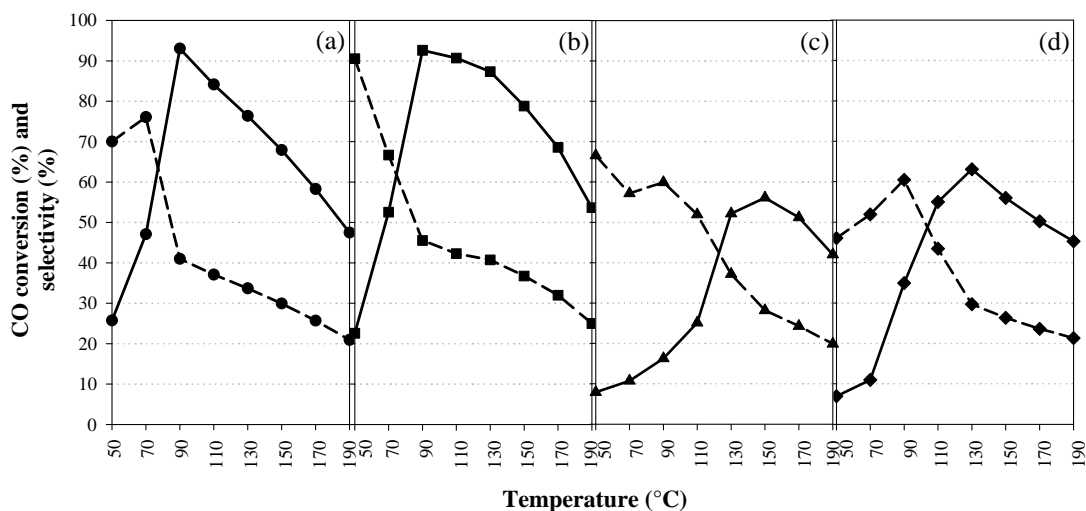


Figure 7.1 Catalytic performance of 1%(1:1)PtAu/(1:1)CeO₂-ZnO catalyst in operating temperature range of 50 °C to 190 °C when feeding the feedstream with various compositions:

- (a) 1% CO, 1% O₂, and 40% H₂ in He balance
- (b) 1% CO, 1% O₂, 10% H₂O, and 40% H₂ in He balance
- (c) 1% CO, 1% O₂, 20% CO₂, and 40% H₂ in He balance
- (d) 1% CO, 1% O₂, 10% H₂O, 20% CO₂, and 40% H₂ in He balance.

CO conversion (solid line) and CO selectivity (dot line)

7.2 Factors screening in a full 2³ factorial design

Based on the catalytic activities for PROX of CO, CO conversion and selectivity were then used as a response. A full 2³ factorial design with 3 central points was applied to evaluate an importance of the three independent factors on the

catalytic activities. The statistically designed set of experiments matrix and the responses were presented in Table 7.1.

Table 7.1 Statistically designed set of PROX-experiments over PtAu/CeO₂-ZnO catalyst for a full 2³ factorial design with three central points

Factors	Variables	Unit	Low (-1)	Medium (0)	High (1)
A	Temperature	°C	50	120	190
B	H ₂ O content	%	0	5	10
C	CO ₂ content	%	0	10	20

Standard order	Run order	A	B	C	CO conversion (%)	CO selectivity (%)
1	9	-1	-1	-1	25.74	70.04
2	10	1	-1	-1	47.47	20.93
3	6	-1	1	-1	22.56	70.52
4	3	1	1	-1	53.61	24.99
5	11	-1	-1	1	7.91	66.58
6	2	1	-1	1	42.02	19.91
7	1	-1	1	1	6.92	66.04
8	4	1	1	1	45.24	21.29
9	5	0	0	0	87.21	37.10
10	7	0	0	0	83.05	33.00
11	8	0	0	0	83.93	39.97

A normal probability plot of the effect estimates was constructed in order to evaluate each independent factor and its interactions, as shown in Figure 7.2a for CO conversion as a response and Figure 7.2b for CO selectivity as a response. These graphs could be divided in two regions. A region with normal probability more than 50% represents positive influence on the response while a region with normal probability less than 50% represents negative influence on the response. The factors and interaction positioned out of the line that cross the zero value of abscissa at 50% normal probability, being a significant influence on the response. For CO conversion

as a response (Figure 7.2a), H₂O content (B) in feedstream and interactions among the factors lied in the line, having no influence on the response. Operating temperature (A) and CO₂ content (C) in feedstream have a significant effect on the CO conversion. The operating temperature positioned in the positive effect region, giving higher CO conversion at higher temperature. CO₂ content positioned in the negative effect region. Less CO conversion was obtained when adding more CO₂ in the feedstream. For CO selectivity as a response (Figure 7.2b), only the operating temperature (A) has a significant negative effect on the CO selectivity, giving less CO selectivity when increasing temperature. This statistical analysis also confirmed the experimental results in the activity measurement, as shown in Figure 7.1.

The Pareto chart displays the absolute standardized effect at 95% confidence interval for CO conversion response and CO selectivity response, as displayed in Figures 7.3a and 7.3b, respectively. The absolute standardized value of the effect of each factor and its interaction appear at the right of each bar. For CO conversion response in Figure 7.3a, it is notice that only operating temperature (A) and CO₂ content (C) in the feedstream expressed an absolute value higher than 7.50. This implies that the entire factors except operating temperature (A) and CO₂ content (C) have no influence on the CO conversion. For CO selectivity response in Figure 7.3b, only operating temperature (A) with absolute standardized value higher than 5.65, having a significant influence on the CO selectivity. Moreover, a curvature in CO conversion and selectivity responses displayed an absolute value higher than 7.50 and 5.65, respectively. This implied a curvature when changing a level of the factors studied. It is surprising that H₂O content (B) in the feedstream has no significant effect on the CO conversion and selectivity responses.

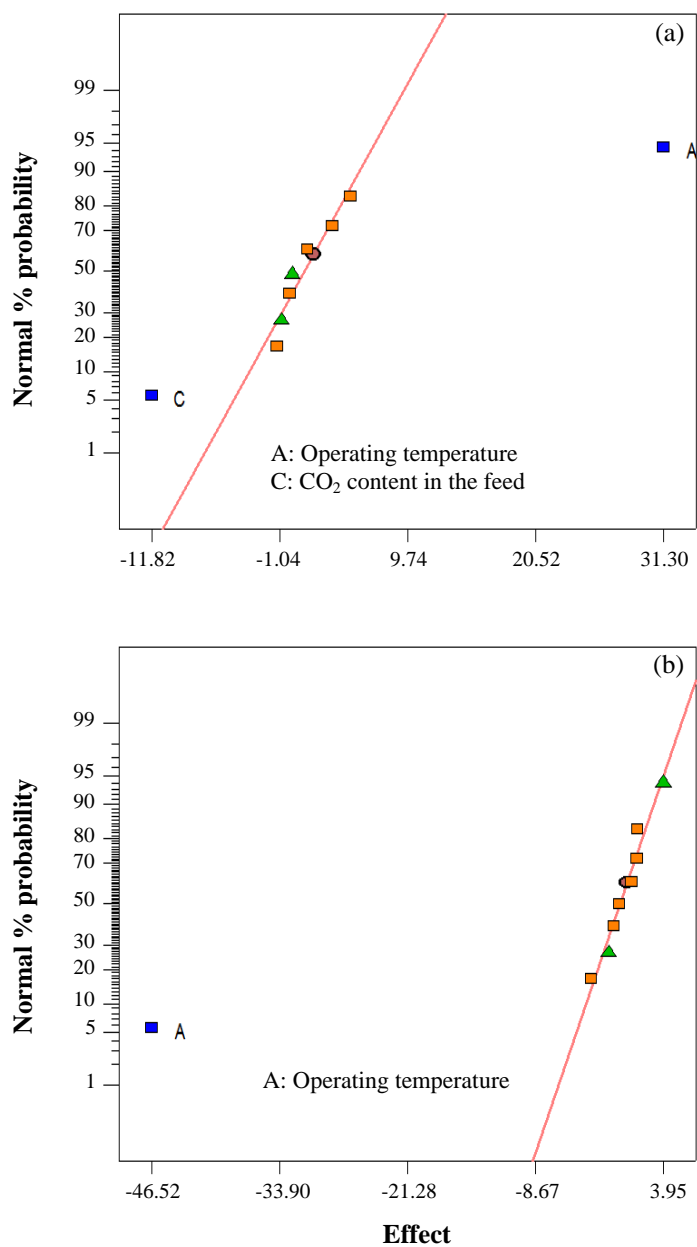


Figure 7.2 Normal probability plot of the effects for a full 2^3 factorial design with 3 central points when using: (a) CO conversion as response and (b) CO selectivity as response.

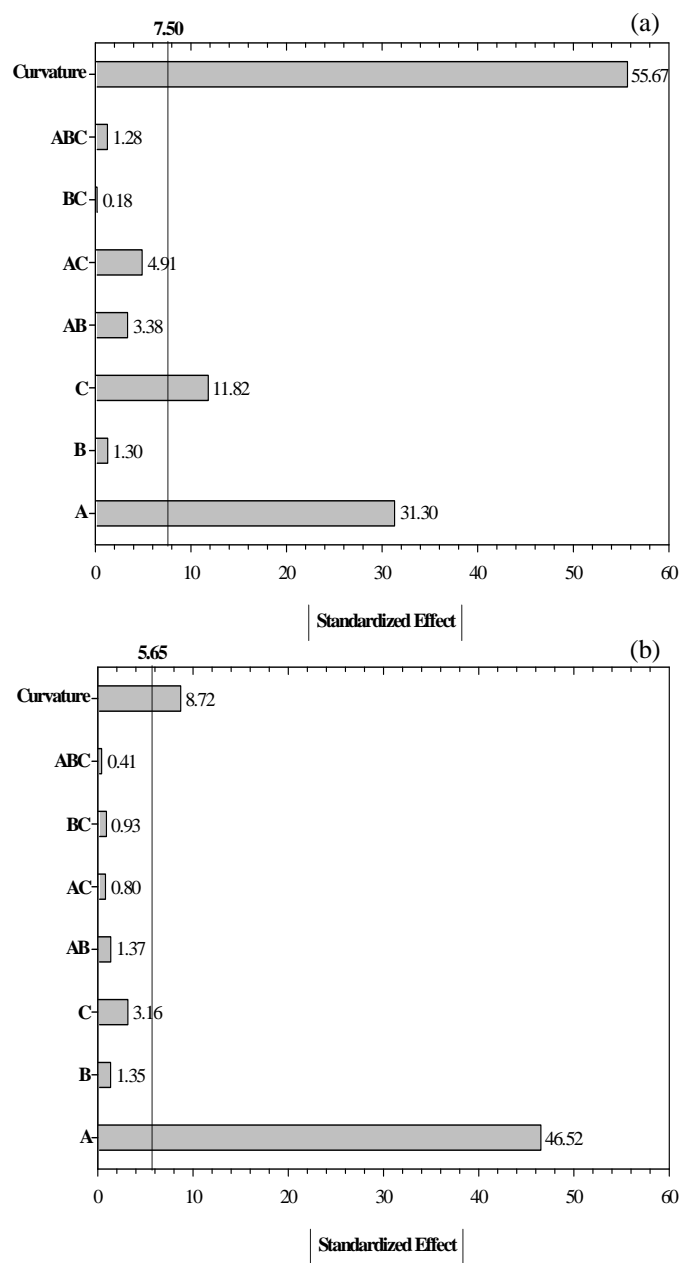


Figure 7.3 The Pareto chart for a full 2^3 factorial design with 3 central points when using: (a) CO conversion as response and (b) CO selectivity as response.

An analysis of variance (ANOVA) of the catalytic performance at a 95% confidence interval is shown in Table 7.2. Based on P-value, any factors or interactions that presented their probability less than 0.05 have a significant influence on response. It also displayed the same factors which have an influence on the response, as obtained from Figures 7.2 and 7.3. For CO conversion response, only operating temperature (A) and CO₂ content (C) in feedstream were significant. By employing the contribution of factor, the importance of the factors was ordering as operating temperature (A) (22.99%) and CO₂ content (C) in feedstream (3.28%), respectively, where the value in a parenthesis represents to its contribution. For CO selectivity response as also shown in Table 7.3, only operating temperature (A) was significant at 95.43% contribution. In addition, the ANOVA revealed that the relationship between the important factors and the response was not in a linear-form since the probability of a curvature was $P = 0.008$ for CO conversion response and $P = 0.0421$ for CO selectivity response. In order to verify the curvature, the mean changes that occurred in the response when changing the level of the factor from lower level through the central point to higher level. As can be seen in the Figure 7.4, the average of the response value for all the factors studied did not correspond to the average of the response value at the central point. This suggested that there should be a quadratic term in the CO conversion and selectivity. From the results of statistical analysis, it can be concluded that an operating temperature and CO₂ content in feedstream have a significant effect on the CO conversion whilst only operating temperature has an influence on CO selectivity. Therefore, the operating temperature and CO₂ content in feedstream were employed for a surface analysis design in order to achieve an optimal CO conversion and CO selectivity.

Table 7.2 Analysis of variance of for a full 2^3 factorial design with three central points of PROX-experiments over PtAu/CeO₂-ZnO catalyst when considering CO conversion and CO selectivity as a response

(a) Response: CO conversion

Source	Sum of squares	DF	Mean square	F-value	Probability (P-value)	Contribution (%)
Model	2317.08	7	331.01	68.87		
A	1959.69	1	1959.69	407.73	0.0024	22.99
B	3.37	1	3.37	0.70	0.4907	0.04
C	279.54	1	279.54	58.16	0.0168	3.28
AB	22.88	1	22.88	4.76	0.1608	0.27
AC	48.27	1	48.27	10.04	0.0868	0.57
BC	0.067	1	0.067	0.014	0.9170	0.0007
ABC	3.26	1	3.26	0.68	0.4965	0.04
Curvature	6197.43	1	6197.43	1289.41	0.008	72.70
Residual	9.61	2	4.81			0.11
Cor Total	8524.13	10				

R-Squared = 0.9959; Adj R-Squared = 0.9814

(b) Response: CO selectivity

Source	Sum of squares	DF	Mean square	F-value	Probability (P-value)	Contribution (%)
Model	4358.08	7	622.68	50.73		
A	4327.29	1	4327.29	352.64	0.0028	95.43
B	3.62	1	3.62	0.29	0.6416	0.08
C	20.03	1	20.03	1.63	0.3296	0.44
AB	3.78	1	3.78	0.31	0.6346	0.08
AC	1.30	1	1.30	0.11	0.7760	0.03
BC	1.71	1	1.71	0.14	0.7447	0.04
ABC	0.34	1	0.34	0.028	0.8824	0.01
Curvature	152.03	1	152.03	12.39	0.0421	3.35
Residual	24.54	2	12.27			0.54
Cor Total	4534.65	10				

R-Squared = 0.9944; Adj R-Squared = 0.9748

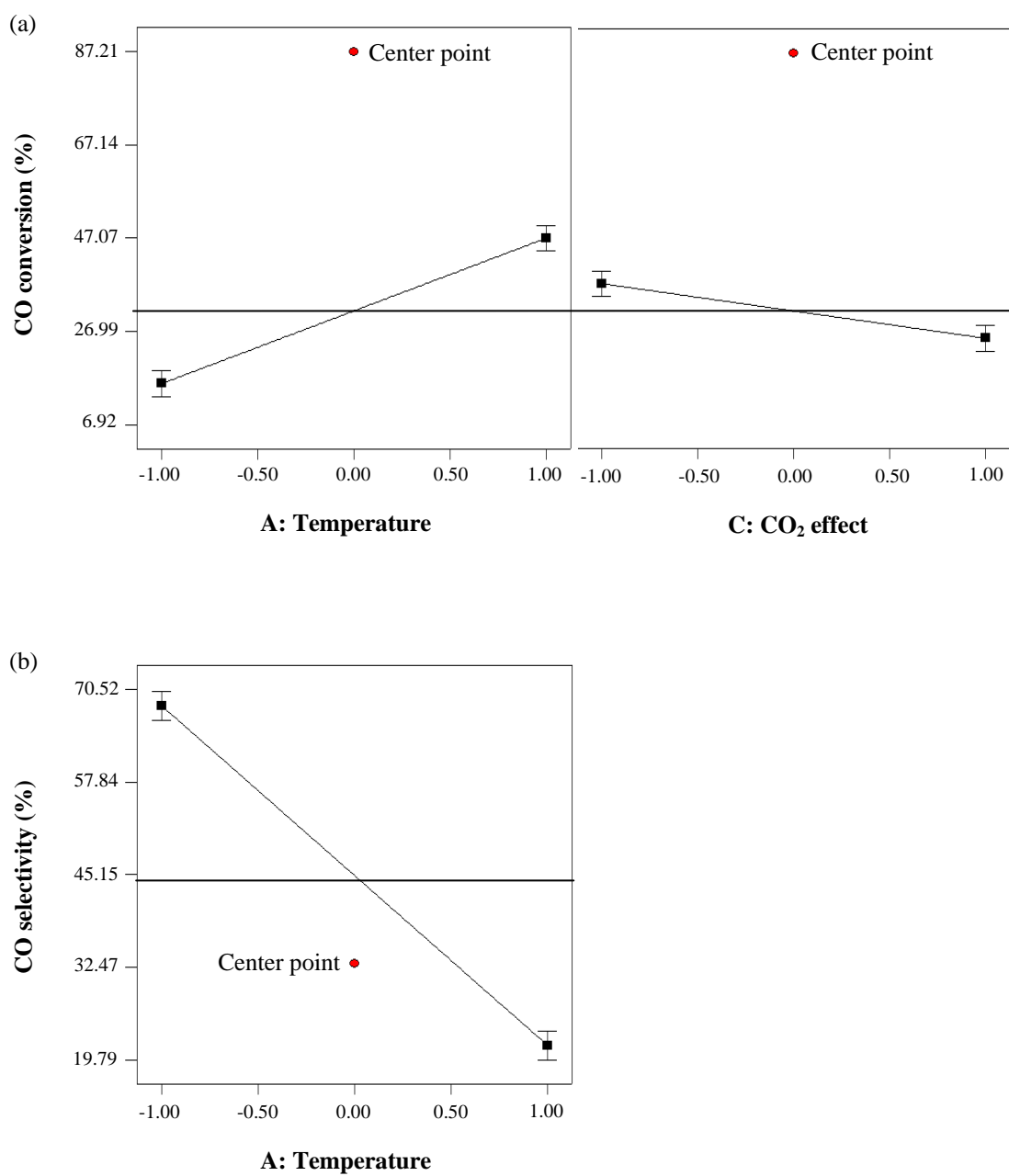


Figure 7.4 Main effect plot with its response: (a) CO conversion and (b) CO selectivity.

7.3 Response surface methodology (RSM)

After screening an important factor on the responses using a full factorial design with central points, face-centered central composite design (FCCCD) with two independent screened factors was performed in order to achieve the optimum condition for CO conversion and CO selectivity in PROX unit over PtAu/CeO₂-ZnO catalysts. The criterion of this design is chosen base on the previous factorial design were designed as shown in Table 7.3. The levels of the screened factors were set based on the previous full factorial design described above. Based on the components of a realistic reformat gas from SRM unit and the results of statistical analysis and catalytic activities, H₂O content in feedstream was hold constant at medium level. An appropriate response surface model for each response was generated. The corresponding response surface model for CO conversion and CO selectivity are in coded term, as shown in Equations 7.1 and 7.2:

$$CO\ conversion\ (\%) = + 58.52 + 3.68A - 21.70C + 16.23AC \quad (7.1)$$

$$CO\ selectivity(\%) = + 39.60 - 10.70A + 4.38C - 5.17AC \quad (7.2)$$

where A is operating temperature, C is CO₂ content in feedstream, and AC is the interaction between operating temperature and CO₂ content in feedstream.

Table 7.3 Experimental variables for faced-centered central composite design (FCCCD) of response surface methodology with three central points over PtAu/CeO₂-ZnO catalyst

Factors	Variables	Unit	Low (-1)	Medium (0)	High (1)
A	Temperature	°C	90	120	150
C	CO ₂ content	%	0	10	20

Standard order	Run order	A	C	CO conversion (%)	CO selectivity (%)
1	9	90	0	93.02	41.01
2	2	150	0	67.92	29.95
3	8	90	20	16.28	59.92
4	10	150	20	56.09	28.18
5	5	90	10	54.65	50.47
6	1	150	10	62.01	29.07
7	4	120	0	80.25	35.38
8	3	120	20	38.62	44.55
9	7	120	10	59.41	37.10
10	11	120	10	58.21	39.96
11	6	120	10	57.23	39.97

The FCCCD results were treated by ANOVA, as shown in Table 7.4. All the factors and their interaction were significant at a 95% confidence interval. For both responses, the probability of each factor and its interaction were less than 0.05, having a significant influence. It is notice that lack of fit in the developed models was not significant. This implied that all required independent factors studied were adequate for representing the actual relationship between the factors and the response within the selected range. The R-Squared value provides a variability measurement in the estimated response value when using the factors and their interaction.

Table 7.4 Analysis of variance of for response surface methodology of PROX-experiments over PtAu/CeO₂-ZnO catalyst when considering CO conversion and CO selectivity as a response

(a) Response: CO conversion

Source	Sum of squares	DF	Mean square	F-value	Probability (P-value)
Model	3959.85	3	1319.95	1359.42	
A	81.18	1	81.18	83.61	< 0.0001
C	2825.34	1	2825.34	2909.82	< 0.0001
AC	1053.33	1	1053.33	1084.82	< 0.0001
Lack of fit	4.41	5	0.88	0.74	0.6604
Residual	2.38	2	1.19		
Cor Total	3966.64	10			

R-Squared = 0.9983; Adj R-Squared = 0.9976; Adeq Precision = 127.66

(b) Response: CO selectivity

Source	Sum of squares	DF	Mean square	F-value	Probability (P-value)
Model	909.22	3	303.07	300.10	
A	686.94	1	686.94	680.19	< 0.0001
C	115.37	1	115.37	114.24	< 0.0001
AC	106.92	1	106.92	105.86	< 0.0001
Lack of fit	1.60	5	0.32	0.12	0.9757
Residual	5.47	2	2.74		
Cor Total	916.29	10			

R-Squared = 0.9923; Adj R-Squared = 0.9890; Adeq Precision = 52.38

The R-Squared value of 0.9983 for CO conversion response and 0.9923 for CO selectivity revealed to the accuracy of the response surface quadratic model. The R-Squared value of these two models is very close to 1, indicating accuracy of the model. Just only 0.17% and 0.77% of the total variation for CO conversion and CO selectivity response, respectively, was not explained by the model. There is a little difference between R-Squared and adjusted R-Squared (Adj R-Squared). To monitor the signal to noise ratio by adequate precision (Adeq Precision), it was suggested that the signal was adequate when the ratio was greater than 4. An adequate precision for

CO conversion and selectivity were 127.66 and 52.38, respectively. This implied a good agreement between the estimated value and the experimental response value for CO conversion and selectivity.

Figures 7.5a and 7.5b show the three-dimensional response surface and contour plot of the CO conversion and CO selectivity, respectively. As can be seen, the highest CO conversion occurred at high level of operating temperature (A) and at low level of CO₂ content (C) in feedstream while the highest CO selectivity yielded at the high level of operating temperature and at high CO₂ content. A relatively straightforward approach to optimizing the two responses is to overlay the contour plot for each response, as shown in Figure 7.5c. Since the realistic reformat gas from SRM unit over Au/CuO–CeO₂ was routed to the PROX of CO unit to test the performance of hydrogen fuel processor unit; therefore, the CO₂ content in the reformat gas (9% to 12%) and temperature of the feedstream (>100 °C) were also used as a constrain for optimizing the responses. The optimal condition that estimated by simultaneous considering the maximal CO conversion response, the maximal CO selectivity response, and the constrains is in the shaded portion, represented by an operating temperature from ~100 °C to ~115 °C and CO₂ content less than 12%.

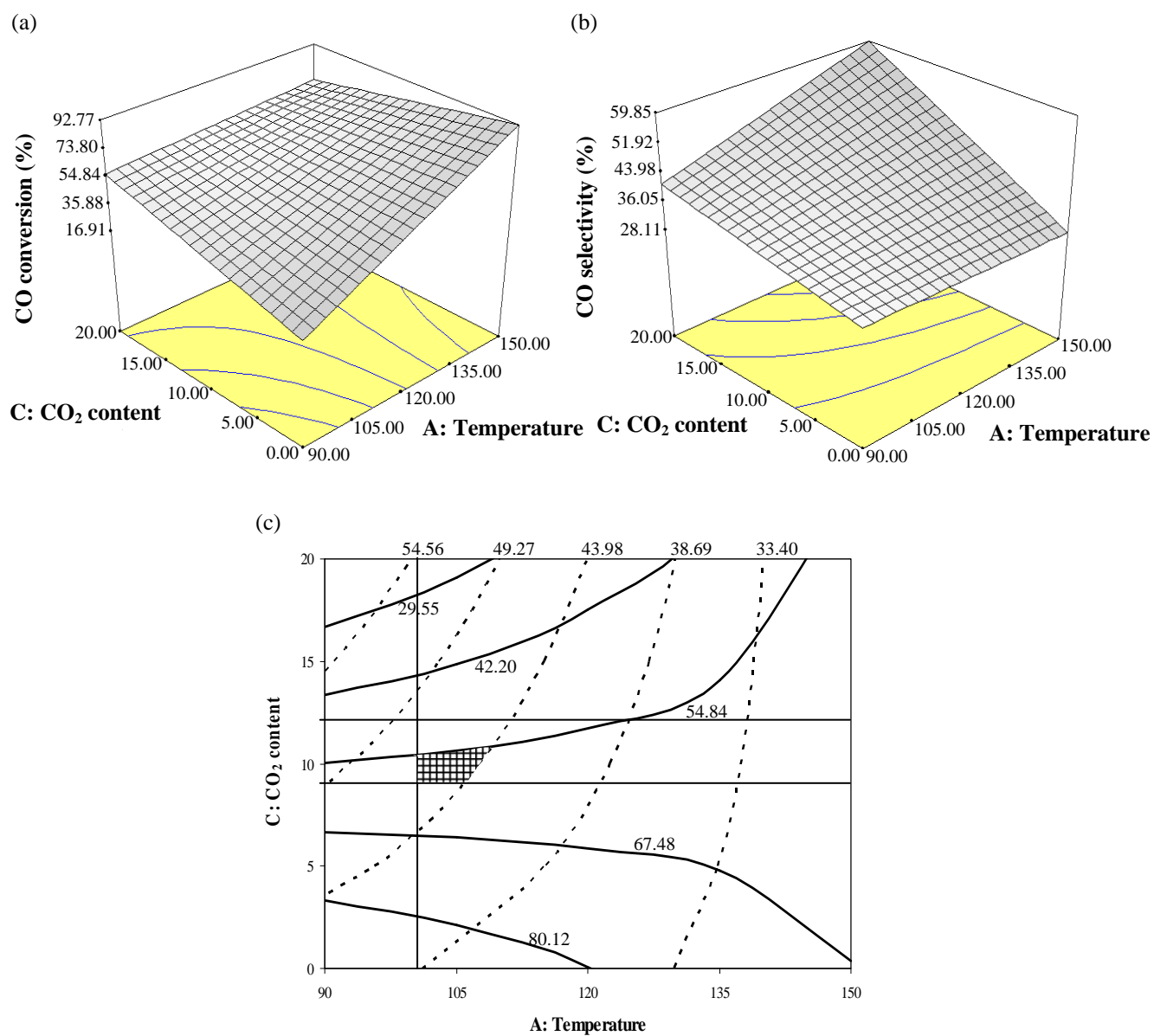


Figure 7.5 Response surface and contour plot of: (a) CO conversion response, (b) CO selectivity response, and (c) region of the optimum (shaded portion) found by overlaying yield between CO conversion response (solid line) and CO selectivity response (dot line).

7.4 Validation of the response surface models

To investigate an accuracy of the models, 4 experiments were sets by using the two independent screened factors. The factor of H₂O content was constant. Table 7.5 shows the CO conversion and CO selectivity of an individual experiment along with the estimated responses under simulated reformat gas and realistic reformat gas. In this work, the realistic reformat gas composition from SRM unit over Au/CuO–CeO₂ consisted of 36.8% H₂, 1.1% CO, 1.1% O₂, 11.6% CO₂, 8.2% H₂O, and He balance. The realistic reformat gas was routed directly from SRM unit to PROX of CO unit. The estimated responses are much closed to the experimental one in all cases. The difference between estimated response and the experimental one, which was reported in term of residual (%), was plotted against the experimental one, as shown in Figure 7.6a for CO conversion response and Figure 7.6b for CO selectivity response. The residual distribution with regard to the response does not follow a trend. For simulated reformat gas, all the residuals are less than 2% for CO conversion and selectivity response. For realistic reformat gas, all the residuals are less than 5% for CO conversion response and 4% for CO selectivity response, indicating an accuracy of the models over the factors studied. The experimental design in this work can be applied to examine the CO conversion and CO selectivity over PtAu/CeO₂–ZnO; although, the reactant gas for PROX unit may be a realistic reformat gas.

Table 7.5 Validation of FCCCD using various levels of operating temperature and CO₂ content when feeding (a) simulated reformat gas with 40% H₂ and 5% H₂O in He balance and (b) realistic reformat gas

(a) Simulated reformat gas

Operating condition		CO conversion (%)		CO selectivity (%)	
Temperature (°C)	CO ₂ content (%)	Estimation	Experiment	Estimation	Experiment
90	10	54.84	54.65	50.30	50.47
110	0	84.40	84.13	37.05	37.1
120	10	58.52	59.41	39.6	39.97
130	0	76.03	76.36	33.37	33.67
150	0	67.67	67.92	29.68	29.95
150	10	62.20	62.01	28.9	29.07
150	20	56.73	56.09	28.12	28.18
170	0	59.30	58.27	25.99	25.69

Note: the simulated reformat gas consisted of 40% H₂, 1% CO, 1% O₂, 5% H₂O, desired amount of CO₂ (as shown in Table), and He balance.

(b) Realistic reformat gas

Operating condition		CO conversion (%)		CO selectivity (%)	
Temperature (°C)	CO ₂ content (%)	Estimation	Experiment	Estimation	Experiment
100	11.6	55.05	57.50	40.30	39.10
110	11.6	57.14	56.27	36.46	35.93
120	11.6	59.23	60.00	32.62	33.22
130	11.6	61.32	64.35	28.78	28.35

Note: the realistic reformat gas composition from SRM unit over Au/CuO–CeO₂ consisted of 36.8% H₂, 1.1% CO, 1.1% O₂, 11.6% CO₂, 8.2% H₂O, and He balance.

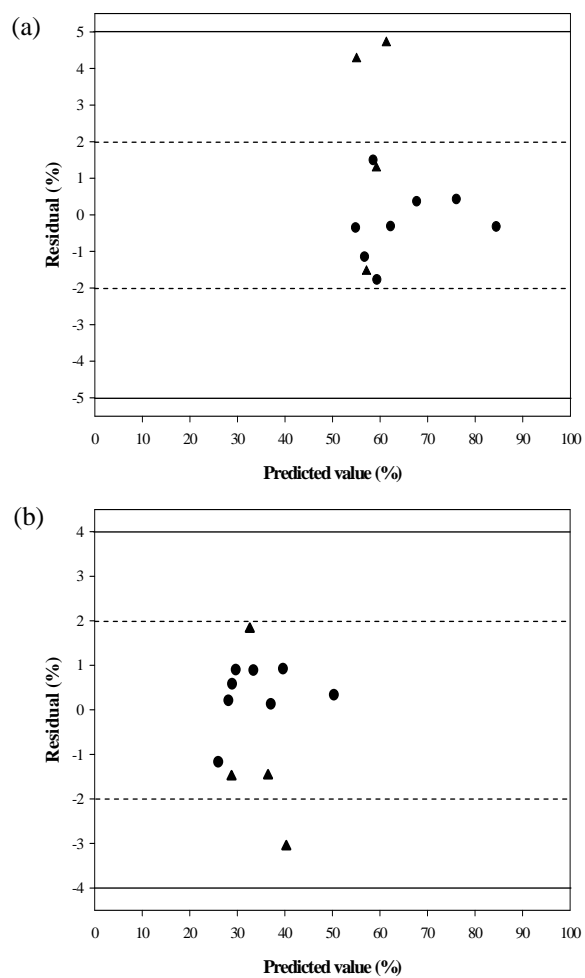


Figure 7.6 Residual plots of the response surface model: (a) CO conversion response and (b) CO selectivity response.

(●) simulated reformat gas and (▲) realistic reformat gas

CHAPTER VIII

INTEGRATION OF STEAM REFORMING UNIT AND PREFERENTIAL OXIDATION UNIT

In this chapter, integration of steam reforming of methanol (SRM) and preferential oxidation (PROX) of CO for pure hydrogen production was investigated. The effective catalyst for each unit was employed in the integration system. The SRM unit was operated at optimum condition over 5% Au/(50:50)CuO–CeO₂ catalyst which obtained from Chapters 4 and 5. The yield distribution for a period of 2 h operating time from SRM unit was exhibited to ensure the composition of the effluent. The operating condition for PROX unit over 1%(1:1)PtAu/(1:1)CeO₂–ZnO catalyst was achieved from Chapters 6 and 7. To achieve complete CO conversion in PROX unit, double-stage was then applied. The optimal condition for integration system with respect to the maximal methanol conversion with negligible CO content was then studied in this chapter. Durability of the effective catalysts and characterization of the fresh and spent catalysts were also considered.

8.1 Yield distribution of SRM unit

After determining the optimal condition of SRM-performance for complete methanol conversion with minimal CO selectivity as described in Chapters 4 and 5, the stability test was done for a period of 2 h at optimal condition for SRM unit; ~ 306 °C of operating temperature, 2 of S/M ratio, $1 \text{ cm}^3 \text{ h}^{-1}$ of liquid feed rate, and 0.17 g s cm^{-3} of W/F ratio. Distribution of product yield from SRM unit over high potential Au/CuO–CeO₂ catalyst was illustrated in Figure 8.1. The real reformat gas consisted of $\sim 75.1\%$ H₂, $\sim 23.4\%$ CO₂, and $\sim 1.5\%$ CO (dry basis) at 100% methanol conversion, approximately.

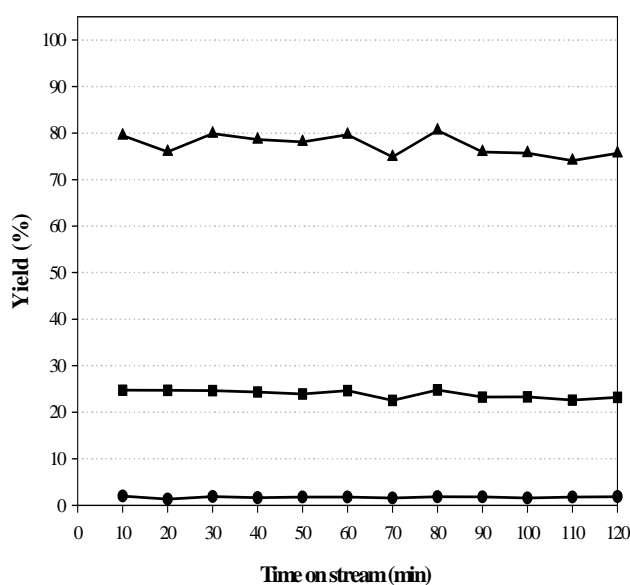


Figure 8.1 Distribution of product yield from SRM unit over Au/CuO–CeO₂ catalyst at optimum condition for 2 h: (▲) H₂, (■) CO₂, and (●) CO, at optimal condition for SRM unit; Operating temperature = ~ 306 °C, S/M ratio = 2, Liquid feed rate = $1 \text{ cm}^3 \text{ h}^{-1}$, and W/F ratio = 0.17 g s cm^{-3} .

8.1.1 Single-stage reactor of PROX unit

From the experimental results and the statistical analysis for PROX unit as shown in Chapters 6 and 7, CO₂ content and operating temperature had a significant influence on catalytic activities. It was found that the maximum CO conversion was shifted to 130 °C from 90 °C to when adding more amount of CO₂ (20-fold) with 10% H₂O to feedstream. Eventually, the realistic reformat gas composition consisted of 36.8% H₂, 1.1% CO, 11.6% CO₂, 8.2% H₂O, and He balance. Therefore, it is necessary to determine the optimal temperature of a single-stage reactor to approach the maximum CO conversion with regard to the operating temperature and catalyst weight to total flow of gas inlet (W/F) ratio. More O₂ was added to the feedstream to maintain the ratio of O₂ to CO at 1:1.

From the experimental results as shown in Figure 8.2, increase in CO conversion was approached when employing higher W/F ratio in whole range of operating temperature selected. The maximum CO conversion with selectivity was around ~87% and ~37%, respectively at 120 °C and W/F ratio of 0.13 g s cm⁻³. At higher W/F ratio, the reactant gas had longer contact time for reaction and thus enhanced the catalytic activities. Additionally the improvement of contact time for reaction also promoted oxidation of H₂ therefore the selectivity decreased when increasing in W/F ratio. However, second-stage reactor is more effective than single-stage reactor for CO clean-up.

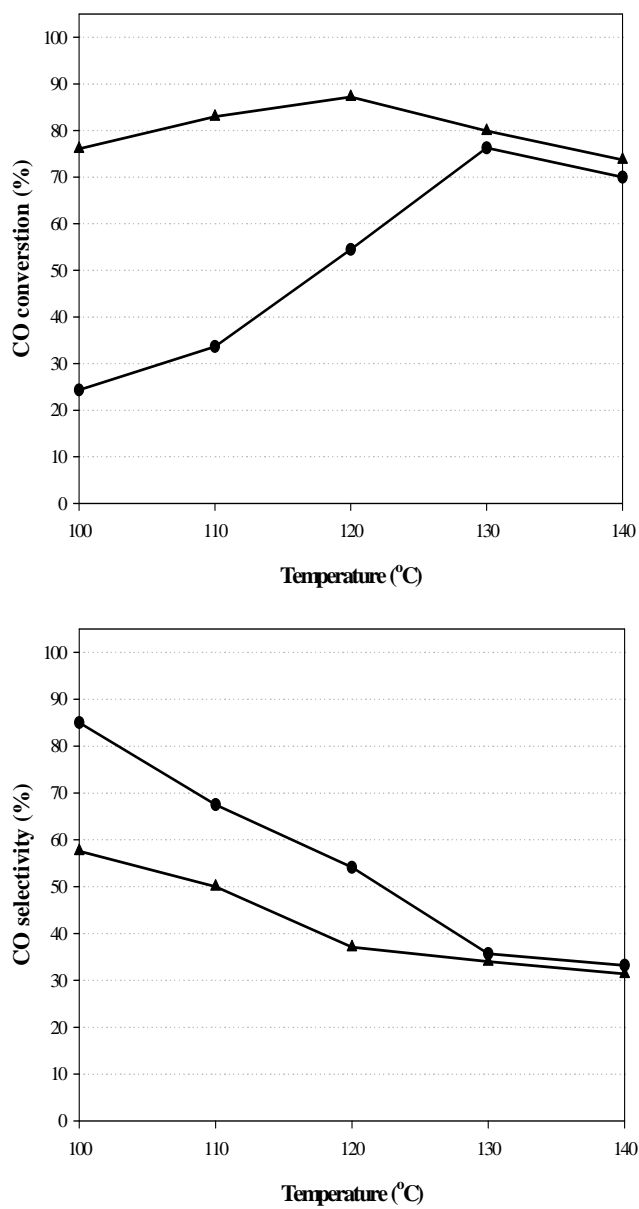


Figure 8.2 Catalytic activities of PROX unit in single-stage reactor over PtAu/CeO₂-ZnO at W/F ratio of: (●) 0.08 g s cm⁻³ and (▲) 0.13 g s cm⁻³.

8.1.2 Double-stage reactor of PROX unit

Attempt to remove CO completely, the PROX unit with double-stage reactor was employed over PtAu/CeO₂-ZnO under realistic reformat gas. The first-stage reactor was operated at constant temperature of 120 °C while the second-stage operating temperature was varied in a range of 100 °C to 130 °C. To examine the effect of the double-stage reactor on the catalytic activities, the total of catalyst weight was split into each reactor keeping at weight ratio of 1:1. The effluent from the first-reactor was then routed directly to the second reactor, thereby providing the double-stage reactor. The O₂ split ratio was constant at 1:1 whereas the entire O₂/CO ratio was kept constant at 1; the same as the single-stage reaction. Figure 8.3 shows the catalytic performance in double-stage reactor at W/F = 0.13 and 0.17 g s cm⁻³. At W/F ratio of 0.17 g s cm⁻³, complete CO conversion was obtained in temperature range of 120 °C to 130 °C for the second-stage reactor while the CO selectivity decreased from ~57% to ~50% when increasing temperature. The results illustrated that enhancing of W/F ratio increased the CO conversion while decreased the CO selectivity in agreed with our previous work.

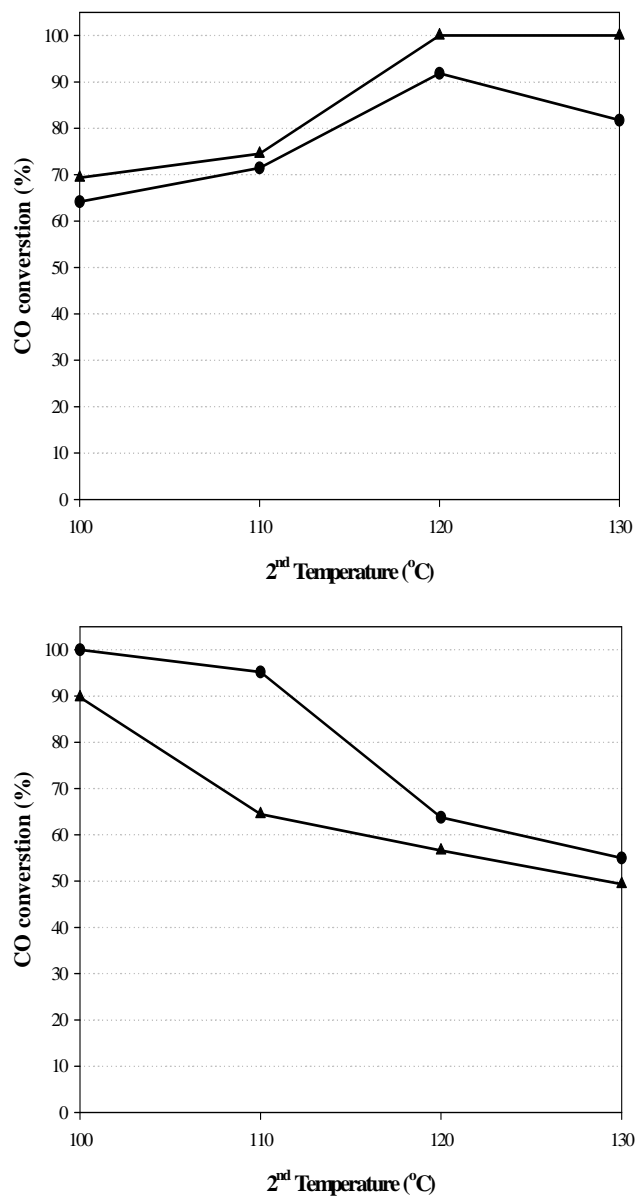


Figure 8.3 Catalytic activities of PROX unit in double-stage reactor over PtAu/CeO₂-ZnO at W/F ratio of: (●) 0.13 g s cm⁻³ and (▲) 0.17 g s cm⁻³. Operating temperature of 1st = 120 °C and catalyst weight ratio, O₂ split ratio, and O₂/CO ratio = 1:1.

8.2 Stability test

Durability of the catalyst performance for SRM unit was test in period of 1200 min, as shown in Figure 8.4a. Complete methanol conversion was obtained in the first 600 min after that it decreased to ~90% at 1200 min operating time. H₂ and CO selectivity were still constant at ~75% and ~0%, respectively. However, production yield as shown in Figure 8.4b displayed that the reformat gas consisted of ~75% H₂, ~25% CO₂, and < 0.005% CO (dry basis). The behavior of rate of H₂ production in Figure 8.4c was similar to the methanol conversion.

From mentioned above, the reformat gas produced in the first 600 min operating time was then routed to the PROX unit to determine the optimize condition for the furl processor system. The catalytic performance, yield distribution, and H₂ production rate for PROX unit were presented in Figures 8.5a to 8.5c, respectively. Complete CO conversion with ~50% selectivity was achieved in whole period of 600 min. This implied that catalyst was active and stable in whole period work. The yield consists of ~75% H₂, ~25% CO₂, and < 0.005% CO (dry basis) at H₂ production rate of ~320 L d⁻¹ g_{cat}⁻¹.

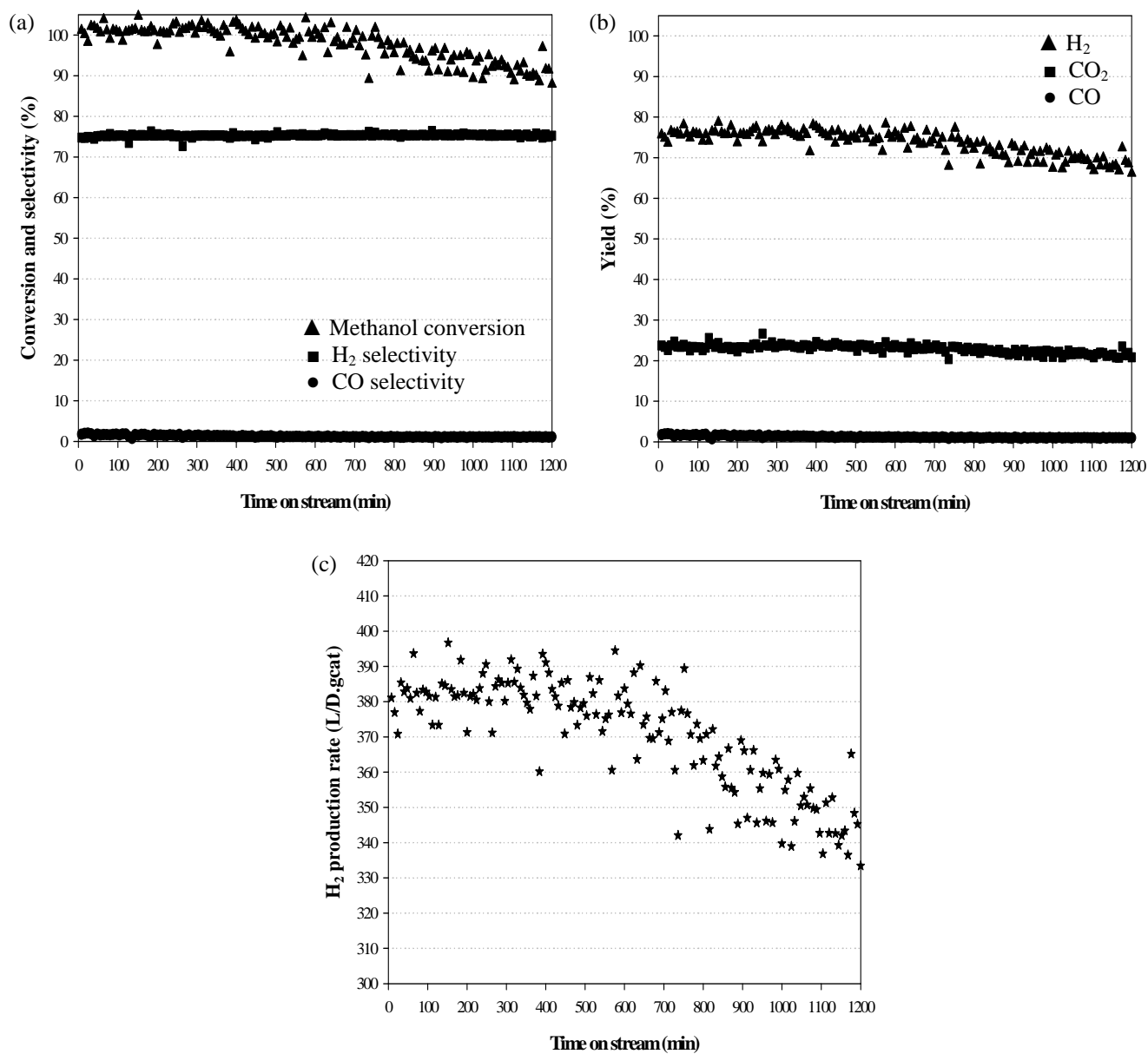


Figure 8.4 Deactivation test of SRM unit on Au/CuO–CeO₂ at optimum condition: Operating temperature = ~ 306 °C, S/M ratio = 2, Liquid feed rate = $1 \text{ cm}^3 \text{ min}^{-1}$, and W/F ratio = 0.17 g s cm^{-3} .

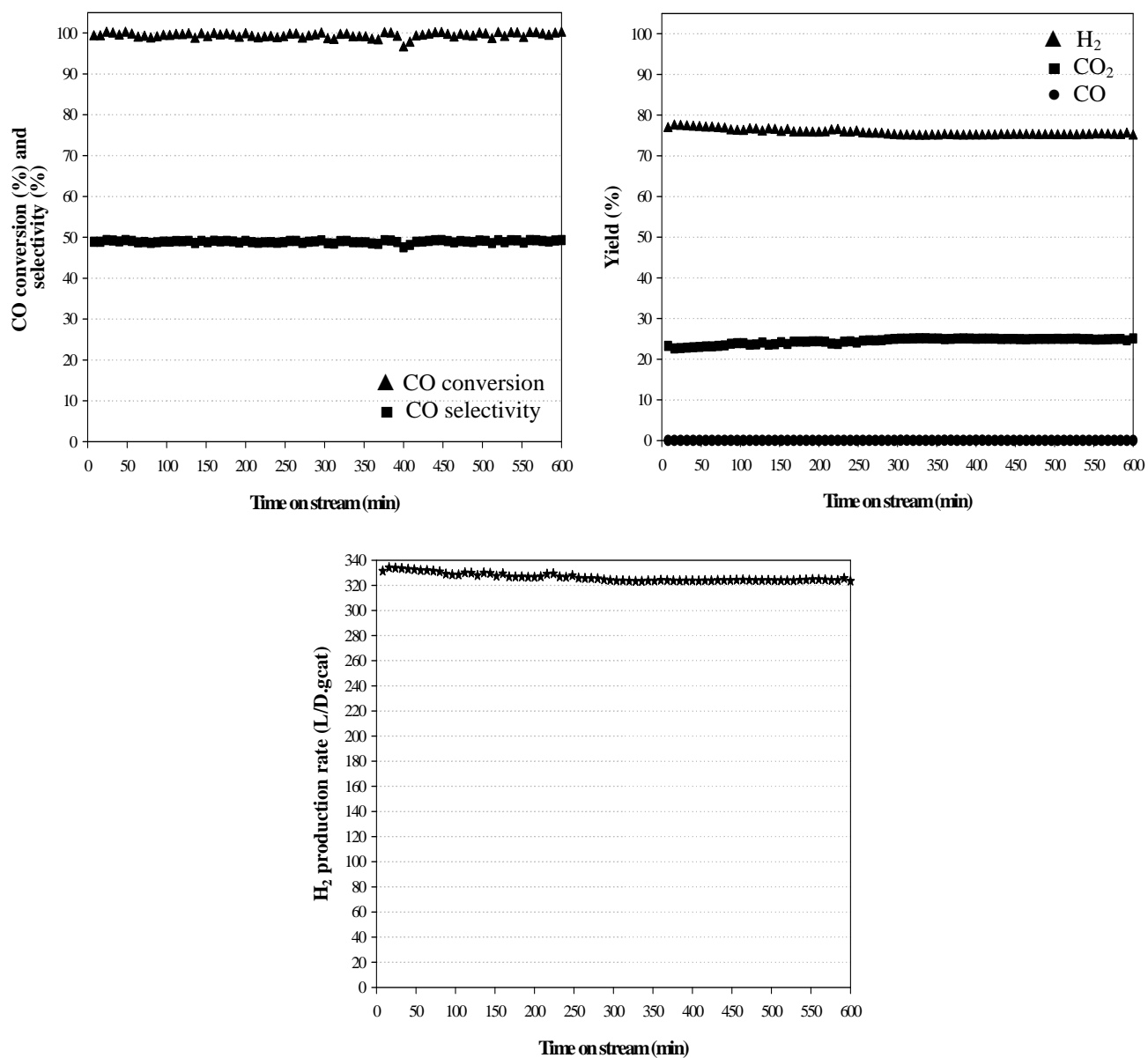


Figure 8.5 Deactivation test of PROX unit for overall process for 600 min at optimum condition:

SRM unit: Operating temperature = ~ 306 °C, S/M ratio = 2, Liquid feed rate = $1 \text{ cm}^3 \text{ h}^{-1}$, and W/F ratio = 0.17 g s cm^{-3} .

PROX unit: 1st temperature = 120 °C, 2nd temperature = ~ 125 °C, W/F ratio = 0.17 g s cm^{-3} , and catalyst weight, O₂ split ratio, and O₂/CO = 1:1.

8.3 Characterization of fresh and spent catalysts

Physical properties of the catalysts, fresh and spent, for SRM and PROX unit are presented in Table 8.1. There is no much difference in the characteristic of fresh and spent catalysts. The BET surface area and pore volume of the spent catalyst closed to the fresh one.

XRD patterns of the catalysts are displayed in Figure 8.6. The peaks of mixed metal oxide support were observed in the fresh and spent catalysts. For SRM catalysts, the XRD patterns only appeared the peaks of tenorite (CuO) ($2\theta = 33.5^\circ, 38.7^\circ, 66.2^\circ$) and cerianite (CeO₂) ($2\theta = 28.6^\circ, 33.1^\circ, 47.5^\circ, 56.3^\circ, 69.4^\circ, 76.7^\circ, 88.4^\circ$) for the fresh catalyst. Compared to the spent catalyst CuO phase disappeared and metallic copper phase was observed at 2θ of 43.3° and 50.4° . This result is caused by CuO reduction to metallic copper with H₂ during the reaction. Moreover, the broad peaks of the spent catalyst were obtained. There is no peak of Au oxide species or metallic Au species represent in the pattern. There is even the possibility that these species are too small (< 5 nm) to be detected by X-ray diffractometer. For PROX catalysts, the reflection peaks at $28.6^\circ, 33.1^\circ, 47.5^\circ, 56.3^\circ, 59.1^\circ, 69.4^\circ, 76.7^\circ, 79.1^\circ,$ and 88.4° responded to cerianite phase (CeO₂) while the diffraction peaks at $32.0^\circ, 34.6^\circ, 36.5^\circ, 62.9^\circ,$ and 68.0° display to zincite phase (ZnO). It was observe from the XRD patterns that the fresh catalyst was more crystalline compared to the spent one due to its higher peak intensity. There was no peak represent to characteristic peaks of Pt ($2\theta = 39.8^\circ$ and 46.2°) and Au ($2\theta = 38.2^\circ, 44.4^\circ, 77.6^\circ$). This suggests that Pt and Au particles are highly dispersed on the mixed metal oxide support surface or they may be overlapped

by CeO₂ or ZnO or are too small (< 5 nm) to be detected by X-ray diffractometer, as mention above.

These results also confirm the results of transmission electron microscope (TEM) images. The particle size of catalyst was very clear in TEM images as shown in Figure 8.7. Black spots on the area were metallic phase Pt or Au or Cu on the mixed oxide support of all were observed in the gray one. The fresh metallic particles were nano-particles in a range of 3–5 nm. It was noted that size of the spent catalyst was almost the same as the fresh one. The crystallite size of metal and metal oxide phases (Cu, CuO, CeO₂, and ZnO) was calculated by Debye-Scherrer equation at the X-ray line broadening of the (1 1 -1), (1 1 1), (1 1 1), and (1 0 1) diffraction peak for CuO, Cu, CeO₂, and ZnO, respectively as shown in Table 8.1.

Table 8.1 Physical properties of the prepared catalysts

Catalyst	Status	S _{BET} ^a (m ² g ⁻¹)	Pore volume ^a (cm ³ g ⁻¹)	Crystallite size ^b (nm)		
				CuO	CeO ₂	ZnO
Au/CuO–CeO ₂	Fresh	77.3	0.29	19.7	5.5	-
Au/CuO–CeO ₂	Spent	73.8	0.26	22.6*	5.7	-
PtAu/CeO ₂ –ZnO	Fresh	58.6	0.16	-	6.9	15.4
PtAu/CeO ₂ –ZnO	Spent	54.7	0.15	-	6.6	11.7

* Cu crystallite phase

^a Determined by BET surface area analyzer

^b Determined by XRD from line broadening of CuO (1 1 -1), Cu (1 1 1), CeO₂ (1 1 1), and ZnO (1 0 1) peak

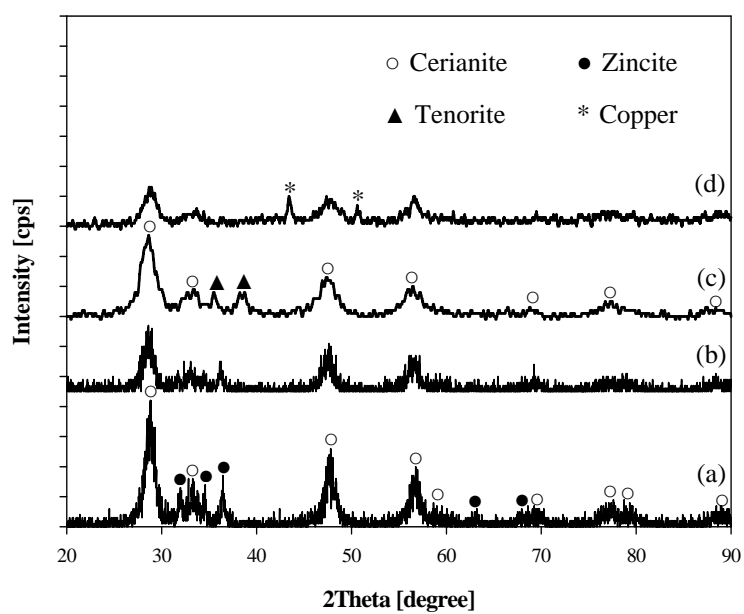


Figure 8.6 XRD patterns of (a) PROX-Fresh, (b) PROX-Spent, (c) SRM-Fresh, and (d) SRM-Spent catalysts.

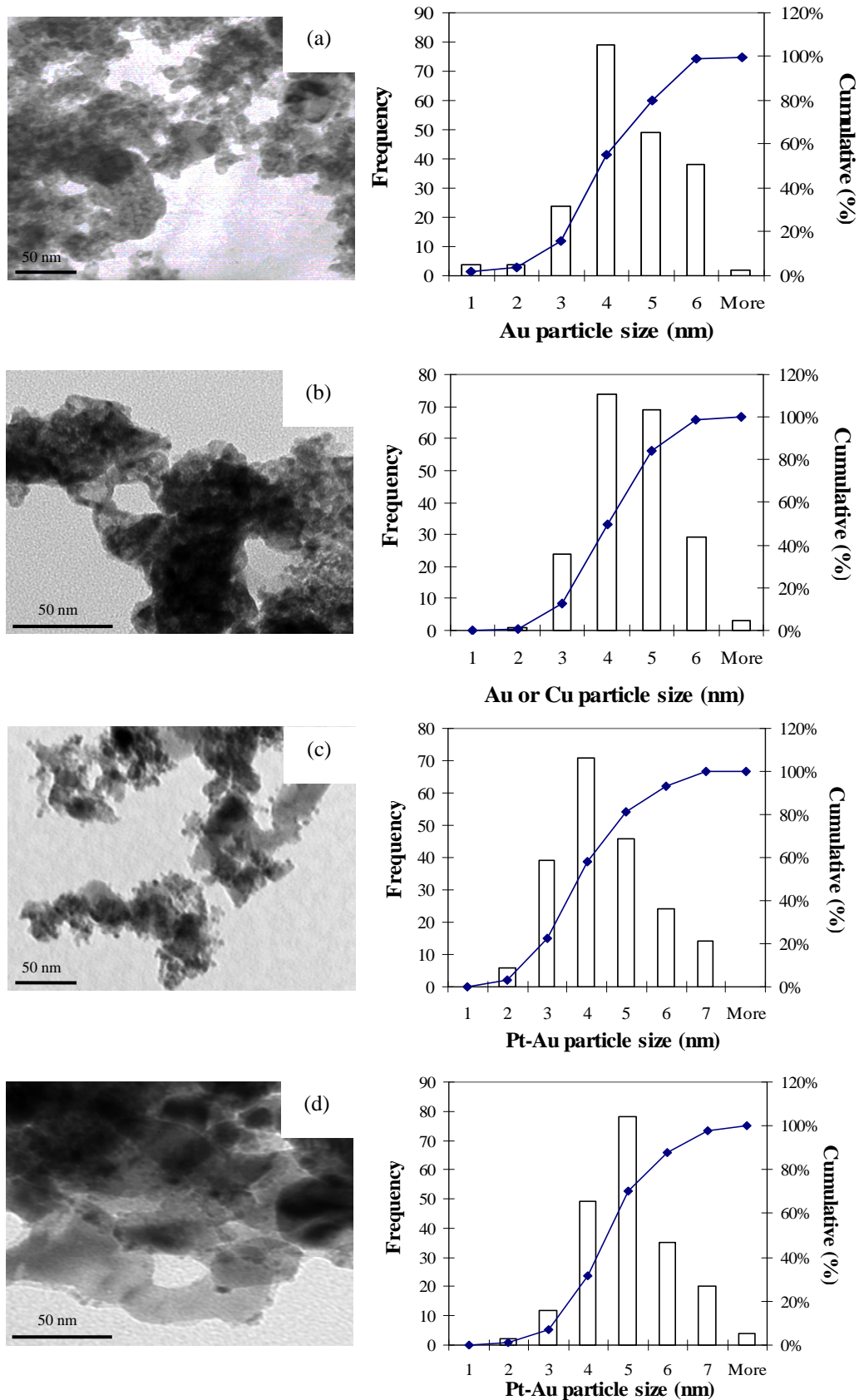


Figure 8.7 TEM images of (a) SRM-Fresh, (b) SRM-Spent, (c) PROX-Fresh, and (d) PROX-Spent catalysts.

The FTIR spectra of the samples are presented in Figure 8.8. There are three small peaks in the C–H stretching region at 2852, 2921, and 2960 cm^{-1} . The C–H stretching peak at 2852 and 2960 cm^{-1} represents to either formate [92] or methoxy groups [93]. These results agreed with Martínez-Arias et al. [94]. The peaks responded to C–H stretching were not observed in the fresh catalyst only. The wavenumbers range of $\sim 3100 \text{ cm}^{-1}$ to 3700 cm^{-1} at absorbance centered of $\sim 3500 \text{ cm}^{-1}$ signify O–H stretching which can be observed in both fresh and spent catalyst samples [95,96]. For the spent catalysts, the band in range of $\sim 1200\text{--}1700 \text{ cm}^{-1}$ referred to carbonate group which come from CO_2 over the catalyst surface [96,97]. The spent catalysts of both showed the intensity peak higher than the fresh one. In this dissertation, there are infrared absorption frequencies at 1384, 1500, and 1639 cm^{-1} for PROX-spent while SRM-spent catalyst presented at 1360 and 1530 cm^{-1} and overlapping peak at 1407 and 1469 cm^{-1} . The observed peaks of SRM-spent catalyst were corresponding vibrational modes of surface carbonate with different bonding configurations match with bidentate, monodentate, and free— CO_3 [97] while only bidentate peak was noticed in the PROX-spent catalyst.

From FTIR results in Figure 8.8d, it implied that, in case of SRM-spent catalyst, CO_2 reacted with oxygen on the catalyst surface and then formed carbonated group such as bidentate, monodentate, and free— CO_3 [97]. Monodentate carbonate then reacted with H from dissociation of water to form formate group, as shown in Figure 8.9a. In case of PROX-spent catalyst, CO_2 reacted with oxygen on the catalyst surface to form carbonated group such as bidentate, monodentate, and free— CO_3 . It was noted that there was only bidentate peak in FTIR spectra in Figure 8.8b since monodentate carbonate could form CO_2 , as shown in Figure 8.9b.

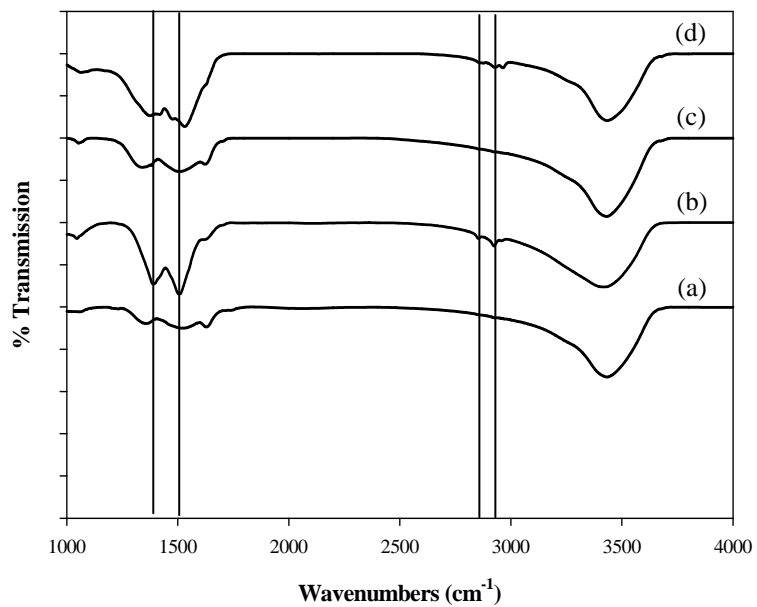


Figure 8.8 FTIR spectra of (a) PROX-Fresh, (b) PROX-Spent, (c) SRM-Fresh, and (d) SRM-Spent catalysts.

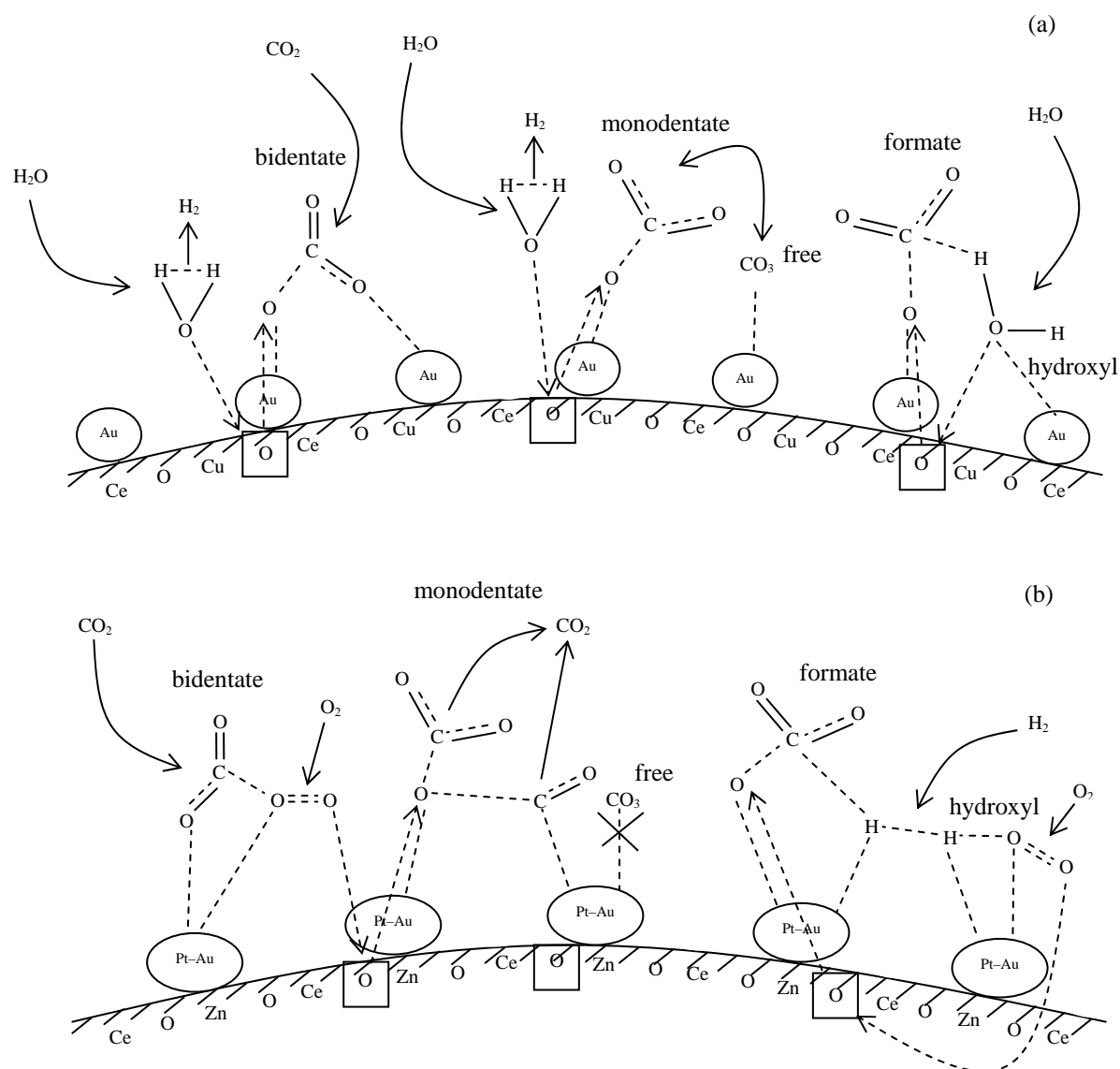


Figure 8.9 Mechanism of carbonate and hydroxyl group formation on (a) SRM and (b) PROX catalysts surface.

CHAPTER IX

CONCLUSIONS

9.1 Steam reforming of methanol (SRM)

In this research, the production of a H₂-rich stream with a low concentration of CO via SRM over 5% Au/CuO, 5% Au/CeO₂, (50:50)CuO–CeO₂, 5% Au/(50:50)CuO–CeO₂ and commercial MegaMax 700 catalysts was investigated over reaction temperatures between 200 °C to 300 °C at atmospheric pressure. The 5% Au/(50:50)CuO–CeO₂ catalyst yielded a higher methanol conversion level than the others due to the integration of CuO particles into the CeO₂ lattice to form a solid solution (as evidenced by XRD) and a strong interaction of the Au and CuO species to promote CuO reduction (as evidenced by TPR). It is noted that a small amount of CO was observed with the prepared catalysts, especially with the 5% Au/(50:50)CuO–CeO₂ catalyst, compared to that obtained with the commercial MegaMax 700 catalyst. The optimum Cu:Ce atomic ratio for CuO–CeO₂ supported 5 wt% Au catalysts was found to be 50:50 and to be able to perform SRM. With this optimal catalyst, an overall 100% methanol conversion level with ~82% and ~1.3% H₂ and CO selectivity, respectively, was observed with a liquid feed rate of 1.5 cm³ h⁻¹ and a reaction temperature of 300 °C. The 5% Au/(50:50)CuO–CeO₂ catalyst was still active for 540

min even though CuO in this catalyst was reduced to metallic Cu. Therefore, metallic Cu is one of the active components of the catalysts for SRM.

From the statistically designed set of experiments for H₂ production from methanol by SRM over 5% Au/(50:50)CuO–CeO₂ catalysts, complete methanol conversion with a minimal CO selectivity (~1.5%) could be achieved when operated at temperature of ~306 °C, a S/M molar ratio of 2, a liquid feed of 1 cm³ h⁻¹ and a W/F ratio of 0.17 g s cm⁻³. The catalytic activities increased as the operating temperature increased, as expected for an endothermic reaction. A molar excess of water above the stoichiometric level is an important driving force to move the SRM reaction forward. An improved catalytic performance for methanol conversion with a lower CO selectivity can be achieved by decreasing the liquid feed rate. Higher W/F ratios, and thus a longer contact time, results in a higher catalytic activity. The liquid feed rate is the main factor influencing the methanol conversion and CO selectivity obtained, but masks the also important contribution of the operating temperature on the methanol conversion, and this plus the S/M molar ratio and its interaction with temperature on the CO selectivity. The optimized conditions for complete methanol conversion with a minimal CO selectivity in a SRM unit over 5 wt% Au/CuO–CeO₂ catalysts was evaluated using CCRD within the response surface method at a constant low liquid flow rate and subsequently experimentally tested, and was found to be an operating temperature of ~295 °C to ~307 °C and an S/M ratio of ~1.82 to 2.00 with good empirical-theoretical agreement.

9.2 Preferential oxidation (PROX) of CO

In the first part, the catalysts prepared by single step sol-gel (SSG) appeared an excellent catalyst performance for PROX of CO. Especially, bimetallic of Pt–Au catalyst improved the activity because of forming a new phase as evident by TPR. The 1%(1:1)PtAu/CeO₂ had the highest performance (90% conversion and 50% selectivity) at 90 °C. The presence of CO₂ and H₂O had a negatively effect on CO conversion and selectivity due to blocking of carbonate and water on active sites. For improvement, the reaction was studied in the double-stage reactor system and compared to the single-stage reactor system. The total inlet gas composition was maintained the same for both of systems. From the experiment, it was indicated that the double-stage reactor gave higher CO oxidation than the single stage reactor. The first-stage and the second-stage temperature showed the best activity in the range of 90 °C to 110 °C. Increase the total O₂ inlet stream and the amount of catalyst supported CO removal due to a lot of reactants and active sites of catalyst. However, the total O₂ inlet stream affected the selectivity significantly. After that, the effect of preparation method (compared with our previous works), addition of metal oxide (ZnO and Fe₂O₃), pretreatment condition and the composition of metal oxide in catalysts were studied. From the experiment, we can conclude that the catalytic activity of catalyst depend on the preparation method. Comparing the influence of catalytic preparation on the activities of the 1%(1:1)PtAu/(1:1)CeO₂–ZnO, the maximum CO conversion when prepared by the CP method was higher than SSG method ~15% at 90 °C. This may be because the CP method produces a catalyst that had a higher metallic surface area and a smaller particle size. The effective catalyst

for PROX unit was 1%(1:1)PtAu/(1:1)CeO₂-ZnO that was prepared by coprecipitation method, calcined at 500 °C for 5 h, and pretreated by H₂ before reaction. The incorporation of the Ce⁴⁺ ions and the Zn²⁺ ions in the lattice forms a solid solution and consequently promotes the oxygen mobility to react in CO oxidation. When adding H₂O or CO₂ or co-adding to the feedstream, the catalytic performance is dramatically decreased due to the competition adsorption of CO and CO₂ on the active sites and to the blockage by water vapor. Moreover, we also compared between single- and double-stage reactor for the best catalyst. The total inlet gas composition was maintained the same for both of systems. The double-stage reactor is an effective choice for increasing efficiency of PROX unit and had a good durability for ~60 h under simulated gas composition.

For second part, the statistically designed set of experiments to investigate the effect of H₂O and CO₂ which are important component under real reformat gas in single-stage reactor. To screen three factors; operating temperature, H₂O content, and CO₂ content, a full 2³ factorial design was carried out. The presence of H₂O had a slight effect on CO conversion and selectivity. Operating temperature and CO₂ content effected on CO conversion while only operating temperature that effected on CO selectivity significantly. After screening, face-centered central composite design (FCCCD) was used to fit models. The fitted models at desired condition were successful to use in simulated or real reformat gas. Indicating that a statistics can evaluate CO conversion and selectivity of PROX unit over 1%(1:1)PtAu/(1:1)CeO₂-ZnO catalyst. This is a useful tool to economize the experiment.

9.3 Fuel processing for hydrogen production

In this part, integration of steam reforming of methanol (SRM) and preferential oxidation (PROX) of CO was continuously operated. The effective catalysts of each unit were used. The real reformat gas produced from SRM unit at optimum condition (from section 9.1) consisted of 36.8% H₂, 1.1% CO, 1.1% O₂, 11.6% CO₂, 8.2% H₂O, and He balance. Nevertheless, CO in H₂-rich stream was not removed completely in single-stage reactor. The complete CO conversion was achieved by double-stage reactor in temperature range of 120 °C to 130 °C (1st = 120 °C, 2nd = 120–130 °C) at W/F of 0.17 g s cm⁻³. This hydrogen fuel process system could produce hydrogen at a rate of ~320 L d⁻¹ g_{cat}⁻¹.

9.4 Recommendations

Although, 5% Au/(50:50)CuO–CeO₂ catalyst for SRM unit and 1%(1:1)PtAu/(1:1)CeO₂–ZnO catalyst for PROX unit exhibited an excellent catalytic performance for pure hydrogen production. Nevertheless, it was first introduced to a lab scale H₂ production system as shown in this dissertation. To apply to the H₂ industry, more parameters were continued for further study. Moreover, the life time of 5% Au/(50:50)CuO–CeO₂ catalyst was not enough for H₂ production on-board PEMFC; though, the performance of 1%(1:1)PtAu/(1:1)CeO₂–ZnO was stable on ~60 h time stream. However, both catalysts are one of the potential candidates in H₂ processing due to a higher performance than commercial one.

REFERENCES

- [1] Barbir, F. PEM Fuel Cells: Theory and Practice. Elsevier Inc.: USA, 2005.
- [2] Agrell, J. et al. Production of hydrogen from methanol over Cu/ZnO catalysts promoted by ZrO₂ and Al₂O₃. Journal of Catalysis 219(2003): 389–403.
- [3] Brown, L.F. A comparative study of fuels for on-board hydrogen production for fuel-cell-powered automobiles. International Journal of Hydrogen Energy 26(2001): 381–397.
- [4] Qi, Z., He, C., and Kaufman, A. Effect of CO in the anode fuel on the performance of PEM fuel cell cathode. Journal of Power Sources 111(2002): 239-247.
- [5] Bartholomew, C.H. and Farrauto, R.J. Fundamentals of industrial catalytic processes 2nd edition, Hoboken, N.J.: Wiley, 2006.
- [6] Okada, O. et al. Process for steam reforming of hydrocarbons. U.S. Patent 5(1997): 685–890.
- [7] Wiese, W., Emonts, B., and Peters R. Methanol steam reforming in a fuel cell drive system. Journal of Power Sources 84(1999): 187–193.
- [8] Agrell, J., Lindström, B., Pettersson, L.J., and Järås, S.G. Catalytic hydrogen generation from methanol. Catalysis Volume 15, A review of recent literature, USA, 2002.
- [9] Takahashi, K., Takezawa, N., and Kobayashi, H. The mechanism of steam reforming of methanol over a copper-silica catalyst. Applied Catalysis A 2(1982): 363–366.

- [10] Peppley, B.A., Amphlett, J.C., Kearns, L.M., and Mann, R.F. Methanol±steam reforming on Cu/ZnO/Al₂O₃. Part 1: the reaction network. Applied Catalysis A 179(1999): 21–29.
- [11] Peppley, B.A., Amphlett, J.C., Kearns, L.M., and Mann, R.F. Methanol±steam reforming on Cu/ZnO/Al₂O₃ catalysts. Part 2. A comprehensive kinetic model. Applied Catalysis A 179(1999): 31–49.
- [12] Ritzkopf, I., Vukojević, S., Weidenthaler, C., Grunwaldt, J.-D., and Schüth, F. Decreased CO production in methanol steam reforming over Cu/ZrO₂ catalysts prepared by the microemulsion technique. Applied Catalysis A 302(2006): 215–223.
- [13] Huang, C.-Y., Sun, Y.-M., Chou, C.-Y., and Su, C.-C. Performance of catalysts CuO–ZnO–Al₂O₃, CuO–ZnO–Al₂O₃–Pt–Rh, and Pt–Rh in a small reformer for hydrogen generation. Journal of Power Sources 166(2007): 450–457.
- [14] Mastalir, Á. et al. Steam reforming of methanol over Cu/ZnO/Al₂O₃ modified with hydrotalcites. Catalysis Communications 8(2007): 1684–1690.
- [15] Yang, H.-M., and Liao, P.-H. Preparation and activity of Cu/ZnO-CNTs nano-catalyst on steam reforming of methanol. Applied Catalysis A 317(2007): 226–233.
- [16] Papavasiliou, J., Avgouropoulos, G., and Ioannides, T. Effect of dopants on the performance of CuO–CeO₂ catalysts in methanol steam reforming. Applied Catalysis B 69(2007): 226–234.

- [17] Shishido, T., Yamamoto, Y., Morioka, H., Takaki, K., and Takehira, K. Active Cu/ZnO and Cu/ZnO/Al₂O₃ catalysts prepared by homogeneous precipitation method in steam reforming of methanol. Applied Catalysis A 263(2004): 249–253.
- [18] Jones, S.D., Neal, L.M., and Hagelin-Weaver, H.E. Steam reforming of methanol using Cu–ZnO catalysts supported on nanoparticle alumina. Applied Catalysis B 84(2008): 631–642.
- [19] Matsumura, Y., and Ishibe, H. Selective steam reforming of methanol over silica-supported copper catalyst prepared by sol–gel method. Applied Catalysis B 86(2009): 114–120.
- [20] Udani, P.P.C., Gunawardana, P.V.D.S., Lee, H.C., and Kim, D.H. Steam reforming and oxidative steam reforming of methanol over CuO–CeO₂ catalysts. International Journal of Hydrogen Energy 34(2009): 7648–7655.
- [21] Jones, S.D., and Hagelin-Weaver, H.E. Steam reforming of methanol over CeO₂- and ZrO₂-promoted Cu–ZnO catalysts supported on nanoparticle Al₂O₃. Applied Catalysis B 90(2009):195–204.
- [22] Shen, J.-P., and Song, C. Influence of preparation method on performance of Cu/Zn-based catalysts for low-temperature steam reforming and oxidative steam reforming of methanol for H₂ production for fuel cells. Catalysis Today 77(2002): 89–98.
- [23] Jeong, H. et al. Hydrogen production by steam reforming of methanol in a micro-channel reactor coated with Cu/ZnO/ZrO₂/Al₂O₃ catalyst. Journal of Power Sources 159(2006): 1296–1299.

- [24] Chen, G., Li, S., and Yuan, Q. Pd-Zn/Cu-Zn-Al catalysts prepared for methanol oxidation reforming in microchannel reactors. Catalysis Today 120(2007): 63–70.
- [25] Oguchi, H., Kanai, H., Utani, K., Matsumura, Y., and Imamura, S. Cu₂O as active species in the steam reforming of methanol by CuO/ZrO₂ catalysts. Applied Catalysis A 293(2005): 64–70.
- [26] Huang, G., Liaw, B.-J., Jhang, C.-J., and Chen, Y.-Z. Steam reforming of methanol over CuO/ZnO/CeO₂/ZrO₂/Al₂O₃ catalysts. Applied Catalysis A 358(2009): 7–12.
- [27] Liu, Y., Hayakawa, T., Suzuki, K., and Hamakawa, S. Production of hydrogen by steam reforming of methanol over Cu/CeO₂ catalysts derived from Ce_{1-x}Cu_xO_{2-x} precursors. Catalysis Communications 2(2001): 195–200.
- [28] Zhang, X., and Shi, P. Production of hydrogen by steam reforming of methanol on CeO₂ promoted Cu/Al₂O₃ catalysts. Journal of Molecular Catalysis A 194(2003): 99–105.
- [29] Manzoli, M., Chiorino, A., and Boccuzzi, F. Decomposition and combined reforming of methanol to hydrogen: a FTIR and QMS study on Cu and Au catalysts supported on ZnO and TiO₂. Applied Catalysis B 57(2004): 201–209.
- [30] Yang, H.-C., Chang, F.-W., and Roselin, L.-S. Hydrogen production by partial oxidation of methanol over Au/CuO/ZnO catalysts. Journal of Molecular Catalysis A 276(2007): 184–190.
- [31] Ou, T.-C., Chang, F.-W., and Roselin, L.-S. Production of hydrogen via partial oxidation of methanol over bimetallic Au–Cu/TiO₂ catalysts. Journal of Molecular Catalysis A 293(2008): 8–16.

- [32] Wu, G. et al. H₂ production with ultra-low CO selectivity via photocatalytic reforming of methanol on Au/TiO₂ catalyst. International Journal of Hydrogen Energy 33(2008): 1243–1251.
- [33] Mariño, F., Descorme, C., and Duprez, D. Noble metal catalysts for the preferential oxidation of carbon monoxide in the presence of hydrogen (PROX). Applied Catalysis B 54(2004): 59–66.
- [34] Suh, D.J., Kwak, C., Kim, J.-H., Kwon, S.M., and Park, T.-J. Removal of carbon monoxide from hydrogen-rich fuels by selective low-temperature oxidation over base metal added platinum catalysts. Journal of Power Sources 142(2005): 70–74.
- [35] Oh, S.H., and Sinkevitch, R.M. Carbon Monoxide removal from hydrogen-rich fuel cell feedstream by selective catalytic oxidation. Journal of Catalysis 142(1993): 254–262.
- [36] Luengnaruemitchai, A., Osuwan, S., and Gulari, E. Selective catalytic oxidation of CO in the presence of H₂ over gold catalyst. International Journal of Hydrogen Energy 29(2004): 429–435.
- [37] Luengnaruemitchai, A., Osuwan, S., and Gulari, E. Comparative studies of low-temperature water–gas shift reaction over Pt/CeO₂, Au/CeO₂, and Au/Fe₂O₃ catalysts. Catalysis Communications 4(2003): 215–221.
- [38] Panzera, G. et al. CO selective oxidation on ceria-supported Au catalysts for fuel cell application. Journal of Power Sources 135(2004): 177–183.
- [39] Haruta, M., Yamada, N., Kobayashi, T., and Iijima, M., Gold catalysts prepared by coprecipitation for low-temperature oxidation of hydrogen and of carbon monoxide. Journal of Catalysis 115(1989): 301–309.

- [40] Grunwaldt, J.-D., Maciejewski, M., Becker, O.S., Fabrizioli, P., and Baiker, A. comparative study of Au/TiO₂ and Au/ZrO₂ catalysts for low-temperature CO oxidation. Journal of Catalysis 186(1999): 458–469.
- [41] Boccuzzi, F. et al. Au/TiO₂ nanosized samples: A catalytic, TEM, and FTIR study of the effect of calcination temperature on the CO oxidation. Journal of Catalysis 202(2001): 256–267.
- [42] Choudhary, T.V. et al. CO oxidation on supported nano-Au catalysts synthesized from a [Au₆(PPh₃)₆](BF₄)₂ Complex. Journal of Catalysis 207(2002): 247–255.
- [43] Okumura, M., Tsubota, S., and Haruta, M. Preparation of supported gold catalysts by gas-phase grafting of gold acetylacetonate for low-temperature oxidation of CO and of H₂. Journal of Molecular Catalysis A 199(2003): 73–84.
- [44] Sanchez, R.M.T., Ueda, A., Tanaka, K., and Haruta, M. Selective oxidation of CO in hydrogen over gold supported on manganese oxides. Journal of Catalysis 168(1997): 125–127.
- [45] Deng, W., Jesus, J.D., Saltsburg, H., and Flytzani-Stephanopoulos, M. Low-content gold-ceria catalysts for the water–gas shift and preferential CO oxidation reactions. Applied Catalysis B 291(2005): 126–135.
- [46] Barbier Jr., and Dopez, D. Steam effects in three-way catalysis. Applied Catalysis B 4(1994): 105–140.
- [47] Diwell, A.F., Rajaram, R.R., Shaw, H.A., and Truex, T.J. The role of ceria in three-way catalysts. Studies in Surface Science and Catalysis 71(1991): 139–148.

- [48] Mariño, F., Descorme, C., and Duprez, D. Supported base metal catalysts for the preferential oxidation of carbon monoxide in the presence of excess hydrogen (PROX). Applied Catalysis B 58(2005): 175–183.
- [49] Pozdnyakova, O. et al. Preferential CO oxidation in hydrogen (PROX) on ceria-supported catalysts, part I: Oxidation state and surface species on Pt/CeO₂ under reaction conditions. Journal of Catalysis 237(2006): 1–16.
- [50] Pozdnyakova, O. et al. Preferential CO oxidation in hydrogen (PROX) on ceria-supported catalysts, part II: Oxidation states and surface species on Pd/CeO₂ under reaction conditions, suggested reaction mechanism. Journal of Catalysis 237(2006): 17–28.
- [51] Vayssieres, L., Keis, K., Hagfeldt, A., and Lindquist, S.-E. Three-dimensional array of highly oriented crystalline ZnO Microtubes. Chemistry of Materials 13(2001): 4395–4398.
- [52] Huang, M.H. et al. Room-Temperature ultraviolet nanowire nanolasers. Science 292(2001): 1897–1899.
- [53] Leiter, F. et al. Oxygen vacancies in ZnO. Physica B 340–342(2003): 201–204.
- [54] Wang, G.Y., Zhang, W.X., Lian, H.L., Jiang, D.Z., and Wu, T.H. Effect of calcination temperatures and precipitant on the catalytic performance of Au/ZnO catalysts for CO oxidation at ambient temperature and in humid circumstances. Applied Catalysis A 239(2003): 1–10.
- [55] Iwasa, N., Arai, S., and Arai, M. Effect of Cs promoter on the activity of Pd/ZnO catalyst for selective oxidation of CO in H₂-rich gas. Catalysis Communications 7(2006): 839–842.

- [56] Iwasa, N., Arai, S., and Arai, M. Selective oxidation of CO with modified Pd/ZnO catalysts in the presence of H₂: Effects of additives and preparation variables. Applied Catalysis B 79(2007): 132–141.
- [57] Zhang, J. et al. Selective oxidation of CO in hydrogen rich gas over platinum–gold catalyst supported on zinc oxide for potential application in fuel cell. Energy Conversion and Management 44(2003): 1805–1815.
- [58] Wang, Y.H. et al. Selective oxidation of CO in hydrogen–rich mixtures and kinetics investigation on platinum–gold supported on zinc oxide catalyst. Journal of Power Sources 155(2006): 440–446.
- [59] Souza, K.R., Lima, A.F.F., Sous, F.F., and Appel, L.G. Preparing Au/ZnO by precipitation–deposition technique. Applied Catalysis A 340(2008): 133–139.
- [60] Guo, J. et al. Preparation of nanometric CeO₂–ZrO₂–Nd₂O₃ solid solution and its catalytic performances. Journal of Alloys and Compounds 460(2008): 485–490.
- [61] Ayastuy, J.L., González–Marcos, M.P., Gil–Rodríguez, A., González–Velasco, J.R., and Gutiérrez–Ortiz, M.A. Selective CO oxidation over Ce_xZr_{1-x}O₂–supported Pt catalysts. Catalysis Today 116(2006): 391–399.
- [62] Kumar, K.S., and Mathews, T. Sol-gel synthesis microwave assisted sintering of zirconia–ceria solid solution. Journal of Alloys and Compounds 391(2005): 177–180.
- [63] Thammachart, M., Meeyoo, V., Risksomboon, T., and Osuwan, S. Catalytic activity of CeO₂–ZrO₂ mixed oxide catalysts prepared via sol-gel technique: CO oxidation. Catalysis Today 68(2001): 53–61.

- [64] Wu, X., Fan, J., Ran, R., and Weng, D. Effect of preparation methods on the structure and redox behavior of platinum–ceria–zirconia catalysts. Chemical Engineering Journal 109(2005): 133–139.
- [65] de Jong, K.P. Synthesis of Solid Catalysts Weinheim: Wiley-VCH, 2009.
- [66] Ertl, G., Knözinger, H., and Schüth, F. Handbook of Heterogeneous Catalysis Volume 1, 2nd edition, Weinheim: Wiley-VCH Verlag, 2008.
- [67] Zhou, S., Yuan, Z., and Wang, S. Selective CO oxidation with real methanol reformat over monolithic Pt group catalysts: PEMFC applications. International Journal of Hydrogen Energy 31(2006): 924–933.
- [68] Parinyaswan, A., Pongstabodee, S., and Luengnaruemitchai, A. Catalytic performances of Pt–Pd/CeO₂ catalysts for selective CO oxidation. International Journal of Hydrogen Energy 31(2006): 1942–1949.
- [69] Srinivas, S., and Gulari, E. Preferential CO oxidation in a two-stage packed-bed reactor: Optimization of oxygen split ratio and evaluation of system robustness. Catalysis Communications 7(2006): 819–826.
- [70] Scirè, S., Crisafulli, C., Minicò, S., Condorelli, G.G., and Mauro, A.D. Selective oxidation of CO in H₂-rich stream over gold/iron oxide: An insight on the effect of catalyst pretreatment. Journal of Molecular Catalysis A 284(2008): 24–32.
- [71] Chang, L.-H., Yeh, Y.L., and Chen, Y.-W. Preferential oxidation of CO in hydrogen stream over nano-gold catalysts prepared by photodeposition method. International Journal of Hydrogen Energy 33(2008): 1965–1974.

- [72] Brasil, J.L. et al. Statistical design of experiments as a tool for optimizing the batch conditions to Cr(VI) biosorption on *Araucaria angustifolia* wastes. Journal of Hazardous Materials B 133(2006): 143–153.
- [73] Lima, E.C. et al. Adsorption of Cu(II) on *Araucaria angustifolia* wastes: Determination of the optimal conditions by statistic design of experiments. Journal of Hazardous Materials 140(2007): 211–220.
- [74] Erickson, P.A., and Liao, C.-h Statistical validation and an empirical model of hydrogen production enhancement found by utilizing passive flow disturbance in the steam-reformation process. Experimental Thermal and Fluid Science 32(2007): 467–474.
- [75] Aslan, N. Application of response surface methodology and central composite rotatable design for modeling the influence of some operating variables of a Multi-Gravity Separator for coal cleaning. Fuel 86(2007): 769–776.
- [76] Meshkini, F., Taghizadeh, M., and Bahmani, M. Investigating the effect of metal oxide additives on the properties of Cu/ZnO/Al₂O₃ catalysts in methanol synthesis from syngas using factorial experimental design. Fuel 89(2010): 170–175.
- [77] Thouchprasitchai, N., Luengnaruemitchai, A., and Pongstabodee, S. Statistical optimization by response surface methodology for water–gas shift reaction in a H₂-rich stream over Cu–Zn–Fe composite-oxide catalysts. Journal of the Taiwan Institute of Chemical Engineers (2010) doi:10.1016/j.jtice.2010.10.008.

- [78] Charoenchaitrakool, M., and Thienmethangkoon, J. Statistical optimization for biodiesel production from waste frying oil through two-step catalyzed process. Fuel Processing Technology 92(2011): 112–118.
- [79] Pan, C. et al. Integration of high temperature PEM fuel cells with a methanol reformer. Journal of Power Sources 145(2005): 392–398.
- [80] Men, Y. et al. A complete miniaturized microstructured methanol fuel processor/fuel cell system for low power applications. International Journal of Hydrogen Energy 33(2008): 1374–1382.
- [81] Montgomery, D.C. Design and Analysis of Experiments 7th edition New York, John Wiley and Sons, 2009.
- [82] Avgouropoulos, G., and Ioannides, T. Selective CO oxidation over CuO–CeO₂ catalysts prepared via the urea–nitrate combustion method Applied Catalysis A 244(2003): 155–167.
- [83] Hwang, S.-M., Kwon, O.J., and Kim, J.J. Method of catalyst coating in micro-reactors for methanol steam reforming. Applied Catalysis A 316(2007): 83–89.
- [84] Datè, M., and Haruta, M. Moisture Effect on CO Oxidation over Au/TiO₂ Catalyst. Journal of Catalysis 201(2001): 221–224.
- [85] Schubert, M.M., Venugopal, A., Kahlich, M.J., Plzak, V., and Behm, R.J. Influence of H₂O and CO₂ on the selective CO oxidation in H₂-rich gases over Au/a-Fe₂O₃. Journal of Catalysis 222(2004): 32–40.
- [86] Monyanon, S., Luengnaruemitchai, A., and Pongstabodee, S. Catalytic activity of Pt–Au/CeO₂ catalyst for the preferential oxidation of CO in H₂-rich stream. Journal of Power Sources 163(2006): 547–554.

- [87] Li, R. et al. Synthesis and UV-shielding properties of ZnO- and CaO doped CeO₂ via soft solution chemical process. Solid State Ionics 151(2002): 235–241.
- [88] Naknam, P., Luengnaruemitchai, A., and Sujitra Wongkasemjit. Preferential CO oxidation over Au/ZnO and Au/ZnO–Fe₂O₃ catalysts prepared by photodeposition, International Journal of Hydrogen Energy 34(2009): 9838–9846.
- [89] Ayastuy, J.L., Gil-Rodríguez, A., González-Marcos, M.P., and Gutiérrez-Ortiz, M.A. Effect of process variables on Pt/CeO₂ catalyst behaviour for the PROX reaction. International Journal of Hydrogen Energy 31(2006): 2231–2242.
- [90] Wu, Z. et al. CO preferential oxidation in H₂-rich stream over a CuO/CeO₂ catalyst with high H₂O and CO₂ tolerance. Fuel (2010) doi:10.1016/j.fuel.2010.03.001.
- [91] Guo, Q., and Liu, Y. MnO_x modified Co₃O₄-CeO₂ catalysts for the preferential oxidation of CO in H₂-rich gases. Applied Catalysis B 82(2008): 19–26.
- [92] Boccuzzi, F., Chiorino, A., and Manzoli, M. FTIR study of methanol decomposition on gold catalyst for fuel cells. Journal of Power Sources 118(2003): 304–310.
- [93] Vargas, M.A.L. et al. An IR study of methanol steam reforming over ex-hydrotalcite Cu–Zn–Al catalysts. Journal of Molecular Catalysis A 266(2007): 188–197.
- [94] Martínez-Arias, A., Hungría, A.B., Fernández-García, M., Conesa, J.C., and Munuera, G. Preferential oxidation of CO in a H₂-rich stream over CuO/CeO₂ and CuO/(Ce,M)O_x (M = Zr, Tb) catalysts. Journal of Power Sources 151(2005): 32–42.

- [95] Zaki, M.I., Hasan, M.A., Al-Sagheer, F.A., and Pasupulety, L. In situ FTIR spectra of pyridine adsorbed on $\text{SiO}_2\text{-Al}_2\text{O}_3$, TiO_2 , ZrO_2 and CeO_2 : general considerations for the identification of acid sites on surfaces of finely divided metal oxides. Colloids and Surfaces A 190(2001): 261–274.
- [96] Chowdhury, A., Thompson, P.R., and Milne, S.J. TGA–FTIR study of a lead zirconate titanate gel made from a triol-based sol–gel system. Thermochimica Acta 475(2008): 59–64.
- [97] Liao, L.-F., Lien, C.-F., Shieh, D.-L., Chen, M.-T., and Lin, J.-L. FTIR study of adsorption and photoassisted oxygen isotopic exchange of carbon monoxide, carbon dioxide, carbonate, and formate on TiO_2 . Journal of Physic Chemical B 106(2002): 11240–11245.

APPENDICES

$$= \frac{805.93}{14.01}$$

$$= 57.53 \text{ ml of solution}$$

Using of mixed solution between urea and $\text{Ce}(\text{NO}_3)_3 \cdot 6\text{H}_2\text{O}$ at 3:1 volume ratio;

So, the required volume of urea from stock solution

$$= 3 \times 57.53$$

$$= 172.59 \text{ ml}$$

In part of active metal;

$$1 \text{ g of catalyst consists of} = 10 \text{ mg of Pt-Au}$$

$$\text{M.W. of Pt} = 195.08 \text{ g}, \quad \text{M.W. of Au} = 196.97 \text{ g}$$

At Pt : Au = 1 : 1 atomic ratio;

	Pt	:	Au	
	$1 \times 6.02 \times 10^{23}$:	$1 \times 6.02 \times 10^{23}$	atom by mole
or	1	:	1	atom by mole
	$1 \times \frac{195.08}{195.08}$:	$1 \times \frac{196.97}{195.08}$	by weight
	1	:	1.0097	by weight

Total amount of Pt-Au = 10 mg; so,

$$1 \times \frac{10}{(1+1.0097)} : 1.0097 \times \frac{10}{(1+1.0097)}$$

$$4.98 : 5.02 \text{ mg}$$

Stock solution:

$$\text{M.W. of H}_2\text{PtCl}_6 \cdot 6\text{H}_2\text{O} = 517.93 \text{ g}, \quad \text{M.W. of H AuCl}_4 \cdot 3\text{H}_2\text{O} = 394.79 \text{ g}$$

$\text{H}_2\text{PtCl}_6 \cdot 6\text{H}_2\text{O}$ solution 200 ml from 5 g of $\text{H}_2\text{PtCl}_6 \cdot 6\text{H}_2\text{O}$; so,

$$\begin{aligned}
 \text{Pt} &= \frac{195.08 \times 5}{517.93} \\
 &= 1.8833 \text{ g} \\
 \text{Concentration of Pt} &= \frac{1883.3}{200} \\
 &= 9.42 \text{ mg/ml}
 \end{aligned}$$

H₂AuCl₄·3H₂O solution 200 ml from 5 g of H₂AuCl₄·3H₂O

$$\begin{aligned}
 \text{Au} &= \frac{196.97 \times 5}{394.79} \\
 &= 2.4946 \text{ g} \\
 \text{Concentration of Au} &= \frac{2494.6}{200} \\
 &= 12.47 \text{ mg/ml}
 \end{aligned}$$

From stock solution of H₂PtCl₆·6H₂O and H₂AuCl₄·3H₂O;

Need Pt 4.98 mg, the required volume of stock solution

$$\begin{aligned}
 &= \frac{4.98}{9.42} \\
 &= 0.528 \text{ ml of solution}
 \end{aligned}$$

Need Au 5.02 mg, the required volume of stock solution

$$\begin{aligned}
 &= \frac{5.02}{12.47} \\
 &= 0.403 \text{ ml of solution}
 \end{aligned}$$

Therefore, the solution for 1%(1:1)PtAu/CeO₂ preparation by single step sol-gel method are:

$$\begin{aligned}
 \text{Ce(NO}_3)_3 \cdot 6\text{H}_2\text{O solution} &= 57.53 \text{ ml} \\
 \text{urea solution} &= 172.59 \text{ ml}
 \end{aligned}$$

$$\text{H}_2\text{PtCl}_6 \cdot 6\text{H}_2\text{O} \text{ solution} = 0.528 \text{ ml}$$

$$\text{HAuCl}_4 \cdot 3\text{H}_2\text{O} \text{ solution} = 0.403 \text{ ml}$$

A2 Precipitation method

Example: Preparation of 1%(1:1)PtAu/(1:1)CeO₂-ZnO 1000 mg

In part of support;

1000 mg of catalyst consists of mixed CeO₂-ZnO = 990 mg

At Ce : Zn = 1 : 1 atomic ratio;

	Ce	:	Zn	
	$1 \times 6.02 \times 10^{23}$:	$1 \times 6.02 \times 10^{23}$	atom by mole
or	1	:	1	atom by mole
	140.11	:	65.41	by weight
or	CeO ₂	:	ZnO	
	172.11	:	81.41	by weight

Total amount of CeO₂-ZnO = 990 mg; so,

$$\frac{172.11}{(172.11 + 81.41)} \times 990 \quad : \quad \frac{81.41}{(172.11 + 81.41)} \times 990$$

$$672.09 \quad : \quad 317.91 \quad \text{mg}$$

Stock solution;

$$\text{Ce}(\text{NO}_3)_3 \cdot 6\text{H}_2\text{O} \quad \quad \quad 0.1 \quad \quad \text{M}$$

$$\text{Zn}(\text{NO}_3)_2 \cdot 4\text{H}_2\text{O} \quad \quad \quad 0.1 \quad \quad \text{M}$$

$$\text{M.W. of Zn}(\text{NO}_3)_2 \cdot 4\text{H}_2\text{O} = 261.44 \text{ g}, \quad \text{M.W. of ZnO} = 81.41 \text{ g}$$

$$\text{M.W. of Ce}(\text{NO}_3)_3 \cdot 6\text{H}_2\text{O} = 434.23 \text{ g}, \quad \text{M.W. of CeO}_2 = 172.11 \text{ g}$$

$$\begin{aligned}
 \text{So, concentration of CeO}_2 &= \frac{172.11 \times 43.423}{434.23} \\
 &= 17.21 \text{ g/L or mg/ml} \\
 \text{and concentration of ZnO} &= \frac{81.41 \times 26.144}{261.44} \\
 &= 8.14 \text{ g/L or mg/ml}
 \end{aligned}$$

From stock solution of 0.1 M of $\text{Ce}(\text{NO}_3)_3 \cdot 6\text{H}_2\text{O}$;

Need CeO_2 672.09 mg, the required volume of stock solution

$$\begin{aligned}
 &= \frac{672.09}{17.21} \\
 &= 39.05 \text{ ml of solution}
 \end{aligned}$$

And from stock solution of 0.1 M of $\text{Zn}(\text{NO}_3)_2 \cdot 4\text{H}_2\text{O}$;

Need ZnO 317.91 mg, the required volume of stock solution

$$\begin{aligned}
 &= \frac{317.91}{8.14} \\
 &= 39.05 \text{ ml of solution}
 \end{aligned}$$

In part of active metal;

1 g of catalyst consists of 10 mg of Pt–Au

M.W. of Pt = 195.08 g, M.W. of Au = 196.97 g

At Pt : Au = 1 : 1 atomic ratio;

$$\begin{array}{rcccl}
 & \text{Pt} & : & \text{Au} & \\
 & 1 \times 6.02 \times 10^{23} & : & 1 \times 6.02 \times 10^{23} & \text{atom by mole} \\
 \text{or} & 1 & : & 1 & \text{atom by mole} \\
 & 1 \times \frac{195.08}{195.08} & : & 1 \times \frac{196.97}{196.97} & \text{by weight} \\
 & 1 & : & 1.0097 & \text{by weight}
 \end{array}$$

Total amount of Pt–Au = 10 mg; so,

$$1 \times \frac{10}{(1+1.0097)} : 1.0097 \times \frac{10}{(1+1.0097)}$$

$$4.98 : 5.02 \quad \text{mg}$$

Stock solution:

$$\text{M.W. of H}_2\text{PtCl}_6 \cdot 6\text{H}_2\text{O} = 517.93 \text{ g}, \quad \text{M.W. of HAuCl}_4 \cdot 3\text{H}_2\text{O} = 394.79 \text{ g}$$

H₂PtCl₆·6H₂O solution 200 ml from 5 g of H₂PtCl₆·6H₂O; so,

$$\text{From above, concentration of Pt} = 9.42 \text{ mg/ml}$$

HAuCl₄·3H₂O solution 200 ml from 5 g of HAuCl₄·3H₂O

$$\text{From above, concentration of Au} = 12.47 \text{ mg/ml}$$

From stock solution;

$$\text{Pt } 4.976 \text{ mg} = \frac{4.98}{9.42}$$

$$= 0.528 \text{ ml of solution}$$

$$\text{Au } 5.02 \text{ mg} = \frac{5.02}{12.47}$$

$$= 0.403 \text{ ml of solution}$$

Therefore, the solution for 1%(1:1)PtAu/CeO₂ preparation by single step sol-gel

method are:

$$\text{Ce(NO}_3)_3 \cdot 6\text{H}_2\text{O solution} = 39.05 \text{ ml}$$

$$\text{Zn(NO}_3)_2 \cdot 4\text{H}_2\text{O} = 39.05 \text{ ml}$$

$$\text{H}_2\text{PtCl}_6 \cdot 6\text{H}_2\text{O solution} = 0.528 \text{ ml}$$

$$\text{HAuCl}_4 \cdot 3\text{H}_2\text{O solution} = 0.403 \text{ ml}$$

APPENDIX B

CATALYST CHARACTERIZATION

B1 X-ray diffraction (XRD)

XRD calculation for crystallite size particle from Debye Scherrer's equation;

$$D_b = \frac{K \times \lambda}{\beta \times \cos \theta}$$

where;

D_b = crystallite diameter (Å)

K = Scherrer constant = 0.9

λ = X-ray wave length (Å) = 1.54

β = angular width of peak in term of 2θ

θ = Bragg's angle of reflection (degree)

For example: PtAu/CeO₂ single step sol-gel

To calculate CeO₂ crystallite size from the XRD pattern of PtAu/CeO₂ is shown in Figure B-1 and giving data

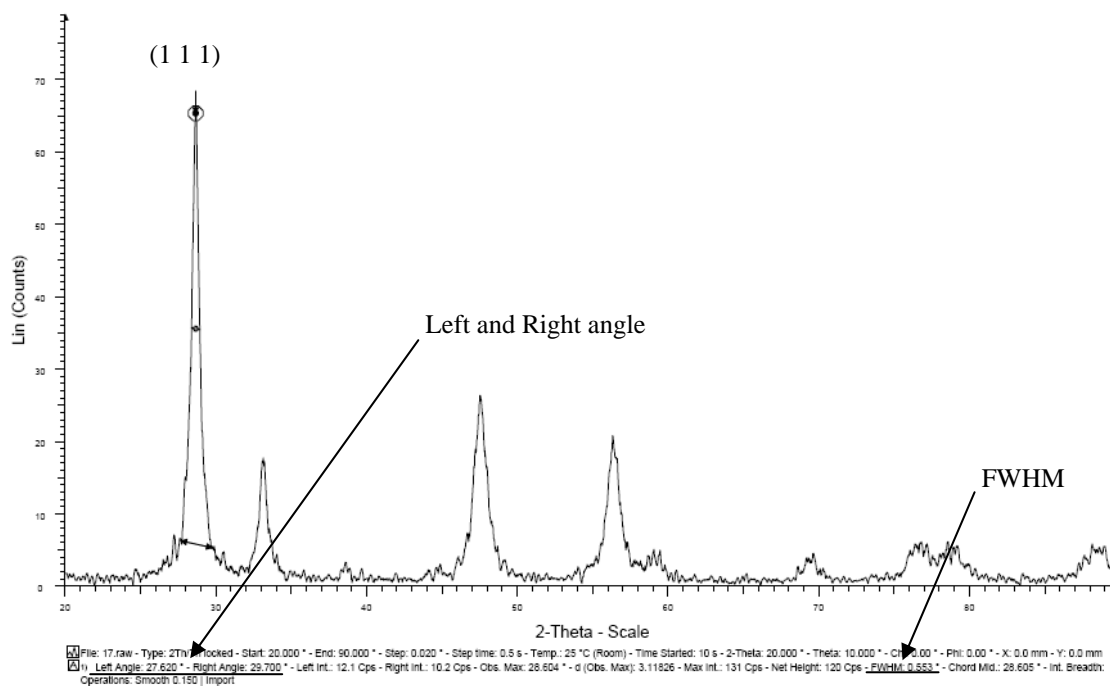


Figure B–1 XRD pattern of 1%(1:1)PtAu/CeO₂ catalyst

At center of major peak, (1 1 1) plane,

$$2\theta = \frac{\text{Left angle} + \text{Right angle}}{2}$$

$$= \frac{27.62 + 29.7}{2}$$

$$= 28.66$$

$$\theta = \frac{28.66}{2} \times \frac{\pi}{180}$$

$$= 0.25$$

Form graph,

$$\text{Full width at half maximum (FWHM)} = 0.553$$

$$\text{So, } \beta = 0.553 \times \frac{\pi}{180}$$

$$= 0.01$$

Therefore,

$$\begin{aligned} \text{CeO}_2 \text{ crystallite size } (D_b) &= D_b = \frac{K \times \lambda}{\beta \times \cos \theta} \\ &= \frac{0.9 \times 1.54}{0.01 \times \cos 0.25} \\ &= 138.6 \text{ \AA} \\ &= 13.9 \text{ nm} \end{aligned}$$

B2 Transmission electron microscope (TEM)

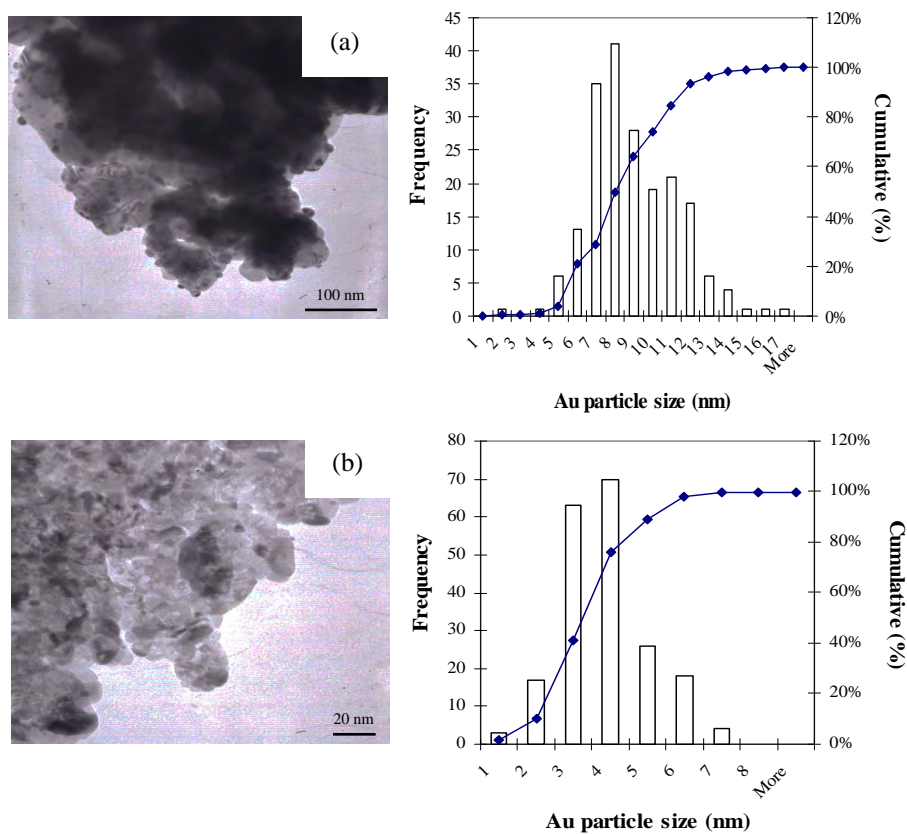


Figure B-2 TEM images of (a) 5% Au/CuO and (b) 5% Au/CeO₂ catalysts.

VITA

Miss Sutarawadee Monyanon was born on December 15, 1981 in Songkhla, Thailand.

University Education:

2000–2004 Bachelor Degree of Science*

(Scholarship: Senior Project Endowment Fund)

2004–2006 Master Degree of Science*

(Scholarship: Asian Development Bank (ADB) Endowment Fund)

2006–2010 Doctor of Philosophy Degree of Science*

(Scholarships: The 90th Anniversary of Chulalongkorn University Fund under Ratchadaphiseksomphot Endowment Fund and Fuels Research Center Endowment Fund)

* Department of Chemical Technology, Faculty of Science, Chulalongkorn University, Bangkok, Thailand.

Publications:

1. “Catalytic Activity of Pt–Au/CeO₂ Catalyst for the Preferential Oxidation of CO in H₂-Rich Stream”. *Journal of Power Sources* 163 (2006) 547–554.
2. “Preferential Oxidation of Carbon Monoxide over Pt, Au Monometallic Catalyst, and Pt–Au Bimetallic Catalyst Supported on Ceria in Hydrogen-rich Reformate”. *Journal of the Chinese Institute of Chemical Engineers* 38 (2007) 435–441.
3. “Preferential Oxidation of Carbon Monoxide in Simulated Reformatted Gas over PtAu/Ce_xZn_yO₂ Catalysts”. *International Journal of Hydrogen Energy* 35 (2010) 3234–3242.